

**UCSF**

**UC San Francisco Electronic Theses and Dissertations**

**Title**

Regulation of bacterial outer membrane homeostasis by the  $\sigma$ -factor,  $\sigma^E$

**Permalink**

<https://escholarship.org/uc/item/6z62v1t6>

**Author**

Guo, Monica

**Publication Date**

2014

Peer reviewed|Thesis/dissertation

Regulation of Bacterial Outer Membrane Homeostasis by the  $\sigma$ -  
factor,  $\sigma^E$

by

Monica S. Guo

DISSERTATION

Submitted in partial satisfaction of the requirements for the degree of

DOCTOR OF PHILOSOPHY

in


Biochemistry and Molecular Biology

in the

GRADUATE DIVISION

of the

UNIVERSITY OF CALIFORNIA, SAN FRANCISCO







## Dedication & Acknowledgements

This work would not have been possible without the support and guidance of various people: mentors, colleagues, family and friends. Thank you, to my amazing advisor, Carol Gross, who always believed in me, even when I didn't believe in myself.

I would also like to thank my thesis committee members, Hana El-samad and Jeffrey Cox for guidance and encouragement. Also a major thank you to all my amazing collaborators – Bob Sauer and Santiago Lima, for the fantastic work in the LPS project, and Gisela Storz, Taylor Updegrave, and Svetlana Shabalina, for the fantastic work on the Lpp project. It was these collaborations that made this thesis possible.

Additionally, all the amazing members of the Carol Gross lab, especially Rachna Chaba, Bentley Lim, David Burkhardt, and Andrew Gray, who were major influencer on the direction of my PhD. Additionally, I'd like to thank Jason Peters for keeping me company at night and for eating some of my ruffles. Also Gene-Wei Li, for putting up with the nonsense and for the suggestions and support.

To my friends, especially my Tetrad classmates who were so helpful and supportive along the way, and those who aren't in biologists, who now actually believe me when I say, "I'm graduating soon." To my family, my parents and relatives who helped me along this path, and especially Victor Chubukov, who made the last few years a really fun journey together.

## Abstract

The outer membrane (OM) is the first line of defense for Gram-negative bacteria against the exterior environment, as it forms an impermeable lipid barrier to protect the cell from antibiotics and other stresses. This impermeability is due to the fact that the OM is an asymmetric lipid bilayer, consisting of outer leaflet lipopolysaccharides and inner leaflet phospholipids. Additionally, there are many proteins unique to the OM, mainly the Outer Membrane Porins (OMPs) and OM lipoproteins. The cell utilizes dedicated machines to assemble each of the proteins and lipids into this complex folding environment. As OM integrity is vital, the cell needs to have complex surveillance systems to monitor folding and assembly of all OM components. In *E. coli* and related bacteria, homeostasis of the OM is monitored by the essential transcription factor,  $\sigma^E$ , which regulates OM assembly by transcribing a suite of ~100 protein encoding genes and two small, regulatory RNAs (sRNAs).

$\sigma^E$  activity is controlled by the degradation rate of its anti- $\sigma^E$ , RseA, which holds  $\sigma^E$  inactive in the inner membrane.  $\sigma^E$  is further regulated by RseB, which binds to RseA and protects RseA from proteolytic cleavage. While mechanisms that can cause RseA degradation are known, the *in vivo* signal that relieves the inhibitory effect of RseB was not understood.

In this thesis, I set out to understand the role of RseB in the  $\sigma^E$  signaling system, and to identify the signal that inactivated RseB *in vivo*. I found that the presence of RseB significantly inhibited the dynamic range of  $\sigma^E$  activation, such that  $\sigma^E$  is activated only when signals to activate RseA cleavage and inhibit RseB were both present in the cell. I next discovered that RseB is inactivated by lipopolysaccharide, thus only in the presence of two concomitant sources of envelope stress is  $\sigma^E$  maximally activated. As the  $\sigma^E$ , RseA, and RseB operon is conserved in genomes with  $\sigma^E$ , we hoped that our findings regarding the role of RseB in *Escherichia coli*

would be a broadly applicable paradigm for how Gram-negative bacteria regulate OM homeostasis.

I found it curious that the assembly machines for the lipoproteins of the OM were not represented in the  $\sigma^E$  regulon, even though this regulon encodes genes involved in every step of lipopolysaccharide and OMP transport and assembly. As lipoproteins are the major proteins of the OM, I set out to determine whether  $\sigma^E$  senses lipoprotein folding stresses and whether  $\sigma^E$  had additional mechanisms to regulate lipoprotein folding. I discovered a new  $\sigma^E$ -dependent sRNA (MicL) that decreases translation of the lipoprotein Lpp, the most abundant protein in the cell. By regulating Lpp translation through MicL,  $\sigma^E$  is able to regulate a major fraction of cellular translation and control the majority of protein flux destined to the OM. Additionally, misaccumulation of Lpp induces the  $\sigma^E$  response and proper regulation of Lpp plays an important role in envelope homeostasis.

## Table of Contents

|   |            |
|---|------------|
| <b>Dedication &amp; Acknowledgements</b> .....  | <b>iii</b> |
| <b>Abstract</b> .....   | <b>iv</b>  |
| <b>Table of Contents</b> .....  | <b>vi</b>  |
| <b>List of Tables</b> .....   | <b>ix</b>  |
| <b>List of Figures</b> .....  | <b>x</b>   |
| <b>Introduction</b> .....   | <b>1</b>   |
| Preface .....   | 2          |
| Introduction .....  | 3          |
| Transcriptional Remodeling in Response to Stress.....   | 3          |
| Regulatory Proteolysis in Stress Responses.....   | 17         |
| Perspectives .....  | 25         |
| References .....  | 26         |
| <b>Chapter 1 - Signal Integration by DegS and RseB governs the <math>\sigma^E</math>-mediated<br/>    envelope stress response in <i>Escherichia coli</i></b> ..... | <b>46</b>  |
| Preface: .....  | 47         |
| Abstract .....  | 48         |
| Introduction .....  | 49         |
| Results.....  | 52         |

|  |            |
|--|------------|
| Discussion .....   | 63         |
| Materials and Methods .....  | 66         |
| References .....   | 68         |
| Supplemental Information.....  | 72         |
| <b>Chapter 2 - Dual molecular signals mediate the bacterial response to outer-</b>                     |            |
| <b>membrane stress .....</b>   | <b>77</b>  |
| Preface: .....   | 78         |
| Abstract .....   | 79         |
| Main Text:.....  | 80         |
| References and Notes:.....   | 92         |
| Materials and Methods .....  | 98         |
| Supplemental References (27-32).....   | 122        |
| <b>Chapter 3 - MicL, a new <math>\sigma^E</math>-dependent sRNA, combats envelope stress by</b>        |            |
| <b>repressing synthesis of Lpp, the major outer membrane lipoprotein.....</b>                          | <b>123</b> |
| Preface: .....   | 124        |
| Abstract .....   | 126        |
| Introduction.....  | 127        |
| Results.....   | 130        |
| Discussion .....   | 147        |
| Materials and methods .....  | 154        |
| References .....   | 160        |
| Supplemental Figures.....  | 169        |
| <b>Conclusions .....</b>   | <b>194</b> |
| <b>Appendix 1 - Suppressors of the lethality due to <math>\sigma^E</math> activity depletion .....</b> | <b>195</b> |

|   |            |
|---|------------|
| Introduction .....  | 196        |
| Results.....  | 197        |
| Discussion/Future Directions .....  | 205        |
| Methods .....   | 206        |
| References .....  | 207        |
| <b>Appendix 2 - MicL overexpression alters global sRNA regulation.....</b>    | <b>208</b> |
| Introduction .....  | 209        |
| Results.....  | 210        |
| Discussion .....  | 213        |
| References .....  | 214        |
| <b>Appendix 3 - Comparison of sequencing approaches to identify TSS .....</b> | <b>215</b> |
| Introduction .....  | 216        |
| Results.....  | 217        |
| References .....  | 222        |

## List of Tables

### Chapter 1

|  |    |
|--|----|
| <b>Supplemental Table S1.</b> Stains and plasmids used in this study ..... | 76 |
|--|----|

### Chapter 2

|   |     |
|---|-----|
| <b>Supplemental Table S1.</b> Stains used in this study ..... | 120 |
|---|-----|

### Chapter 3

|                                      |     |
|--------------------------------------|-----|
| <b>Supplemental Table List</b> ..... | 185 |
|--------------------------------------|-----|

|  |          |
|--|----------|
| <b>Supplemental Table S3.</b> Outer membrane and MicA, RybB, and MicL regulated proteins<br>as a fraction of total ..... | 186, 190 |
|--|----------|

|   |     |
|---|-----|
| <b>Supplemental Table S4.</b> Stains used in this study ..... | 191 |
|---|-----|

|   |     |
|---|-----|
| <b>Supplemental Table S5.</b> Plasmids used in this study ..... | 193 |
|---|-----|

### Appendix 3

|   |     |
|---|-----|
| <b>Table 1.</b> Sites in TSS-seq that correspond with peaks in mRNA-seq ..... | 221 |
|---|-----|



## List of Figures

### Introduction

|  |    |
|--|----|
| <b>Figure 1.</b> Regulation of $\sigma^{32}$ at the inner membrane .....                         | 15 |
| <b>Figure 2.</b> Two signals are required for $\sigma^E$ activation .....                        | 19 |
| <b>Figure 3.</b> Activation of $\sigma^B$ by different stresses leads to distinct responses..... | 22 |
| <b>Figure 4.</b> ClpXP degradation of $\sigma^S$ is regulated via two mechanisms.....            | 27 |
| <b>Figure 5.</b> Many cellular functions of Lon .....  | 31 |

### Chapter 1

|   |    |
|---|----|
| <b>Figure 1.</b> Components controlling $\sigma^E$ activity .....   | 50 |
| <b>Figure 2.</b> Synergistic effect of DegS activation and RseB removal on $\sigma^E$ activity.....   | 53 |
| <b>Figure 3.</b> RseB determines the threshold of OMP signal required for $\sigma^E$ activation .....   | 55 |
| <b>Figure 4.</b> OMP peptide relieves RseB inhibition of RseA .....   | 58 |
| <b>Figure 5.</b> Residues upstream of the C-terminal YxF motif encode RseB modulatory<br>sequences.....   | 59 |
| <b>Figure 6.</b> Comparison of $\sigma^E$ activation, DegS activation, and RseB inactivation strengths of<br>OmpC <sub>20</sub> and OmpX <sub>20</sub> .....                  | 61 |
| <b>Figure 7.</b> OmpX fusion protein induces $\sigma^E$ in a DegS $\Delta$ PDZ strain.....  | 62 |
| <b>Figure S1.</b> Differential $\sigma^E$ activation in WT and $\Delta rseB$ cells does not result from differential<br>protein expression in the two strain backgrounds..... | 74 |
| <b>Figure S2.</b> DegS activation <i>in vivo</i> follows the inhibition-relief model.....   | 75 |

### Chapter 2

|   |     |
|---|-----|
| <b>Figure 1.</b> LPS displaces RseA from RseB .....   | 81  |
| <b>Figure 2.</b> Lipid-A fragments disrupt RseA <sup>P</sup> -RseB complexes .....  | 83  |
| <b>Figure 3.</b> Lipid-A fragments bind RseB/MucB and coactivate cleavage of RseA <sup>P</sup> /MucA <sup>P</sup> ..                                  | 85  |
| <b>Figure 4.</b> Activation of $\sigma^E$ -dependent rpoHp3-LacZ reporter under nonstress conditions by<br>LPS-biogenesis mutations .....             | 87  |
| <b>Figure 5.</b> Dual-signal model for $\sigma^E$ activation.....   | 89  |
| <b>Figure S1.</b> $\sigma^E$ response to envelope stress .....  | 106 |
| <b>Figure S2.</b> Partially acylated LPS species eluted <sup>S35</sup> RseB from RseA <sup>P</sup> -agarose.....                                      | 107 |
| <b>Figure S3.</b> LPS from $\Delta rfaG$ retains the ability to elute <sup>S35</sup> RseB from RseA <sup>P</sup> -agarose.....                        | 108 |
| <b>Figure S4.</b> Expected structure and mass spectrometry of the purified fragment produced by<br>NaOH hydrolysis of Kdo <sub>2</sub> -lipid A ..... | 109 |
| <b>Figure S5.</b> Competitive inhibition mechanism of L-IIA fragment.....   | 110 |
| <b>Figure S6.</b> Gel filtration of RseB with L-IIA fragments .....   | 111 |
| <b>Figure S7.</b> Individual replicates from Figure 4A.....   | 112 |
| <b>Figure S8.</b> $\Delta dsbA$ increases $\sigma^E$ activity.....  | 113 |
| <b>Figure S9.</b> Structures of mutant LPS species.....   | 114 |
| <b>Figure S10.</b> $\sigma^E$ activity in DegS <sup>WT</sup> vs DegS <sup><math>\Delta PDZ</math></sup> .....   | 115 |
| <b>Figure S11.</b> LPS mutants may also generate an OMP signal .....  | 116 |
| <b>Figure S12.</b> Effect of the chloramphenicol marker between <i>lptD</i> and <i>surA</i> on $\sigma^E$ activity and<br>SurA expression.....        | 117 |
| <b>Figure S13.</b> Histogram of the correlation of the chemical signature of all deletions with<br>$\Delta rseB$ .....                                | 118 |
| <b>Figure S14.</b> Mutations in LPS induce $\sigma^E$ to similar extents in DegS <sup>WT</sup> and DegS <sup><math>\Delta PDZ</math></sup> .....      | 119 |

## Chapter 3

|   |     |
|---|-----|
| <b>Figure 1.</b> MicL expression is regulated by $\sigma^E$ .....   | 131 |
| <b>Figure 2.</b> <i>lpp</i> is the sole target of MicL .....  | 135 |
| <b>Figure 3.</b> MicL regulation of <i>lpp</i> is physiologically important.....                                    | 137 |
| <b>Figure 4.</b> MicL base-pairs with <i>lpp</i> .....  | 139 |
| <b>Figure 5.</b> MicL repression of <i>lpp</i> is dependent on translation .....                                    | 142 |
| <b>Figure 6.</b> Copper sensitivity of $\Delta cutC$ is due to loss of MicL .....                                   | 144 |
| <b>Figure 7.</b> MicL and Lpp are part of an envelope protective regulatory loop.....                               | 146 |
| <b>Figure 8.</b> Model of the envelope protective $\sigma^E$ -MicL-Lpp loop .....                                   | 149 |
| <b>Figure S1.</b> Re-annotation of <i>cutC</i> region .....   | 169 |
| <b>Figure S2.</b> Conservation of $\sigma^E$ promoter within <i>cutC</i> .....                                      | 171 |
| <b>Figure S3.</b> Processing of MicL-S .....  | 173 |
| <b>Figure S4.</b> <i>lpp</i> is the sole target of MicL and MicL-S .....  | 175 |
| <b>Figure S5.</b> Control plates for Figure 3A .....  | 177 |
| <b>Figure S6.</b> Identification of region of base pairing between MicL-S and <i>lpp-lacZ</i> .....                 | 178 |
| <b>Figure S7.</b> Prediction of potential MicL sRNA targets in <i>lpp</i> mRNAs from several<br>enterobacteria..... | 179 |
| <b>Figure S8.</b> MicL repression of <i>lpp</i> confers copper resistance .....                                     | 180 |
| <b>Figure S9.</b> MicL is responsible for <i>cutC</i> copper sensitivity phenotype.....                             | 181 |
| <b>Figure S10.</b> MicL and Lpp are part of an envelope-protective regulatory loop .....                            | 182 |
| <b>Figure S11.</b> $\sigma^E$ Regulates the majority of OM proteins through its sRNAs .....                         | 184 |

## Appendix 1

|  |     |
|--|-----|
| <b>Figure 1.</b> Rescue of lethality due to loss of $\sigma^E$ activity by sRNA under various stress<br>conditions ..... | 198 |
| <b>Figure 2.</b> Plasmid map for pXG10-RybB .....  | 199 |

**Figure 3.** New vector (pMSG15) for sRNA cloning ..... 200

**Figure 4.** Overexpression of new sRNA plasmids rescues growth defect of pRseAB  
overexpression ..... 202

**Figure 5.** Deletion of major porins rescues viability when RseA and RseB are  
overexpressed ..... 203

**Figure 6.** Deletion of *lpp* has a small but significant rescue phenotype ..... 204

**Appendix 2**

**Figure 1.** Global change in sRNA levels after 20 min of MicL-S overexpression ..... 211

**Figure 2.** Effect of MicL-S overexpression on *hfq* ..... 212

**Appendix 3**

**Figure 1.** Examples comparing promoters in mRNA-seq with TSS-seq ..... 220

## Introduction

# Stress Induced Remodeling of the Bacterial Proteome

**Contributing Authors:** Carol A. Gross

*Citation:* Guo M.S., and Gross C.A. Stress-induced remodeling of the bacterial proteome.

*Current Biology* (2014) vol. 24 (10) pp. R424-34.

## **Preface**

Microorganisms live in fluctuating environments, requiring stress response pathways to resist environmental insults and stress. These pathways dynamically monitor cellular status, and mediate adaptive changes by remodeling the proteome, largely accomplished by remodeling transcriptional networks and protein degradation. The complementarity of fast, specific proteolytic degradation and slower, broad transcriptomic changes gives cells the mechanistic repertoire to dynamically adjust cellular processes and optimize response behavior. Together, this enables cells to minimize the 'cost' of the response while maximizing the ability to survive environmental stress.

The following general introduction on microbial stress responses is from a review Carol and I were invited to write for a special stress response issue of *Current Biology*. As we were the only group writing a review on microbes, we chose to write a general review on the recent advances in the field. We wished to highlight recent progress in understanding of transcriptional networks and proteolysis thus illustrating the design principles used by bacteria to generate the complex behaviors required to resist stress. Importantly, this review incorporates several major findings from Chapters 1 and 2 of my thesis, which were published at the time. This review appears in *Current Biology*, volume 24 (10).

## **Introduction**

Bacteria and other single-celled organisms have evolved to survive in variable and at times extreme conditions, and must sense and mount effective responses to environmental challenges as diverse as heat, oxidative damage, anti-microbial agents, and nutritional limitation. While bacteria have a number of programs that they can use to combat these environmental challenges, mounting a costly response in the absence of stress is detrimental, as resources that could be utilized for growth are wastefully funneled into unneeded adaptations [1]. Because bacteria are in constant competition with other species in their environment, organisms with more efficient stress responses have a competitive advantage. Thus, stress responses are carefully regulated so that they are activated only when required and to the extent necessary.

In this review we shall consider emerging stories in bacterial stress responses that highlight the design principles used by bacteria to mount stress responses that are fast, accurate, cost efficient, and successful. We focus on two complementary mechanisms that remodel the proteome to oppose stress: rewiring the transcriptome, and modulating proteolysis. While transcription can activate broad swathes of genes in concert, proteolysis allows rapid adjustments to be made to the availability of specific cellular proteins to favor required processes. Together, these mechanisms allow cells to maintain a dynamic equilibrium, continually re-optimizing processes in response to changing environmental cues.

## **Transcriptional Remodeling in Response to Stress**

The first step in a transcriptional response is to convert the signals from the environment into transcriptional change, leading to production of new proteins and adaptation. Regulators

can sense stress through two general mechanisms: first, consequence sensing, for example sensing heat by the accumulation of unfolded proteins; and second, direct or ‘feed-forward’ sensing, for example *via* a regulatory RNA whose structure is melted by heat [2] (note that this is distinct from the ‘feed-forward loop’ regulatory motif [3,4]). Notably, these stress signals often control transcription factors post-transcriptionally, for example by protein degradation or regulation of activity. This decreases the lag time of transcriptional responses, enabling both a rapid initial response and rapid adaptation. As stresses are alleviated, the activity of stress-responsive transcription factors then decreases to reach a new homeostasis.

In this section, we review emerging stories about bacterial stress-responsive transcription factors, focusing on two large families: two-component systems, and alternative sigma factors. Two-component systems are comprised of a sensor histidine kinase and a cognate response regulator [5,6]; when activated, the histidine kinase auto-phosphorylates and then transfers the phosphate group to the response regulator, which modulates gene expression [5–11]. Sigma factors ( $\sigma$ s) are subunits of RNA polymerase holoenzyme that mediate promoter recognition; alternative, non-housekeeping  $\sigma$ s are widely used in stress responsive signal transduction pathways [12–14]. Typically, every bacterial species contains multiple members of each of these families. We discuss how these transcription factors sense and relieve the deleterious effects of stress as quickly and accurately as possible, and how stress systems limit spurious cross-activation between pathways to ensure an accurate and specific response.

### *Stress sensory domains in two-component systems*

How do two-component systems sense stress signals? For histidine kinases, which auto-phosphorylate on a specific histidine residue, the current model is that ligand binding induces conformational changes that properly position the catalytic domain and facilitate phosphorylation of the target histidine, activating the response [10,15–21]. Indeed, this is the



mechanism proposed for the *Escherichia coli* histidine kinase EnvZ, which, with its response regulator OmpR regulates the membrane porins OmpC and OmpF [22–24]. EnvZ crosses the inner membrane and monitors a variety of signals — such as osmolarity, pH, and temperature — though the location of the primary signal, in particular whether it is periplasmic or cytoplasmic, is not known [22,23].

Recent work has demonstrated that high osmolarity directly alters the conformation of the cytoplasmic fragment of EnvZ (EnvZ-C) [24], an example of feed-forward sensing. High osmolarity drives EnvZ-C to adopt a more compact structure, properly positioning the catalytic and auto-phosphorylation sites, and activating OmpR [24]. While EnvZ-C may be sufficient for osmo-sensing [24,25], the other domains of EnvZ may still play a role in the response, as substitutions in the EnvZ transmembrane domains are known to affect EnvZ activity [26]. Like many histidine kinases, EnvZ contains inner membrane proximal HAMP domains, which mediate transduction of periplasmic or transmembrane stimuli into conformational changes in the cytoplasm [20,21,27,28]. Thus, the periplasmic portions of EnvZ may sense other types of signal, play a role in EnvZ dimerization, or sense osmolarity in a concerted fashion with EnvZ-C by mediating conformational change of EnvZ-C [22]. Lastly, the periplasmic portion of EnvZ interacts with MzrA, which modulates EnvZ activity, but does not preclude EnvZ signal sensing [29]. While the direct signals that modulate MzrA activity are not known, MzrA may be regulated by both CpxA/CpxR and  $\sigma^E$ , two sensors of membrane status [29,30]. While EnvZ-C may be a feed-forward sensor for osmolarity, the EnvZ periplasmic domains may have a role in sensing other EnvZ signals and properly modulating the activity of EnvZ.

Other two-component systems often contain Per–ARNT–Sim (PAS) domains, a structural motif found across all kingdoms of life that can act as a feed-forward sensor for signals as varied as light, redox potential, and metabolites, though the mechanisms that activate most PAS domains remain unknown [31–33]. As PAS domains are highly modular, they can be exchanged or conjugated to alternative proteins to reprogram signaling and response [34–38].

This allows development of various genetic tools; for example, a light activated histidine kinase, by switching the oxygen sensitive PAS domain of *Bradyrhizobium japonicum* FixL for the light sensitive PAS domain of *Bacillus subtilis* YtvA [36], or a chimeric histidine kinase that cooperatively responds to both light and oxygen, by fusing the YtvA light sensitive PAS domain to the FixL oxygen sensing domain [35].

Unfortunately, the activating signals and the mechanism of activation are unknown for most signaling pathways. We have excellent tools — such as microarrays, proteomics, CHIP analysis — to identify the downstream targets of regulatory systems, but the methods for identifying the signals that activate the relevant regulators and the mechanisms for this activation have yet to mature. This is an important area of investigation, as identification of these signals is critical for both understanding the organism and systems biology.

#### *How $\sigma^{32}$ maintains protein-folding homeostasis*

Maintaining protein-folding homeostasis is a critical task for all cells. It is especially important for cells living in environments with variable temperature, as heat alters protein folding. The highly regulated universal heat shock response controls expression of a core set of chaperones in all organisms, as well as many additional organism-specific proteins, including a set of conserved proteases in bacteria [39–42]. In *E. coli* and other proteobacteria, the heat shock response is controlled by  $\sigma^{32}$ , the master regulator of ~100 genes [42,43]. Recent progress in understanding *E. coli*  $\sigma^{32}$  illustrates the complexity of control that allows  $\sigma^{32}$  to monitor protein folding in the cytoplasm and inner membrane (Figure 1).

There are two mechanisms by which  $\sigma^{32}$  is controlled to enable a rapid response:  $\sigma^{32}$  translation is regulated by a feed-forward sensing mechanism, as heat directly melts an inhibitory mRNA structure that dampens  $\sigma^{32}$  translation [44,45]; and both the activity and stability of  $\sigma^{32}$  is controlled by two feedback loops that sense protein folding status [42]. The activity of  $\sigma^{32}$  is regulated by the cytoplasmic chaperones, such as DnaK/DnaJ, which bind

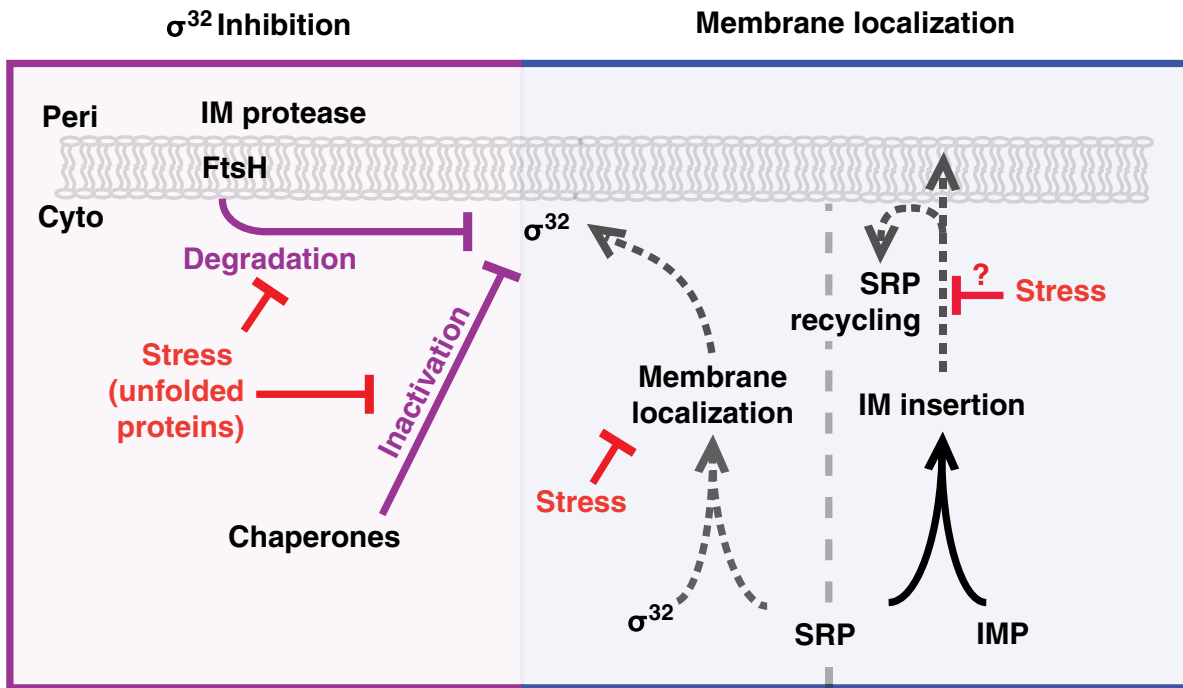


**Figure 1.** Regulation of  $\sigma^{32}$  at the inner membrane.

Left:  $\sigma^{32}$  inhibition. Membrane localized  $\sigma^{32}$  is inhibited via degradation by FtsH and inactivation by the cytoplasmic chaperones. Unfolded proteins relieve inhibition by competing for FtsH and titrating chaperones away from  $\sigma^{32}$ . Right:  $\sigma^{32}$  membrane localization.  $\sigma^{32}$  is brought to the membrane by the signal recognition particle (SRP), which also traffics inner membrane proteins to the membrane. When stress stalls or prevents proper SRP-dependent inner membrane protein insertion, this may prevent  $\sigma^{32}$  from being trafficked to the membrane for inactivation.

directly to  $\sigma^{32}$  to inhibit its activity; and the  $\sigma^{32}$  protein level is modulated by the inner membrane localized FtsH protease, which degrades  $\sigma^{32}$  (Figure 1) [46–49]. When stresses induce protein unfolding, the chaperones and proteases are titrated away from  $\sigma^{32}$ , activating the heat shock response [42]. These regulators are also themselves transcriptionally activated by  $\sigma^{32}$ , forming a negative feedback loop [42]. Thus, regulation of  $\sigma^{32}$  is responsive both to heat and to cellular protein folding status.

Despite this complexity, the known circuitry could not explain two key features of the  $\sigma^{32}$  response: first, mutations in a small region of  $\sigma^{32}$  (a ‘homeostatic control region’) disrupt inhibition of  $\sigma^{32}$  by chaperones and FtsH *in vivo*, leading to hyperactive  $\sigma^{32}$ , but do not alter  $\sigma^{32}$  regulation by these factors *in vitro* [50–53]; and second,  $\sigma^{32}$  is thought to monitor the folding status of inner membrane proteins, but the mechanism for this was until recently not known [42,54]. These observations suggest that  $\sigma^{32}$  may monitor the inner membrane through a key regulator that had not been found.

The missing regulator was recently identified as the Signal Recognition Particle (SRP), a complex of protein Ffh and 4.5S RNA [54]. SRP is part of the co-translational membrane trafficking system that mediates inner membrane protein biogenesis. SRP binds to and targets ribosomes carrying nascent proteins that contain hydrophobic amino-terminal signal sequences to the inner membrane for co-translational insertion and folding [55–57]. Surprisingly, although  $\sigma^{32}$  does not have a signal sequence, SRP also traffics  $\sigma^{32}$  to the inner membrane; membrane localization of  $\sigma^{32}$  is essential for proper regulation by chaperones and FtsH (Figure 1) [54]. In fact, mutants in the  $\sigma^{32}$  homeostatic control region are hyperactive because they reduce binding to SRP, so that they are not membrane localized by SRP and cannot be inhibited by chaperones and FtsH [54]. Thus, membrane localization is vital for proper  $\sigma^{32}$  regulation.

SRP allows  $\sigma^{32}$  to sense the protein folding status of the inner membrane. As SRP is substoichiometric relative to the ribosome (the intracellular ratio of SRP:ribosome is ~1:100), free SRP levels depend on efficient SRP recycling [58,59]. As almost all inner membrane

proteins are trafficked by SRP, defects in trafficking may alter SRP recycling or lead to accumulation of ribosomes with signal sequence proteins, preventing SRP from interacting with  $\sigma^{32}$  or localizing  $\sigma^{32}$  to the membrane [54,55]. Thus, the amount and activity of  $\sigma^{32}$  will dynamically adjust in response to flux of proteins through the inner membrane.

Why would  $\sigma^{32}$  sense inner membrane protein folding? The  $\sigma^{32}$  regulon contains SRP and FtsH, and is additionally enriched in proteins that are involved in or reside in the inner membrane [42,43]. Furthermore, FtsH not only degrades  $\sigma^{32}$  but also is the main protease that mediates quality control of membrane proteins [60,61]. Active  $\sigma^{32}$  will reduce inner membrane dysfunction by increasing levels of SRP (to ameliorate trafficking) and FtsH (to reduce unfolded protein load). As  $\sigma^{32}$  activity is further regulated by cytoplasmic chaperones,  $\sigma^{32}$  is able to integrate the folding status of both inner membrane and cytosolic proteins, a significant advantage as inner membrane proteins comprise 20–30% of total cellular protein [55,62].

#### *How $\sigma^E$ maintains homeostasis of the outer membrane*

The first line of defense for gram-negative bacteria is the outer membrane, which presents a formidable permeability barrier to protect against antibiotics and other stresses [63,64]. The outer membrane is an asymmetric lipid bilayer: its outer leaflet is composed of lipopolysaccharides (LPS) and its inner leaflet of phospholipids [63,65]. The outer membrane additionally contains proteins, including the outer membrane proteins (OMPs) that allow access to selected solutes [63,64,66,67]. Both LPS and OMPs rely on complex machines for their transport and assembly into the outer membrane [65,68–72]. As outer membrane integrity depends on proper balance of its components [63,64,71], maintaining appropriate levels of assembly machines and substrates is vital.

To monitor stress in this compartment, *E. coli* and other  $\gamma$ -proteobacteria employ  $\sigma^E$ , which regulates genes required for assembly of all major components of the outer membrane [73,74]. The major challenge for the  $\sigma^E$  system is how to convey the information about the status

of the outer membrane into the cytoplasm to mediate transcriptional change. We discuss the current model for how each  $\sigma^E$  regulator senses assembly of a different outer membrane component to generate an integrated portrait of envelope status (Figure 2).

The  $\sigma^E$  system monitors outer membrane protein folding through the rate of cleavage of the negative regulator RseA [75–77]. RseA, an inner membrane protein that sequesters  $\sigma^E$  in an inactive conformation, can be cleaved by the protease DegS, which permits secondary cleavage by RseP and subsequent degradation of RseA, freeing  $\sigma^E$  to activate transcription [78–83]. DegS is activated only when it binds to unfolded OMP carboxyl termini in the periplasm [77,84–86]; as these unfolded species are thought to accumulate when OMPs are inefficiently assembled into the outer membrane, activation of DegS is a reflection of outer membrane dysfunction (Figure 2) [87,88].

How is the status of outer membrane LPS sensed? The  $\sigma^E$  system has a second negative regulator, RseB, which binds to RseA and protects it from cleavage by DegS (Figure 2) [89–92]. Recent studies have shown that LPS can bind to and dissociate RseB from RseA [93]. *In vitro*, RseA degradation in the presence of RseB requires both OMPs and LPS: OMPs activate DegS, and LPS dissociates the RseA/RseB complex [93]. Similarly, *in vivo*, perturbations that lead to accumulation of off-pathway LPS (for example, mutations that partially inactivate the LPS assembly machinery or alter LPS structure), in combination with activated DegS, lead to dramatic activation of  $\sigma^E$  [93,94]. Thus, maximal activation of  $\sigma^E$  *in vivo* requires two signals of outer membrane stress (Figure 2).

Why do cells integrate these two signals of outer membrane assembly? OMPs and LPS are the major unique components of the bacterial outer membrane, and thus excellent indicators of outer membrane status [65]. Requiring concomitant defects in the assembly of both OMPs and LPS reduces the chances for spurious activation, ensuring that a large and costly response is not provoked by normal variation in the flux of proteins or LPS through the periplasm. For this mechanism to be an effective response, sustained defects in either OMP or LPS assembly must

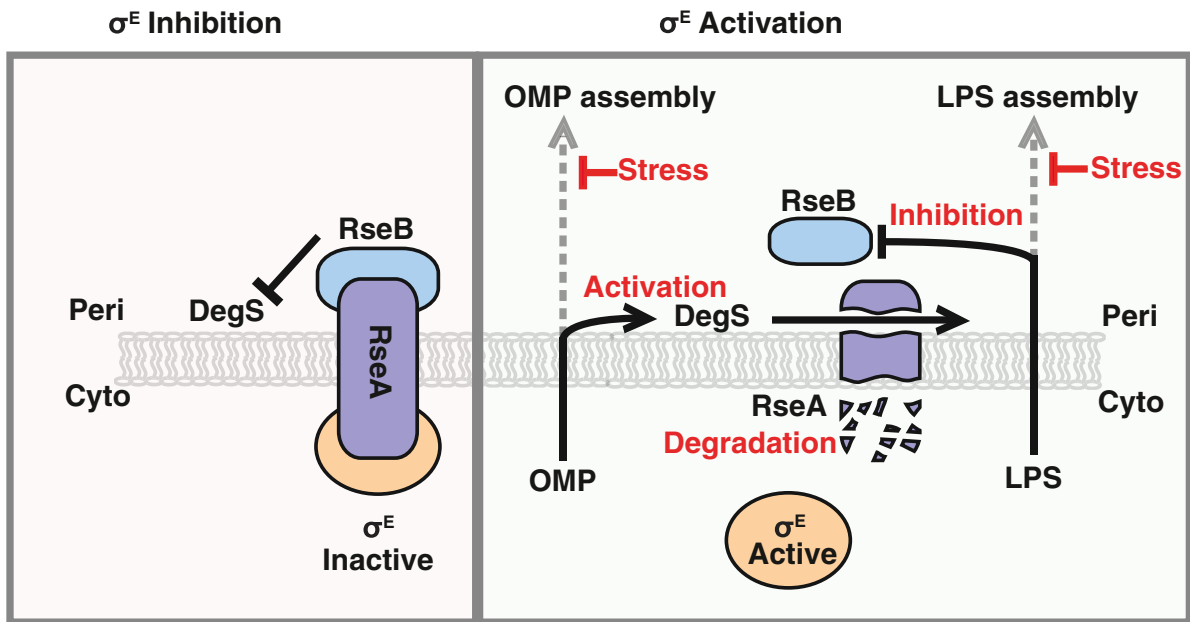


**Figure 2.** Two signals are required for  $\sigma^E$  activation.

Left:  $\sigma^E$  inhibition.  $\sigma^E$  is held inactive by RseA in the inner membrane. DegS, a protease, can cleave RseA if activated, but RseA cleavage is prevented by RseB. Right:  $\sigma^E$  activation. When concomitant defects in OMP assembly and LPS assembly occur,  $\sigma^E$  is activated. Periplasmic LPS dissociates RseB from RseA, and periplasmic OMPs activate DegS to cleave RseA. This leads to a proteolytic cascade that degrades RseA, releasing and activating  $\sigma^E$ .

provoke defects in assembly of the other, ensuring  $\sigma^E$  activation. Indeed, certain LPS species have been shown to reduce the efficiency of OMP assembly, as the altered outer membrane environment may be less conducive to proper OMP assembly [63,95,96]. Similarly, the major component of the LPS assembly machine is inserted into the outer membrane by the same mechanism as is used for other OMPs, so that defects in OMP assembly will eventually lead to defects in LPS assembly [97,98]. Thus, sensing assembly intermediates for multiple outer membrane components allows bacteria to monitor outer membrane status more accurately and comprehensively.

OMPs are among the most abundant proteins in the cell and there is tremendous OMP flux to the outer membrane [63]. For this reason, increasing the production of OMP chaperones, proteases and assembly factors may be insufficient to rapidly restore proper folding. Thus,  $\sigma^E$  also reduces OMP synthesis by inducing two small RNAs (sRNAs), MicA and RybB, which target OMP mRNA for degradation, thereby dramatically decreasing the flow of OMP precursors to the envelope [99–103]. The vital role of these sRNAs is demonstrated by the fact that overexpression of either sRNA can protect the cell from the deleterious effects of depleting  $\sigma^E$ , which normally leads to lysis and cell death [104,105]. Interestingly, the strategy employed by bacteria to address OMP folding is reminiscent of the intercompartmental eukaryotic unfolded protein response (UPR). Upon sensing stress in the endoplasmic reticulum, the UPR opposes folding stress both by upregulating folding factors and by downregulating the flow of precursors to the endoplasmic reticulum [106–108].

#### *Dynamic responses in $\sigma^B$ activation*

To optimize stress responses, cells must tailor the timing, amplitude, and dynamics of the response to each stress. Indeed, many responses contain entwined positive and negative feedback loops that can generate distinct, sophisticated behaviors such as bistability or oscillation [4,109]. Furthermore, while many systems, such as the  $\sigma^E$  system (see above), have



regulators that suppress stochastic fluctuations (noise) to prevent spurious activation, noise can also be utilized to generate sophisticated response behaviors [4,92,110–113]. Indeed, recent studies have demonstrated that noise is used in the *Bacillus subtilis*  $\sigma^B$  system to generate vastly different dynamic behaviors depending on the inducing stress (Figure 3) [114,115].

In *B. subtilis* and related gram-positive bacteria,  $\sigma^B$  is a ‘general stress factor’, which induces a core stress regulon that is expressed in concert with stress-specific responses [116,117]. In steady-state,  $\sigma^B$  is bound and inhibited by its anti- $\sigma$ , RsbW [117–119]. Under stress, the antagonist RsbV binds RsbW and frees  $\sigma^B$ , activating the response [119-121]. This partner-switching mechanism is regulated by the phosphorylation state of RsbV: unphosphorylated RsbV binds RsbW, but RsbV~P cannot [119,120]. RsbW is the kinase that phosphorylates RsbV [119], so that RsbW keeps  $\sigma^B$  activity in check both by binding  $\sigma^B$  and phosphorylating RsbV [119,120]. To activate  $\sigma^B$ , two different phosphatase systems can dephosphorylate RsbV~P: first, RsbP, activated by a limitation in nutrients, such as NTPs; and second, RsbU, activated by an environmental stress, such as ethanol. Environmental stress induces the highly conserved 1.8 MDa supermolecular ‘stressosome’ complex to release RsbT, which, in turn, activates RsbU phosphatase activity (Figure 3) [121–125].

Although energy and environmental stresses both modulate  $\sigma^B$  activity through RsbV dephosphorylation, each stress leads to different dynamics in the  $\sigma^B$  response (Figure 3) [114,115]. Nucleotide limitation, for example as a result of mycophenoic acid treatment, leads to continuous stochastic pulses of  $\sigma^B$  activity that vary in timing but not in intensity from cell-to-cell [114,115]. In contrast, ethanol induces a single pulse of  $\sigma^B$  activity that is synchronous across the population [114,115]. How does the circuitry governing  $\sigma^B$  generate these diverse responses? Opposing kinase (RsbW) and phosphatase (RsbP or RsbU) activities leads to an ultrasensitive response, so that  $\sigma^B$  is activated in a sharp, switch-like manner [114]. Cell-to-cell variability in either the initial level phosphatase or RsbW would mean that different cells would require different levels of phosphatase to oppose RsbW and cross the threshold of activation.

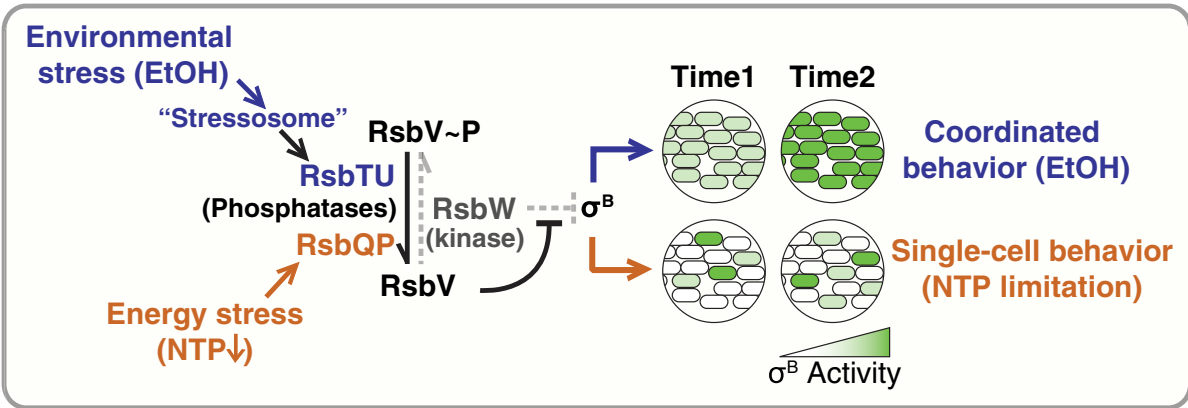


**Figure 3.** Activation of  $\sigma^B$  by different stresses leads to distinct responses.

Activation of  $\sigma^B$  by environmental stress, such ethanol (EtOH, blue) and energy stress (decreased NTP, orange) lead to two different  $\sigma^B$  behaviors: EtOH induces a coordinated response, while nucleotide limitation induces stochastic pulses (same maximum amplitude) on a single-cell level.  $\sigma^B$  is inhibited by RsbW, which is in turn inhibited by RsbV. RsbW, a kinase, phosphorylates RsbV to relieve its own inhibition. Countering this, stress-specific phosphatases such as RsbTU (activated by EtOH, blue) and RsbQP (activated by NTP limitation, orange) dephosphorylate RsbV~P, allowing RsbV to bind to and inhibit RsbW and thereby promoting release and activation of  $\sigma^B$ .

Thus, during energy stress, small fluctuations (noise) in RsbW/RsbP ratio per cell could lead to cell–cell variability in the timing of  $\sigma^B$  activation [114]. In contrast, environmental stress induces mass release of RsbT from the stressosome, enabling RsbT to activate RsbU and overwhelm inhibition by RsbW, thus activating  $\sigma^B$  in a synchronous manner in all cells [115].

What could be the advantage in responding differently to these distinct stresses? This is an important question that requires investigation. As *Bacillus* devotes up to 40% of its translational capacity to the  $\sigma^B$  regulon during stress, misregulation of  $\sigma^B$  is an enormous metabolic cost [126]. One possibility is that different patterns of  $\sigma^B$  activity are optimized to minimize the cost of response for each stress. Another possibility could be that  $\sigma^B$  pulsing is a bet-hedging mechanism, as the cell may anticipate that nutrient limitation is a precursor for other stresses that may require  $\sigma^B$  [115]. This view is supported by the fact that  $\sigma^B$  pulses occur indefinitely under conditions of nucleotide limitation, suggesting that  $\sigma^B$  activity does not lead to adaptation in this condition [114]. Testing these types of hypothesis is a difficult but important challenge, as these different dynamic response behaviors will be present in other systems, particularly those that sense multiple types of stress. These studies suggest that single-cell analysis of stress systems will continue to reveal novel behaviors not previously appreciated in bulk studies.

### *Cross-talk in signaling systems*

Most bacteria have dozens if not hundreds of paralogous two-component systems, each recognizing their own signals [127,128]. As these systems evolved and proliferated via genomic duplication events, they often share considerable sequence and structural similarity, creating significant potential for spurious cross-activation, or ‘cross-talk’ [128,129]. Indeed, histidine kinases have been observed to activate non-cognate response regulators when their cognate regulator is lost [130,131]. As cross-talk may activate non-beneficial responses, networks that are prone to cross-talk will evolve mechanisms to insulate responses [128,129].

The current model is that the co-evolution of residues in the interaction surfaces of histidine kinases and their cognate response regulators is a major way of preventing cross-talk in two-component systems [128,132–134]. As these ‘specificity’ residues determine the histidine kinase/response regulator interaction, amino-acid substitutions on either the histidine kinase or response regulator can lead to recognition of non-cognate histidine kinases or response regulators [132,134–136]. For example, a single amino-acid change to the specificity residues of the histidine kinase EnvZ is sufficient to allow phosphorylation of the non-cognate response regulator RstA [132]. Global approaches have demonstrated that a lack of cross-talk, referred to as ‘orthogonality’, is the norm for nearly all histidine kinases within a genome, ensuring proper insulation of signaling [133,137].

How is orthogonality maintained during genome evolution? This was examined for the broadly conserved PhoB/PhoR two-component system, present in a, b, and g-proteobacteria. Interestingly, while the specificity residues of PhoR are highly similar in b- and g-proteobacteria, there is lower conservation between g- and a-proteobacteria [133]. Analysis revealed this to be an evolutionary adaptation in a-proteobacteria to insulate PhoB/R from an a-specific paralog, NtrY/NtrX, preventing cross-talk between these two systems. Indeed, *E. coli* PhoR (g) can phosphorylate both *Caulobacter* PhoB and NtrX (a), whereas *Caulobacter* PhoR is specific for PhoB [133]. Furthermore, a mutant PhoR that cross-activates NtrX is detrimental to growth under PhoR-inducing conditions; this growth defect is almost fully suppressed by deletion of *ntrX* [133]. Thus, cross-talk can produce selective pressure that drives newly acquired signaling pathways to diverge and insulate themselves against paralogous systems.

These principles are also observed for the extra-cytoplasmic  $\sigma$  factors, a highly diverse group of alternative  $\sigma$  factors, which comprise 43 phylogenetically distinct subgroups [14,138]. Recent work with 40  $\sigma$  factors from 20 different subgroups indicates that, in general,  $\sigma$  factors are inhibited only by their cognate anti- $\sigma$ , and recognize only promoters within their subgroup [139]. However, questions remain as to whether  $\sigma$  factors within a subgroup are as well

insulated. For example, the soil bacterium *Streptomyces coelicolor* contains an astonishing 63  $\sigma$  factors, with four  $\sigma$  factors derived from subgroup 39 [138]. Do these  $\sigma$  factors initiate cooperative response, or are they well-insulated from each other? Furthermore, the evolutionary trajectories that mediate  $\sigma$  orthogonality are not well understood. Such analyses are key to understanding the design of signaling systems and the selective pressures that drive their evolution.

### **Regulatory Proteolysis in Stress Responses**

As a counterpoint to transcriptional remodeling, regulatory proteolysis is an alternative way of altering the protein content of the cell in response to stress. In all organisms, failure to degrade proteins that are unfolded or damaged by stress leads to protein aggregation and deleterious consequences such as cell death in bacteria and disease and aging in eukaryotes [39,40,140]. Proteolytic control is particularly important in bacteria, as most proteins are otherwise stable and diluted only by cell division [141]. Recently, it has emerged that, as well as being direct sensors and effectors for stress, proteolytic machines play a role in regulating the transcriptional response. We have already described how proteolysis controls the amount of  $\sigma^{32}$  and the activity of  $\sigma^E$  (see above); in this section, we focus on recent stories about how the major cytoplasmic proteases ClpXP and Lon directly sense stress and modulate their proteolytic activity in response.

The AAA+ proteases ClpXP and Lon, are members of a large, well-conserved family of proteins that assemble into heptameric or hexameric rings [142–144]. Proteolysis occurs in a central pore that acts as a degradation chamber [142,143]. Cycles of ATP hydrolysis drive conformational changes that promote target protein unfolding and translocation into this chamber [142]. It is estimated that, together, Clp and Lon are responsible for ~75% of ATP-dependent proteolysis in bacteria [141,145]. Importantly, as degradation is irreversible, these

proteases utilize adaptor proteins to specifically recognize intended targets and thus avoid spurious degradation [142,143,146].

#### *The intimate role of proteolysis in controlling the general stress response*

In *E. coli* and related gram-negative bacteria, the 'general stress response' is mediated by  $\sigma^S$ , which is induced by many different conditions, including DNA damage, low  $Mg^{2+}$  or  $PO_4$ , and low nutrients/stationary phase [147]. While  $\sigma^S$  is controlled in multiple ways,  $\sigma^S$  protein level is regulated specifically by proteolysis [147,148]. In unstressed cells, the adaptor protein RssB targets  $\sigma^S$  to ClpXP for degradation [149–151]. In appropriately stressed cells,  $\sigma^S$  is stabilized, activating its regulon. Recent studies demonstrate that  $\sigma^S$  is stabilized by two discrete mechanisms (Figure 4).

In the first mechanism, a suite of stress responsive 'anti-adaptor' proteins (IraD, IraM, IraP) bind to RssB and prevent it from targeting  $\sigma^S$  to ClpXP for degradation [147,152, 153]. Each Ira protein is induced by a different stress condition — in *E. coli*, IraD is induced by nutrient limitation/stationary phase or DNA-damage, IraM by low  $Mg^{2+}$  or  $Ca^{2+}$ , and IraP by low  $PO_4$  [147,152–155] — thereby communicating each discrete stress to ClpXP by interfering with RssB function (Figure 4). Although Ira proteins all bind to RssB, they are not members of the same protein family, do not exhibit sequence similarity, and interact with different residues of RssB [147,156], indicating that they have arisen independently to tune  $\sigma^S$  proteolysis. How Ira proteins are themselves inhibited to turn off the  $\sigma^S$  response remains unclear. An additional question is how  $\sigma^S$  responds to stresses that activate multiple Ira proteins. Most laboratory experiments focus on examining effects of a single stress, but in the environment, multiple stresses may occur simultaneously. These stresses may have combinatorial effects, encouraging bacteria to evolve systems that process information from multiple stresses in an integrated way.

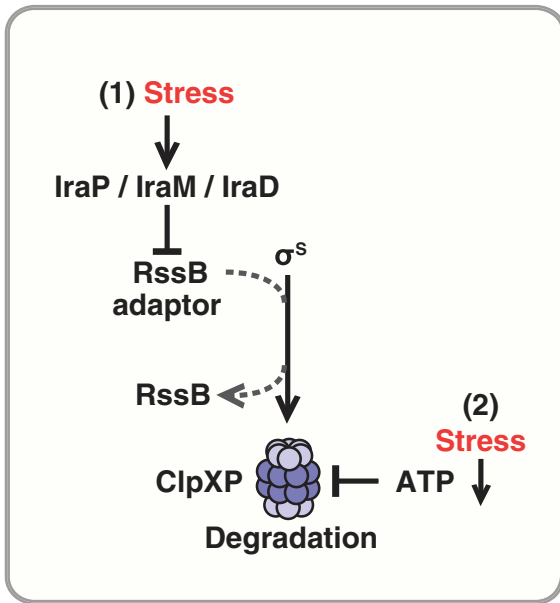


**Figure 4.** ClpXP degradation of  $\sigma^S$  is regulated via two mechanisms. The adaptor RssB targets  $\sigma^S$  to ClpXP for degradation. Stress prevents  $\sigma^S$  degradation via two mechanisms. First, specific stresses induce expression of corresponding anti-adaptor proteins (low  $\text{PO}_4$ , IraP; low  $\text{Mg}^{2+}$ , IraM; stationary phase/DNA damage, IraD), which prevent RssB from interacting with  $\sigma^S$ . Second, ClpXP degradation of  $\sigma^S$  is particularly sensitive to ATP levels; low ATP (nutrient limitation) thus specifically prevents ClpXP degradation of  $\sigma^S$ .

In the second mechanism, ClpXP tunes its own proteolytic capacity to alter  $\sigma^S$  degradation in response to ATP limitation [157]. ClpXP is ATP-dependent, creating the potential for ATP availability to affect rates of substrate degradation [158]. ClpXP degradation of  $\sigma^S$  is in fact exceptionally sensitive to the intracellular ATP concentration: at low levels of ATP, many canonical ClpXP substrates are degraded normally, but degradation of  $\sigma^S$  is blocked (Figure 4) [157]. Though the mechanism for this ATP dependence is not known, it is thought that reducing ATP levels slows ClpXP translocation and may cause accumulation of partially folded substrates that interfere with further unfolding or degradation [157–159]. Interestingly, as low ATP is an indicator of nutrient stress, nutrient limitation regulates ClpXP degradation of  $\sigma^S$  both directly by ATP and indirectly by the nutrient responsive anti-adaptor IraD [155]. What differentiates these two mechanisms? Direct ATP control of  $\sigma^S$  proteolysis may be a feed-forward response that couples  $\sigma^S$  activity directly and dynamically to cellular metabolism. In contrast, while accumulation of IraD during transition to stationary phase may be slower, once made, IraD can constitutively block  $\sigma^S$  degradation, as it is not degraded with  $\sigma^S$  [153]. These complementary mechanisms may allow  $\sigma^S$  to be highly responsive to nutrient state, leading to both rapid and sustained activation of  $\sigma^S$ .

#### *Proteolysis can generate alternative forms of proteins required during stress*

The proteome can also be altered by programmed ribosomal frame-shifting that generates alternative forms of proteins, such as the two forms of DnaX in *E. coli* (a shorter  $\gamma$  form and full-length  $\tau$  form). DnaX is a subunit of the complex that loads the DNA replication sliding clamp, which is required for processive replication in all organisms [160]. Both forms of DnaX protein are present in the cell, with the full-length  $\tau$  form generated by a frame-shifting event [161–163]. However, the significance of these two forms of DnaX and whether and how bacteria other than *E. coli* and *Salmonella* produced these forms was until recently unclear.



Recent work has shown that *Caulobacter* produces the shorter  $\gamma$  form of DnaX from the full-length  $\tau$  form by ClpXP proteolysis, rather than by ribosomal frameshifting [164].

*Caulobacter* DnaX contains a glycine-rich 'slippery' tract adjacent to a stably folded domain that promotes release of partially degraded DnaX  $\gamma$  from ClpXP [164]. *In vitro*, ClpXP had been observed to release degradation intermediates of specific artificial substrates, but native substrates with this property had not been previously identified [165–168].

Both long and short form of DnaX are required for growth in *Caulobacter* [164]. Importantly, processing of  $\tau$  DnaX to the  $\gamma$  form is required for proper recovery from DNA damage, as cells that constitutively express  $\gamma$  DnaX and a form of  $\tau$  that cannot be processed are sensitive to DNA damaging agents [164]. Processing to  $\gamma$  DnaX may be required for efficient exchange to alternative, mutagenic DNA polymerases, which are employed during DNA damage [164]. Indeed, loss of  $\tau$  DnaX processing leads to a reduced level of UV-induced mutagenesis, suggesting that proper usage of the alternative DNA polymerases has been inhibited [164]. This suggests that there is a stress-related rationale for generating two variants of the clamp loader.

Interestingly, there are several known eukaryotic examples of partial proteolysis by the ubiquitin-proteasome system [169–171]. Ci, a regulator of Hedgehog signaling, and NF $\kappa$ B, a mammalian transcription factor involved in inflammatory response, are both released when the proteasome encounters a low complexity sequence, such as a glycine tract, adjacent to a stably folded domain [169-171]. As this is the same mechanism that causes release of DnaX, this conservation suggests that there are likely more examples of partial proteolysis in other organisms.

### *Proteome remodeling by Lon*

Lon, the first protease to be discovered, is thought to be the most widely conserved of all energy-dependent proteases [172]. Its housekeeping function is degradation of unfolded and

abnormally folded proteins [144,172]. This model is supported by the recent realization that the recognition tags for Lon comprise aromatic and hydrophobic residues that are buried in folded proteins [142,173,174]. Like ClpXP, Lon also participates in regulating stress responses. Indeed, the first phenotype determined for a deletion of *lon* was extreme UV-sensitivity [144, 172]. New studies highlight three further activities for Lon and additionally suggest that Lon may target additional proteins when stimulated by stress (Figure 5).

Recently, it was realized that Lon can act as a chaperone as well as a protease. Lon variants that neither hydrolyse ATP nor degrade substrates can suppress severe unfolded protein stress, by binding to target proteins [175]. This chaperone activity is proposed to arise from ATP-independent conformational changes that are coupled to protein remodeling [175,176]. Thus, chaperone activity may be a dominant function when ATP is limiting. Lon can also use its ATPase activity to inactivate the cell-division inhibitor SulA [177–179]. As Lon mutants that are defective in chaperone activity can still inhibit SulA, this suggests that chaperone activity and SulA inhibition are distinct mechanisms for Lon [175].

Additionally, Lon can remodel its substrate specificity by altering its quaternary structure. Normally hexameric, Lon can also exist in a dodecameric state that closes off the entryway to its degradation chamber [180]. This may gate this chamber so that large substrates (>12–25 kDa) can no longer enter and be proteolyzed [180]. Importantly, the cellular concentration of Lon is high enough to support dodecamer formation, and constitutively dodecameric Lon mutants can complement many *lon* deletion phenotypes *in vivo* [180,181]. As dodecamers cannot recognize large protein aggregates, dodecamer formation can realign the powerful degradation capacity of Lon to focus on important small regulatory proteins during times of high protein unfolding and aggregation [180].

Although it is an open question whether specific conditions or stresses promote chaperone activity or dodecamer formation, it is already known that heat can alter the substrate specificity of Lon. Under conditions of severe heat shock (as after a shift to 45°C), replication is

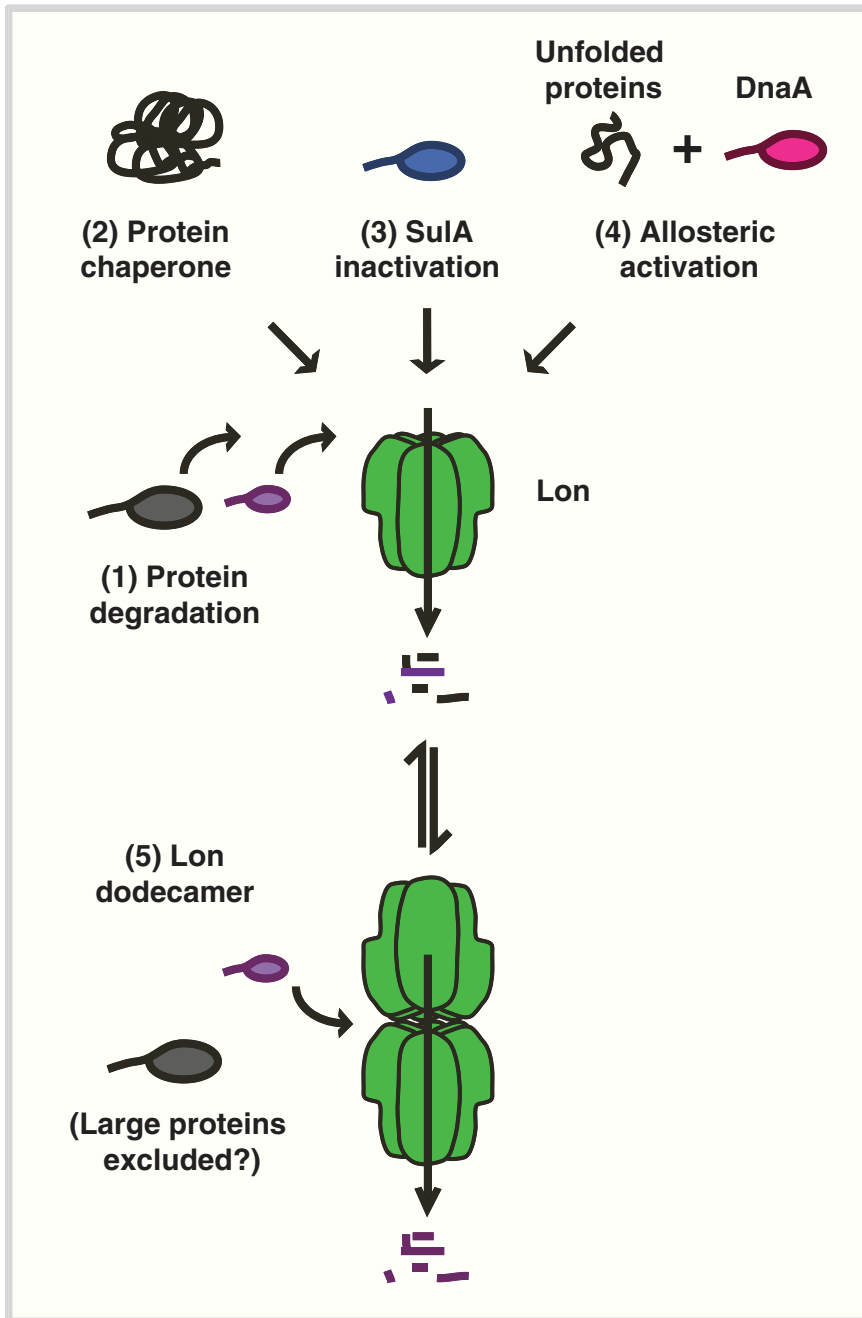


**Figure 5.** Many cellular functions of Lon.

(1) Lon is responsible for degradation of many cellular proteins. (2) Lon can act as a chaperone to prevent protein aggregation. (3) Lon inactivates the cell division inhibitor SulA. (4) Lon is allosterically activated by unfolded proteins to degrade the initiation protein DnaA. (5) Lon exists as a hexamer and a dodecamer. Large proteins are thought to be excluded from entering the pore of the dodecamer and being degraded by Lon. It is not known if the dodecamer may also have chaperone activity, mediate SulA inhibition, or degrade DnaA.

arrested in *C. crescentus* as a result of degradation of the DNA replication initiation protein DnaA [182,183]. DnaA is stable in rich media, but rapidly depleted during severe temperature upshift and in several other stress conditions, leading to growth arrest [183–186]. This effect was recently traced to Lon-mediated degradation of DnaA [187].

Intriguingly, while DnaA is not a normal substrate for Lon *in vitro*, addition of a model unfolded protein substrate stimulated specific, robust degradation of DnaA [187]. Folded substrates of Lon could not stimulate degradation of DnaA, nor did unfolded protein significantly increase the degradation rate of other known Lon substrates [187]. In normal *in vivo* conditions, unfolded proteins are continually removed by cytoplasmic chaperones, such as Hsp70, and thus unavailable to activate Lon degradation of DnaA. However, after the sudden stress of a shift to 45°C, unfolded proteins exceed the capacity of the protein refolding machinery, activating DnaA degradation and arresting replication [187]. As Lon and the chaperone machinery are widely distributed among bacteria, regulated DnaA degradation by Lon may be a broad mechanism for inducing growth arrest during stress. Intriguingly, there is an additional example of Lon targeting proliferation proteins for degradation: In *E. coli* that have lost the Hsp70 chaperone machine ( $\Delta dnaKJ$  mutants), Hsp33 (HslO) can interact with the ribosomal elongation factor Tu (Ef-Tu) and target it for degradation by Lon, thereby inhibiting translation of proteins and leading to growth arrest [188].

Why would cells want to target proliferation factors for degradation? During times of severe stress, if cells cannot maintain genome integrity or ensure survival during growth, it may become better for them to assume a non-proliferative (persister) state [189–193]. In fact, persister cells are highly resistant to stresses and antibiotics [189–192]. By stopping replication and reducing protein synthesis, the cell can focus on stress response while waiting for a more opportune condition to resume growth. Such behavior would be a form of bet-hedging, trading current fitness for future benefits [194,195]. These may be examples of general mechanism, whereby stress exposes vital proliferation factors as proteolytic targets to induce growth arrest.

## Perspectives

Stress responses are not disconnected pathways, but are closely integrated into bacterial physiology. As there is no limit in the variety of ways that stress can alter cellular pathways, responses have evolved to be equally complex, monitoring and maintaining every cellular process. As stress responses are so intimately connected to cellular state, studying them has provided an elegant window into the mechanisms that regulate the homeostasis of the cell. We have started to develop an understanding of the mechanisms that sense stress, the molecular tools that comprise responses, the logic of how responses are constructed and linked, and the dynamic outcomes that can result.

However, many questions remain. For many responses, we still do not know the inducing signal, all the players, how the players fit together, or the behaviors that can result. As there are only a finite number of sensors and regulators to face an infinite variety of stresses, not all responses may be perfectly adaptive [196]. Additionally, we do not know how bacteria integrate the combinatorial stresses they are likely to have faced in the environment. This is especially important for pathogens, as they experience a characteristic set of stresses in a defined temporal order, and responses may be optimized to reflect this [197,198]. Lastly, we are only beginning to grasp at the variability that may occur on the single-cell level. How pervasive are these behaviors in stress? Why have particular response behaviors been selected over others? Answering these and other questions will be crucial for understanding bacterial physiology and engineering.

## References

1. Scott, M., Gunderson, C.W., Mateescu, E.M., Zhang, Z., and Hwa, T. (2010). Interdependence of cell growth and gene expression: origins and consequences. *Science* **330**, 1099-1102.
2. Kortmann, J., and Narberhaus, F. (2012). Bacterial RNA thermometers: molecular zippers and switches. *Nat. Rev. Microbiol.* **10**, 255-265.
3. Mangan, S., and Alon, U. (2003). Structure and function of the feed-forward loop network motif. *Proc. Natl. Acad. Sci. USA* **100**, 11980-11985.
4. Silva-Rocha, R., and De Lorenzo, V. (2010). Noise and robustness in prokaryotic regulatory networks. *Annu. Rev. Microbiol.* **64**, 257-275.
5. Stock, A.M., Robinson, V.L., and Goudreau, P.N. (2000). Two-component signal transduction. *Annu. Rev. Biochem.* **69**, 183-215.
6. Inouye, M., and Dutta, R. (2002). *Histidine kinases in signal transduction*, (San Diego, California: Elsevier Science).
7. Utsumi, R. (2008). *Bacterial Signal Transduction: Networks and Drug Targets*, Volume 631, (Austin, TX: Landes Bioscience).
8. Galperin, M.Y. (2010). Diversity of structure and function of response regulator output domains. *Curr. Opin. Microbiol.* **13**, 150-159.
9. Stewart, R.C. (2010). Protein histidine kinases: assembly of active sites and their regulation in signaling pathways. *Curr. Opin. Microbiol.* **13**, 133-141.
10. Jung, K., Fried, L., Behr, S., and Heermann, R. (2012). Histidine kinases and response regulators in networks. *Curr. Opin. Microbiol.* **15**, 118-124.
11. Göpel, Y., and Görke, B. (2012). Rewiring two-component signal transduction with small RNAs. *Curr. Opin. Microbiol.* **15**, 132-139.

12. Gruber, T.M., and Gross, C.A. (2003). Multiple sigma subunits and the partitioning of bacterial transcription space. *Annu. Rev. Microbiol.* *57*, 441-466.
13. Österberg, S., del Peso-Santos, T., and Shingler, V. (2011). Regulation of alternative sigma factor use. *Annu. Rev. Microbiol.* *65*, 37-55.
14. Mascher, T. (2013). Signaling diversity and evolution of extracytoplasmic function (ECF)  $\sigma$  factors. *Curr. Opin. Microbiol.* *16*, 148-155.
15. Cho, U.S., Bader, M.W., Amaya, M.F., Daley, M.E., Klevit, R.E., Miller, S.I., and Xu, W. (2006). Metal bridges between the PhoQ sensor domain and the membrane regulate transmembrane signaling. *J. Mol. Biol.* *356*, 1193-1206.
16. Parkinson, J.S. (2010). Signaling mechanisms of HAMP domains in chemoreceptors and sensor kinases. *Annu. Rev. Microbiol.* *64*, 101-122.
17. Cheung, J., and Hendrickson, W.A. (2010). Sensor domains of two-component regulatory systems. *Curr. Opin. Microbiol.* *13*, 116-123.
18. Krell, T., Lacal, J., Busch, A., Silva-Jiménez, H., Guazzaroni, M.-E., and Ramos, J.L. (2010). Bacterial sensor kinases: diversity in the recognition of environmental signals. *Annu. Rev. Microbiol.* *64*, 539-559.
19. Ferris, H.U., Dunin-Horkawicz, S., Mondéjar, L.G., Hulko, M., Hantke, K., Martin, J., Schultz, J.E., Zeth, K., Lupas, A.N., and Coles, M. (2011). The mechanisms of HAMP-mediated signaling in transmembrane receptors. *Structure* *19*, 378-385.
20. Ferris, H.U., Dunin-Horkawicz, S., Hornig, N., Hulko, M., Martin, J., Schultz, J.E., Zeth, K., Lupas, A.N., and Coles, M. (2012). Mechanism of regulation of receptor histidine kinases. *Structure* *20*, 56-66.
21. Wang, C., Sang, J., Wang, J., Su, M., Downey, J.S., Wu, Q., Wang, S., Cai, Y., Xu, X., Wu, J., et al. (2013). Mechanistic insights revealed by the crystal structure of a histidine kinase with signal transducer and sensor domains. *PLoS Biol.* *11*, e1001493.

22. Egger, L.A., Park, H., and Inouye, M. (1997). Signal transduction via the histidyl-aspartyl phosphorelay. *Genes Cells* 2, 167-184.
23. Pratt, L.A., Hsing, W., Gibson, K.E., and Silhavy, T.J. (1996). From acids to osmZ: multiple factors influence synthesis of the OmpF and OmpC porins in *Escherichia coli*. *Mol. Microbiol.* 20, 911-917.
24. Wang, L.C., Morgan, L.K., Godakumbura, P., Kenney, L.J., and Anand, G.S. (2012). The inner membrane histidine kinase EnvZ senses osmolality via helix-coil transitions in the cytoplasm. *EMBO J.* 31, 2648-2659.
25. Park, H., Saha, S.K., and Inouye, M. (1998). Two-domain reconstitution of a functional protein histidine kinase. *Proc. Natl. Acad. Sci. USA* 95, 6728-6732.
26. Tokishita, S., Kojima, A., and Mizuno, T. (1992). Transmembrane signal transduction and osmoregulation in *Escherichia coli*: functional importance of the transmembrane regions of membrane-located protein kinase, EnvZ. *J. Biochem.* 111, 707-713.
27. Hulko, M., Berndt, F., Gruber, M., Linder, J.U., Truffault, V., Schultz, A., Martin, J., Schultz, J.E., Lupas, A.N., and Coles, M. (2006). The HAMP domain structure implies helix rotation in transmembrane signaling. *Cell* 126, 929-940.
28. Airola, M.V., Huh, D., Sukomon, N., Widom, J., Sircar, R., Borbat, P.P., Freed, J.H., Watts, K.J., and Crane, B.R. (2013). Architecture of the soluble receptor Aer2 indicates an in-line mechanism for PAS and HAMP domain signaling. *J. Mol. Biol.* 425, 886-901.
29. Gerken, H., Charlson, E.S., Cicirelli, E.M., Kenney, L.J., and Misra, R. (2009). MzrA: a novel modulator of the EnvZ/OmpR two-component regulon. *Mol. Microbiol.* 72, 1408-1422.
30. Gerken, H., and Misra, R. (2010). MzrA-EnvZ interactions in the periplasm influence the EnvZ/OmpR two-component regulon. *J. Bacteriol.* 192, 6271-6278.
31. Taylor, B.L., and Zhulin, I.B. (1999). PAS domains: internal sensors of oxygen, redox potential, and light. *Microbiol. Mol. Biol. Rev.* 63, 479-506.



32. Möglich, A., Ayers, R.A., and Moffat, K. (2009). Structure and signaling mechanism of Per-ARNT-Sim domains. *Structure* 17, 1282-1294.
33. Henry, J.T., and Crosson, S. (2011). Ligand-binding PAS domains in a genomic, cellular, and structural context. *Annu. Rev. Microbiol.* 65, 261-286.
34. Zelzer, E., Wappner, P., and Shilo, B.Z. (1997). The PAS domain confers target gene specificity of *Drosophila* bHLH/PAS proteins. *Genes Dev.* 11, 2079-2089.
35. Möglich, A., Ayers, R.A., and Moffat, K. (2010). Addition at the molecular level: signal integration in designed Per-ARNT-Sim receptor proteins. *J. Mol. Biol.* 400, 477-486.
36. Möglich, A., Ayers, R.A., and Moffat, K. (2009). Design and signaling mechanism of light-regulated histidine kinases. *J. Mol. Biol.* 385, 1433-1444.
37. Wu, Y.I., Frey, D., Lungu, O.I., Jaehrig, A., Schlichting, I., Kuhlman, B., and Hahn, K.M. (2009). A genetically encoded photoactivatable Rac controls the motility of living cells. *Nature* 461, 104-108.
38. Lungu, O.I., Hallett, R.A., Choi, E.J., Aiken, M.J., Hahn, K.M., and Kuhlman, B. (2012). Designing photoswitchable peptides using the AsLOV2 domain. *Chem. Biol.* 19, 507-517.
39. Morimoto, R.I. (2011). The heat shock response: systems biology of proteotoxic stress in aging and disease. *Cold Spring Harbor Symp. Quant. Biol.* 76, 91-99.
40. Mogk, A., Huber, D., and Bukau, B. (2011). Integrating protein homeostasis strategies in prokaryotes. *Cold Spring Harbor Perspectives in Biology* 3.
41. Anckar, J., and Sistonen, L. (2011). Regulation of HSF1 function in the heat stress response: implications in aging and disease. *Annu. Rev. Biochem.* 80, 1089-1115.
42. Guisbert, E., Yura, T., Rhodius, V.A., and Gross, C.A. (2008). Convergence of molecular, modeling, and systems approaches for an understanding of the *Escherichia coli* heat shock response. *Microbiol. Mol. Biol. Rev.* 72, 545-554.

43. Nonaka, G., Blankschien, M., Herman, C., Gross, C.A., and Rhodius, V.A. (2006). Regulon and promoter analysis of the *E. coli* heat-shock factor, sigma32, reveals a multifaceted cellular response to heat stress. *Genes Dev.* *20*, 1776-1789.
44. Morita, M., Kanemori, M., Yanagi, H., and Yura, T. (1999). Heat-induced synthesis of sigma32 in *Escherichia coli*: structural and functional dissection of rpoH mRNA secondary structure. *J. Bacteriol.* *181*, 401-410.
45. Morita, M.T., Tanaka, Y., Kodama, T.S., Kyogoku, Y., Yanagi, H., and Yura, T. (1999). Translational induction of heat shock transcription factor sigma32: evidence for a built-in RNA thermosensor. *Genes Dev.* *13*, 655-665.
46. Guisbert, E., Herman, C., Lu, C.Z., and Gross, C.A. (2004). A chaperone network controls the heat shock response in *E. coli*. *Genes Dev.* *18*, 2812-2821.
47. Gamer, J., Multhaup, G., Tomoyasu, T., McCarty, J.S., Rüdiger, S., Schönfeld, H.J., Schirra, C., Bujard, H., and Bukau, B. (1996). A cycle of binding and release of the DnaK, DnaJ and GrpE chaperones regulates activity of the *Escherichia coli* heat shock transcription factor sigma32. *EMBO J.* *15*, 607-617.
48. Herman, C., Thévenet, D., D'Ari, R., and Boulloc, P. (1995). Degradation of sigma 32, the heat shock regulator in *Escherichia coli*, is governed by HflB. *Proc. Natl. Acad. Sci. USA* *92*, 3516-3520.
49. Tomoyasu, T., Gamer, J., Bukau, B., Kanemori, M., Mori, H., Rutman, A.J., Oppenheim, A.B., Yura, T., Yamanaka, K., and Niki, H. (1995). *Escherichia coli* FtsH is a membrane-bound, ATP-dependent protease which degrades the heat-shock transcription factor sigma 32. *EMBO J.* *14*, 2551-2560.
50. Horikoshi, M., Yura, T., Tsuchimoto, S., Fukumori, Y., and Kanemori, M. (2004). Conserved region 2.1 of *Escherichia coli* heat shock transcription factor sigma32 is required for modulating both metabolic stability and transcriptional activity. *J. Bacteriol.* *186*, 7474-7480.

51. Obrist, M., and Narberhaus, F. (2005). Identification of a turnover element in region 2.1 of *Escherichia coli* sigma32 by a bacterial one-hybrid approach. *J. Bacteriol.* *187*, 3807-3813.
52. Yura, T., Guisbert, E., Poritz, M., Lu, C.Z., Campbell, E., and Gross, C.A. (2007). Analysis of sigma32 mutants defective in chaperone-mediated feedback control reveals unexpected complexity of the heat shock response. *Proc. Natl. Acad. Sci. USA* *104*, 17638-17643.
53. Suzuki, H., Ikeda, A., Tsuchimoto, S., Adachi, K.-i., Noguchi, A., Fukumori, Y., and Kanemori, M. (2012). Synergistic binding of DnaJ and DnaK chaperones to heat shock transcription factor  $\sigma$ 32 ensures its characteristic high metabolic instability: implications for heat shock protein 70 (Hsp70)-Hsp40 mode of function. *J. Biol. Chem.* *287*, 19275-19283.
54. Lim, B., Miyazaki, R., Neher, S., Siegele, D.A., Ito, K., Walter, P., Akiyama, Y., Yura, T., and Gross, C.A. (2013). Heat Shock Transcription Factor  $\sigma$ 32 ensures its characteristic high metabolic instability: implications for heat shock protein 70 (Hsp70)-Hsp40 mode of function. *J. Biol. Chem.* *287*, 19275-19283.
55. Driessen, A.J.M., and Nouwen, N. (2008). Protein translocation across the bacterial cytoplasmic membrane. *Annu. Rev. Biochem.* *77*, 643-667.
56. Bibi, E. (2011). Early targeting events during membrane protein biogenesis in *Escherichia coli*. *Biochim. Biophys. Acta* *1808*, 841-850.
57. Saraogi, I., and Shan, S.-o. (2013). Co-translational protein targeting to the bacterial membrane. *Biochim. Biophys. Acta*.
58. Jensen, C.G., and Pedersen, S. (1994). Concentrations of 4.5S RNA and Ffh protein in *Escherichia coli*: the stability of Ffh protein is dependent on the concentration of 4.5S RNA. *J. Bacteriol.* *176*, 7148-7154.
59. Holtkamp, W., Lee, S., Bornemann, T., Senyushkina, T., Rodnina, M.V., and Wintermeyer, W. (2012). Dynamic switch of the signal recognition particle from scanning to targeting. *Nat. Struct. Mol. Biol.* *19*, 1332-1337.
60. Okuno, T., and Ogura, T. (2013). FtsH Protease-Mediated Regulation of Various Cellular Functions. *Subcell. Biochem.* *66*, 53-69.

61. Ito, K., and Akiyama, Y. (2005). Cellular functions, mechanism of action, and regulation of FtsH protease. *Annu. Rev. Microbiol.* *59*, 211-231.
62. Krogh, A., Larsson, B., von Heijne, G., and Sonnhammer, E.L. (2001). Predicting transmembrane protein topology with a hidden Markov model: application to complete genomes. *J. Mol. Biol.* *305*, 567-580.
63. Nikaido, H. (2003). Molecular basis of bacterial outer membrane permeability revisited. *Microbiol. Mol. Biol. Rev.* *67*, 593-656.
64. Delcour, A.H. (2009). Outer membrane permeability and antibiotic resistance. *Biochim. Biophys. Acta* *1794*, 808-816.
65. Silhavy, T.J., Kahne, D., and Walker, S. (2010). The bacterial cell envelope. *Cold Spring Harbor Perspectives in Biology* *2*, a000414.
66. Tokuda, H. (2009). Biogenesis of outer membranes in Gram-negative bacteria. *Bioscience, Biotechnology, and Biochemistry* *73*, 465-473.
67. Okuda, S., and Tokuda, H. (2011). Lipoprotein sorting in bacteria. *Annu. Rev. Microbiol.* *65*, 239-259.
68. Sperandio, P., Dehò, G., and Polissi, A. (2009). The lipopolysaccharide transport system of Gram-negative bacteria. *Biochim. Biophys. Acta* *1791*, 594-602.
69. Ricci, D.P., and Silhavy, T.J. (2012). The Bam machine: a molecular cooper. *Biochim. Biophys. Acta* *1818*, 1067-1084.
70. Raetz, C.R.H., Guan, Z., Ingram, B.O., Six, D.A., Song, F., Wang, X., and Zhao, J. (2009). Discovery of new biosynthetic pathways: the lipid A story. *The Journal of Lipid Research* *50 Suppl*, S103-108.
71. Zhang, G., Meredith, T.C., and Kahne, D. (2013). On the essentiality of lipopolysaccharide to Gram-negative bacteria. *Curr. Opin. Microbiol.* *16*, 779-785.
72. Hagan, C.L., Silhavy, T.J., and Kahne, D. (2011). ). he essentiality of lipopolysaccharide to Gram-negative bacteri *Biochem.* *80*, 189-210.

73. Rhodius, V.A., Suh, W.C., Nonaka, G., West, J., and Gross, C.A. (2006). Conserved and variable functions of the sigmaE stress response in related genomes. *PLoS Biol.* 4, e2.
74. Barchinger, S.E., and Ades, S.E. (2013). Regulated Proteolysis: Control of the Escherichia coli  $\sigma(E)$ -Dependent Cell Envelope Stress Response. *Subcell. Biochem.* 66, 129-160.
75. Missiakas, D., Mayer, M.P., Lemaire, M., Georgopoulos, C., and Raina, S. (1997). Modulation of the Escherichia coli sigmaE (RpoE) heat-shock transcription-factor activity by the RseA, RseB and RseC proteins. *Mol. Microbiol.* 24, 355-371.
76. De Las Peñas, A., Connolly, L., and Gross, C.A. (1997). The sigmaE-mediated response to extracytoplasmic stress in Escherichia coli is transduced by RseA and RseB, two negative regulators of sigmaE. *Mol. Microbiol.* 24, 373-385.
77. Walsh, N.P., Alba, B.M., Bose, B., Gross, C.A., and Sauer, R.T. (2003). OMP peptide signals initiate the envelope-stress response by activating DegS protease via relief of inhibition mediated by its PDZ domain. *Cell* 113, 61-71.
78. Ades, S.E., Connolly, L.E., Alba, B.M., and Gross, C.A. (1999). The Escherichia coli sigma(E)-dependent extracytoplasmic stress response is controlled by the regulated proteolysis of an anti-sigma factor. *Genes Dev.* 13, 2449-2461.
79. Alba, B.M., Leeds, J.A., Onufryk, C., Lu, C.Z., and Gross, C.A. (2002). DegS and YaeL participate sequentially in the cleavage of RseA to activate the sigma(E)-dependent extracytoplasmic stress response. *Genes Dev.* 16, 2156-2168.
80. Campbell, E.A., Tupy, J.L., Gruber, T.M., Wang, S., Sharp, M.M., Gross, C.A., and Darst, S.A. (2003). Crystal structure of Escherichia coli sigmaE with the cytoplasmic domain of its anti-sigma RseA. *Mol. Cell* 11, 1067-1078.
81. Kanehara, K., Ito, K., and Akiyama, Y. (2003). YaeL proteolysis of RseA is controlled by the PDZ domain of YaeL and a Gln-rich region of RseA. *EMBO J.* 22, 6389-6398.
82. Bohn, C., Collier, J., and Boulloc, P. (2004). Dispensable PDZ domain of Escherichia coli YaeL essential protease. *Mol. Microbiol.* 52, 427-435.

83. Grigorova, I.L., Chaba, R., Zhong, H.J., Alba, B.M., Rhodius, V., Herman, C., and Gross, C.A. (2004). Fine-tuning of the Escherichia coli sigmaE envelope stress response relies on multiple mechanisms to inhibit signal-independent proteolysis of the transmembrane anti-sigma factor, RseA. *Genes Dev.* *18*, 2686-2697.
84. Sohn, J., Grant, R.A., and Sauer, R.T. (2007). Allosteric activation of DegS, a stress sensor PDZ protease. *Cell* *131*, 572-583.
85. Sohn, J., and Sauer, R.T. (2009). OMP peptides modulate the activity of DegS protease by differential binding to active and inactive conformations. *Mol. Cell* *33*, 64-74.
86. Sohn, J., Grant, R.A., and Sauer, R.T. (2009). OMP peptides activate the DegS stress-sensor protease by a relief of inhibition mechanism. *Structure* *17*, 1411-1421.
87. Meccas, J., Rouviere, P.E., Erickson, J.W., Donohue, T.J., and Gross, C.A. (1993). The activity of sigma E, an Escherichia coli heat-inducible sigma-factor, is modulated by expression of outer membrane proteins. *Genes Dev.* *7*, 2618-2628.
88. Alba, B.M., and Gross, C.A. (2004). Regulation of the Escherichia coli sigma-dependent envelope stress response. *Mol. Microbiol.* *52*, 613-619.
89. Collinet, B., Yuzawa, H., Chen, T., Herrera, C., and Missiakas, D. (2000). RseB binding to the periplasmic domain of RseA modulates the RseA:sigmaE interaction in the cytoplasm and the availability of sigmaE:RNA polymerase. *J. Biol. Chem.* *275*, 33898-33904.
90. Cezairliyan, B.O., and Sauer, R.T. (2007). Inhibition of regulated proteolysis by RseB. *Proc. Natl. Acad. Sci. USA* *104*, 3771-3776.
91. Kim, D.Y., Kwon, E., Choi, J., Hwang, H.-Y., and Kim, K.K. (2010). Structural basis for the negative regulation of bacterial stress response by RseB. *Protein Sci.* *19*, 1258-1263.
92. Chaba, R., Alba, B.M., Guo, M.S., Sohn, J., Ahuja, N., Sauer, R.T., and Gross, C.A. (2011). Signal integration by DegS and RseB governs the sigmaE-mediated envelope stress response in Escherichia coli. *Proc. Natl. Acad. Sci. USA* *108*, 2106-2111.

93. Lima, S., Guo, M.S., Chaba, R., Gross, C.A., and Sauer, R.T. (2013). Dual molecular signals mediate the bacterial response to outer-membrane stress. *Science* **340**, 837-841.
94. Tam, C., and Missiakas, D. (2005). Changes in lipopolysaccharide structure induce the sigma(E)-dependent response of *Escherichia coli*. *Mol. Microbiol.* **55**, 1403-1412.
95. Ames, G.F., Spudich, E.N., and Nikaido, H. (1974). Protein composition of the outer membrane of *Salmonella typhimurium*: effect of lipopolysaccharide mutations. *J. Bacteriol.* **117**, 406-416.
96. Austin, E.A., Graves, J.F., Hite, L.A., Parker, C.T., and Schnaitman, C.A. (1990). Genetic analysis of lipopolysaccharide core biosynthesis by *Escherichia coli* K-12: insertion mutagenesis of the *rfa* locus. *J. Bacteriol.* **172**, 5312-5325.
97. Ruiz, N., Chng, S.-S., Hiniker, A., Kahne, D., and Silhavy, T.J. (2010). Nonconsecutive disulfide bond formation in an essential integral outer membrane protein. *Proc. Natl. Acad. Sci. USA*.
98. Vertommen, D., Ruiz, N., Leverrier, P., Silhavy, T.J., and Collet, J.-F. (2009). Characterization of the role of the *Escherichia coli* periplasmic chaperone SurA using differential proteomics. *Proteomics* **9**, 2432-2443.
99. Udekwi, K.I., Darfeuille, F., Vogel, J., Reimegård, J., Holmqvist, E., and Wagner, E.G.H. (2005). Hfq-dependent regulation of OmpA synthesis is mediated by an antisense RNA. *Genes Dev.* **19**, 2355-2366.
100. Rasmussen, A.A., Eriksen, M., Gilany, K., Udesen, C., Franch, T., Petersen, C., and Valentin-Hansen, P. (2005). Regulation of ompA mRNA stability: the role of a small regulatory RNA in growth phase-dependent control. *Mol. Microbiol.* **58**, 1421-1429.
101. Johansen, J., Rasmussen, A.A., Overgaard, M., and Valentin-Hansen, P. (2006). Conserved small non-coding RNAs that belong to the sigmaE regulon: role in down-regulation of outer membrane proteins. *J. Mol. Biol.* **364**, 1-8.

102. Pappenfort, K., Pfeiffer, V., Mika, F., Lucchini, S., Hinton, J.C.D., and Vogel, J. (2006). SigmaE-dependent small RNAs of Salmonella respond to membrane stress by accelerating global omp mRNA decay. *Mol. Microbiol.* *62*, 1674-1688.
103. Thompson, K.M., Rhodius, V.A., and Gottesman, S. (2007). SigmaE regulates and is regulated by a small RNA in Escherichia coli. *J. Bacteriol.* *189*, 4243-4256.
104. Hayden, J.D., and Ades, S.E. (2008). The extracytoplasmic stress factor, sigmaE, is required to maintain cell envelope integrity in Escherichia coli. *PLoS ONE* *3*, e1573.
105. Gogol, E.B., Rhodius, V.A., Pappenfort, K., Vogel, J., and Gross, C.A. (2011). Small RNAs endow a transcriptional activator with essential repressor functions for single-tier control of a global stress regulon. *Proc. Natl. Acad. Sci. USA* *108*, 12875-12880.
106. Walter, P., and Ron, D. (2011). The unfolded protein response: from stress pathway to homeostatic regulation. *Science* *334*, 1081-1086.
107. Pavitt, G.D., and Ron, D. (2012). New insights into translational regulation in the endoplasmic reticulum unfolded protein response. *Cold Spring Harbor Perspectives in Biology* *4*.
108. Maurel, M., and Chevet, E. (2013). Endoplasmic reticulum stress signaling: the microRNA connection. *Am. J. Physiol. Cell Physiol.* *304*, C1117-1126.
109. Alon, U. (2007). Network motifs: theory and experimental approaches. *Nat. Rev. Genet.* *8*, 450-461.
110. Thattai, M., and Van Oudenaarden, A. (2004). Stochastic gene expression in fluctuating environments. *Genetics* *167*, 523-530.
111. El-Samad, H., and Khammash, M. (2006). Regulated degradation is a mechanism for suppressing stochastic fluctuations in gene regulatory networks. *Biophys. J.* *90*, 3749-3761.
112. Eldar, A., and Elowitz, M.B. (2010). Functional roles for noise in genetic circuits. *Nature* *467*, 167-173.



113. Cağatay, T., Turcotte, M., Elowitz, M.B., Garcia-Ojalvo, J., and Süel, G.M. (2009). Architecture-dependent noise discriminates functionally analogous differentiation circuits. *Cell* 139, 512-522.
114. Locke, J.C.W., Young, J.W., Fontes, M., Hernández Jiménez, M.J., and Elowitz, M.B. (2011). Stochastic pulse regulation in bacterial stress response. *Science* 334, 366-369.
115. Young, J.W., Locke, J.C.W., and Elowitz, M.B. (2013). Rate of environmental change determines stress response specificity. *Proc. Natl. Acad. Sci. USA* 110, 4140-4145.
116. Hecker, M., and Völker, U. (1998). Non-specific, general and multiple stress resistance of growth-restricted *Bacillus subtilis* cells by the expression of the sigmaB regulon. *Mol. Microbiol.* 29, 1129-1136.
117. Hecker, M., Pané-Farré, J., and Völker, U. (2007). SigB-dependent general stress response in *Bacillus subtilis* and related gram-positive bacteria. *Annu. Rev. Microbiol.* 61, 215-236.
118. Benson, A.K., and Haldenwang, W.G. (1993). *Bacillus subtilis* sigma B is regulated by a binding protein (RsbW) that blocks its association with core RNA polymerase. *Proc. Natl. Acad. Sci. USA* 90, 2330-2334.
119. Alper, S., Dufour, A., Garsin, D.A., Duncan, L., and Losick, R. (1996). Role of adenosine nucleotides in the regulation of a stress-response transcription factor in *Bacillus subtilis*. *J. Mol. Biol.* 260, 165-177.
120. Dufour, A., and Haldenwang, W.G. (1994). Interactions between a *Bacillus subtilis* anti-sigma factor (RsbW) and its antagonist (RsbV). *J. Bacteriol.* 176, 1813-1820.
121. Voelker, U., Voelker, A., Maul, B., Hecker, M., Dufour, A., and Haldenwang, W.G. (1995). Separate mechanisms activate sigma B of *Bacillus subtilis* in response to environmental and metabolic stresses. *J. Bacteriol.* 177, 3771-3780.

122. Yang, X., Kang, C.M., Brody, M.S., and Price, C.W. (1996). Opposing pairs of serine protein kinases and phosphatases transmit signals of environmental stress to activate a bacterial transcription factor. *Genes Dev.* *10*, 2265-2275.
123. Vijay, K., Brody, M.S., Fredlund, E., and Price, C.W. (2000). A PP2C phosphatase containing a PAS domain is required to convey signals of energy stress to the sigmaB transcription factor of *Bacillus subtilis*. *Mol. Microbiol.* *35*, 180-188.
124. Kim, T.-J., Gaidenko, T.A., and Price, C.W. (2004). In vivo phosphorylation of partner switching regulators correlates with stress transmission in the environmental signaling pathway of *Bacillus subtilis*. *J. Bacteriol.* *186*, 6124-6132.
125. Marles-Wright, J., and Lewis, R.J. (2010). The stressosome: molecular architecture of a signalling hub. *Biochem. Soc. Trans.* *38*, 928-933.
126. Bernhardt, J., Völker, U., Völker, A., Antelmann, H., Schmid, R., Mach, H., and Hecker, M. (1997). Specific and general stress proteins in *Bacillus subtilis*--a two-dimensional protein electrophoresis study. *Microbiology* *143*, 999-1017.
127. Szurmant, H., and Hoch, J.A. (2010). Interaction fidelity in two-component signaling. *Curr. Opin. Microbiol.* *13*, 190-197.
128. Podgornaia, A.I., and Laub, M.T. (2013). Determinants of specificity in two-component signal transduction. *Curr. Opin. Microbiol.* *16*, 156-162.
129. Laub, M.T., and Goulian, M. (2007). Specificity in two-component signal transduction pathways. *Annu. Rev. Genet.* *41*, 121-145.
130. Siryaporn, A., and Goulian, M. (2008). Cross-talk suppression between the CpxA-CpxR and EnvZ-OmpR two-component systems in *E. coli*. *Mol. Microbiol.* *70*, 494-506.
131. Groban, E.S., Clarke, E.J., Salis, H.M., Miller, S.M., and Voigt, C.A. (2009). Kinetic buffering of cross talk between bacterial two-component sensors. *J. Mol. Biol.* *390*, 380-393.
132. Capra, E.J., Perchuk, B.S., Lubin, E.A., Ashenberg, O., Skerker, J.M., and Laub, M.T. (2010). Systematic dissection and trajectory-scanning mutagenesis of the molecular

- interface that ensures specificity of two-component signaling pathways. *PLoS Genet.* **6**, e1001220.
133. Capra, E.J., Perchuk, B.S., Skerker, J.M., and Laub, M.T. (2012). Adaptive mutations that prevent crosstalk enable the expansion of paralogous signaling protein families. *Cell* **150**, 222-232.
134. Podgornaia, A.I., Casino, P., Marina, A., and Laub, M.T. (2013). Structural basis of a rationally rewired protein-protein interface critical to bacterial signaling. *Structure* **21**, 1636-1647.
135. Skerker, J.M., Perchuk, B.S., Siryaporn, A., Lubin, E.A., Ashenberg, O., Goulian, M., and Laub, M.T. (2008). Rewiring the specificity of two-component signal transduction systems. *Cell* **133**, 1043-1054.
136. Siryaporn, A., Perchuk, B.S., Laub, M.T., and Goulian, M. (2010). Evolving a robust signal transduction pathway from weak cross-talk. *Mol. Syst. Biol.* **6**, 452.
137. Willett, J.W., Tiwari, N., Müller, S., Hummels, K.R., Houtman, J.C.D., Fuentes, E.J., and Kirby, J.R. (2013). Specificity residues determine binding affinity for two-component signal transduction systems. *mBio* **4**, e00420-00413.
138. Staroń, A., Sofia, H., Dietrich, S., Ulrich, L., Liesegang, H., and Mascher, T. (2009). The third pillar of bacterial signal transduction: classification of the extracytoplasmic function (ECF) sigma factor protein family. *Mol. Microbiol.*
139. Rhodius, V.A., Segall-Shapiro, T.H., Sharon, B.D., Ghodasara, A., Orlova, E., Tabakh, H., Burkhardt, D.H., Clancy, K., Peterson, T.C., Gross, C.A., et al. (2013). Design of orthogonal genetic switches based on a crosstalk map of  $\sigma$ s, anti- $\sigma$ s, and promoters. *Mol. Syst. Biol.* **9**, 702.
140. Gur, E., Biran, D., and Ron, E.Z. (2011). Regulated proteolysis in Gram-negative bacteria--how and when? *Nat. Rev. Microbiol.* **9**, 839-848.

141. Maurizi, M.R. (1992). Proteases and protein degradation in *Escherichia coli*. *Experientia* *48*, 178-201.
142. Sauer, R.T., and Baker, T.A. (2011). AAA+ proteases: ATP-fueled machines of protein destruction. *Annu. Rev. Biochem.* *80*, 587-612.
143. Gur, E., Ottofueling, R., and Dougan, D.A. (2013). Machines of Destruction - AAA+ Proteases and the Adaptors That Control Them. *Subcell. Biochem.* *66*, 3-33.
144. Gur, E. (2013). The Lon AAA+ Protease. *Subcell. Biochem.* *66*, 35-51.
145. Rosen, R., Biran, D., Gur, E., Becher, D., Hecker, M., and Ron, E.Z. (2002). Protein aggregation in *Escherichia coli*: role of proteases. *FEMS Microbiol. Lett.* *207*, 9-12.
146. Gottesman, S. (2003). Proteolysis in bacterial regulatory circuits. *Annu. Rev. Cell Dev. Biol.* *19*, 565-587.
147. Battesti, A., Majdalani, N., and Gottesman, S. (2011). The RpoS-mediated general stress response in *Escherichia coli*. *Annu. Rev. Microbiol.* *65*, 189-213.
148. Hengge, R. (2009). Proteolysis of sigmaS (RpoS) and the general stress response in *Escherichia coli*. *Res. Microbiol.* *160*, 667-676.
149. Muffler, A., Fischer, D., Altuvia, S., Storz, G., and Hengge-Aronis, R. (1996). The response regulator RssB controls stability of the sigma(S) subunit of RNA polymerase in *Escherichia coli*. *EMBO J.* *15*, 1333-1339.
150. Pratt, L.A., and Silhavy, T.J. (1996). The response regulator SprE controls the stability of RpoS. *Proc. Natl. Acad. Sci. USA* *93*, 2488-2492.
151. Zhou, Y., Gottesman, S., Hoskins, J.R., Maurizi, M.R., and Wickner, S. (2001). The RssB response regulator directly targets sigma(S) for degradation by ClpXP. *Genes Dev.* *15*, 627-637.
152. Bougdour, A., Wickner, S., and Gottesman, S. (2006). Modulating RssB activity: IraP, a novel regulator of sigma(S) stability in *Escherichia coli*. *Genes Dev.* *20*, 884-897.

153. Bougdour, A., Cuning, C., Baptiste, P.J., Elliott, T., and Gottesman, S. (2008). Multiple pathways for regulation of sigmaS (RpoS) stability in *Escherichia coli* via the action of multiple anti-adaptors. *Mol. Microbiol.* *68*, 298-313.
154. Merrikh, H., Ferrazzoli, A.E., Bougdour, A., Olivier-Mason, A., and Lovett, S.T. (2009). A DNA damage response in *Escherichia coli* involving the alternative sigma factor, RpoS. *Proc. Natl. Acad. Sci. USA* *106*, 611-616.
155. Merrikh, H., Ferrazzoli, A.E., and Lovett, S.T. (2009). Growth phase and (p)ppGpp control of IraD, a regulator of RpoS stability, in *Escherichia coli*. *J. Bacteriol.* *191*, 7436-7446.
156. Battesti, A., Hoskins, J.R., Tong, S., Milanesio, P., Mann, J.M., Kravats, A., Tsegaye, Y.M., Bougdour, A., Wickner, S., and Gottesman, S. (2013). Anti-adaptors provide multiple modes for regulation of the RssB adaptor protein. *Genes Dev.* *27*, 2722-2735.
157. Peterson, C.N., Levchenko, I., Rabinowitz, J.D., Baker, T.A., and Silhavy, T.J. (2012). RpoS proteolysis is controlled directly by ATP levels in *Escherichia coli*. *Genes Dev.* *26*, 548-553.
158. Martin, A., Baker, T.A., and Sauer, R.T. (2008). Protein unfolding by a AAA+ protease is dependent on ATP-hydrolysis rates and substrate energy landscapes. *Nat. Struct. Mol. Biol.* *15*, 139-145.
159. Nager, A.R., Baker, T.A., and Sauer, R.T. (2011). Stepwise unfolding of a f<sub>1</sub> F<sub>1</sub> ATPase is dependent on ATP-hydrolysis rates and substrates. *PNAS* *108*, 4-16.
160. Johnson, A., and O'donnell, M. (2005). Cellular DNA replicases: components and dynamics at the replication fork. *Annu. Rev. Biochem.* *74*, 283-315.
161. Tsuchihashi, Z., and Kornberg, A. (1990). Translational frameshifting generates the gamma subunit of DNA polymerase III holoenzyme. *Proc. Natl. Acad. Sci. USA* *87*, 2516-2520.

162. Blinkowa, A.L., and Walker, J.R. (1990). Programmed ribosomal frameshifting generates the Escherichia coli DNA polymerase III gamma subunit from within the tau subunit reading frame. *Nucleic Acids Res.* *18*, 1725-1729.
163. Flower, A.M., and McHenry, C.S. (1990). The gamma subunit of DNA polymerase III holoenzyme of Escherichia coli is produced by ribosomal frameshifting. *Proc. Natl. Acad. Sci. USA* *87*, 3713-3717.
164. Vass, R.H., and Chien, P. (2013). Critical clamp loader processing by an essential AAA+ protease in *Caulobacter crescentus*. *Proc. Natl. Acad. Sci. USA* *110*, 18138-18143.
165. Kenniston, J.A., Baker, T.A., and Sauer, R.T. (2005). Partitioning between unfolding and release of native domains during ClpXP degradation determines substrate selectivity and partial processing. *Proc. Natl. Acad. Sci. USA* *102*, 1390-1395.
166. Aubin-Tam, M.-E., Olivares, A.O., Sauer, R.T., Baker, T.A., and Lang, M.J. (2011). Single-molecule protein unfolding and translocation by an ATP-fueled proteolytic machine. *Cell* *145*, 257-267.
167. Maillard, R.A., Chistol, G., Sen, M., Righini, M., Tan, J., Kaiser, C.M., Hodges, C., Martin, A., and Bustamante, C. (2011). ClpX(P) Generates Mechanical Force to Unfold and Translocate Its Protein Substrates. *Cell* *145*, 459-469.
168. Too, P.H.-M., Eralles, J., Simen, J.D., Marjanovic, A., and Coffino, P. (2013). Slippery substrates impair function of a bacterial protease ATPase by unbalancing translocation versus exit. *J. Biol. Chem.* *288*, 13243-13257.
169. Tian, L., Holmgren, R.A., and Matouschek, A. (2005). A conserved processing mechanism regulates the activity of transcription factors Cubitus interruptus and NF-kappaB. *Nat. Struct. Mol. Biol.* *12*, 1045-1053.
170. Palombella, V.J., Rando, O.J., Goldberg, A.L., and Maniatis, T. (1994). The ubiquitin-proteasome pathway is required for processing the NF-kappa B1 precursor protein and the activation of NF-kappa B. *Cell* *78*, 773-785.

171. Aza-Blanc, P., Ramírez-Weber, F.A., Laget, M.P., Schwartz, C., and Kornberg, T.B. (1997). Proteolysis that is inhibited by hedgehog targets Cubitus interruptus protein to the nucleus and converts it to a repressor. *Cell* **89**, 1043-1053.
172. Gottesman, S. (1996). Proteases and their targets in *Escherichia coli*. *Annu. Rev. Genet.* **30**, 465-506.
173. Gur, E., and Sauer, R.T. (2008). Recognition of misfolded proteins by Lon, a AAA(+) protease. *Genes Dev.* **22**, 2267-2277.
174. Gur, E., Vishkautzan, M., and Sauer, R.T. (2012). Protein unfolding and degradation by the AAA+ Lon protease. *Protein Sci.* **21**, 268-278.
175. Wohlever, M.L., Baker, T.A., and Sauer, R.T. (2014). Roles of the N domain of the AAA+ Lon protease in substrate recognition, allosteric regulation and chaperone activity. *Mol. Microbiol.* **91**, 66-78.
176. Gur, E., and Sauer, R.T. (2009). Degrons in protein substrates program the speed and operating efficiency of the AAA+ Lon proteolytic machine. *Proc. Natl. Acad. Sci. USA* **106**, 18503-18508.
177. Gottesman, S., Halpern, E., and Trisler, P. (1981). Role of *sulA* and *sulB* in filamentation by lon mutants of *Escherichia coli* K-12. *J. Bacteriol.* **148**, 265-273.
178. Mizusawa, S., and Gottesman, S. (1983). Protein degradation in *Escherichia coli*: the lon gene controls the stability of *sulA* protein. *Proc. Natl. Acad. Sci. USA* **80**, 358-362.
179. Van Melder, L., and Gottesman, S. (1999). Substrate sequestration by a proteolytically inactive Lon mutant. *Proc. Natl. Acad. Sci. USA* **96**, 6064-6071.
180. Vieux, E.F., Wohlever, M.L., Chen, J.Z., Sauer, R.T., and Baker, T.A. (2013). Distinct quaternary structures of the AAA+ Lon protease control substrate degradation. *Proc. Natl. Acad. Sci. USA* **110**, E2002-2008.

181. Wohlever, M.L., Baker, T.A., and Sauer, R.T. (2013). A Mutation in the N Domain of *Escherichia coli* Lon Stabilizes Dodecamers and Selectively Alters Degradation of Model Substrates. *J. Bacteriol.* *195*, 5622-5628.
182. Leonard, A.C., and Grimwade, J.E. (2011). Regulation of DnaA assembly and activity: taking directions from the genome. *Annu. Rev. Microbiol.* *65*, 19-35.
183. Collier, J. (2012). Regulation of chromosomal replication in *Caulobacter crescentus*. *Plasmid* *67*, 76-87.
184. Gorbatyuk, B., and Marczynski, G.T. (2005). Regulated degradation of chromosome replication proteins DnaA and CtrA in *Caulobacter crescentus*. *Mol. Microbiol.* *55*, 1233-1245.
185. Lesley, J.A., and Shapiro, L. (2008). SpoT regulates DnaA stability and initiation of DNA replication in carbon-starved *Caulobacter crescentus*. *J. Bacteriol.* *190*, 6867-6880.
186. Jonas, K., Chen, Y.E., and Laub, M.T. (2011). Modularity of the bacterial cell cycle enables independent spatial and temporal control of DNA replication. *Curr. Biol.* *21*, 1092-1101.
187. Jonas, K., Liu, J., Chien, P., and Laub, M.T. (2013). Proteotoxic stress induces a cell-cycle arrest by stimulating Lon to degrade the replication initiator DnaA. *Cell* *154*, 623-636.
188. Bruel, N., Castanié-Cornet, M.-P., Cirinesi, A.-M., Koningstein, G., Georgopoulos, C., Luirink, J., and Genevaux, P. (2012). Hsp33 controls elongation factor-Tu stability and allows *Escherichia coli* growth in the absence of the major DnaK and trigger factor chaperones. *J. Biol. Chem.* *287*, 44435-44446.
189. Balaban, N.Q., Merrin, J., Chait, R., Kowalik, L., and Leibler, S. (2004). Bacterial persistence as a phenotypic switch. *Science* *305*, 1622-1625.
190. Lewis, K. (2010). Persister Cells. *Annu. Rev. Microbiol.* *64*, 357-372.
191. Balaban, N.Q. (2011). Persistence: mechanisms for triggering and enhancing phenotypic variability. *Curr. Opin. Genet. Dev.* *21*, 768-775.



192. Gerdes, K., and Maisonneuve, E. (2012). Bacterial persistence and toxin-antitoxin loci. *Annu. Rev. Microbiol.* 66, 103-123.
193. Maisonneuve, E., Castro-Camargo, M., and Gerdes, K. (2013). (p)ppGpp Controls Bacterial Persistence by Stochastic Induction of Toxin-Antitoxin Activity. *Cell* 154, 1140-1150.
194. Dubnau, D., and Losick, R. (2006). Bistability in bacteria. *Mol. Microbiol.* 61, 564-572.
195. Veening, J.-W., Smits, W.K., and Kuipers, O.P. (2008). Bistability, epigenetics, and bet-hedging in bacteria. *Annu. Rev. Microbiol.* 62, 193-210.
196. Price, M.N., Deutschbauer, A.M., Skerker, J.M., Wetmore, K.M., Ruths, T., Mar, J.S., Kuehl, J.V., Shao, W., and Arkin, A.P. (2013). Indirect and suboptimal control of gene expression is widespread in bacteria. *Mol. Syst. Biol.* 9, 660.
197. Tagkopoulos, I., Liu, Y.-C., and Tavazoie, S. (2008). Predictive behavior within microbial genetic networks. *Science* 320, 1313-1317.
198. Mitchell, A., Romano, G.H., Groisman, B., Yona, A., Dekel, E., Kupiec, M., Dahan, O., and Pilpel, Y. (2009). Adaptive prediction of environmental changes by microorganisms. *Nature* 460, 220-224.

## Chapter 1

Signal integration by DegS and RseB governs the  $\sigma^E$ -mediated envelope stress response in *Escherichia coli*

**Contributing Authors:** Rachna Chaba, Benjamin M. Alba, Jungsan Sohn, Nidhi Ahuja, Robert T. Sauer, Carol A. Gross.

*Citation:* Chaba et al. Signal integration by DegS and RseB governs the  $\sigma^E$ -mediated envelope stress response in *Escherichia coli*. *Proceedings of the National Academy of Sciences USA* (2011) vol. 108 (5) pp. 2106-11.

## Preface:

As discussed in the introduction, the  $\sigma^E$  response regulates a broad swathe of genes involved in OM biogenesis [5].  $\sigma^E$  is well conserved in  $\gamma$ -proteobacteria, and importantly, is always co-transcribed with its negative regulators, RseA and RseB [5]. RseA was known to bind to  $\sigma^E$  and inhibit its activity. In response to unfolded OMPs in the periplasm, the DegS protease would bind these OMPs and initiate cleavage of RseA, activating  $\sigma^E$ . However role of RseB was obscure. *In vivo*, RseB seemed to only play a minor role ( $\Delta rseB$  cells had only 2-fold  $\sigma^E$  activation), but *in vitro*, RseB was able to fully inhibit cleavage of RseA. How could these two observations be reconciled? This required understanding the role of RseB in the cell.

This chapter of my thesis describes how we determined the cellular role of RseB. Rachna Chaba, a postdoc in the lab, initiated this project to tease apart the separate roles of OMP activation and RseB inactivation. We discovered that *rseB*<sup>+</sup> cells were much less sensitive to overexpression of OMPs than  $\Delta rseB$  cells. Thus, RseB functioned to repress activation of  $\sigma^E$  in response to fluctuations in OMP level, uncovering the role an additional signal to inactivate RseB that was required to initiate  $\sigma^E$  activation *in vivo*.

This work was published in *PNAS* (2011) vol. 108 (5) pp. 2106-11. I helped Rachna by generating a key DegS mutation in the chromosome, and also with writing the final manuscript. Ben Alba, a previous graduate student in the lab, performed some of the genetic experiments, Nidi Ahuja, a previous post-doc in the lab, helped analyze data, and our collaborators, Bob Sauer and his postdoc Jungsan Sohn performed biochemical experiments to demonstrate that different OMP peptides had the same ability to activate DegS *in vitro*, and helped write the final manuscript.

## Abstract

In *Escherichia coli*, the  $\sigma^E$  transcription factor monitors and maintains outer membrane (OM) integrity by activating genes required for assembly of its two key components, outer membrane proteins (OMPs) and lipopolysaccharide (LPS), and by transcribing small RNAs to down-regulate excess unassembled OMPs.  $\sigma^E$  activity is governed by the rate of degradation of its membrane-spanning anti- $\sigma$  factor, RseA. Importantly, the DegS protease can initiate RseA cleavage only when activated by binding to unassembled OMPs. The prevalent paradigm has been that the  $\sigma^E$  response is controlled by the amount of activated DegS. Here we demonstrate that inactivation of a second negative regulator, the periplasmic protein RseB, is also required for  $\sigma^E$  induction *in vivo*. Moreover, OMPs, previously known only to activate DegS, also generate a signal to antagonize RseB inhibition. This signal may be lipid related, as RseB is structurally similar to proteins that bind lipids. We propose that the use of an AND gate enables  $\sigma^E$  to sense and integrate multivariate signals from the envelope.

## Introduction

The outer membrane (OM) of gram-negative bacteria is their first line of defense against harsh environments. Both key components of the OM, outer membrane proteins (OMPs) and lipopolysaccharide (LPS) have complex assembly and insertion pathways (1-4). In *Escherichia coli*, OM homeostasis is primarily maintained by a transcription factor,  $\sigma^E$ , whose regulon includes machinery for assembly and insertion of OMPs into the OM, small RNAs that down-regulate OMP expression, and components controlling LPS synthesis and transport (5, 6).

An elaborate regulatory apparatus monitors envelope status to control  $\sigma^E$  activity. Under steady-state growth,  $\sigma^E$  is predominantly bound to RseA,  $\sigma^E$ 's inner membrane (IM)-spanning anti- $\sigma$  factor (Fig. 1A) (7-9). Accumulation of unassembled OMPs in the periplasm activates DegS, a trimeric IM-anchored serine protease, to initiate RseA degradation. Free DegS lacks significant catalytic activity because the oxyanion hole of the active site is inappropriately positioned (Fig. 1A) (10). However, binding of the YxF tripeptide at the C-terminus of unassembled OMPs to the DegS PDZ domain stabilizes the active protease conformation, allowing it to cleave the periplasmic domain of RseA (Fig. 1B) (11-13), thereby activating the protease cascade that degrades RseA (14-18). This “activation” signal is an excellent indicator of OMP assembly problems, as the OMP C-termini are inaccessible in properly assembled OM-localized OMPs (19). Once released from its inhibitory interactions with RseA,  $\sigma^E$  binds RNA polymerase and activates transcription. Thus, the intracellular concentration of active  $\sigma^E$  primarily reflects the rate of RseA degradation, enabling fine temporal control over  $\sigma^E$  activity (16).

$\sigma^E$  also has a second negative regulator, the periplasmic protein RseB, which binds to RseA (Fig. 1A) (8, 20). There is conflicting data about the role of RseB. Strains lacking RseB display only a ~2-fold increase in  $\sigma^E$  activity, suggesting that RseB plays a minor role in the response (8), but *in vitro*, RseB completely inhibits RseA degradation by OMP-activated DegS (21). Moreover *in vivo*,

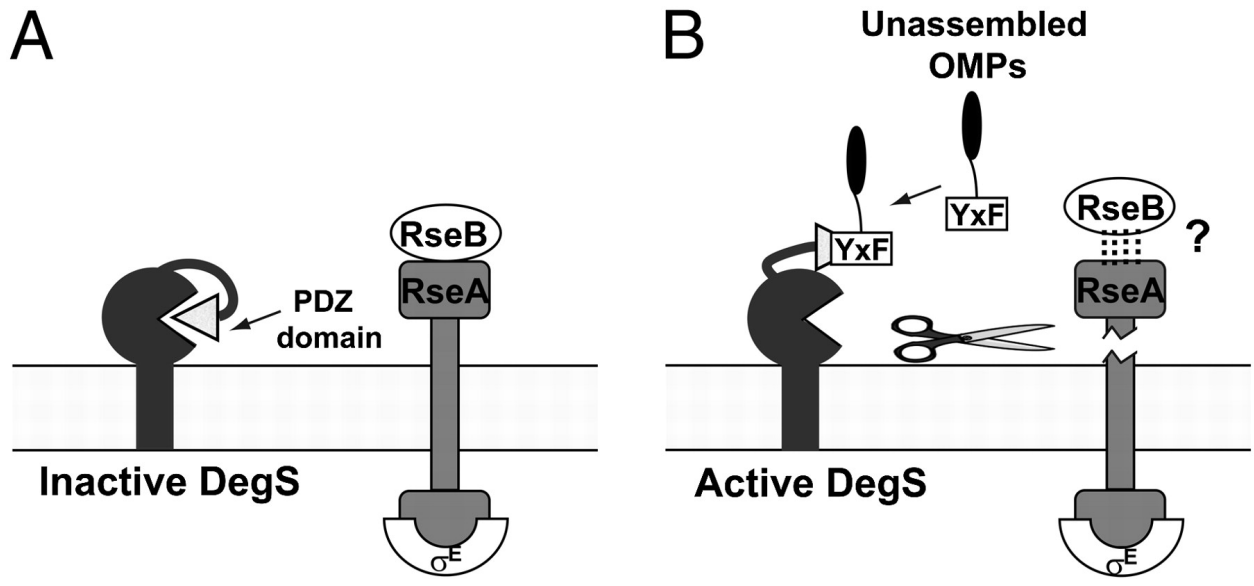


**Figure 1.** Components controlling  $\sigma^E$  activity.

(A)  $\sigma^E$  is sequestered at the IM by binding to the membrane-spanning anti- $\sigma$  factor, RseA. The second negative regulator of  $\sigma^E$ , the periplasmic protein RseB, binds to RseA. Unliganded DegS lacks significant catalytic activity. (B)  $\sigma^E$  activity is controlled by an AND gate, requiring both DegS activation by unassembled OMPs and RseB inactivation by an alternate cellular signal.

OMP peptides are sufficient for  $\sigma^E$  induction, yet were thought only to activate DegS, suggesting that antagonizing RseB inhibition was not critical to the response. Our work clarifies this issue. We show that  $\sigma^E$  activity is controlled by an AND gate, requiring both DegS activation and RseB inactivation for robust response (Fig. 1B). Consistent with this finding, RseB sets the sensitivity of the  $\sigma^E$  response to OMP signal. Additionally, we find that OMPs, previously known only to activate DegS, also antagonize RseB by inducing another cellular signal. Since RseB is structurally similar to proteins that bind lipids (22, 23), it suggests that this signal is lipid related. We propose that the  $\sigma^E$  pathway employs DegS and RseB to sense and integrate multivariate signals from the envelope.

## Results

**Intertwined roles of DegS and RseB in  $\sigma^E$  induction.** A variant of DegS lacking its PDZ domain (DegS $\Delta$ PDZ) cleaves RseA in an OMP-independent fashion *in vitro*, but cells harboring this truncated enzyme display only ~1.5-fold induction of  $\sigma^E$  *in vivo* (Fig. 2A) (11, 12), raising the possibility that DegS activation *per se* may not be sufficient for full  $\sigma^E$  induction. The logical candidate for an additional regulator is RseB, which binds tightly to RseA and impedes DegS cleavage of RseA *in vitro*. Indeed, removal of RseB in a DegS $\Delta$ PDZ strain led to synergistic  $\sigma^E$  induction (Fig. 2A). Although  $\Delta$ rseB and DegS $\Delta$ PDZ single mutants each activated  $\sigma^E$  only ~1.5 to 2-fold, the double mutant  $\Delta$ rseB DegS $\Delta$ PDZ strain showed ~12-fold activation. Additionally, amino acid substitutions in DegS that decrease the free-energy gap between its active and inactive conformations and increase basal cleavage activity *in vitro* (12, 13, 24) are also synergistic with  $\Delta$ rseB (Fig. 2B). K243D, which breaks the inhibitory interactions between the PDZ and protease domains of DegS, and H198P, which stabilizes the functional conformation of the oxyanion hole, each induce  $\sigma^E$  only a few fold, but in combination with  $\Delta$ rseB showed ~15-20-fold  $\sigma^E$  induction. Thus, both DegS activation and RseB removal are required for robust activation of  $\sigma^E$ .

**RseB determines the threshold of OMP signal required for  $\sigma^E$  activation.** RseB modulates the  $\sigma^E$  induction of active DegS variants, leading us to consider whether it might also modulate  $\sigma^E$  induction when DegS is activated by OMPs. We compared  $\sigma^E$  induction in wildtype (WT) and  $\Delta$ rseB cells using a library of inducers, which consisted of periplasmic cytochrome b<sub>562</sub> fused to the C-terminal 50 amino acids of OmpC (Cyt-OmpC<sub>50</sub>) and variants in which the penultimate residue of the OmpC C-terminus (YQF) was changed to correspond to each YxF motif identified in *E. coli* OMPs (11).



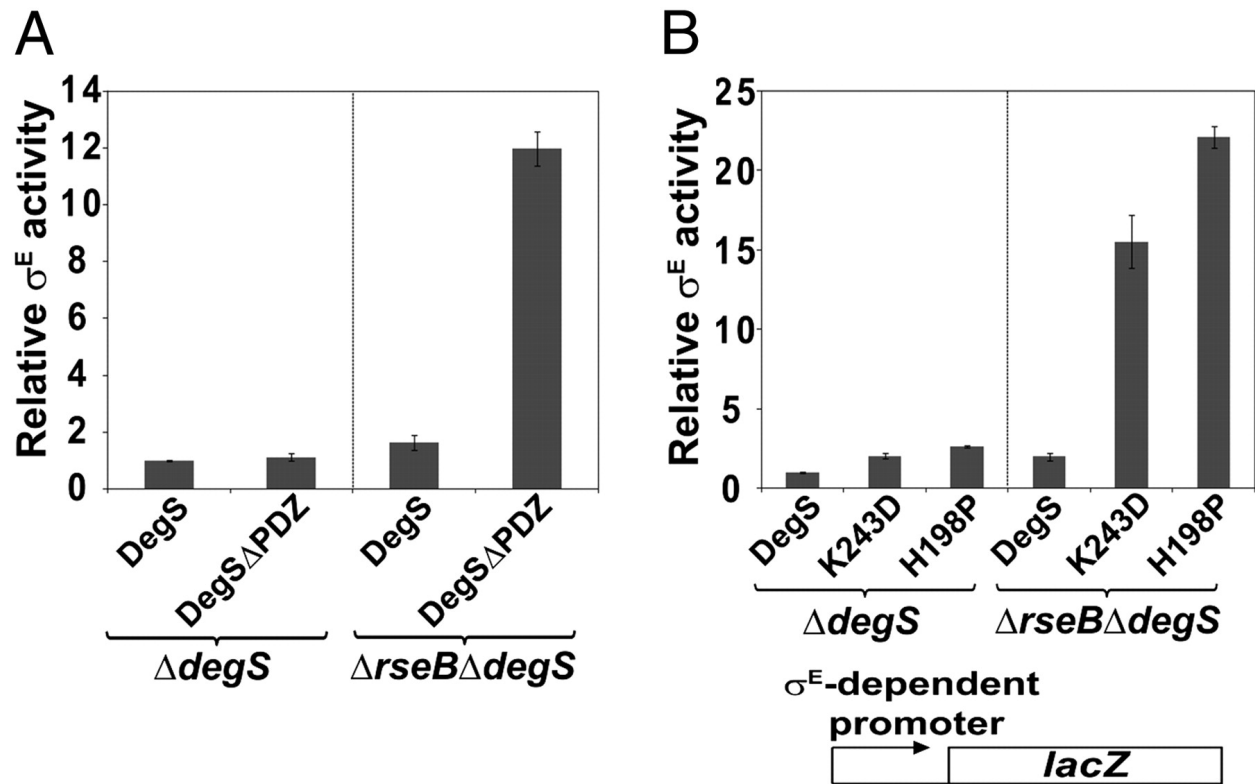


**Figure 2.** Synergistic effect of DegS activation and RseB removal on  $\sigma^E$  activity.

$\Delta degS$  and  $\Delta rseB \Delta degS$  strains carried plasmids for **(A)** WT DegS or DegS $\Delta$ PDZ; or **(B)** WT DegS, K243D DegS, or H198P DegS. Cells were grown to  $OD_{600} \sim 0.1$  and  $\sigma^E$  activity was measured by monitoring  $\beta$ -gal expression from a chromosomal  $\sigma^E$ -dependent *lacZ* reporter. Data were normalized to the  $\Delta degS$  strain expressing WT DegS from the plasmid and represent averages ( $\pm$  SD) of three independent experiments.

We expressed each YxF fusion protein from the  $P_{trc}$  promoter in the presence of 1 mM IPTG and measured  $\sigma^E$  activity. In WT cells,  $\sigma^E$  activation correlated with binding affinity of the YxF motif for the PDZ domain of DegS (Fig. 3A), consistent with the fact that this parameter governs DegS activation *in vitro* (12). In contrast, in  $\Delta rseB$  cells, all YxF peptides displayed similar activation of  $\sigma^E$  and were significantly better inducers than in the WT background (Fig. 3B). Therefore, we tested whether the absence of RseB lowered the threshold for OMP activation by assaying  $\sigma^E$  induction from basal expression of fusion proteins (no IPTG; basal expression from the  $P_{trc}$  promoter). Under these conditions, graded  $\sigma^E$  activation was observed in  $\Delta rseB$  cells, but no induction was observed in WT cells (Fig. 3C). These results are consistent with the idea that RseB modulates  $\sigma^E$  activation by increasing the OMP peptide threshold.

We explored alternative explanations for the effect of RseB on  $\sigma^E$  activation. We tested whether differential  $\sigma^E$  activation in WT and  $\Delta rseB$  cells resulted from differential expression of the fusion proteins using SDS-PAGE of periplasmic extracts to examine the proteins in the high-expression regime, and quantitative RT-PCR to examine transcription of fusion proteins in the low-expression regime. Both studies showed that fusion proteins and their transcripts were present at equivalent levels in WT and  $\Delta rseB$  cells, thus ruling out differential fusion protein expression as the cause of differential  $\sigma^E$  activation (Fig. S1A,B). Moreover, the increase in  $\sigma^E$  activity in  $\Delta rseB$  cells was not due to cleavage by another protease. Using a  $\Delta rseB\Delta degS$  strain expressing either WT DegS or catalytically inactive DegS (DegS-S201A), we demonstrate that active DegS is required for  $\sigma^E$  induction upon expression of the YQF fusion (Fig. 3D). These findings together with data that  $\Delta rseB$  cells expressing low concentrations of YxF fusions exhibit  $\sigma^E$  activation roughly proportional to the YxF affinities for DegS (Fig. 3C) strongly support a model in which RseB modulates the threshold for OMP-peptide activation of DegS.

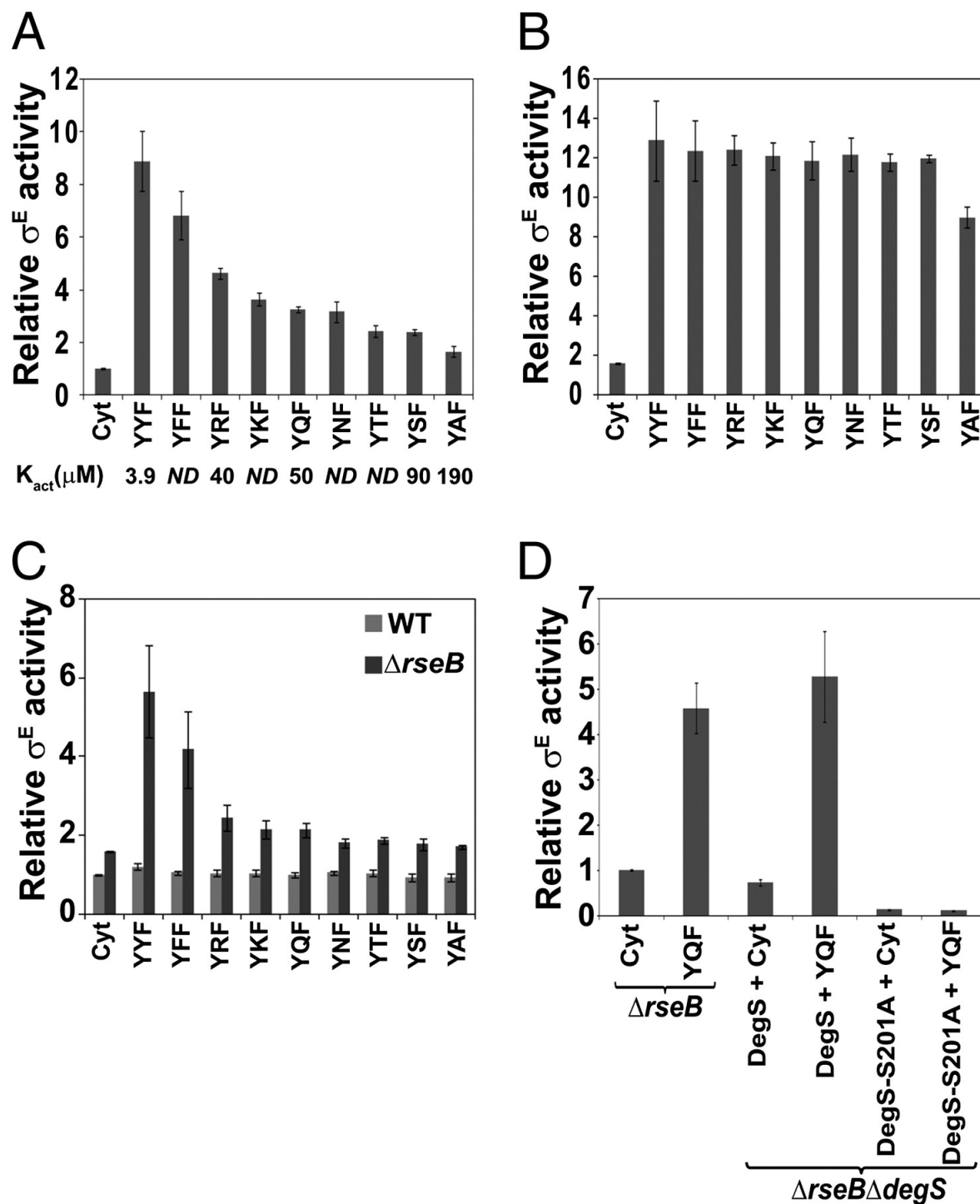


**Figure 3.** RseB determines the threshold of OMP signal required for  $\sigma^E$  activation.

**(A)**  $\sigma^E$  activity of WT strain expressing high levels of YxY fusion proteins. WT strain carried plasmids for cytochrome  $b_{562}$  (Cyt), a fusion of this protein to the C-terminal 50 residues of OmpC (Cyt-OmpC<sub>50</sub>(YQF); YQF), or its variants with the C-terminal motifs YYF, YFF, YRF, YKF, YNF, YTF, YSF, YAF. Cells were grown to OD<sub>600</sub> ~0.1 and induced with 1 mM IPTG. Samples were collected at four time points during exponential phase and assayed for  $\beta$ -gal activity.

Data were normalized to  $\sigma^E$  activity of the WT strain expressing cytochrome  $b_{562}$  and represent averages ( $\pm$  SD) of three independent experiments.  $K_{act}$  represents the concentration of YxF peptide required for half-maximal activation of DegS cleavage of RseA *in vitro* (12); *ND*: not determined. **(B)**  $\sigma^E$  activity of  $\Delta rseB$  strain expressing high levels of YxF fusion proteins.  $\Delta rseB$  cells carrying plasmids for cytochrome  $b_{562}$  or YxF OMP-fusion proteins were grown to  $OD_{600} \sim 0.1$ , induced with 1 mM IPTG, and assayed as described in the Fig. 3A legend. Data were normalized to the WT strain expressing cytochrome  $b_{562}$  and represent averages ( $\pm$  SD) of three independent experiments. **(C)**  $\sigma^E$  activity of WT and  $\Delta rseB$  strains under basal-level expression of YxF fusion proteins (no IPTG). The uninduced sample at  $OD_{600} \sim 0.1$  from Figs. 3A and 3B was used to measure  $\sigma^E$  activity from basal fusion-protein expression. Data were normalized to the WT strain expressing cytochrome  $b_{562}$  and represent averages ( $\pm$  SD) of three independent experiments. **(D)** Catalytically active DegS is required for  $\sigma^E$  activation in the absence of RseB.  $\Delta rseB$  cells carried plasmids for cytochrome  $b_{562}$  (Cyt) or the YQF fusion protein, and  $\Delta rseB\Delta degS$  cells carried either Cyt or YQF fusion protein, and plasmid for constitutive expression of either WT DegS or DegS-S201A. Cells were grown to  $OD_{600} \sim 0.1$ , and induced with 0.02 mM IPTG. At an  $OD_{600}$  of 0.25-0.3, samples were harvested for  $\beta$ -gal assays. Data were normalized to the  $\Delta rseB$  strain expressing cytochrome  $b_{562}$  and represent averages ( $\pm$  SD) of three independent experiments.

**Sequence elements upstream of the C-terminal YxF motif affect RseB inhibition in vivo.** The three C-terminal residues of OMP peptides are sufficient for activating DegS *in vitro*; additional residues N-terminal to these generally inhibit and sometimes enhance activation (13). We found that significantly more C-terminal OMP residues were necessary for induction *in vivo*. Using a C-terminal deletion series of fusion proteins containing 10, 20, 30, 40, and 50 C-terminal residues, we found that fusions ending with 20 (OmpC<sub>20</sub>) or more OmpC residues activated  $\sigma^E$  similarly, whereas the fusion ending with 10 OmpC residues (OmpC<sub>10</sub>) displayed weak activity (Fig. 4A,B). Because  $\sigma^E$  induction *in vivo* involves both DegS activation and antagonizing RseB, we tested whether these additional OMP amino acids might be used for the latter process. Indeed, OmpC<sub>10</sub> activated  $\sigma^E$  ~75% as well as OmpC<sub>20</sub> in  $\Delta rseB$  cells using basal-expression conditions to ensure that  $\sigma^E$  activity is in the linear range (Fig. 4C). Increasing OmpC<sub>10</sub> affinity for DegS by changing its terminal tripeptide to YYF did not significantly activate WT cells but did show full activation in  $\Delta rseB$  cells, indicating that a process other than DegS activation limits the ability of OmpC<sub>10</sub> to induce  $\sigma^E$  in WT cells (compare Fig. 4B,C). These results demonstrate that an element located between 10 and 20 residues is required to antagonize RseB inhibition.

We asked whether upstream OMP sequences vary in their ability to counter RseB inhibition. Our test system compared  $\sigma^E$  induction by “natural inducers” comprised of the authentic 50 C-terminal residues of several OMPs with that of an OmpC<sub>50</sub> fusion protein having the same YxF motif as its “natural inducer” counterpart. Four natural inducers (OmpX, MipA, OmpG, and FadL) were better than their respective OmpC controls at inducing  $\sigma^E$  (Fig. 5A). Importantly, these same natural inducers performed the same as or worse than their OmpC counterparts in  $\Delta rseB$  cells, where induction is dependent solely on DegS activation (Fig. 5B). We conclude that OMPs vary in their ability to antagonize RseB inhibition, just as they vary in their ability to affect DegS activation.

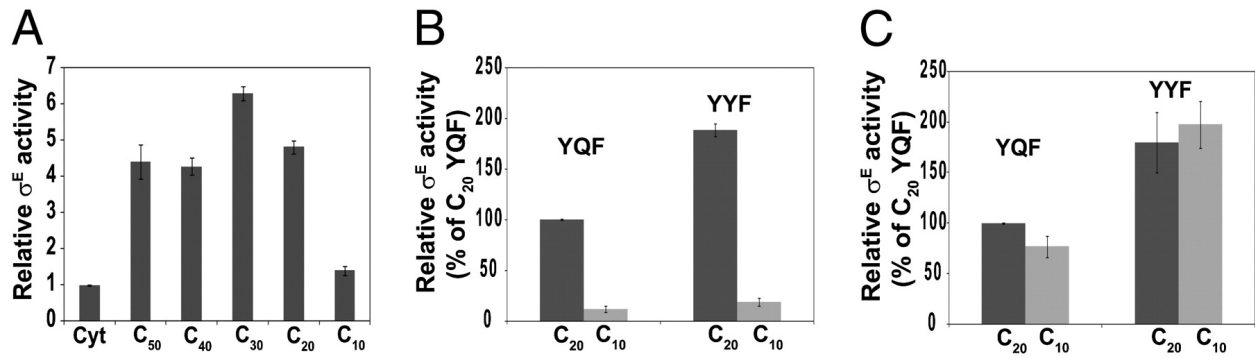


**Figure 4.** OMP peptide relieves RseB inhibition of RseA.

**(A)** C-terminal 20 amino acids of OmpC are required for  $\sigma^E$  activation in WT cells. WT strain carried plasmids for either cytochrome *b*<sub>562</sub> (Cyt) or a fusion of this protein to the C-terminal 50 (C<sub>50</sub>), 40 (C<sub>40</sub>), 30 (C<sub>30</sub>), 20 (C<sub>20</sub>), and 10 (C<sub>10</sub>) residues of OmpC. Cells were grown to OD<sub>600</sub> ~0.1 and induced with 1 mM IPTG. Samples were collected at four time points during exponential phase and assayed for  $\beta$ -gal activity. Data were normalized to the  $\sigma^E$  activity of WT strain expressing cytochrome *b*<sub>562</sub> and represent averages ( $\pm$  SD) of two independent experiments. **(B)** Increasing affinity of the C-terminal 10 residues of OmpC for DegS does not promote significant activation in WT cells. WT cells carried plasmids expressing cytochrome *b*<sub>562</sub>, a fusion of cytochrome *b*<sub>562</sub> to the C-terminal 20 or 10 residues of OmpC (C<sub>20</sub> YQF, C<sub>10</sub> YQF) or its variant with YYF C-terminal motif (C<sub>20</sub> YYF, C<sub>10</sub> YYF). Strains were grown and sampled as in Fig. 4A. The background  $\beta$ -gal activity of cytochrome *b*<sub>562</sub> was subtracted from the  $\beta$ -gal activity of fusion proteins and the data is presented as % activity of C<sub>20</sub> YQF. Data represent averages ( $\pm$  SD) of three independent experiments. **(C)** C-terminal 10 amino acids of OmpC are sufficient for  $\sigma^E$  activation in  $\Delta rseB$  cells.  $\Delta rseB$  cells carrying plasmids mentioned in Fig. 4B were grown to OD<sub>600</sub> ~0.1.  $\beta$ -gal activity was measured under basal protein expression. The background  $\beta$ -gal activity of cytochrome *b*<sub>562</sub> was subtracted from the  $\beta$ -gal activity of fusion proteins and the data is presented as % activity of C<sub>20</sub> YQF. Data represent averages ( $\pm$  SD) of three independent experiments.

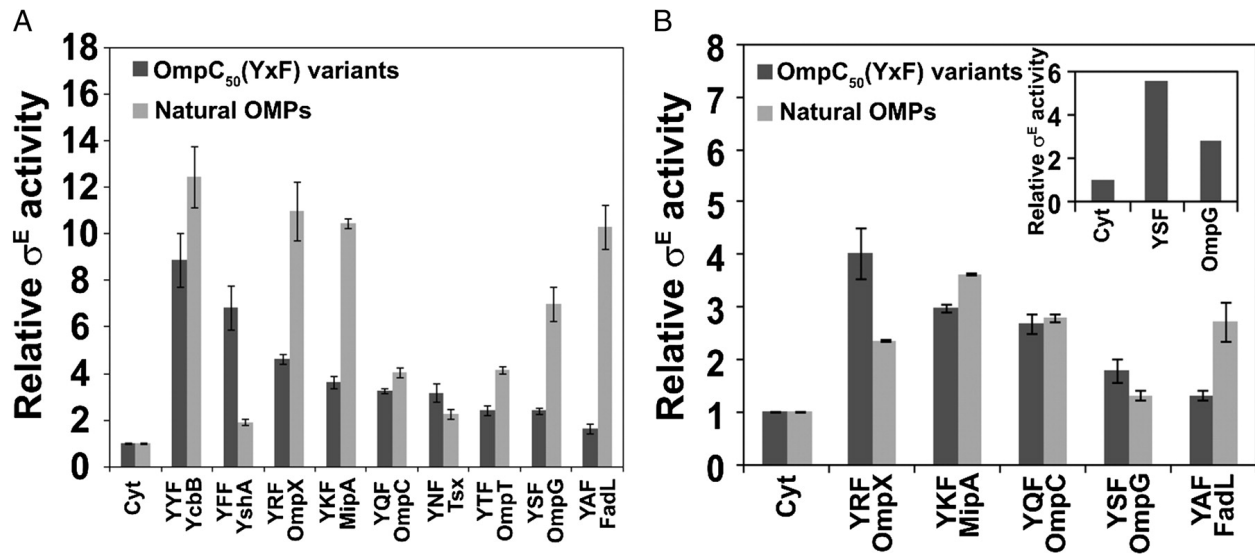


**Figure 5.** Residues upstream of the C-terminal YxF motif encode RseB modulatory sequences.

**(A)** Comparison of  $\sigma^E$  activation strengths of natural OMPs with OmpC carrying matched YxF C-terminus in WT cells. WT strain carried plasmids expressing cytochrome  $b_{562}$  (Cyt), a fusion of this protein to the C-terminal 50 residues of OmpC (Cyt-OmpC<sub>50</sub>(YQF); YQF), or its variants with the C-terminal motifs YFF, YFF, YRF, YKF, YNF, YTF, YSF, YAF, and a fusion of cytochrome  $b_{562}$  to ~50 C-terminal residues of YcbB, YshA, OmpX, MipA, Tsx, OmpT, OmpG, or FadL. Cells were grown to OD<sub>600</sub> ~0.1 and induced with 1 mM IPTG. Samples were collected at four time points during exponential phase and assayed for  $\beta$ -gal activity. Data were normalized to  $\sigma^E$  activity of WT strain expressing cytochrome  $b_{562}$ . Data shown are the averages ( $\pm$  SD) of three independent experiments. **(B)** Comparison of  $\sigma^E$  activation strengths of natural OMPs with OmpC carrying matched YxF C-terminus in  $\Delta rseB$  cells.  $\Delta rseB$  cells carried plasmids expressing cytochrome  $b_{562}$  (Cyt), a fusion of this protein to the C-terminal 50 residues of OmpC (Cyt-OmpC<sub>50</sub>(YQF); YQF), or its variants with C-terminal motifs YRF, YKF, YSF, YAF, and a fusion of cytochrome  $b_{562}$  to ~50 C-terminal residues of OmpX, MipA, OmpG, or FadL. Cells were grown to OD<sub>600</sub> ~0.1 and induced with 0.003mM IPTG. Samples were collected at four time points during exponential phase and assayed for  $\beta$ -gal activity. Data were normalized to  $\sigma^E$  activity of  $\Delta rseB$  strain expressing cytochrome  $b_{562}$ . Data shown are the averages ( $\pm$  SD) of three independent experiments. (*Inset*) To show clear difference in the  $\sigma^E$  activation strengths of OmpG and YSF fusion proteins in  $\Delta rseB$  strain,  $\beta$ -gal activity was measured following protein expression with 0.02 mM IPTG.

We examined the DegS activation parameters of the OmpX<sub>20</sub> and OmpC<sub>20</sub> fusion proteins. As OmpX<sub>20</sub> activated WT cells 2-fold better than OmpC<sub>20</sub>, but was equivalent to OmpC<sub>20</sub> in activating in  $\Delta rseB$  cells, their differential activation of  $\sigma^E$  *in vivo* is attributed to differential antagonism of RseB (Fig. 6A,B). In an *in vitro* assay measuring DegS cleavage of the periplasmic domain of RseA, both OmpC<sub>20</sub> and OmpX<sub>20</sub> peptides supported roughly equal rates of DegS cleavage at peptide concentrations below 5  $\mu$ M, with the OmpC<sub>20</sub> peptide showing higher activity at saturating concentrations (Fig. 6C). These results are consistent with our hypothesis that the induction potential of OmpX<sub>20</sub> *in vivo* reflects stronger antagonism of RseB, as OmpX is not better than OmpC at activating DegS *in vitro*. Importantly, OmpX<sub>20</sub> did not antagonize RseB repression of RseA cleavage *in vitro* (Fig. 6D). Therefore, relief of RseB inhibition is not mediated via direct binding by OmpX<sub>20</sub> to RseB, and likely requires additional regulatory components not present in our biochemical assays (see below and Discussion).

**OMPs generate two  $\sigma^E$  induction signals *in vivo*.** If OMP accumulation *in vivo* activates DegS and also induces a second signal that antagonizes RseB, then OMP accumulation might activate  $\sigma^E$  in a DegS variant unable to bind OMP peptides (DegS $\Delta$ PDZ). We previously found that overexpression of OmpC<sub>50</sub> did not alter DegS $\Delta$ PDZ activity *in vivo* (11). Here, we tested whether OmpX<sub>50</sub>, a strong antagonist of RseB, activated  $\sigma^E$  in a DegS $\Delta$ PDZ strain. Indeed, in DegS $\Delta$ PDZ, overexpression of OmpX<sub>50</sub> induced  $\sigma^E$  activity ~2-fold, whereas overexpression of OmpC<sub>50</sub> did not alter  $\sigma^E$  activity (Fig. 7). This result is consistent with the idea that some OMPs induce a second signal *in vivo* that antagonizes RseB inhibition.



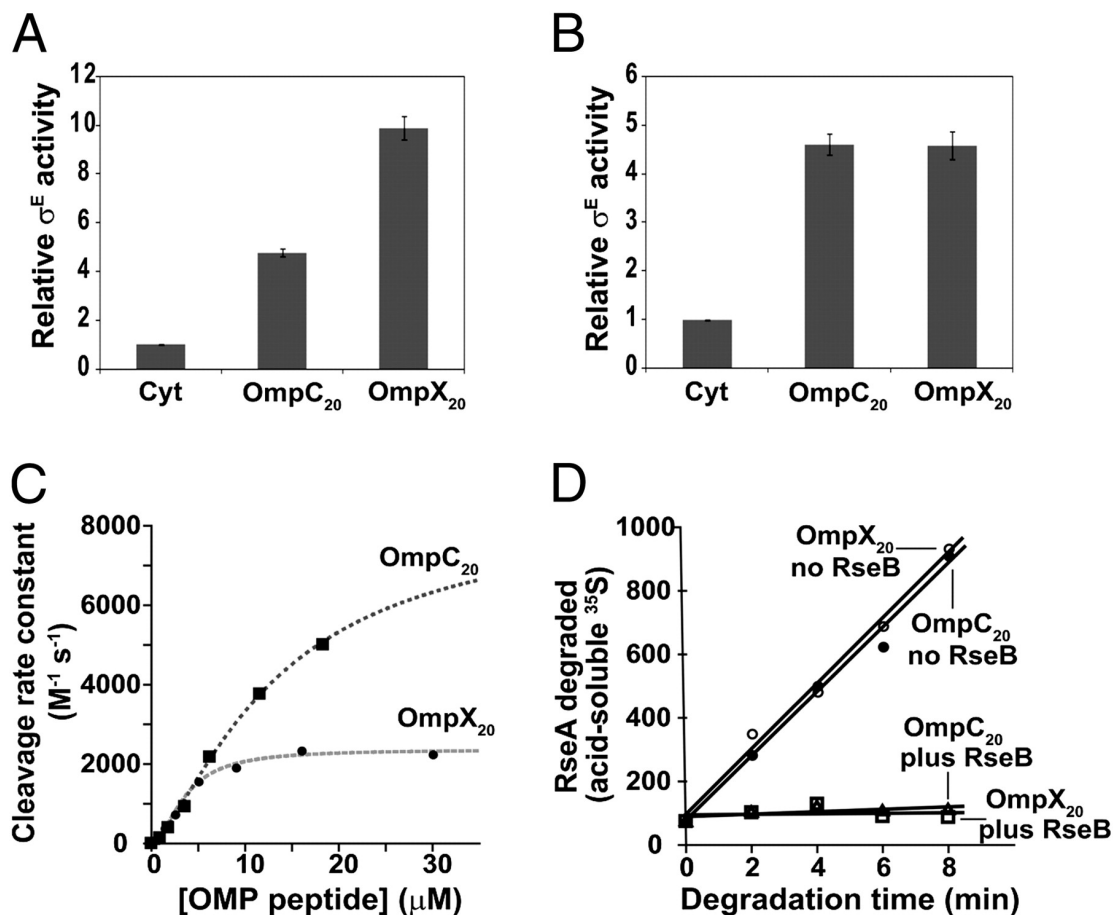


**Figure 6.** Comparison of  $\sigma^E$  activation, DegS activation, and RseB inactivation strengths of OmpC<sub>20</sub> and OmpX<sub>20</sub>. **(A)**  $\sigma^E$  activation of WT cells by OmpC<sub>20</sub> and OmpX<sub>20</sub>. Cells carrying plasmids for cytochrome b<sub>562</sub> (Cyt), a fusion of this protein to the C-terminal 20 residues of OmpC (OmpC<sub>20</sub>) or OmpX (OmpX<sub>20</sub>) were grown to OD<sub>600</sub> ~0.1 and induced with 1 mM IPTG. Samples were collected at four time points during exponential phase and assayed for  $\beta$ -gal activity. Data were normalized to  $\sigma^E$  activity of WT strain expressing cytochrome b<sub>562</sub>. Data shown are the averages ( $\pm$  SD) of three independent experiments. **(B)**  $\sigma^E$  activation of  $\Delta rseB$  cells by OmpC<sub>20</sub> and OmpX<sub>20</sub>. Cells carrying plasmids mentioned in Fig. 6A were grown to OD<sub>600</sub> ~0.1.  $\beta$ -gal activity was measured under basal protein expression. Data were normalized to  $\sigma^E$  activity of  $\Delta rseB$  strain expressing cytochrome b<sub>562</sub>. Data shown are the averages ( $\pm$  SD) of three independent experiments. **(C)** Rates of cleavage *in vitro* of  $^{35}\text{S}$ -RseA<sup>121-261</sup> (100  $\mu\text{M}$ ) by DegS (0.5  $\mu\text{M}$  trimer) were determined in the presence of different concentrations of the OmpX<sub>20</sub> or OmpC<sub>20</sub> peptides. Data were fit to the Hill equation. For the OmpX<sub>20</sub> peptide, half-maximal stimulation was observed at a peptide concentration of 3.6  $\mu\text{M}$ , and the maximal degradation rate constant was 2350  $\text{M}^{-1}\text{s}^{-1}$ . For the OmpC<sub>20</sub> peptide, half-maximal stimulation was achieved at a peptide concentration of 10  $\mu\text{M}$ , and the maximal degradation rate constant was 6860  $\text{M}^{-1}\text{s}^{-1}$ . **(D)** Kinetics of the cleavage *in vitro* of  $^{35}\text{S}$ -RseA<sup>121-261</sup> (31  $\mu\text{M}$ ) by DegS (0.84  $\mu\text{M}$  trimer) was assayed using the OmpX<sub>20</sub> or OmpC<sub>20</sub> peptides (6.5  $\mu\text{M}$ ) with RseB present (33  $\mu\text{M}$ ) or absent. The lines are linear fits.

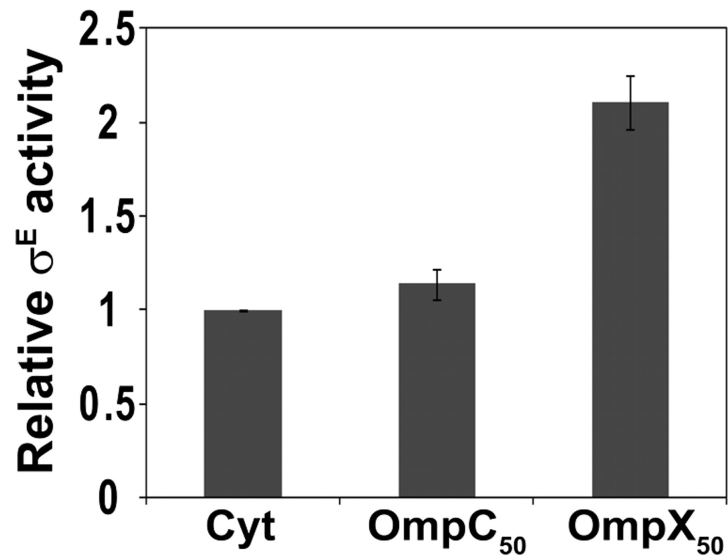


**Figure 7.** OmpX fusion protein induces  $\sigma^E$  in a DegS $\Delta$ PDZ strain.

Strains carrying DegS $\Delta$ PDZ on the chromosome as the sole copy of DegS carried plasmids expressing cytochrome *b*<sub>562</sub> (Cyt), and a fusion of this protein to the C-terminal 50 residues of OmpC (OmpC<sub>50</sub>), or OmpX (OmpX<sub>50</sub>). Cells were grown to OD<sub>600</sub> ~0.1 and induced with 1 mM IPTG. Samples were collected at four time points during exponential phase and assayed for  $\beta$ -gal activity. Data were normalized to  $\sigma^E$  activity of strain expressing cytochrome *b*<sub>562</sub> and represent averages ( $\pm$  SD) of three independent experiments.

## Discussion

We have dissected the intertwined roles of DegS and RseB in control of the  $\sigma^E$ -response. Our results discriminate between two models for allosteric activation of DegS, and show that DegS and RseB serve as joint gate-keepers for the response. Perturbing either gatekeeper leads to minor induction of the  $\sigma^E$ -response but joint perturbation leads to complete derepression. Two events are thus required for maximal  $\sigma^E$ -response, (i) OMP activation of DegS, and (ii) relief of RseB inhibition by an envelope signal. We argue that the use of an AND gate enables the cell to simultaneously sense and integrate multivariate envelope signals.

**Activation of DegS *in vivo*.** There are two competing models for the role of the PDZ domain in allosteric activation of DegS. In the ‘peptide-activation’ model, the PDZ domain positions a bound OMP peptide, allowing its penultimate side chain to contact the protease domain and alter the conformation or dynamics of the active site to increase activity of DegS (10, 25). Conversely, in the ‘inhibition-relief’ model, the unliganded PDZ domain stabilizes the inactive conformation of the protease domain, and OMP-peptide binding relieves these inhibitory interactions (11-13, 24). Our *in vivo* results provide two lines of evidence that support the inhibition-relief model. First, weakening the PDZ/protease interface increases rather than decreases DegS activity. K243D eliminates a salt-bridge between the PDZ and protease domains (13), and has 3-fold higher basal  $\sigma^E$  activity and 4-5 fold higher peptide stimulated  $\sigma^E$  activity compared to WT DegS (Fig. 2B and Fig. S2A). Importantly, K243D does not increase activity in the context of DegS $\Delta$ PDZ (Fig. S2B), as expected if K243 exerts its effect solely by altering the PDZ/protease interface. Mutations such as H198P, which stabilize the active conformation of DegS (24, 26), provide a second line of evidence that the PDZ domain is inhibitory. H198P increases  $\sigma^E$  activity both in strains containing DegS $\Delta$ PDZ, which does not bind OMP peptides, and WT DegS (Fig. 2B and Fig. S2A,B). In summary, our results

indicate that the behavior of DegS *in vivo* is consistent with the predictions of the “inhibition relief” model for allosteric activation of DegS.

**Relief of RseB inhibition requires a second signal.** The role of OMP peptides in activating DegS has been well characterized (12, 13, 24). Here we show that OMP peptides also antagonize RseB inhibition. OMP amino acids between 10 and 20 residues from the C-terminus are uniquely required for  $\sigma^E$  induction in the presence of RseB (Fig. 4). OMP peptides differ in their ability to antagonize RseB (Fig. 5 and Fig. 6A,B), just as they differ in their ability to activate DegS. Moreover, the OmpX peptide, identified as more proficient at RseB antagonism can induce  $\sigma^E$  even in a DegS variant that lacks the OMP docking domain (DegS $\Delta$ PDZ), whereas the OmpC peptide, which is less proficient at RseB antagonism cannot (Fig. 7). Taken together, these results argue that OMP peptides play a dual role in inducing the  $\sigma^E$  response, both activating DegS and relieving RseB inhibition.

How might OMPs generate a signal that antagonizes RseB *in vivo*? Our results argue strongly that they generate this signal indirectly, as OmpX is not able to antagonize RseB inhibition in an *in vitro* cleavage system (Fig. 6D). Because RseB is structurally similar to the LolA, LolB, and LppX lipid-binding proteins (22, 23), the RseB signal is most likely a lipophilic compound such as a periplasmic lipid, lipoprotein, or LPS. Intriguingly, there is a connection between OMP and LPS assembly. The  $\beta$ -barrel assembly machinery (BAM complex) is necessary to insert both OMPs and LptD, the critical player in LPS assembly, into the OM (27-31). Accumulation of OMPs in the periplasm could therefore titrate the BAM machinery away from LptD. Decreased levels of LptD would reduce LPS insertion at the OM resulting in its accumulation in the periplasm, which could signal the  $\sigma^E$  pathway via RseB. This model is consistent with the previous data that changes in LPS structure induce  $\sigma^E$  response (32, 33). We are currently testing whether defects in LPS synthesis/transport activate  $\sigma^E$  in an RseB-dependent manner.

**The output regime of the  $\sigma^E$  pathway.** To provide an optimal response to inducing signals, signal-transduction pathways must sense signals over a wide concentration range, but at the same time discriminate between “stressed” and “unstressed” conditions. The *E. coli*  $\sigma^E$  pathway achieves this distinction by employing an AND gate to trigger the system. A robust response requires both activating DegS and antagonizing RseB inhibition. The synergistic nature of these two events is shown by differential  $\sigma^E$  induction by activated DegS variants with and without RseB. When RseB is present, these variants show only minor  $\sigma^E$  activation, but in the absence of RseB, each of these variants shows high  $\sigma^E$  induction, consistent with their demonstrated ability to cleave RseA in an *in vitro* assay (Fig. 2).

This dual requirement for  $\sigma^E$  induction is also evident in a physiological setting. Whereas high-level expression of a majority of YxF peptides failed to strongly activate  $\sigma^E$  in WT cells, even weak peptides could achieve significant  $\sigma^E$  induction in the absence of RseB (Fig. 3A,B). Thus, removal of RseB magnifies the effects of OMP activation of DegS. RseB can be viewed as a ‘noise-filtering gatekeeper’ that suppresses the contribution of noise in the signaling process, and improves the information quality of the stress signal. This effect of RseB could be explained if RseB and active DegS (stabilized by OMP peptide) compete for binding to RseA. In WT cells, a larger number of active DegS molecules and therefore higher peptide amounts would be required for RseA cleavage compared to  $\Delta rseB$  cells.

Use of an AND gate enables the cell to integrate multiple signals from the OM prior to committing to significant activation of  $\sigma^E$ . Whereas the DegS gatekeeper responds to an unfolded OMP signal, RseB is likely to respond to a lipid signal. Because the  $\sigma^E$  regulon encodes the machinery for assembly and insertion of both OM proteins and lipids, this signal integration would permit  $\sigma^E$  to finely tune production of OM biogenesis machinery to the stresses at hand.

## Acknowledgments

We thank Dr. Hana El-Samad and members of the Gross lab for helpful suggestions. This work was supported by National Institutes of Health Grants GM-036278-27 (to C.A.G) and AI-16982-31 (to R.T.S).

## Materials and Methods

**Media and antibiotics.** Luria-Bertani (LB) broth was prepared as described (34). When required, LB was supplemented with 100  $\mu\text{g/ml}$  ampicillin (Ap) or 20  $\mu\text{g/ml}$  chloramphenicol (Cm). IPTG was added to induce the expression of cytochrome b562-OMP-protein fusions from P<sub>trc</sub> promoter.

**Strains and plasmids.** Strains and plasmids used are listed in Table S1, and details of their construction are available upon request. The  $\Delta\text{rseB}$  strain carrying plasmids for strong  $\sigma\text{E}$ -activating OMP peptides and the  $\Delta\text{rseB}\Delta\text{degS}$  strain carrying plasmids for constitutively active DegS variants were unstable as glycerol stocks and lost  $\sigma\text{E}$  activity over time. Plasmids were freshly transformed to construct these strains.

**$\beta$ -galactosidase assays.**  $\sigma\text{E}$  activity was measured by monitoring  $\beta$ -galactosidase ( $\beta$ -gal) expression from a chromosomal  $\sigma\text{E}$ -dependent lacZ reporter gene in  $\Phi\lambda(\text{rpoHP3}::\text{lacZ})$ , as described (35-37). Cells were diluted from overnight cultures to OD<sub>600</sub> ~0.01 in LB and grown at 30°C. For single point assays, the sample was harvested at an OD<sub>600</sub> listed in the figure legends, and  $\sigma\text{E}$  activity was calculated as Miller units. For differential plots, several samples were collected between 0.1-0.4 OD<sub>600</sub>, and  $\beta$ -gal activity/0.5 ml cells was plotted against OD<sub>600</sub>. The slope of these plots is the differential rate of  $\beta$ -gal synthesis and was used as the

measure of  $\sigma$ E activity. All assays were performed at least twice and usually thrice to ensure reproducibility. For  $\beta$ -gal assays involving OMP fusions, the proteins were overexpressed with 1mM IPTG in WT cells and with low induction in  $\Delta$ rseB cells, enabling quantifiable  $\sigma$ E activity measurements within the linear range of each strain.

**Biochemical assays.** DegS variants (residues 27-355) with an N-terminal His6 tag and RseA (residues 121-216) with a C-terminal His6 tag were expressed and purified as described (12). RseB (residues 24-318) with a C-terminal Leu-Glu-His6 tag was expressed in *E. coli* strain X90(DE3) and purified by Ni<sup>++</sup>-NTA chromatography. The active dimeric fraction of RseB was separated from the inactive oligomeric fraction by gel-filtration chromatography and stored in 50 mM NaHPO<sub>4</sub> (pH 8.0), 200 mM NaCl, and 10% glycerol (21). The OmpX20 and OmpC20 peptides were synthesized by the MIT Biopolymers Laboratory and purified by reverse-phase HPLC; their molecular weights were confirmed by MALDI-TOF mass spectrometry. DegS cleavage of <sup>35</sup>S-labeled RseA<sub>121-216</sub> was performed as described and quantified by scintillation counting of cleavage products soluble in cold trichloroacetic acid (12).

## References

1. Sperandeo P, Deho G, & Polissi A (2009) The lipopolysaccharide transport system of Gram-negative bacteria. *Biochim Biophys Acta* 1791(7):594-602.
2. Bos MP, Robert V, & Tommassen J (2007) Biogenesis of the gram-negative bacterial outer membrane. *Annu Rev Microbiol* 61:191-214.
3. Silhavy TJ, Kahne D, & Walker S (2010) The bacterial cell envelope. *Cold Spring Harb Perspect Biol* 2(5):a000414.
4. Knowles TJ, Scott-Tucker A, Overduin M, & Henderson IR (2009) Membrane protein architects: the role of the BAM complex in outer membrane protein assembly. *Nat Rev Microbiol* 7(3):206-214.
5. Rhodius VA, Suh WC, Nonaka G, West J, & Gross CA (2006) Conserved and variable functions of the  $\sigma^E$  stress response in related genomes. *PLoS Biol* 4(1):e2.
6. Valentin-Hansen P, Johansen J, & Rasmussen AA (2007) Small RNAs controlling outer membrane porins. *Curr Opin Microbiol* 10(2):152-155.
7. Campbell EA, et al. (2003) Crystal structure of *Escherichia coli*  $\sigma^E$  with the cytoplasmic domain of its anti- $\sigma$  RseA. *Mol Cell* 11(4):1067-1078.
8. De Las Penas A, Connolly L, & Gross CA (1997) The  $\sigma^E$ -mediated response to extracytoplasmic stress in *Escherichia coli* is transduced by RseA and RseB, two negative regulators of  $\sigma^E$ . *Mol Microbiol* 24(2):373-385.
9. Missiakas D, Mayer MP, Lemaire M, Georgopoulos C, & Raina S (1997) Modulation of the *Escherichia coli*  $\sigma^E$  (RpoE) heat-shock transcription-factor activity by the RseA, RseB and RseC proteins. *Mol Microbiol* 24(2):355-371.



10. Wilken C, Kitzing K, Kurzbauer R, Ehrmann M, & Clausen T (2004) Crystal structure of the DegS stress sensor: How a PDZ domain recognizes misfolded protein and activates a protease. *Cell* 117(4):483-494.
11. Walsh NP, Alba BM, Bose B, Gross CA, & Sauer RT (2003) OMP peptide signals initiate the envelope-stress response by activating DegS protease via relief of inhibition mediated by its PDZ domain. *Cell* 113(1):61-71.
12. Sohn J, Grant RA, & Sauer RT (2007) Allosteric activation of DegS, a stress sensor PDZ protease. *Cell* 131(3):572-583.
13. Sohn J & Sauer RT (2009) OMP peptides modulate the activity of DegS protease by differential binding to active and inactive conformations. *Mol Cell* 33(1):64-74.
14. Akiyama Y, Kanehara K, & Ito K (2004) RseP (YaeL), an *Escherichia coli* RIP protease, cleaves transmembrane sequences. *EMBO J* 23(22):4434-4442.
15. Alba BM, Leeds JA, Onufryk C, Lu CZ, & Gross CA (2002) DegS and YaeL participate sequentially in the cleavage of RseA to activate the  $\sigma^E$ -dependent extracytoplasmic stress response. *Genes Dev* 16(16):2156-2168.
16. Chaba R, Grigorova IL, Flynn JM, Baker TA, & Gross CA (2007) Design principles of the proteolytic cascade governing the  $\sigma^E$ -mediated envelope stress response in *Escherichia coli*: keys to graded, buffered, and rapid signal transduction. *Genes Dev* 21(1):124-136.
17. Flynn JM, Levchenko I, Sauer RT, & Baker TA (2004) Modulating substrate choice: the SspB adaptor delivers a regulator of the extracytoplasmic-stress response to the AAA+ protease ClpXP for degradation. *Genes Dev* 18(18):2292-2301.
18. Kanehara K, Ito K, & Akiyama Y (2002) YaeL (EcfE) activates the  $\sigma^E$  pathway of stress response through a site-2 cleavage of anti- $\sigma^E$ , RseA. *Genes Dev* 16(16):2147-2155.
19. Cowan SW, *et al.* (1995) The structure of OmpF porin in a tetragonal crystal form. *Structure* 3(10):1041-1050.

20. Ahuja N, *et al.* (2009) Analyzing the interaction of RseA and RseB, the two negative regulators of the  $\sigma^E$  envelope stress response, using a combined bioinformatic and experimental strategy. *J Biol Chem* 284(8):5403-5413.
21. Cezairliyan BO & Sauer RT (2007) Inhibition of regulated proteolysis by RseB. *Proc Natl Acad Sci U S A* 104(10):3771-3776.
22. Wollmann P & Zeth K (2007) The structure of RseB: a sensor in periplasmic stress response of *E. coli*. *J Mol Biol* 372(4):927-941.
23. Kim DY, Jin KS, Kwon E, Ree M, & Kim KK (2007) Crystal structure of RseB and a model of its binding mode to RseA. *Proc Natl Acad Sci U S A* 104(21):8779-8784.
24. Sohn J, Grant RA, & Sauer RT (2009) OMP peptides activate the DegS stress-sensor protease by a relief of inhibition mechanism. *Structure* 17(10):1411-1421.
25. Hasselblatt H, *et al.* (2007) Regulation of the  $\sigma^E$  stress response by DegS: how the PDZ domain keeps the protease inactive in the resting state and allows integration of different OMP-derived stress signals upon folding stress. *Genes Dev* 21(20):2659-2670.
26. Sohn J, Grant RA, & Sauer RT (2010) Allostery is an intrinsic property of the protease domain of DegS: Implications for enzyme function and evolution *J Biol Chem*:In Press.
27. Bos MP, Tefsen B, Geurtsen J, & Tommassen J (2004) Identification of an outer membrane protein required for the transport of lipopolysaccharide to the bacterial cell surface. *Proc Natl Acad Sci U S A* 101(25):9417-9422.
28. Chng SS, Gronenberg LS, & Kahne D (2010) Proteins required for lipopolysaccharide assembly in *Escherichia coli* form a transenvelope complex. *Biochemistry* 49(22):4565-4567.
29. Hagan CL, Kim S, & Kahne D (2010) Reconstitution of outer membrane protein assembly from purified components. *Science* 328(5980):890-892.

30. Sperandeo P, *et al.* (2008) Functional analysis of the protein machinery required for transport of lipopolysaccharide to the outer membrane of *Escherichia coli*. *J Bacteriol* 190(13):4460-4469.
31. Wu T, *et al.* (2005) Identification of a multicomponent complex required for outer membrane biogenesis in *Escherichia coli*. *Cell* 121(2):235-245.
32. Klein G, Lindner B, Brabetz W, Brade H, & Raina S (2009) *Escherichia coli* K-12 Suppressor-free Mutants Lacking Early Glycosyltransferases and Late Acyltransferases: minimal lipopolysaccharide structure and induction of envelope stress response. *J Biol Chem* 284(23):15369-15389.
33. Tam C & Missiakas D (2005) Changes in lipopolysaccharide structure induce the  $\sigma^E$ -dependent response of *Escherichia coli*. *Mol Microbiol* 55(5):1403-1412.
34. Sambrook J, Fritsch, E.F., and Maniatis, T. (1989) *Molecular Cloning. A Laboratory Manual* (Cold Spring Harbor Laboratory Press, New York, NY).
35. Ades SE, Connolly LE, Alba BM, & Gross CA (1999) The *Escherichia coli*  $\sigma^E$ -dependent extracytoplasmic stress response is controlled by the regulated proteolysis of an anti- $\sigma$  factor. *Genes Dev* 13(18):2449-2461.
36. Mecsas J, Rouviere PE, Erickson JW, Donohue TJ, & Gross CA (1993) The activity of  $\sigma^E$ , an *Escherichia coli* heat-inducible sigma-factor, is modulated by expression of outer membrane proteins. *Genes Dev* 7(12B):2618-2628.
37. Miller JH (1972) *Experiments in molecular genetics* (Cold Spring Harbor Laboratory, NY).

## Supplemental Information

**RNA Isolation, cDNA Preparation, and Quantitative RT-PCR.** Cultures were grown in LB broth containing ampicillin at 30 °C to  $\sim 0.2$  OD<sup>600</sup>. Samples (8 mL) were harvested and added to ice-cold 5% water-saturated acid phenol in ethanol solution, centrifuged at  $6,600 \times g$  for 2 min, and the cell pellets were flash frozen in liquid nitrogen before storing at  $-80$  °C until required. RNA was extracted using the hot-phenol technique, with modifications. Briefly, cell pellets were resuspended in 500  $\mu$ L of lysis solution (40 mM of Na acetate, pH 4.6, 1% SDS, 20 mM of EDTA), and mixed with 1 mL of acid phenol. The samples were incubated at 65 °C for 5 min with intermittent vortexing, placed on ice for 5 min, and centrifuged at  $16,000 \times g$  for 10 min at 4 °C. The supernatant was extracted twice with phenol-chloroform, pre- cipitated with 2.5 volumes of 100% ethanol, and washed with 70% ethanol. The RNA pellet was air dried and resuspended in 85  $\mu$ L of RNase free water. Genomic DNA was then removed from the samples using Turbo DNA-free Turbo DNase Treatment according to the manufacturer's directions for rigorous DNase treatment (Applied Biosystems). cDNA was prepared for qRT-PCR as described (1), using 5  $\mu$ g of input RNA using the Invitrogen SuperScriptIII First Strand cDNA Synthesis system.

Quantitative RT-PCR reactions were carried out using Stratagene Brilliant II SYBR green master mix according to the manufacturer's directions (Agilent Technologies), and 6 pmol of each forward and reverse primer (Integrated DNA Technolo- gies). Real-time PCR was performed with a Stratagene Mx3000P sequence-detection system (Agilent Technologies). Data were analyzed as described (2) with *recA* and *gyrA* as references.

**Preparation of Periplasmic Extracts.** Cultures were grown in LB broth containing ampicillin and 5  $\mu$ g/mL FeCl<sub>2</sub> at 30°C. Peri- plasmic extracts were prepared as described (3).

Samples were loaded on 15% polyacrylamide gels (19:1 acrylamide) and gels were stained with Coomassie Blue.

1. Cummings CA, Bootsma HJ, Relman DA, Miller JF (2006) Species- and strain-specific control of a complex, flexible regulon by *Bordetella BvgAS*. *J Bact* 188:1775–1785.
2. Vandesompele J, et al. (2002) Accurate normalization of real-time quantitative RT-PCR data by geometric averaging of multiple internal control genes. *Genome Biol*, 3(7): RESEARCH0034.
3. Keiler KC, Sauer RT (1996) Sequence determinants of C-terminal substrate recognition by the Tsp protease. *J Biol Chem* 271:2589–2593.

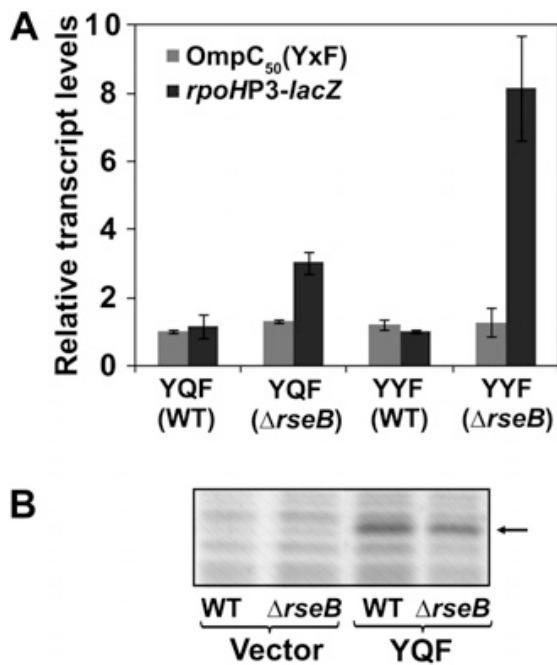


**Figure S1.** Differential  $\sigma^E$  activation in WT and  $\Delta rseB$  cells does not result from differential protein expression in the two strain backgrounds.

**(A)** Levels of YxF and lacZ transcripts under basal expression of YxF fusion proteins. WT and  $\Delta rseB$  cells carrying plasmids for YQF or YYF fusion proteins were grown to  $OD_{600} \sim 0.2$ . Samples were harvested for RNA isolation, cDNA was prepared, and transcript abundance was assayed by qRT-PCR. Data were normalized to the transcript levels in WT cells expressing YQF-fusion protein and represent averages ( $\pm$ SD) of three independent experiments.

**(B)** YQF-fusion protein levels upon high-level expression. WT and  $\Delta rseB$  cells carrying plasmid for YQF fusion were grown to  $OD_{600} \sim 0.1$ . Cultures were induced with 1 mM of IPTG, grown to  $OD_{600} \sim 0.3$ , and harvested. Periplasmic extracts were prepared as described and samples were run on SDS/PAGE.

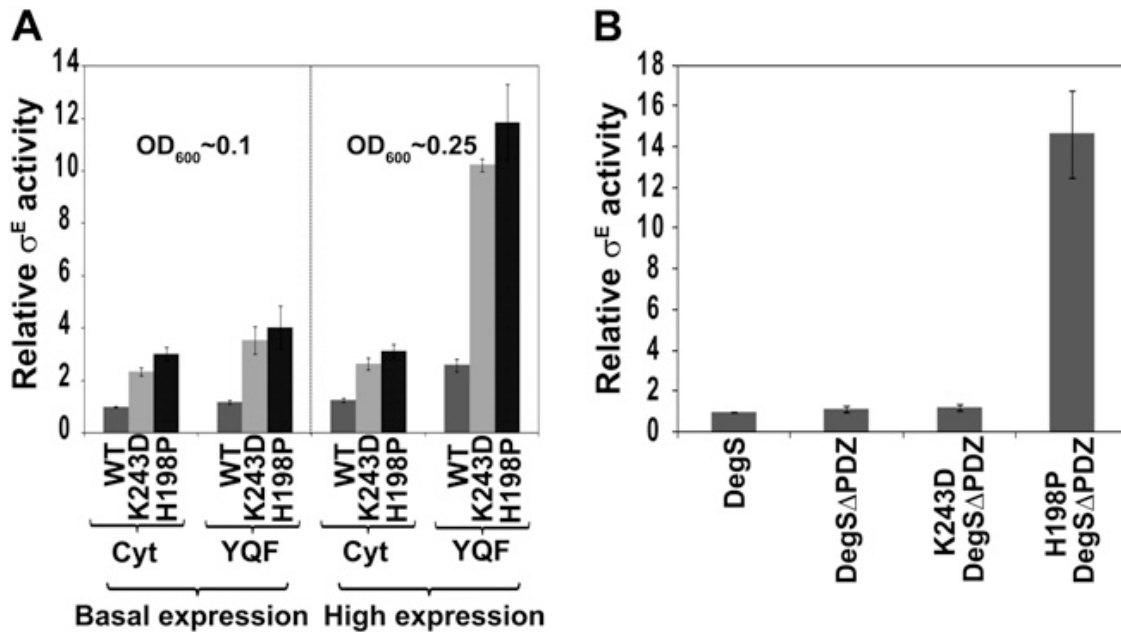


**Figure S2.** DegS activation in vivo follows the inhibition-relief model.

**(A)** Allosteric stabilization of proteolytically active DegS increases  $\sigma^E$  activation. All strains were  $\Delta degS$  and carried one plasmid for WT DegS, K243D DegS, or H198P DegS, and a second plasmid for cytochrome  $b_{562}$ (Cyt) or the YQF-fusion protein. Cells were grown to  $\sim 0.1$   $OD_{600}$  and a portion of each sample was harvested to determine  $\sigma^E$  activity resulting from basal YQF-fusion protein expression from  $P_{trc}$ . The remaining sample was induced with 0.02 mM of IPTG and harvested at  $\sim 0.25$   $OD_{600}$  to determine  $\sigma^E$  activity resulting from YQF-fusion protein over-expression. Data were normalized to the  $\sigma^E$  activity of the  $\Delta degS$  strain expressing WT DegS and cytochrome  $b_{562}$  from plasmids and represent averages ( $\pm$ SD) of three independent experiments. **(B)**  $\sigma^E$  activity of DegS $\Delta$ PDZ variants.  $\Delta degS$  strain carried plasmids for WT DegS, DegS $\Delta$ PDZ, K243D DegS $\Delta$ PDZ, or H198P DegS $\Delta$ PDZ. Cells were grown to  $OD_{600}$  of 0.1–0.15, and samples were harvested for  $\beta$ -gal assay. Data were normalized to the  $\Delta degS$  strain expressing WT DegS from the plasmid and represent averages ( $\pm$ SD) of three independent experiments.

## Supplemental Table S1. Strains and plasmids used in this study.

| Strains/plasmids | Relevant genotype   | Source/reference                         |
|------------------|---|--|
| <b>Strains</b>   |   |  |
| MC1061           | <i>araD</i> $\Delta$ ( <i>ara-leu</i> )7697 $\Delta$ ( <i>codB-lacI</i> ) <i>galk16 galE15 mcrA0 relA1 rpsL150 spoT1 mcrB9999 hsdR2</i> | (1); <i>E. coli</i> Genetic Stock Center |
| CAG16037         | MC1061 [ $\phi$ λ <i>rpoH P3::lacZ</i> ]  | (2)                                      |
| CAG22951         | 16037 $\Delta$ <i>rseB nadB-3140::Tn10</i> , Tet <sup>R</sup>   | (3)                                      |
| CAG33315         | MC1061 $\Delta$ <i>degS</i> $\phi$ λ[ <i>rpoH P3::lacZ</i> ]  | (4)                                      |
| CAG41001         | MC1061 <i>rpoE</i> <sup>*</sup> with suppressor of <i>rpoE::ΩCm</i>   | (5)                                      |
| CAG51025         | 22951 $\Delta$ <i>degS arg::Tn5</i> , Kan <sup>R</sup> , Tet <sup>R</sup>   | (6)                                      |
| CAG51050         | 16037 $\Delta$ <i>rseB nadB::Tn10</i> , Kan <sup>R</sup>  | (6)                                      |
| CAG53524         | 16037 <i>degS</i> $\Delta$ PDZ::Kan, Kan <sup>R</sup>   | This work                                |
| CAG64056         | 41001 pKD46, Ap <sup>R</sup>  | This work                                |
| <b>Plasmids</b>  |   |  |
| pACYC184         | Vector, p15A ori, Cm <sup>R</sup>   | (7)                                      |
| pBA131           | <i>degS</i> promoter and DegS in pACYC184, Cm <sup>R</sup>  | This work                                |
| pRC124           | <i>degS</i> promoter and DegS-S201A in pACYC184, Cm <sup>R</sup>  | This work                                |
| pRC130           | <i>degS</i> promoter and H198P DegS in pACYC184, Cm <sup>R</sup>  | This work                                |
| pRC131           | <i>degS</i> promoter and K243D DegS in pACYC184, Cm <sup>R</sup>  | This work                                |
| pTrc99a          | Vector, pBR322 ori, Ap <sup>R</sup>   | Amersham Pharmacia Biotech               |
| pBA169           | pTrc99a $\Delta$ NcoI, Ap <sup>R</sup>  | (8)                                      |
| pRC21            | cytochrome <i>b</i> <sub>562</sub> (Cyt) in pBA169, Ap <sup>R</sup>   | This work                                |
| pRC24            | Cyt-Tsx <sub>50</sub> in pBA169, Ap <sup>R</sup>  | This work                                |
| pRC37            | Cyt-OmpX <sub>50</sub> in pBA169, Ap <sup>R</sup>   | This work                                |
| pRC39            | Cyt-OmpT <sub>50</sub> in pBA169, Ap <sup>R</sup>   | This work                                |
| pRC40            | Cyt-OmpC <sub>50</sub> in pBA169, Ap <sup>R</sup>   | This work                                |
| pRC42            | Cyt-OmpG <sub>53</sub> in pBA169, Ap <sup>R</sup>   | This work                                |
| pRC43            | Cyt-MipA <sub>48</sub> in pBA169, Ap <sup>R</sup>   | This work                                |
| pRC44            | Cyt-YshA <sub>51</sub> in pBA169, Ap <sup>R</sup>   | This work                                |
| pRC46            | Cyt-FadL <sub>53</sub> in pBA169, Ap <sup>R</sup>   | This work                                |
| pRC58            | Cyt-OmpC <sub>50</sub> (YFF) in pBA169, Ap <sup>R</sup>   | This work                                |
| pRC61            | Cyt-OmpC <sub>50</sub> (YAF) in pBA169, Ap <sup>R</sup>   | This work                                |
| pRC64            | Cyt-OmpC <sub>50</sub> (YTF) in pBA169, Ap <sup>R</sup>   | This work                                |
| pRC65            | Cyt-OmpC <sub>50</sub> (YSF) in pBA169, Ap <sup>R</sup>   | This work                                |
| pRC66            | Cyt-OmpC <sub>50</sub> (YYF) in pBA169, Ap <sup>R</sup>   | This work                                |
| pRC68            | Cyt-OmpC <sub>50</sub> (YNF) in pBA169, Ap <sup>R</sup>   | This work                                |
| pRC72            | Cyt-OmpC <sub>50</sub> (YKF) in pBA169, Ap <sup>R</sup>   | This work                                |
| pRC73            | Cyt-OmpC <sub>50</sub> (YRF) in pBA169, Ap <sup>R</sup>   | This work                                |
| pRC76            | Cyt-YcbB <sub>51</sub> in pBA169, Ap <sup>R</sup>   | This work                                |
| pRC78            | Cyt-OmpC <sub>40</sub> in pBA169, Ap <sup>R</sup>   | This work                                |
| pRC79            | Cyt-OmpC <sub>30</sub> in pBA169, Ap <sup>R</sup>   | This work                                |
| pRC80            | Cyt-OmpC <sub>20</sub> in pBA169, Ap <sup>R</sup>   | This work                                |
| pRC81            | Cyt-OmpC <sub>10</sub> in pBA169, Ap <sup>R</sup>   | This work                                |
| pRC84            | Cyt-OmpX <sub>20</sub> in pBA169, Ap <sup>R</sup>   | This work                                |
| pRC107           | Cyt-OmpC <sub>20</sub> (YYF) in pBA169, Ap <sup>R</sup>   | This work                                |
| pRC108           | Cyt-OmpC <sub>10</sub> (YYF) in pBA169, Ap <sup>R</sup>   | This work                                |
| pBA191           | DegS-6His in pBA169, Ap <sup>R</sup>  | This work                                |
| pBA192           | DegS $\Delta$ PDZ-6His in pBA169, Ap <sup>R</sup>   | This work                                |
| pRC135           | K243D DegS $\Delta$ PDZ-6His in pBA169, Ap <sup>R</sup>   | This work                                |
| pRC136           | H198P DegS $\Delta$ PDZ-6His in pBA169, Ap <sup>R</sup>   | This work                                |
| pKD4             | FRT-flanked Kan <sup>R</sup> gene, pANTS $\gamma$ , Kan <sup>R</sup> , Ap <sup>R</sup>  | (9)                                      |
| pKD46            | <i>oriR101 repA101ts P<sub>araBAD</sub>-λred</i> , Ap <sup>R</sup>  | (9)                                      |

- Casadaban MJ, Cohen SN (1980) Analysis of gene control signals by DNA fusion and cloning in *Escherichia coli*. *J Mol Biol* 138:179–207.
- Mecas J, Rouviere PE, Erickson JW, Donohue TJ, Gross CA (1993) The activity of  $\sigma^E$ , an *Escherichia coli* heat-inducible  $\sigma$ -factor, is modulated by expression of outer membrane proteins. *Genes Dev* 7(12B):2618–2628.
- De Las Peñas A, Connolly L, Gross CA (1997) The  $\sigma^E$ -mediated response to extracytoplasmic stress in *Escherichia coli* is transduced by RseA and RseB, two negative regulators of  $\sigma^E$ . *Mol Microbiol* 24:373–385.
- Ades SE, Connolly LE, Alba BM, Gross CA (1999) The *Escherichia coli*  $\sigma^E$ -dependent extracytoplasmic stress response is controlled by the regulated proteolysis of an anti- $\sigma$  factor. *Genes Dev* 13:2449–2461.
- Alba BM, Zhong HJ, Pelayo JC, Gross CA (2001) *degS* (*hhoB*) is an essential *Escherichia coli* gene whose indispensable function is to provide  $\sigma^E$  activity. *Mol Microbiol* 40:1323–1333.
- GrigoroVA IL, et al. (2004) Fine-tuning of the *Escherichia coli*  $\sigma^E$  envelope stress response relies on multiple mechanisms to inhibit signal-independent proteolysis of the transmembrane anti- $\sigma$  factor, RseA. *Genes Dev* 18:2686–2697.
- Rose RE (1988) The nucleotide sequence of pACYC184. *Nucleic Acids Res* 16:355.
- Walsh NP, Alba BM, Bose B, Gross CA, Sauer RT (2003) OMP peptide signals initiate the envelope-stress response by activating DegS protease via relief of inhibition mediated by its PDZ domain. *Cell* 113:61–71.
- Datsenko KA, Wanner BL (2000) One-step inactivation of chromosomal genes in *Escherichia coli* K-12 using PCR products. *Proc Natl Acad Sci USA* 97:6640–6645.



## Chapter 2

# Dual Molecular Signals Mediate the Bacterial Response to Outer-Membrane Stress

**Contributing Authors:** Santiago Lima, Rachna Chaba, Carol A. Gross, Robert T. Sauer

*Citation:* Lima, S.<sup>†</sup>, Guo M.S.<sup>†</sup> et al. Dual molecular signals mediate the bacterial response to outer-membrane stress. *Science* (2013) vol. 340 (6134) pp. 837-41

<sup>†</sup>*These authors contributed equally to this work.*

## Preface:

In Chapter 1, I described the discovery of the role of RseB, which acts to prevent spurious  $\sigma^E$  activation *in vivo*, and must be inhibited by a separate, OMP-independent mechanism to fully induce  $\sigma^E$  [1]. However, what is the signal to inactivate RseB in the cell? In general, it is very difficult to identify the inducing signals of pathways, as these signals can take any form and are cannot be easily screened for. Importantly, our lab and the Bob Sauer lab (Santiago Lima) independently identified LPS as the putative signal that inactivates RseB. The following Chapter details our collaboration, which presents *in vitro* and *in vivo* evidence suggesting that defects in LPS assembly induce accumulation of off-pathway LPS species that directly bind RseB, dissociating RseB from RseA, thus permitting DegS cleavage of RseA. This work was published in *Science* (2013) vol. 340 (6134) pp. 837-41, where Santiago and I were co-first authors, with Santiago listed first.

Santiago, a postdoc in the Sauer lab, identified LPS as a signal using a biochemical approach, and performed all the biochemistry describing how LPS binds RseB to and dissociates the RseA/RseB interaction. I identified LPS in the chemical genomics screen that was performed by Robert Nichols and Athanasios Typas in the lab [2], this result was not included in the final ms, but is described further in the supplement (Supplemental Figure S13, p. 118). I performed the *in vivo* experiments to show that misassembly of LPS directly activates  $\sigma^E$  response. Rachna Chaba provided helpful advice, helped design experiments, and offered critical commentary on the manuscript. Carol, Bob, Santiago and I wrote the manuscript.

1. Chaba et al. Signal integration by DegS and RseB governs  $\sigma^E$ -mediated envelope stress response in *Escherichia coli*. *Proc Natl Acad Sci USA* (2011) vol. 108 (5) pp. 2106-11.
2. Nichols et al. Phenotypic landscape of a bacterial cell. *Cell* (2011) vol. 144 (1) pp. 143-56

## Abstract

In Gram-negative bacteria, outer-membrane integrity is essential for survival and is monitored by the  $\sigma^E$  stress-response system, which initiates damage-repair pathways. One activating signal is unassembled outer-membrane proteins. Using biochemical and genetic experiments in *Escherichia coli*, we found that off-pathway intermediates in lipopolysaccharide transport and assembly provided an additional required signal. These distinct signals, arising from disruptions in the transport and assembly of the major outer-membrane components, jointly determined the rate of proteolytic destruction of a negative regulator of the  $\sigma^E$  transcription factor, thereby modulating the expression of stress-response genes. This dual-signal system permits a rapid response to dysfunction in outer-membrane biogenesis, while buffering responses to transient fluctuations in individual components, and may represent a broad strategy for bacteria to monitor their interface with the environment.

## Main Text:

The outer membrane (OM) is essential for survival of Gram-negative bacteria. In *Escherichia coli*, the  $\sigma^E$  stress-response system recognizes signals indicative of OM dysfunction and triggers an adaptive response by activating expression of gene products involved in the biogenesis, transport, and/or assembly of the lipopolysaccharides (LPS), phospholipids, and outer-membrane proteins (OMPs) that comprise the OM, as well as the proteases and chaperones that maintain or repair OM integrity (1-3). In this stress-response system, the  $\sigma^E$  transcription factor, the RseA and RseB negative regulatory proteins, and the DegS and RseP inner-membrane (IM) proteases mediate signal transduction (Fig. S1) (4-7). RseA, a single-pass IM protein, has a cytoplasmic domain (RseA<sup>C</sup>) that binds and inhibits  $\sigma^E$  and a periplasmic domain (RseA<sup>P</sup>) that binds RseB (4,5,8-11). Following stress, OMPs accumulate in the periplasm and their C-terminal residues bind to the DegS protease and activate cleavage of RseA<sup>P</sup>, triggering a proteolytic cascade that frees  $\sigma^E$  to activate gene expression (7,9,12-15). However, a signal that inhibits RseB is also required, because RseB binding to RseA<sup>P</sup> prevents activated DegS from cleaving RseA (9,10,16). The RseB-inhibition signal has not been characterized but may be related to LPS, because the  $\sigma^E$  response is activated by alterations in LPS structure (17,18), and a lipid-binding domain in RseB binds RseA (11). Here we test and provide evidence for a model in which intermediates in LPS transport and assembly are the necessary second signal that activates the  $\sigma^E$  response.

**LPS antagonizes RseA•RseB binding in vitro.** To test the hypothesis that LPS binds RseB and competes for RseA<sup>P</sup> binding, we developed an assay to determine if LPS dissociates <sup>35</sup>S-RseB from RseA<sup>P</sup>-agarose. We established that <sup>35</sup>S-RseB was efficiently eluted from RseA<sup>P</sup>-agarose by unlabeled RseB and by RseA<sup>P</sup> but not by unrelated control proteins or an abundant bacterial phospholipid (Fig. 1A). LPS purified from a wild-type *E. coli* K-12 strain had

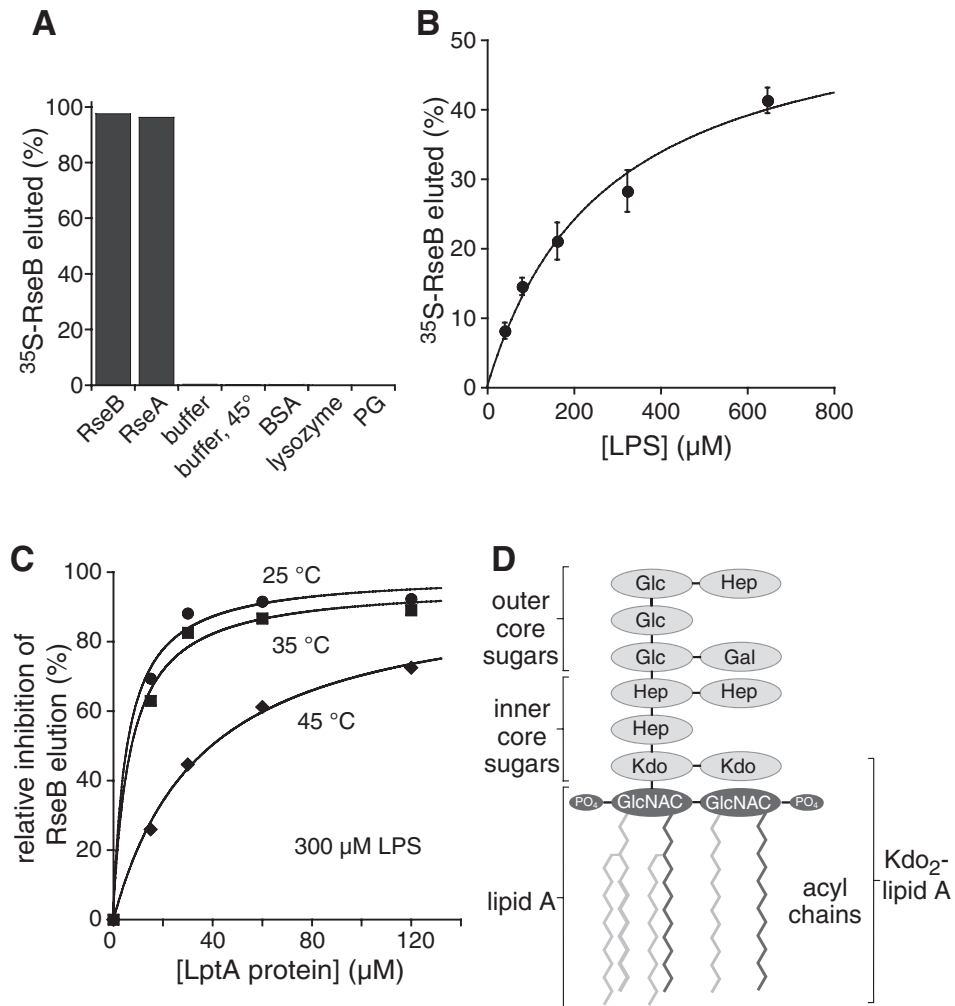


**Figure 1.** LPS displaces RseA from RseB.

(A) Unlabeled RseB (35  $\mu\text{M}$ ) and RseA<sup>P</sup> (100  $\mu\text{M}$ ) efficiently eluted  $^{35}\text{S}$ -RseB (~1  $\mu\text{M}$  total) from an RseA<sup>P</sup>-agarose column, whereas buffer, buffer at 45 °C, bovine serum albumin (BSA; 125  $\mu\text{M}$ ), hen egg lysozyme (125  $\mu\text{M}$ ), or phosphatidylglycerol (PG; 13 mM) eluted less than 0.3% of the radioactivity bound to the column. (B) Purified LPS eluted  $^{35}\text{S}$ -RseB from RseA<sup>P</sup>-agarose at 25 °C. Data are plotted as mean  $\pm$  SD ( $N=3$ , where each replicate was a different purified preparation of LPS). The line is a hyperbolic fit with an apparent interaction constant of 270  $\mu\text{M}$ . (C) LptA inhibited RseB elution by LPS (300  $\mu\text{M}$ ) more efficiently at 25 and 35 °C than at 45 °C. ~40  $\mu\text{M}$  LptA inhibited most of the RseB elution activity of ~300  $\mu\text{M}$  LPS. This sub-stoichiometric inhibition probably arises because only a fraction of LPS is monomeric and able to bind RseB or LptA. LPS was purified from *E. coli* strain CGSC5073 (Yale Coli Genetic Stock Center), a wild-type K12 strain with respect to LPS biosynthesis. (D) LPS consists of lipid A and inner and outer core sugars (GlcNAC, N-acetylglucosamine; Kdo, keto-deoxyoctulosonate; Hep, heptose; Gal, galactose; Glc, glucose) in wild-type *E. coli* K-12 strains. Experiments in this paper show that the structural elements colored dark gray are sufficient for RseB binding.

RseB-elution activity (Fig. 1B), as did LPS variants purified from various mutant strains (Fig. S2, S3).

LptA binds LPS and is part of the periplasmic bridge that shuttles LPS from the IM to the OM (19). Increasing concentrations of purified LptA inhibited LPS elution of RseB from RseA<sup>P</sup>-agarose (Fig. 1C), indicating that LptA and RseB compete for LPS binding. RseB competed more efficiently for LPS binding at 45 °C, a temperature that activates the cellular  $\sigma^E$  response, than at lower temperatures (Fig. 1C), suggesting that altered competitive binding could contribute to  $\sigma^E$  activation.

**Minimal LPS fragments bind RseB and facilitate cleavage of RseA.** We sought to test whether fragments of LPS containing lipid-A or di-[keto-deoxyoctulosonate]-lipid A (Kdo<sub>2</sub>-lipid-A; Fig. 1D) were sufficient for RseB interactions, but both molecules had much lower solubilities than native LPS, precluding interpretation of biochemical studies. However, NaOH hydrolysis of lipid A or Kdo<sub>2</sub>-lipid A, a treatment that partially remove acyl chains, improved solubility and allowed purification of active fragments (called L-IIA and Kdo<sub>2</sub>-L-IIA) with masses expected for retention of the two N-linked acyl chains of the original molecules but hydrolytic loss of all four O-linked acyl chains (Fig. 2A; Fig. S4). Kdo<sub>2</sub>-L-IIA was only slightly more active than L-IIA (Fig. 2B), indicating that the additional Kdo sugars in Kdo<sub>2</sub>-L-IIA (see Fig. 1D) made minor contributions to RseB elution. Derivatives of lipid A devoid of acyl chains had no RseB-elution activity. As observed with LPS, LptA inhibited the RseB-elution activity of Kdo<sub>2</sub>-L-IIA, with inhibition being less efficient at higher temperature (Fig. 2C). Thus, any LPS derivative that contains the phosphorylated GlcNAC disaccharide and N-linked acyl chains of the lipid-A moiety (colored dark gray in Fig. 1D) appears to bind RseB and displace RseA<sup>P</sup>.

Although not metabolically relevant, L-IIA and Kdo<sub>2</sub>-L-IIA were useful LPS surrogates because they did not scatter light, permitting the use of fluorescence anisotropy to monitor RseB binding (9). L-IIA dissociated a complex of fluorescent RseA<sup>P</sup> (fl-RseA<sup>P</sup>) and RseB in a concentration-dependent manner but did not alter anisotropy of fl-RseA<sup>P</sup> alone (Fig. 2D),

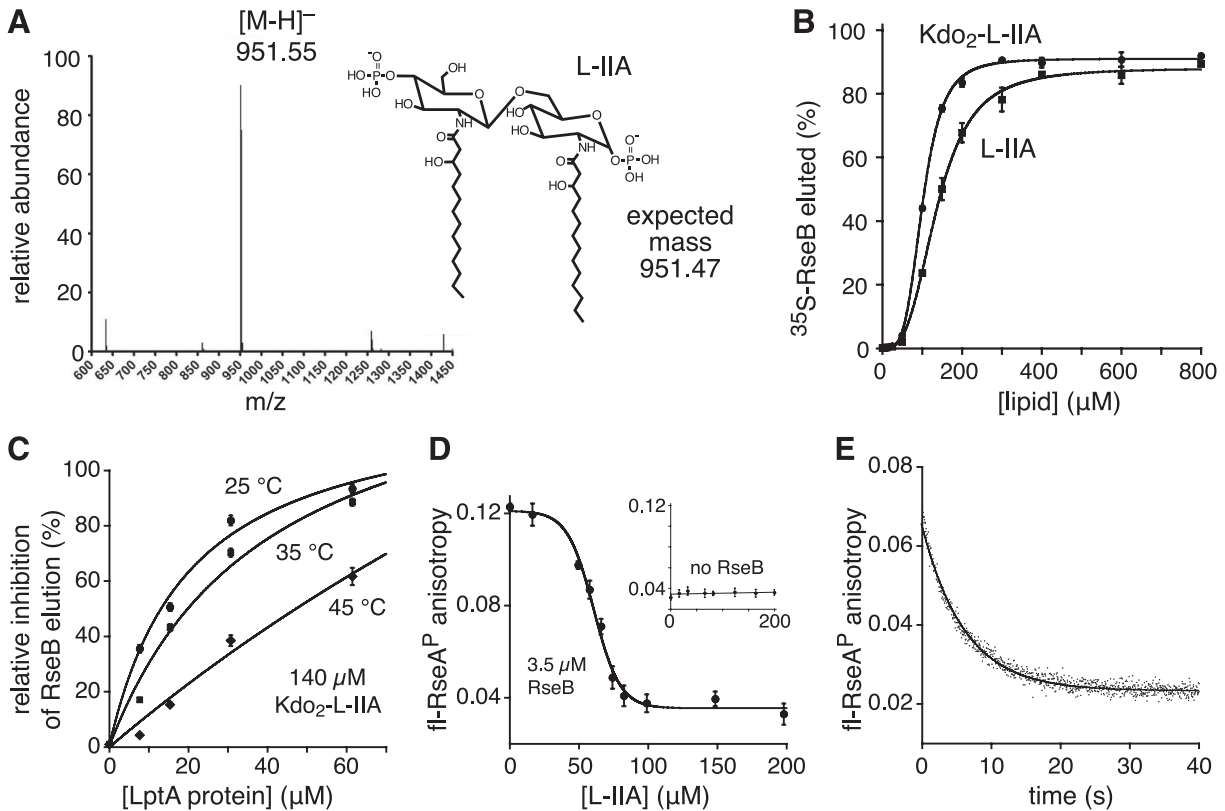


**Figure 2.** Partially acylated lipid-A fragments disrupt RseA<sup>P</sup>•RseB complexes.

**(A)** Mass spectrometry and expected structure of a purified fragment (L-IIA) produced by NaOH hydrolysis of lipid A. **(B)** L-IIA and Kdo<sub>2</sub>-L-IIA eluted  $^{35}\text{S}$ -RseB from RseA<sup>P</sup>-agarose (25 °C). Data were fit to a Hill equation ( $\text{max}/(1 + ([\text{lipid}]/K_{\text{app}})^h)$ ), resulting in  $K_{\text{app}}$  values of  $\sim 140 \mu\text{M}$  (L-IIA;  $h = 3.1$ ) and  $\sim 100 \mu\text{M}$  (Kdo<sub>2</sub>-L-IIA;  $h = 3.9$ ). Data are plotted as mean  $\pm$  SEM ( $N=2$ ). **(C)** In the presence of Kdo<sub>2</sub>-L-IIA (140  $\mu\text{M}$ ), increasing concentrations of LptA decreased the elution of  $^{35}\text{S}$ -RseB from RseA<sup>P</sup>-agarose more efficiently at 25 and 35 °C than 45 °C. Data are plotted as mean  $\pm$  SEM ( $N=2$ ). **(D)** L-IIA competed for RseB (3.5  $\mu\text{M}$ ) binding to fl-RseA<sup>P</sup> (60 nM). Data were fit to a competition equation ( $\text{min} + (\text{max}-\text{min})/(1 + 10^{(\log(\text{EC}_{50})-[\text{lipid}])\cdot h})$ ) (Prism), giving an  $\text{EC}_{50}$  of 65  $\mu\text{M}$ . Data are plotted as mean  $\pm$  SD ( $N=5$ ). Inset: Increasing L-IIA did not change the anisotropy of fl-RseA<sup>P</sup> (60 nM) in the absence of RseB. **(E)** A solution containing 5  $\mu\text{M}$  RseB (monomer equivalents) and 60 nM fl-RseA<sup>P</sup> was mixed with an equal volume of 5 mM L-IIA and fluorescence anisotropy was monitored as a function of time to follow dissociation. The solid line is a single-exponential fit with a rate constant of  $0.16 \text{ s}^{-1}$ .

confirming competition between L-IIA and fl-RseA<sup>P</sup> for RseB binding. Furthermore, increasing quantities of L-IIA raised the RseB concentration required for half-maximal fl-RseA<sup>P</sup> binding but did not change the maximal binding signal (fig. S5). Dissociation of the RseB•fl-RseA<sup>P</sup> complex was complete within 30 s of addition of L-IIA (Fig. 2E), a time rapid enough to account for the kinetics of the cellular  $\sigma^E$  response following a stress treatment (20).

Purified RseB is a mixture of dimers and tetramers, with only the dimer binding RseA (9,21). When we added L-IIA to freshly purified RseB dimers and immediately re-chromatographed the mixture, most protein co-eluted with L-IIA at a position expected for an RseB protein tetramer (Fig. 3A). L-IIA alone eluted from the column near the salt volume (Fig. S6). Thus, L-IIA binds directly to RseB, L-IIA complexes with RseB largely persist during the ~1 h required for chromatography, and L-IIA binding stabilizes RseB in a tetrameric state that does not bind RseA.

We tested the effects of RseB, L-IIA, and OMP peptide on DegS cleavage of RseA<sup>P</sup> in vitro (Fig. 3B). As expected (9), DegS alone did not cleave RseA<sup>P</sup>, addition of OMP peptide activated cleavage and further addition of RseB inhibited this cleavage. However, addition of L-IIA to OMP peptide restored robust DegS cleavage of RseA<sup>P</sup> in the presence of RseB. Other combinations did not restore cleavage, and L-IIA alone did not activate DegS, confirming that it acts as an RseB-inhibition signal.

**LPS plays an evolutionarily conserved role.** Most  $\gamma$  and  $\beta$  proteobacteria have RseA, RseB, and DegS orthologs, with MucA, MucB, and AlgW being their functional equivalents in *Pseudomonas aeruginosa*, a distant relative of *E. coli* (21). We tested the generality of our findings by examining the interaction of *E. coli* LPS fragments with the *P. aeruginosa* proteins. L-IIA converted MucB dimers to tetramers (Fig. 3C) and eluted <sup>35</sup>S-MucB from a MucA<sup>P</sup>-affinity column (Fig. 3D), supporting conservation of an LPS-mediated displacement mechanism. L-IIA also allowed OMP-activated AlgW to cleave MucA in the presence of MucB (Fig. 3E). Thus, in both the *E. coli* and *P. aeruginosa* systems, the combination of an LPS molecule and an OMP



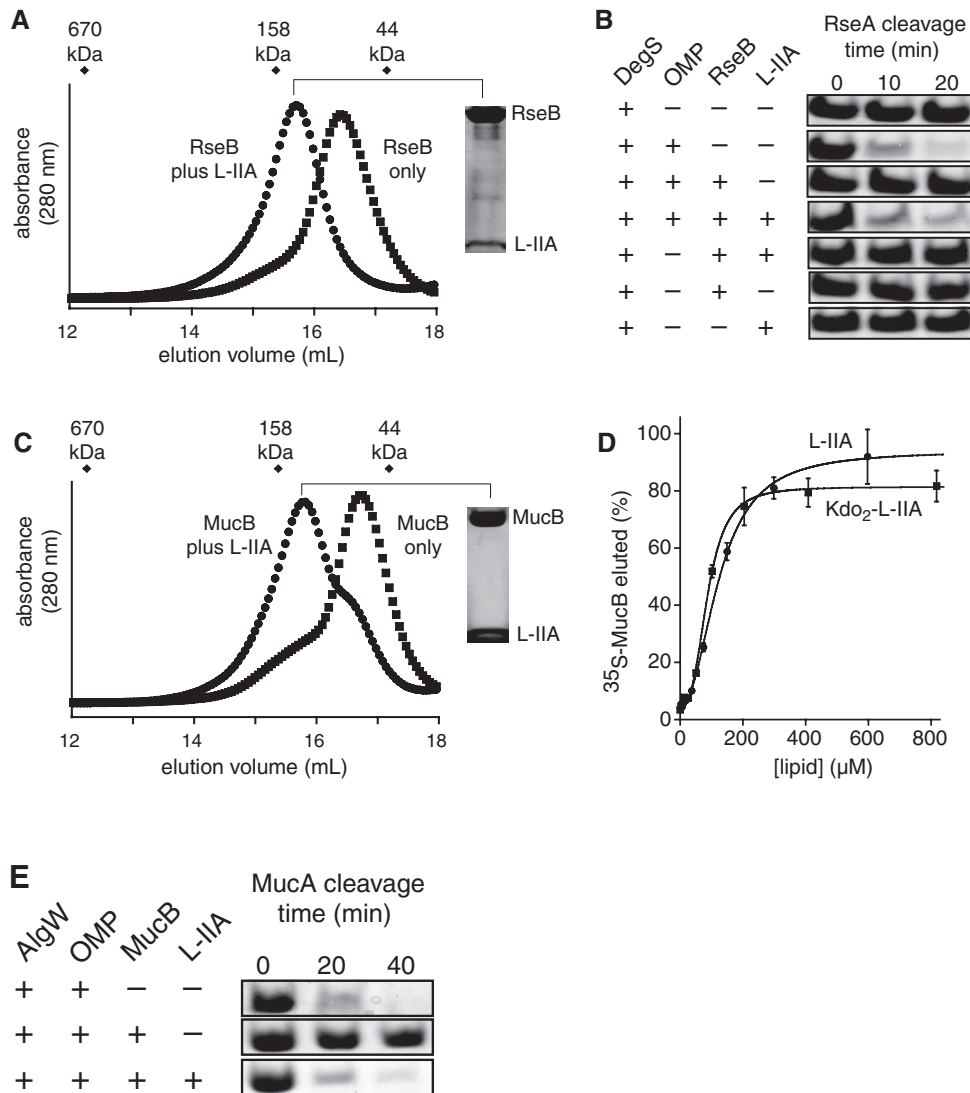


**Figure 3.** Lipid-A fragments bind RseB/MucB and coactivate cleavage of RseA<sup>P</sup>/MucA<sup>P</sup>.

(A) Addition of L-IIA (2 mM) to freshly purified RseB dimer (loading concentration 180  $\mu\text{M}$ ) changed the elution position on a gel-filtration column to one expected for a tetramer (~143 kDa). SDS-PAGE and silver staining of the “tetramer” peak fraction showed co-elution of RseB and L-IIA. Gels across the entire included volume are shown in fig. S6. (B) SDS-PAGE assay of RseA<sup>P</sup> (40  $\mu\text{M}$ ) degradation by DegS (4  $\mu\text{M}$  trimer) in the presence or absence of RseB (40  $\mu\text{M}$  monomer), OMP peptide (200  $\mu\text{M}$ ), and L-IIA (2 mM). (C) Addition of L-IIA (2 mM) to freshly purified MucB dimer (loading concentration 180  $\mu\text{M}$ ) resulted in elution of most protein as a tetramer on a gel-filtration column, although a dimeric shoulder was still evident. SDS-PAGE and silver staining of the “tetramer” peak fraction showed co-elution of MucB and L-IIA. (D) L-IIA and Kdo<sub>2</sub>-L-IIA eluted  $^{35}\text{S}$ -MucB from MucA<sup>P</sup>-agarose. Data were fit to a Hill equation ( $c + \max/(1 + ([\text{lipid}]/K_{\text{app}})^n)$ ), with  $K_{\text{app}}$  values of ~120  $\mu\text{M}$  (L-IIA) and 83  $\mu\text{M}$  (Kdo<sub>2</sub>-L-IIA). Data are plotted as mean  $\pm$  SD ( $N=3$ ). (E) SDS-PAGE assay of MucA<sup>P</sup> (25  $\mu\text{M}$ ) degradation by AlgW (2  $\mu\text{M}$  trimer) in the presence or absence of MucB (40  $\mu\text{M}$  monomer), OMP peptide (75  $\mu\text{M}$ ), and L-IIA (2 mM).

peptide mimic the molecular signals that result in RseA/MucA cleavage in vivo by inactivating RseB/MucB and activating DegS/AlgW, respectively.

**$\sigma^E$  activation by wild-type and mutant LPS.** Our results predict that increases in the levels of periplasmic LPS should activate the cellular  $\sigma^E$  response. Following synthesis on the IM, LPS is shuttled over an Lpt protein bridge and inserted into the OM by the LptD/E translocon at the distal end of the bridge (22-25) (see Fig. 5). In the LptD <sup>$\Delta$ 330-352</sup> variant, the loss of key disulfide bonds results in fewer functional bridges and should cause accumulation of LPS in the periplasm (26-29). We found that the *lptD* <sup>$\Delta$ 330-352</sup> allele increased expression of a  $\beta$ -galactosidase reporter under  $\sigma^E$ -transcriptional control in a strain requiring RseB inhibition but no OMP signal (*degS* <sup>$\Delta$ PDZ</sup>) and in a strain requiring both RseB inhibition and an OMP signal (*degS*<sup>+</sup>) (Fig. 4A; Fig. S7). RseA cleavage neither requires nor is activated by OMPs in *degS* <sup>$\Delta$ PDZ</sup> cells because the autoinhibitory PDZ domain of DegS is missing, but RseB inhibition normally keeps  $\sigma^E$  activity low (9,16,30). Thus, increased  $\sigma^E$  activity in the *lptD* <sup>$\Delta$ 330-352</sup> *degS* <sup>$\Delta$ PDZ</sup> strain supports a model in which accumulation of periplasmic LPS relieves RseB inhibition. The activation of  $\sigma^E$  in *lptD* <sup>$\Delta$ 330-352</sup> *degS*<sup>+</sup> cells suggests that OMP intermediates also accumulate in this strain (12,16), probably as a consequence of defects in LPS assembly, as we discuss below.

As another method of reducing LptD function and slowing LPS transport, we decreased the level of properly disulfide-bonded LptD by deleting the DsbA disulfide oxidoreductase (26,28). Although the  $\Delta$ *dsbA* mutation affects many proteins in addition to LptD, it increased  $\sigma^E$  activity both in *degS* <sup>$\Delta$ PDZ</sup> and in *degS*<sup>+</sup> strains (Fig. S8).

Using *degS*<sup>+</sup> and *degS* <sup>$\Delta$ PDZ</sup> strains, we tested  $\sigma^E$  activity in a panel of 11 LPS-biosynthesis mutants to determine if they relieved RseB inhibition and/or activated DegS. The mutant LPS variants all contained the minimal RseB-interaction motif (Fig. S9). Nine mutants elevated  $\sigma^E$  activity in *degS*<sup>+</sup> and *degS* <sup>$\Delta$ PDZ</sup> strains (Fig. 4B,C), supporting a model in which activation is linked to LPS inhibition of RseB and to the generation of an OMP signal that

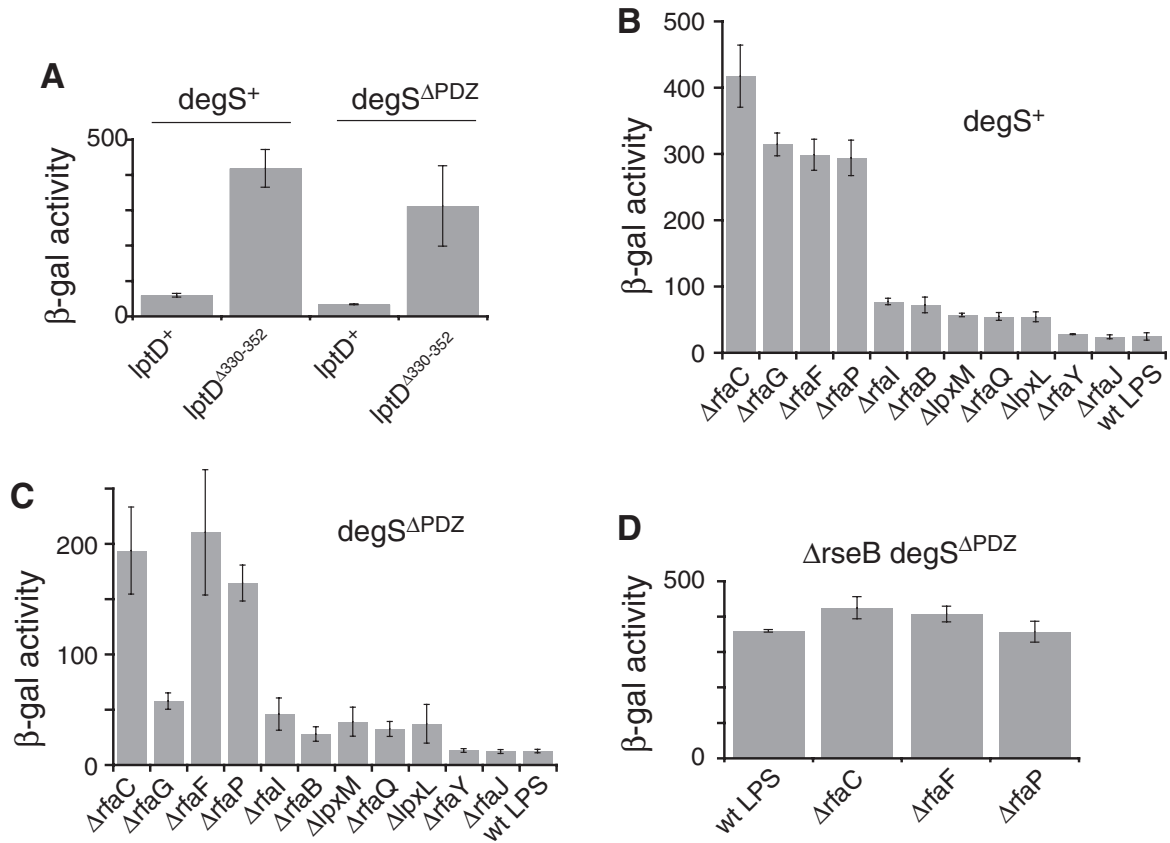


**Figure 4.** Effects of mutations affecting LPS OM insertion or biosynthesis on  $\sigma^E$  activation.

**(A)** The *lptD*<sup>Δ330-352</sup> mutation, which slows insertion of wild-type LPS into the OM, enhanced expression of a  $\sigma^E$ -dependent *rpoHp3-LacZ* reporter under non-stress growth conditions both in *degS*<sup>+</sup> and in *degS*<sup>ΔPDZ</sup> backgrounds. **(B)** Many mutations affecting LPS biosynthesis activated  $\sigma^E$  activity in a *degS*<sup>+</sup> strain. The structures of the major LPS variants produced in each strain are shown in fig. S9. **(C)**  $\sigma^E$  activation by LPS mutations in a *degS*<sup>ΔPDZ</sup> strain. The constitutively active *DegS*<sup>ΔPDZ</sup> enzyme has lower RseA-cleavage activity *in vitro* than the fully OMP-activated wild-type *DegS* enzyme (30), which probably accounts for the lower  $\sigma^E$  activities in *degS*<sup>ΔPDZ</sup> compared to the *degS*<sup>+</sup> strains in panel B (also, see fig. S10). **(D)**  $\sigma^E$  activities were similar in *ΔrseB degS*<sup>ΔPDZ</sup> strains producing wild-type LPS and some of the strongest LPS-biosynthesis mutations from panel C. In all panels, data are plotted as mean ± 1 SD (*N* ≥ 4).

activates DegS. In a  $\Delta rseB$   $degS^{APDZ}$  strain in which an OMP signal is not needed and negative regulation by RseB is abrogated, the most strongly inducing LPS biosynthesis mutations did not further activate  $\sigma^E$  (Fig. 4D). Thus, a major effect of these mutations appears to be relief of RseB inhibition. In general, mutant LPS molecules with the fewest core sugars and phosphates activated to the highest levels in  $rseB^+$  cells (Fig. 4B,C; Fig. S9). We propose that eliminating these polar groups results in accumulation of periplasmic LPS because of loss of synchrony between one or more discrete steps in LPS biosynthesis, transport, or OM insertion.

**RseB as a periplasmic LPS sensor.** Our results support a model in which LPS relieves RseB inhibition of RseA cleavage. Intact LPS or LPS fragments containing a portion of the lipid-A scaffold bind RseB and release RseA, allowing its cleavage by DegS. Functionally, detection of part of the lipid-A moiety of LPS ensures that RseB can sense and respond to many mislocalized LPS species, including wild-type LPS, incompletely synthesized LPS molecules that reach the periplasm, and LPS variants lacking O-linked acyl chains or core sugars that support *E. coli* viability but decrease the ability of the OM to protect against cytotoxic agents. Many mutations affecting LPS biosynthesis or OM insertion stimulate the  $\sigma^E$  response in an RseB-dependent fashion. By analogy with the activation observed when LPS transport was disrupted by partially disabling LptD, LPS-biosynthesis mutations that activate  $\sigma^E$  probably disrupt the coordination between biosynthesis, transport, and OM insertion in ways that increase periplasmic LPS (Fig. 5). During exponential growth, the flux of LPS through the periplasm is  $\sim 70,000$  molecules  $\text{min}^{-1}$ . Changes in the coordination of individual biogenesis and transport steps that diverted  $\sim 10\%$  of these molecules would result in a  $\sim 40$   $\mu\text{M min}^{-1}$  rise in periplasmic LPS (31). Likewise, environmental stress could affect the integrity or function of the Lpt machinery for LPS transport or OM insertion, causing periplasmic accumulation of LPS. Temperature stress might have additional direct effects. LptA, a key component of the transenvelope bridge (19), competed less efficiently with RseB for binding to LPS at  $45^\circ\text{C}$ ,

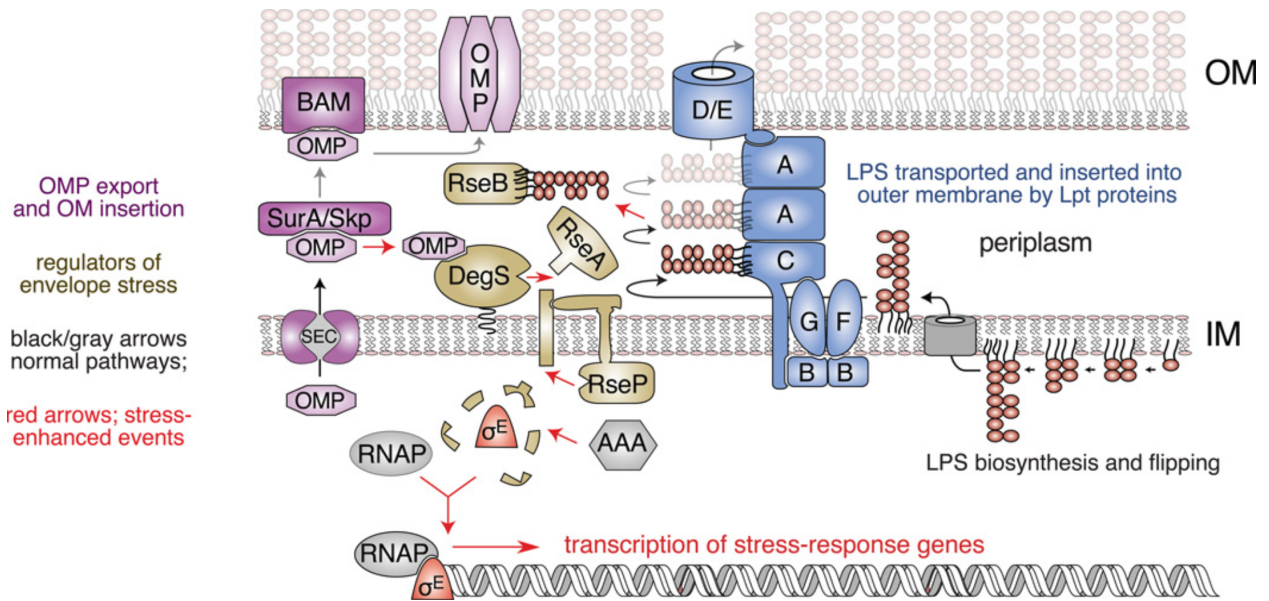


**Figure 5.** Dual-signal model for  $\sigma^E$  activation.

Stress interferes with the transport and/or OM insertion of LPS and OMPs, causing accumulation of these molecules in the periplasm. Periplasmic LPS competes for RseB binding, freeing RseA to be cleaved by OMP-activated DegS, which initiates the  $\sigma^E$  stress response. Thus, a combination of OMP and LPS signals is required for the transcriptional response that attempts to restore homeostasis to the bacterial envelope. Black or gray arrows show the normal pathways for LPS and OMP biogenesis, transport, and OM insertion. Red arrows show altered pathways or events caused by OM stress.

suggesting that heat shock facilitates transfer of LPS from LptA to RseB, providing a “feedforward” mechanism for  $\sigma^E$  activation.

**Dual-signal logic and  $\sigma^E$  control.** Two distinct signals are required for DegS cleavage of RseA when RseB is present in vitro. An OMP signal activates proteolysis by DegS, whereas an LPS signal prevents RseB from inhibiting cleavage of RseA. The importance of both signals is also clear in certain genetic backgrounds in vivo. For example, mutations expected to increase periplasmic LPS activate the  $\sigma^E$  response in *degS*<sup>ΔPDZ</sup> cells, which require RseB inhibition but not OMP activation. Similarly, expression of OMP signals alone is sufficient to strongly induce the  $\sigma^E$  response in  $\Delta rseB$  cells (16). The requirement for dual signals when all of the regulatory components are present is reminiscent of an ‘AND’ operation in symbolic or digital logic.

$\sigma^E$  activates transcription of genes for the chaperones and machines that transport and insert both LPS and OMPs into the OM. Crosstalk between these pathways could add an additional layer of regulation (3,25,32,33). If defects in LPS biogenesis created problems with OMP biogenesis and vice versa, then both signals needed to activate  $\sigma^E$  would be produced when either pathway is perturbed. Indeed, *rfaC*, *rfaF*, and *rfaP* LPS mutations activate  $\sigma^E$  in strains requiring only RseB inhibition (*degS*<sup>ΔPDZ</sup> *rseB*<sup>+</sup>; Fig. 4C), only OMP activation (*degS*<sup>+</sup>  $\Delta rseB$ ; Fig. S11), or both (*degS*<sup>+</sup> *rseB*<sup>+</sup>; Fig. 4B). Supporting this idea, the OM of *rfaC*, *rfaF*, and *rfaP* strains have significantly reduced levels of OMPs (34-37), suggesting problems with OMP biogenesis. Conversely, the LptD component of the LPS translocon is transported and inserted into the OM by the same chaperones and machinery as other OMPs (26,38), and thus defects in OMP biogenesis would soon lead to problems in LPS transport and assembly. A combination of AND logic and cross signaling permits the  $\sigma^E$  response to reflect the stress level. Low levels of off-pathway OMPs and LPS are probably always present in the periplasm, because a basal rate of RseA cleavage by DegS is essential for survival (39), and a transient increase in either signal will therefore result in an increased albeit buffered response, even assuming strict AND

logic. Only when the RseB and DegS sensors detect high concentrations of off-pathway LPS and OMPs, an indicator of extensive envelope-biogenesis dysfunction, will the full and metabolically expensive stress response be mounted.

Most unicellular organisms are enclosed by cell walls or envelopes that provide both a barrier to and an interface with the environment. These external structures are built from components that are synthesized in the cytosol but are assembled outside of the cytoplasmic membrane. Monitoring the flux of these molecules in the vicinity of the membrane coupled with dual-signal logic to buffer spurious responses may be a common regulatory strategy enabling precise homeostatic control of these critical barrier structures.

## References and Notes:

1. B.M Alba, C.A. Gross, Regulation of the *Escherichia coli* sigma-dependent envelope stress response. *Mol. Microbiol.* **52**, 613-619 (2004).
2. S.E. Ades, Regulation by destruction: design of the sigmaE envelope stress response. *Curr. Opin. Microbiol.* **11**, 535-540 (2008).
3. V.A. Rhodius, W.C. Suh, G. Nonaka, J. West, C.A. Gross, Conserved and variable functions of the sigmaE stress response in related genomes. *PLoS Biol.* **4**, e2 (2006)..
4. A. De Las Peñas, L. Connolly, C.A. Gross, The sigmaE-mediated response to extracytoplasmic stress in *Escherichia coli* is transduced by RseA and RseB, two negative regulators of sigmaE. *Mol. Microbiol.* **24**, 373-385 (1997).
5. D. Missiakas, M.P. Mayer, M. Lemaire, C. Georgopoulos, S. Raina, Modulation of the *Escherichia coli* sigmaE (RpoE) heat-shock transcription-factor activity by the RseA, RseB and RseC proteins. *Mol. Microbiol.* **24**, 355-371 (1997)
6. C. Dartigalongue, H. Loferer, S. Raina, EcfE, a new essential inner membrane protease: its role in the regulation of heat shock response in *Escherichia coli*. *EMBO J.* **20**, 5908-5918 (2001).
7. K. Kanehara, K. Ito, Y. Akiyama, YaeL (EcfE) activates the sigma(E) pathway of stress response through a site-2 cleavage of antisigma(E), RseA. *Genes Dev.* **16**, 2147-2155 (2002).
8. E.A. Campbell, *et al.*, Crystal structure of *Escherichia coli* s<sup>E</sup> with the cytoplasmic domain of its anti-s RseA. *Mol. Cell* **11**, 1067-1078 (2003).
9. B.O. Cezairliyan, R.T. Sauer, Inhibition of regulated proteolysis by RseB. *Proc. Natl. Acad. Sci. USA* **104**, 3771-3776 (2007).
10. D.Y. Kim, K.S. Jin, E. Kwon, M. Ree, K.K. Kim, Crystal structure of RseB and a model of its binding mode to RseA. *Proc. Natl. Acad. Sci. USA* **104**, 8779-8784 (2007).



11. D.Y. Kim, E. Kwon, J. Choi, H.Y. Hwang, K.K. Kim, Structural basis for the negative regulation of bacterial stress response by RseB. *Protein Sci.* **19**, 1258-1263 (2010).
12. N.P. Walsh, B.M. Alba, B. Bose, C.A. Gross, R.T. Sauer, OMP peptide signals initiate the envelope-stress response by activating DegS protease via relief of inhibition mediated by its PDZ domain. *Cell* **113**, 61-71 (2003).
13. S.E. Ades, L.E. Connolly, B.M. Alba, C.A. Gross, The *Escherichia coli* sigma(E)-dependent extracytoplasmic stress response is controlled by the regulated proteolysis of an anti-sigma factor. *Genes Dev.* **13**, 2449-2461 (1999).
14. Y. Akiyama, K. Kanehara, K. Ito, RseP (YaeL), an *Escherichia coli* RIP protease, cleaves transmembrane sequences. *EMBO J.* **23**, 4434-4442 (2004).
15. R. Chaba, I.L. Grigorova, J.M. Flynn, T.A. Baker, C.A. Gross, Design principles of the proteolytic cascade governing the sigmaE-mediated envelope stress response in *Escherichia coli*: keys to graded, buffered, and rapid signal transduction. *Genes Dev.* **21**, 124-136 (2007).
16. R. Chaba, *et al.* Signal integration by DegS and RseB governs the s<sup>E</sup>-mediated envelope stress response in *Escherichia coli*. *Proc. Natl. Acad. Sci. USA* **108**, 2106-2111 (2011).
17. Tam, C., and Missiakas, D. (2005). Changes in lipopolysaccharide structure induce the sigma(E)-dependent response of *Escherichia coli*. *Mol. Microbiol.* **55**, 1403-1412.
18. G. Klein, B. Lindner, W. Brabetz, H. Brade, S. Raina, *Escherichia coli* K-12 Suppressor-free mutants lacking early glycosyltransferases and late acyltransferases: minimal lipopolysaccharide structure and induction of envelope stress response. *J. Biol. Chem.* **284**, 15369-15389 (2009).
19. A.X. Tran, M.S. Trent, C. Whitfield, The LptA protein of *Escherichia coli* is a periplasmic lipid A-binding protein involved in the lipopolysaccharide export pathway. *J. Biol. Chem.* **283**, 20342-20349 (2008).

20. S.E. Ades, I.L. Grigorova, C.A. Gross, Regulation of the alternative sigma factor sigma(E) during initiation, adaptation, and shutoff of the extracytoplasmic heat shock response in *Escherichia coli*. *J. Bacteriol.* **185**, 2512-251 (2003).
21. B.O. Cezairliyan, R.T. Sauer, Control of *Pseudomonas aeruginosa* AlgW protease cleavage of MucA by peptide signals and MucB. *Mol. Microbiol.* **72**, 368-379 (2009).
22. T. Wu *et al.*, Identification of a protein complex that assembles lipopolysaccharide in the outer membrane of *Escherichia coli*. *Proc. Natl. Acad. Sci. USA* **103**, 11754-11759 (2006).
23. S.S. Chng, N. Ruiz, G. Chimalakonda, T.J. Silhavy, D. Kahne, Characterization of the two-protein complex in *Escherichia coli* responsible for lipopolysaccharide assembly at the outer membrane. *Proc. Natl. Acad. Sci. USA* **107**, 5363-5368 (2010).
24. E. Freinkman, S.S. Chng, D. Kahne, The complex that inserts lipopolysaccharide into the bacterial outer membrane forms a two-protein plug-and-barrel. *Proc. Natl. Acad. Sci. USA* **108**, 2486-2491 (2011).
25. N. Ruiz, D. Kahne, T.J. Silhavy, Transport of lipopolysaccharide across the cell envelope: the long road of discovery. *Nat. Rev. Microbiol.* **7**, 677-683 (2009).
26. N. Ruiz, S.S. Chng, A. Hiniker, D. Kahne, T.J. Silhavy, Nonconsecutive disulfide bond formation in an essential integral outer membrane protein. *Proc. Natl. Acad. Sci. USA* **107**, 12245-12250 (2010).
27. E. Freinkman, S. Okuda, N. Ruiz, D. Kahne, Regulated assembly of the transenvelope protein complex required for lipopolysaccharide export. *Biochemistry* **51**, 4800-4806 (2012).
28. S.S. Chng *et al.*, Disulfide rearrangement triggered by translocon assembly controls lipopolysaccharide export. *Science* **337**, 1665-1668 (2012).
29. B.A. Sampson, R. Misra, S.A. Benson, Identification and characterization of a new gene of *Escherichia coli* K-12 involved in outer membrane permeability. *Genetics* **122**, 491-501 (1989).

30. J. Sohn, R.A. Grant, R.T. Sauer, Allosteric activation of DegS, a stress sensor PDZ protease. *Cell* **131**, 572-583 (2007).
31. Calculations assume  $2 \cdot 10^6$  LPS molecules per *E. coli* cell, a doubling time of 30 min, and a periplasmic volume of  $3 \cdot 10^{-16}$  liters.
32. J.E. Mogensen, D.E. Otzen, Interactions between folding factors and bacterial outer membrane proteins. *Mol. Microbiol.* **57**, 326-346 (2005).
33. C.L. Hagan, T.J. Silhavy, D. Kahne,  $\beta$ -Barrel membrane protein assembly by the Bam complex. *Annu. Rev. Biochem.* **80**, 189-210 (2011).
34. C.A. Schnaitman, J.D. Klena, Genetics of lipopolysaccharide biosynthesis in enteric bacteria. *Microbiol. Rev.* **57**, 655-682 (1993).
35. G.F. Ames, E.N. Spudich, H. Nikaido, Protein composition of the outer membrane of *Salmonella typhimurium*: effect of lipopolysaccharide mutations. *J. Bacteriol.* **117**, 406-416 (1974).
36. E.A. Austin, J.F. Graves, L.A. Hite, C.T. Parker, C.A. Schnaitman, Genetic analysis of lipopolysaccharide core biosynthesis by *Escherichia coli* K-12: insertion mutagenesis of the *rfa* locus. *J. Bacteriol.* **172**, 5312-5325 (1990).
37. H. Nikaido, Molecular basis of bacterial outer membrane permeability revisited. *Microbiol. Mol. Biol. Rev.* **67**, 593-656 (2003).
38. D. Vertommen, N. Ruiz, P. Leverrier, T.J. Silhavy, J.F. Collet, Characterization of the role of the *Escherichia coli* periplasmic chaperone SurA using differential proteomics. *Proteomics* **9**, 2432-2443 (2009).
39. B.M. Alba, H.J. Zhong, J.C. Pelayo, C.A. Gross, *degS* (*hhoB*) is an essential *Escherichia coli* gene whose indispensable function is to provide sigma (E) activity. *Mol. Microbiol.* **40**, 1323-1333 (2001).

40. T.J. Odegaard, *et al.*, Shortened hydroxyacyl chains on lipid A of *Escherichia coli* cells expressing a foreign UDP-N-acetylglucosamine O-acyltransferase. *J. Biol. Chem.* **272**, 19688-19696 (1997).
41. Z. Zhou, S. Lin, R.J. Cotter, C.R. Raetz, Lipid A modifications characteristic of *Salmonella typhimurium* are induced by  $\text{NH}_4\text{VO}_3$  in *Escherichia coli* K12. Detection of 4-amino-4-deoxy-L-arabinose, phosphoethanolamine and palmitate. *J. Biol. Chem.* **274**, 18503-18514 (1999).
42. C. Galanos, O. Luderitz, O. Westphal, A new method for the extraction of R lipopolysaccharides. *Eur. J. Biochem.* **9**, 245-249 (1969).
43. M. Caroff, A. Tacken, L. Szabo, Detergent-accelerated hydrolysis of bacterial endotoxins and determination of the anomeric configuration of the glycosyl phosphate present in the "isolated lipid A" fragment of the *Bordetella pertussis* endotoxin. *Carbohydr. Res.* **175**, 273-282 (1988).
44. P. Zhou, E. Altman, M.B. Perry, J. Li, Study of matrix additives for sensitive analysis of lipid A by matrix-assisted laser desorption ionization mass spectrometry. *Appl. Environ. Microbiol.* **76**, 3437-3443 (2010).
45. E.C. Yi, M. Hackett, Rapid isolation method for lipopolysaccharide and lipid A from gram-negative bacteria. *Analyst.* **125**, 651-656 (2000).
46. K.A. Datsenko, B.L. Wanner, One-step inactivation of chromosomal genes in *Escherichia coli* K-12 using PCR products. *Proc. Natl. Acad. Sci. USA* **97**, 6640-6645 (2000).
47. T. Baba, *et al.*, Construction of *Escherichia coli* K-12 in-frame, single-gene knockout mutants: the Keio collection. *Mol. Syst. Biol.* **2**, 2006.0008 (2006).
48. M.K. Vorachek-Warren, S. Ramirez, R.J. Cotter, C.R. Raetz, A triple mutant of *Escherichia coli* lacking secondary acyl chains on lipid A. *J. Biol. Chem.* **277**, 14194-14205 (2002).
49. C.R. Raetz, C.M. Reynolds, M.S. Trent, R.E. Bishop, Lipid A modification systems in gram-negative bacteria. *Annu. Rev. Biochem.* **76**, 295-329 (2007).

**Acknowledgments:** We thank B. Cezairliyan, K. Chatman, S. Chng, H. Chung, S. Glynn, D. Kahne, S. Kim, L. Li, D. Pheasant, C. Raetz, D. Six, J. Sohn, and B. Stinson for helpful discussions, advice, and strains. Supported by NIH grants AI-16892 and GM-36278. S.L. was supported by an NIH postdoctoral fellowship (AI-084442). The data reported in this paper are presented in the main text and supplementary materials.

## Materials and Methods

### Proteins and peptides

*E. coli* RseA<sup>P</sup> (residues 121-216 with an N-terminal MGSSH<sub>6</sub>SSGLVPRGSHM tag), mature *E. coli* RseB or <sup>35</sup>S-RseB (residues 24-318 with a C-terminal LEH<sub>6</sub> tag), *E. coli* DegS lacking its membrane anchor (residues 27-355 with an N-terminal MRGSH<sub>6</sub>G tag), *P. aeruginosa* MucA<sup>P</sup> (residues 106-194 with an N-terminal MGSSH<sub>6</sub>SSGLVPRGS HM tag), mature *P. aeruginosa* MucB or <sup>35</sup>S-MucB (residues 22-316 with a C-terminal LEH<sub>6</sub>tag), *P. aeruginosa* AlgW lacking its membrane anchor (residues 24-389 with an N-terminal MGSSH<sub>6</sub>SSGLVPRGSHM tag), H<sub>6</sub>-tagged *E. coli* LptA (expression plasmid provided by S.S. Chng, Harvard University), OMP peptide (YYF), and MucE peptide (DNRDGNVWVF) were purified as described (4,6,10,12,18). For expression of <sup>35</sup>S- proteins, cells were grown in defined medium (Teknova) lacking methionine to OD<sub>600</sub> = 0.4, 1 mM IPTG and 0.04 mCi <sup>35</sup>S-methionine (Perkin-Elmer) per mL of culture were added, growth was continued for 2 h, and cells were harvested and lysed by treatment with lysozyme (0.5 mg/mL), 0.5 mM EDTA, and three freeze-thaw cycles. Dimeric RseB and MucB were isolated by gel-filtration chromatography at 25 °C on a Superose-6 column (GE Healthcare) equilibrated with 25 mM potassium phosphate (KP<sub>i</sub>) [pH 8.2], 10% glycerol. Fractions containing dimers were pooled, concentrated to 180 μM, and frozen at -80 °C.

### RseB-elution assay

RseA<sup>P</sup> was coupled to cyanogen-bromide activated Sepharose CL-4B (Sigma-Aldrich) following the manufacturer's guidelines. RseA<sup>P</sup>-resin was resuspended in 25 mM KP<sub>i</sub> [pH 8.3], and incubated with a 4-fold molar excess of <sup>35</sup>S-RseB over total RseA<sup>P</sup> in a 0.8 x 4 cm Poly-Prep column (Bio-Rad). After 10 min with intermittent mixing at 25 °C, the resin was drained, washed, and resuspended in 16 volumes of 25 mM KP<sub>i</sub> [pH 8.3]. For assays, 30 μL of resin-

slurry was mixed with 20  $\mu\text{L}$  of competitor solution in a microcentrifuge tube with periodic gentle stirring. After 30 min, the slurry was transferred to a 96-well Multiscreen<sub>HTS</sub>-HV Filter Plate (Millipore, #MSHVN4510). Prior to slurry addition, the filter-plate membrane was wet with 10  $\mu\text{L}$  per well of 25 mM  $\text{KPi}$  [pH 8.3] to avoid  $^{35}\text{S}$ -RseB retention. Filter-plates were placed over a 96-well polypropylene receiving plate (Greiner, #651201), and centrifuged at 1500 x g for 1 min to collect the flow-through.  $^{35}\text{S}$ -RseB was quantified by scintillation counting. Assays using  $^{35}\text{S}$ -MucB and MucA<sup>P</sup>-resin were performed in an analogous fashion.

LPS variants were sonicated prior to use in elution assays. Unless noted, these assays also contained 10 mM EDTA titrated to pH 8.2 with triethylamine (EDTA-TEA) to minimize aggregation. Assays performed without EDTA-TEA typically displayed reduced maximum elution of  $^{35}\text{S}$ -RseB from the RseA<sup>P</sup>-resin, probably because larger aggregates are excluded from RseB bound to RseA<sup>P</sup> within the agarose matrix, reducing both the effective concentration and the maximum amount of RseB released. Using dynamic light scattering, we confirmed that EDTA-TEA at concentrations of 10 mM or higher reduced the average particle radius of LPS from ~20 to ~3 nm, as expected for a transition from vesicles or micelles to small aggregates. In the presence of EDTA-TEA, there were still large differences in the maximum elution efficiencies of different LPS species that paralleled the solubility of these species. For example, the highly soluble L-IIA and Kdo<sub>2</sub>-L-IIA fragments eluted ~90% of the RseB (Fig. 2B and 3D), the moderately soluble intact LPS molecule eluted ~40% (Fig. 1A), and the highly insoluble lipid-A fragment eluted less than 5% (not shown).

To generate fluorescently labeled RseA<sup>P</sup> (fl-RseA<sup>P</sup>) the purified His<sub>6</sub>-RseA<sup>P</sup> S154C mutant protein was treated with 50  $\mu\text{M}$  Tris(2-carboxyethyl)phosphine hydrochloride [pH 7.5] for 1 h at 25 °C (4), dialyzed against 50 mM NaPi [pH 7.5] buffer, and finally incubated with a 10-fold molar excess of Oregon Green-488 Maleimide (Invitrogen). After 2 h, fl-RseA<sup>P</sup> and free dye

were separated by adding a small amount of Ni<sup>++</sup>-NTA resin to the mixture, the resin was extensively washed with 50 mM NaPi [pH 7.5], and fl-RseA<sup>P</sup> was eluted with imidazole, concentrated, and then desalted over a PD-10 column (GE Healthcare) equilibrated with 50 mM NaPi [7.5], 10% glycerol.

### **Protease assays**

Cleavage of RseA<sup>P</sup>/MucA<sup>P</sup> by OMP-activated DegS/AlgW was performed at 25 °C as described (4, 12, 18). For reactions containing RseA<sup>P</sup> and RseB, the complex was initially purified by gel filtration on a Superdex S-75 column at 25 °C in 25 mM KP<sub>i</sub> [pH 8.3], 10% glycerol, and then concentrated to 85 μM ( $\epsilon = 34380 \text{ M}^{-1} \text{ cm}^{-1}$ ). Complete cleavage assays contained the RseA<sup>P</sup>•RseB complex (40 μM), DegS (4 μM trimer), YYF OMP peptide (200 μM), and L-IIA (2 mM) in a buffer consisting of 100 mM sodium phosphate (NaP<sub>i</sub>) [pH 8.2], 380 mM NaCl, 4 mM EDTA, and 10% glycerol. Cleavage of MucA<sup>P</sup> (25 μM) was assayed in the presence of MucB (40 μM monomer), AlgW (2 μM trimer), MucE peptide (75 μM), and L-IIA (2 mM) in 50 mM NaP<sub>i</sub> [pH 7.5], 200 mM KCl, and 10% glycerol. In controls, one or more components of the complete reactions were omitted. Cleavage reactions were initiated by peptide addition and quenched by adding SDS-PAGE loading buffer and heating at 100 °C for 1 min. Following SDS-PAGE, gels were stained using Coomassie Blue or the Bio-Rad Silver Stain Kit (Cat. # 161-0443).

### **Lipid purification and characterization**

For small-scale studies, purified lipid A (2 mg/mL; Sigma) was hydrolyzed in 0.1 N NaOH at 100 °C for 1 h, the pH was adjusted to 7, debris was removed by centrifugation, and 1.1X volumes of chloroform and methanol were added to form a two phase Bligh-Dryer mixture (27). After phase separation, the aqueous phase was heated under reduced pressure to remove organic solvent, KP<sub>i</sub> [pH 8.3] was added to a final concentration of 0.65 M, and this material was applied to phenyl Sepharose CL-4B resin equilibrated in 0.65 M KP<sub>i</sub> [pH 8.3]. This resin was



washed with 10 column volumes each of 650 mM  $\text{KPi}$ , a mixture of 300 mM  $\text{KPi}$  and 300 mM ammonium acetate ( $\text{NH}_4\text{OAc}$ ), 300 mM  $\text{NH}_4\text{OAc}$ , 150 mM  $\text{NH}_4\text{OAc}$ , 75 mM  $\text{NH}_4\text{OAc}$ , 25 mM  $\text{NH}_4\text{OAc}$ , 10 mM  $\text{NH}_4\text{OAc}$ , 5 mM  $\text{NH}_4\text{OAc}$ , and water. Fractions were frozen in liquid nitrogen, lyophilized, resuspended in water, and assayed. Activity was recovered in the 5 mM  $\text{NH}_4\text{OAc}$  and water fractions, which were pooled, adjusted to 5 mM  $\text{NH}_4\text{OAc}$  [pH 3.5], and loaded onto a C18 column that had been equilibrated in 95% buffer A (5 mM  $\text{NH}_4\text{OAc}$  adjusted to pH 3.5 with acetic acid) and 5% buffer B (95% acetonitrile, 5 mM  $\text{NH}_4\text{OAc}$  [pH 3.5]). The column was developed with a linear gradient from 5% buffer B to 100% buffer B at 25 °C, and fractions with UV adsorption at 214 nm were dried under reduced pressure at 45 °C to remove acetonitrile, frozen in liquid nitrogen, lyophilized, resuspended in water, and assayed. Hydrolysis products with RseB-elution activity were analyzed by tandem liquid chromatography mass spectrometry (LC-MS, Harvard Small Molecule Mass Spectrometry Facility) in the negative-ion mode with separation on a C18 column as described above.

For large-scale purification of LII-A, we initially isolated  $\text{Kdo}_2$ -lipid A from strain D31m4 (Yale Coli Genetic Stock Center). 20 L of D31m4 cells were grown to stationary phase at 37 °C in LB broth plus 1 mM  $\text{MgSO}_4$ , harvested, washed 3X with 99% ethanol, dried, and resuspended in phenol:chloroform:petroleum ether (2:5:8) at 0.15 g/mL (42). After overnight extraction, the suspension was centrifuged to remove cell debris, and organic solvents were removed from the supernatant by rotary evaporation under reduced pressure at 40 °C.  $\text{Kdo}_2$ -lipid A was precipitated from the phenol layer by the drop-wise addition of water and collected by centrifugation. Crude  $\text{Kdo}_2$ -lipid-A pellets were washed with 99% ethanol to remove phenol and phospholipids. Lipid A was obtained by mild acid hydrolysis; the dried  $\text{Kdo}_2$ -lipid-A extract was resuspended in water at ~4 mg/mL by sonication, the solution was adjusted to 50 mM sodium acetate, [pH 4.5], 1% SDS, and heated at 100 °C for 1 hr. Lipid A was purified on DEAE-cellulose as described (27). To obtain L-IIA, lipid A was suspended by sonication in water

at 2 mg/mL, the solution was adjusted to 0.1 N NaOH and was incubated at 100 °C with moderate stirring. After 60 min, the solution was cooled to 25 °C, and the pH was adjusted to 7. Insoluble debris was removed by centrifugation, and the supernatant was adjusted to 600 mM  $\text{KPi}$  [pH 8.3], and applied to a column containing 10 mL packed phenyl Sepharose CL-4B resin per mg lipid. Lipids were eluted as described for the small-scale purification. Pooled fractions were adjusted to 5 mM  $\text{NH}_4\text{OAc}$ , frozen in liquid nitrogen and lyophilized. For mass spectrometry analysis, lipids were dissolved in water at 20 mg/mL and purified by HPLC on a semi-preparative C18 column as described above, except that the gradient was 0-10 min 5% B, 10-15 min 5-40% B, 15-40 min 40-60%B, 60-65 min 60% B, 65-70 min 100% B. Fractions were collected, adjusted to pH 7.5 with  $\text{NH}_4\text{OH}$ , solvent was removed by rotary evaporation under reduced pressure at 40 °C, and lipids were recovered by lyophilization. Mass was confirmed by MALDI-TOF with a CMBT/ $\text{NH}_4$ -EDTA matrix as described (28).

For  $\text{Kdo}_2$ -L-IIA purification,  $\text{Kdo}_2$ -lipid A from strain D31m4 was hydrolyzed with base and purified as described for L-IIA except a C18 HPLC step was not performed. Final L-IIA or  $\text{Kdo}_2$ -L-IIA products were homogeneous as assayed by thin-layer chromatography.

Lipopolysaccharides from different *E. coli* strains were extracted by a modified Tri-reagent method (29). Briefly, cells were grown to stationary phase at 30 °C in LB broth plus 1 mM  $\text{MgSO}_4$ , harvested, and re-suspended in 25 mM  $\text{NaPi}$  [pH 7.5], 100 mM NaCl. The suspension was centrifuged, and the cell pellet was resuspended in water and adjusted to 0.8 M guanidine thiocyanate, 0.4 M ammonium thiocyanate, 0.1 M sodium acetate [pH 5], and 38% water saturated phenol (v/v) at 0.075 g of cells per mL of tri-reagent. The suspension was vortexed intermittently for 5 min and then incubated for 30 min at 25 °C. Phases were separated by the addition of 0.2 mL of chloroform per mL of suspension followed by centrifugation at 5000 x g. The aqueous phase was collected and LPS was recovered by adding three volumes of 99%

ethanol, adjusting the solution to 30 mM NaOAc, and incubating at  $-20\text{ }^{\circ}\text{C}$  for 2 h to precipitate lipids. The precipitate was collected by centrifugation at  $5000\times g$ , washed with 99% ethanol, and dried. This material was resuspended in water at 10 mg/mL, incubated at  $60\text{ }^{\circ}\text{C}$  for 20 min, followed by extensive sonication, centrifugation at  $10000\times g$  for 10 min to remove debris, and extraction into a Triton X-114 phase. Briefly, Triton X-114 was added to 1% (v/v), and small aliquots of 4 M  $\text{NH}_4\text{OAc}$  were added until the solution became cloudy at  $25\text{ }^{\circ}\text{C}$ . This suspension was incubated at  $4\text{ }^{\circ}\text{C}$  until the solution became clear, incubated at  $50\text{ }^{\circ}\text{C}$  until it became cloudy again, and the detergent phase (bottom) and aqueous phase (top) were separated by centrifugation at  $3000\times g$ . The detergent phase, containing lipids, was re-extracted with  $\text{NH}_4\text{OAc}$  as described above, and the lipids were recovered by ethanol precipitation. This procedure was repeated (typically 4-5 times) until nucleic-acid contamination was not detected by UV absorbance at 260 nm. LPS was recovered by ethanol precipitation and dried under reduced pressure.

### Strain construction

Strains are listed in Supplemental Table S1. Phenotypes were determined in derivatives of *E. coli* MG1655 containing the chromosomal  $\sigma^E$ -dependent *rpoHP3-LacZ* reporter (CAG45114). The DegS PDZ domain (encoded by nucleotides 757-1065) was deleted by recombineering a kanamycin cassette into a  $\sigma^E$ -suppressor strain (CAG41001) as described (30). *degS* <sup>$\Delta$ PDZ</sup> was then transduced into CAG45114, transformed with the FLP recombinase plasmid pCP20, and cured of pCP20 to make CAG64132. Tetracycline (*nadB::Tn10*) tightly linked to  $\Delta$ *rseB* was subsequently transduced into CAG45114 or CAG64132 to yield CAG53505 and CAG64133, respectively. Deletion alleles affecting LPS biosynthesis were transduced from the KEIO collection (31) into CAG45114 (*degS*<sup>+</sup>), CAG64132 (*degS* <sup>$\Delta$ PDZ</sup>), CAG53505 (*degS*<sup>+</sup>  $\Delta$ *rseB*), or CAG64133 (*degS* <sup>$\Delta$ PDZ</sup>  $\Delta$ *rseB*) and selected on kanamycin. To move *lptD* alleles, we inserted a chloramphenicol cassette between *lptD* and *surA* (2365 bases downstream from the

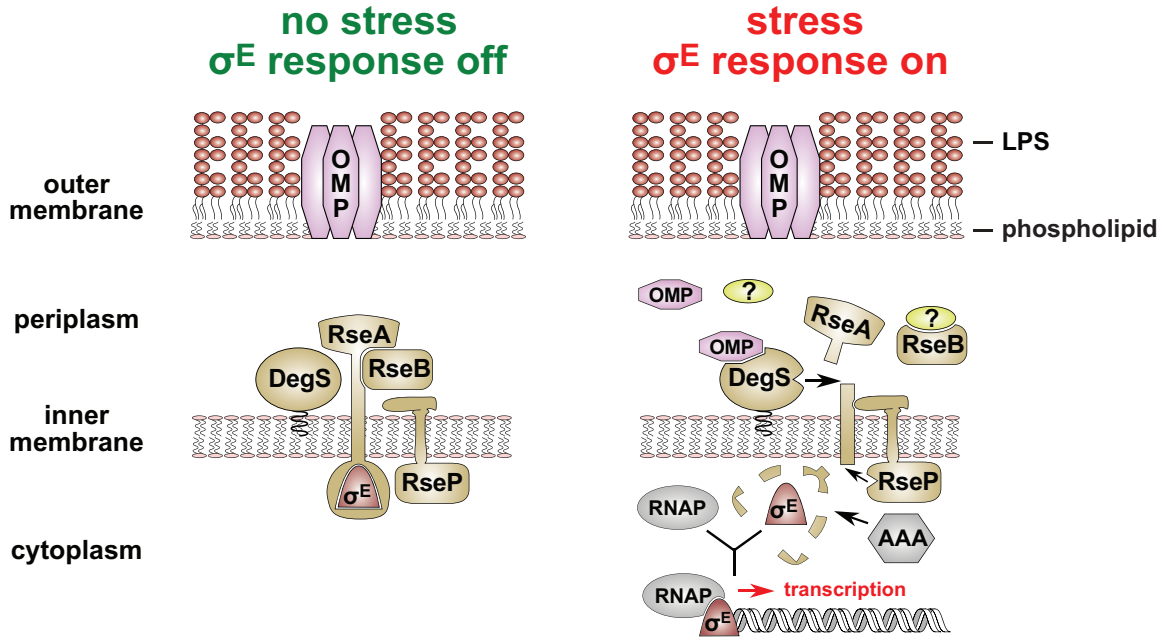
*lptD* start codon) in MC4100 and subsequently transduced this marker, linked either to wild-type *lptD* or *lptD*<sup>Δ330-352</sup> into MG1655 to generate *degS*<sup>+</sup> *lptD*-*cm* (CAG64294), *degS*<sup>ΔPDZ</sup> *lptD*-*cm* (CAG64295), and *degS*<sup>+</sup> *lptD*<sup>Δ330-352</sup>-*cm* (CAG64274). *degS*<sup>ΔPDZ</sup> *lptD*<sup>Δ330-352</sup>-*cm* (CAG64275) was made by transducing kanamycin-marked *degS*<sup>ΔPDZ</sup> into CAG64274 at 37 °C, and plating at 30 °C. Assays of control strains (CAG64294 and CAG64295) with chloramphenicol inserted between wild-type *lptD* and *surA* indicated that the cassette did not perturb  $\sigma^E$  expression (Fig. S12). The chloramphenicol cassette did result in an ~3-fold increase in SurA-protein levels (Fig. S12), presumably because of increased transcription from the chloramphenicol promoter. To make  $\Delta dsbA$  (CAG64257) and *degS*<sup>ΔPDZ</sup>  $\Delta dsbA$  (CAG64258) strains, kanamycin-marked  $\Delta dsbA$  was transduced into CAG45114 and CAG64132, respectively.

### $\sigma^E$ -activity assays

For  $\sigma^E$ -activity measurements, cells were diluted from overnight cultures to OD<sub>600</sub> 0.01 in LB broth (with additives as needed) and grown at 30 °C. Four samples were taken at different times between OD<sub>600</sub> 0.1 and 0.4, and  $\beta$ -galactosidase activity per 0.5 mL of cells was determined and plotted against OD<sub>600</sub> (11). The slope of this plot measures  $\sigma^E$  activity. Four independent assays were performed for each strain. Normally, transductants were purified by replating prior to assay. However, *degS*<sup>ΔPDZ</sup> *lptD*<sup>Δ330-352</sup> cells were very sick and gained suppressors rapidly, as evidenced by variability in growth rates. In this case, we inoculated colonies directly from the transduction plate into LB broth plus chloramphenicol for  $\sigma^E$ -activity measurements. Both *degS*<sup>+</sup> *lptD*<sup>Δ330-352</sup> and *degS*<sup>ΔPDZ</sup> *lptD*<sup>Δ330-352</sup> cells had significantly increased  $\sigma^E$  activity as compared to the respective *degS*<sup>+</sup> and *degS*<sup>ΔPDZ</sup> parental strain, as shown in Fig. 4A. In Fig. S7, we show the variability of  $\sigma^E$  activity in six independent transductants of each strain. Independent *degS*<sup>ΔPDZ</sup> *lptD*<sup>Δ330-352</sup> isolates had variable growth rates (doubling times of 62-83 min versus 44 min for the isogenic *degS*<sup>ΔPDZ</sup> parental strain) and variable increases in  $\sigma^E$

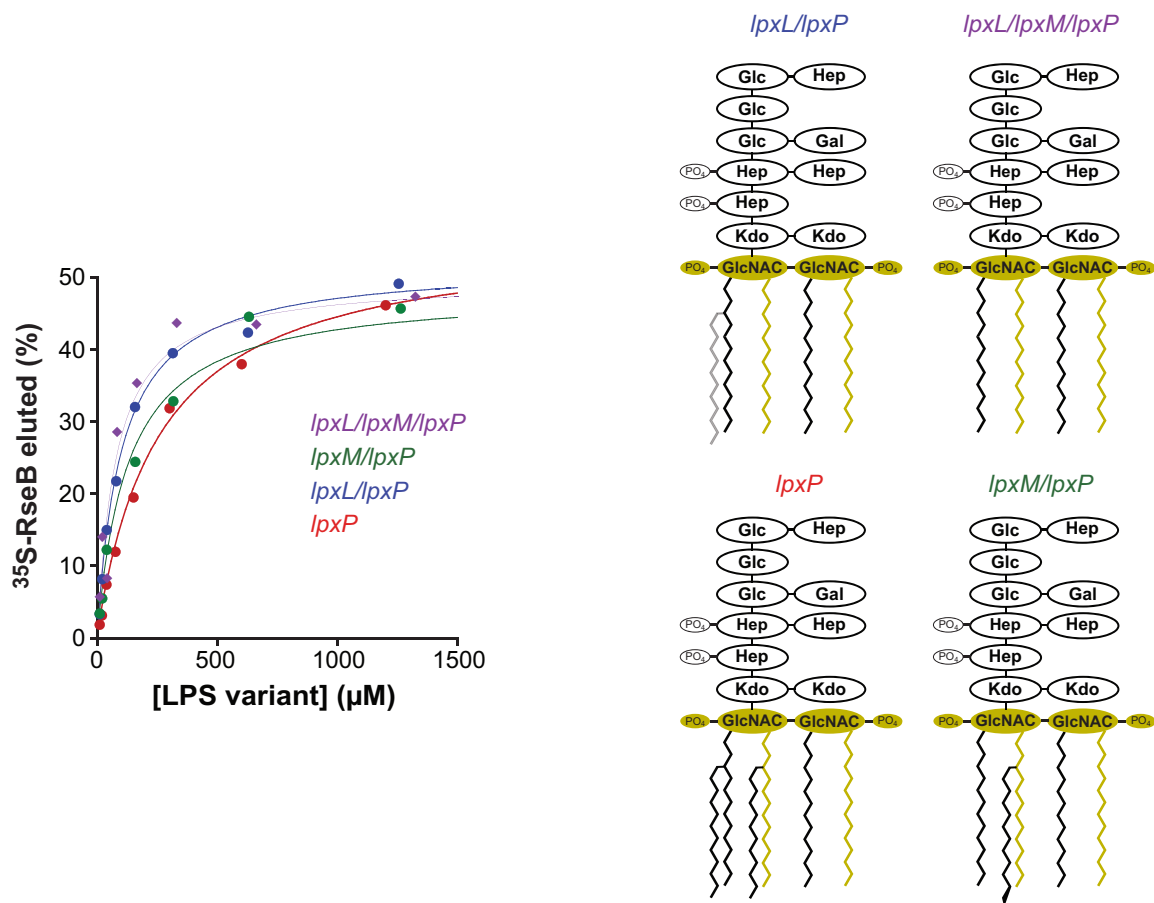
activity (3 to 10-fold), likely caused by differential accumulation of suppressor mutations in transductants. Indeed, upon prolonged growth, *degS*<sup>ΔPDZ</sup> *lptD*<sup>Δ330-352</sup> cells exhibited a decline in  $\sigma^E$  activity, consistent with the accumulation of suppressor mutations that decrease  $\sigma^E$  expression. *ΔrseA*, *degS*<sup>ΔPDZ</sup> *ΔrfaC*, and *degS*<sup>ΔPDZ</sup> *ΔrfaF* strains also showed reduced  $\sigma^E$  activity upon continued subculture. These strains share the common feature of complete deregulation of the  $\sigma^E$  system, either because of loss of the central regulator (*ΔrseA*) or because of constitutive activation of both the DegS protease (*degS*<sup>ΔPDZ</sup>) and LPS-mediated inactivation of RseB (*lptD*<sup>Δ330-352</sup>, *ΔrfaC*, and *ΔrfaF*). These results highlight the importance of the two signals in controlling  $\sigma^E$  activity.

**Author notes:** All authors contributed to experimental design and interpretation. S.L. performed biochemical experiments. M.S.G. performed biological experiments. S.L., M.S.G., C.A.G., and R.T.S. wrote the manuscript.



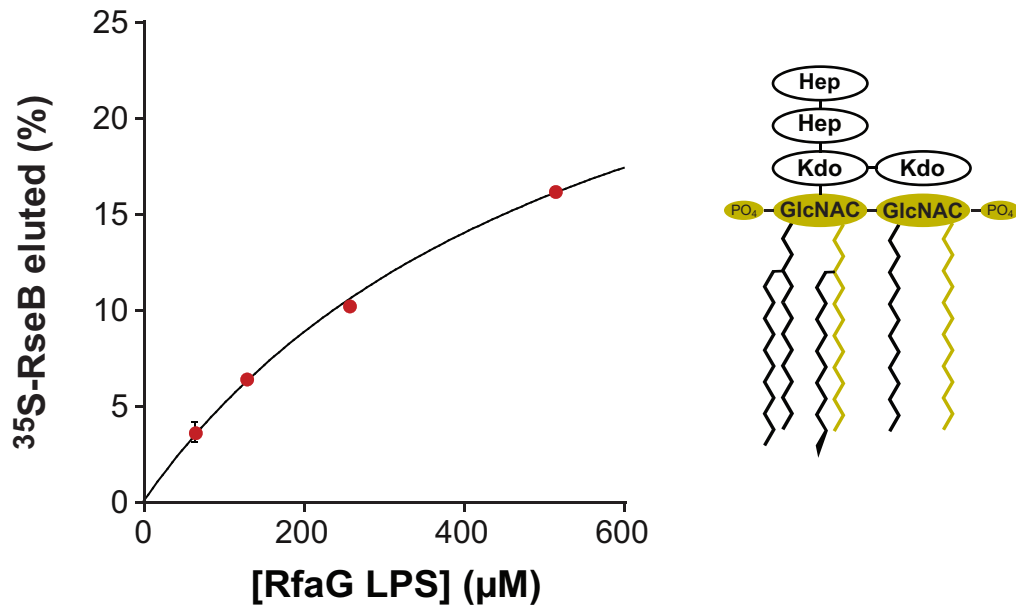
**Supplemental Figure S1:**  $\sigma^E$  response to envelope stress.

Stress activates a proteolytic cascade that destroys RseA, releasing  $\sigma^E$  to activate a transcriptional response. This system requires activation of the DegS protease by OMPs and disruption of RseB binding to RseA by an unknown molecular signal (shown as question mark in this figure; experiments in this paper show that this signal is LPS). Black arrows indicate proteolysis events. The red arrow indicates  $\sigma^E$ -stimulated transcription of genes for proteins that combat envelope stress.



**Supplemental Figure S2:** Partially acylated LPS species eluted <sup>35</sup>S-RseB from RseA<sup>P</sup>-agarose.

LPS species purified from strains with mutations in *lpxL/lpxP*, *lpxM/lpxP*, and *lpxL/lpxM/lpxP* eluted <sup>35</sup>S-RseB from RseA<sup>P</sup>-agarose. The lines are hyperbolic fits with apparent interaction constants of 260 µM (*lpxP*; red symbols), 103 µM (*lpxL/lpxP*; blue symbols), 130 µM (*lpxM/lpxP*; green symbols), and 78 µM (*lpxL/lpxM/lpxP*; purple symbols). LpxL and LpxM add O-linked acyl chains to the lipid-A portion of LPS; LpxP adds a longer acyl chain to the LpxL position at low temperatures (32). The acyl chain colored gray is absent in some LPS molecules synthesized in *lpxL* mutant strains (32). The region colored gold in the structures represents a "minimal" RseB recognition unit.



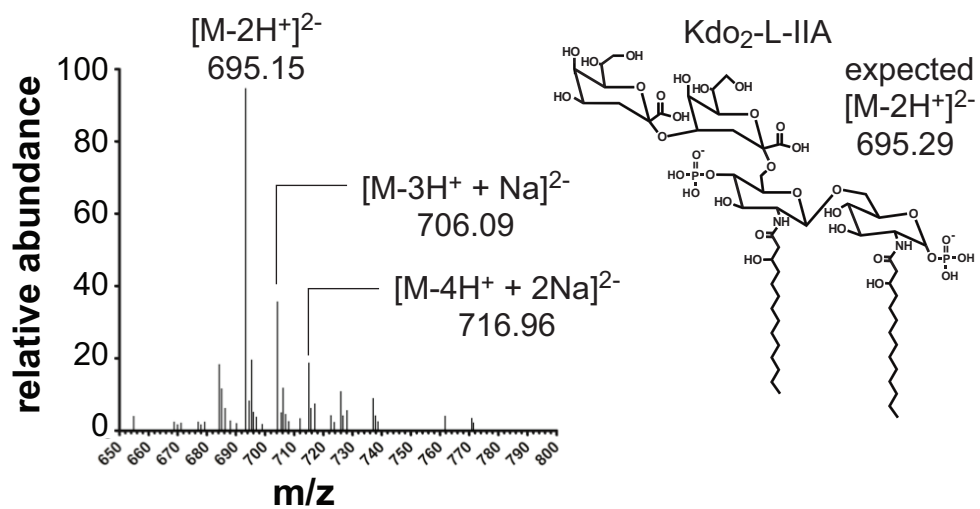
**Supplemental Figure S3:** LPS from  $\Delta rfaG$  retains the ability to elute  $^{35}\text{S}$ -RseB from RseA<sup>P</sup>-agarose.

LPS purified from  $\Delta rfaG$  *E. coli* lacks outer-core sugars but retains the ability to elute  $^{35}\text{S}$ -RseB from RseA<sup>P</sup>-agarose.

The line is a hyperbolic fit with an apparent interaction constant of 570  $\mu\text{M}$ . Data are plotted as mean  $\pm$  SEM ( $N=2$ ).

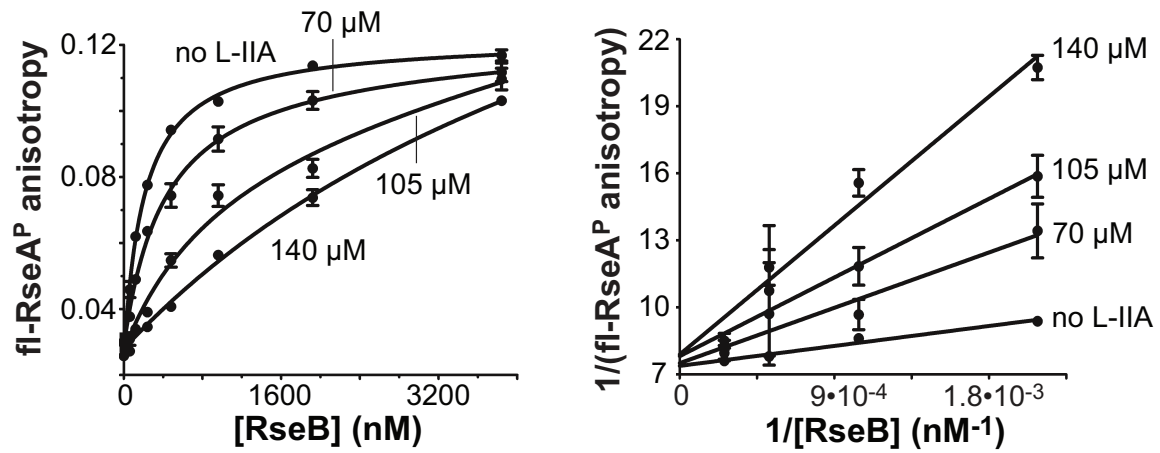
The region colored gold in the structure represents a “minimal” RseB recognition unit.





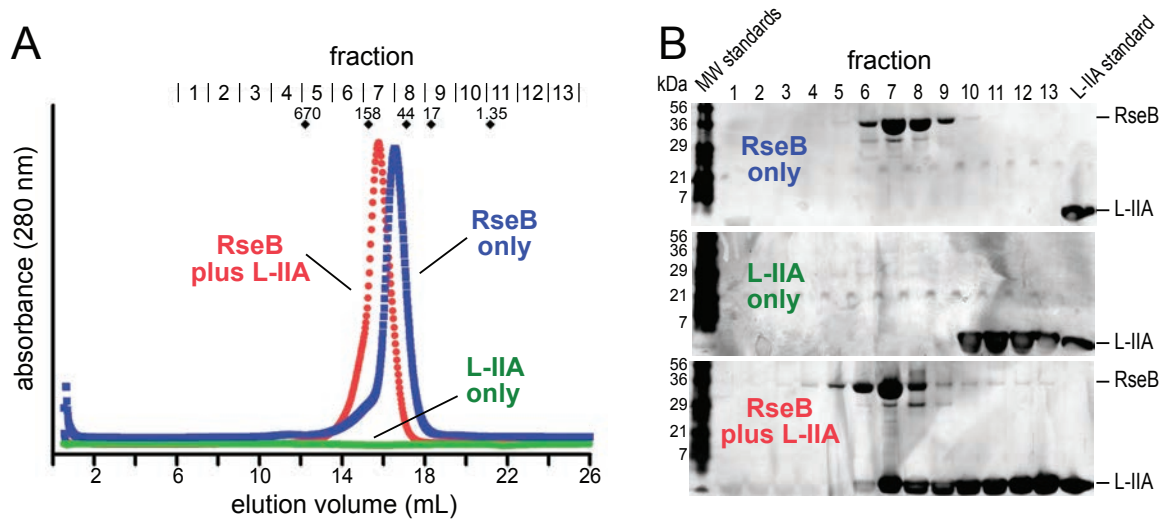
**Supplemental Figure S4:** Expected structure and mass spectrometry of the purified fragment produced by NaOH hydrolysis of Kdo<sub>2</sub>-lipid A.

Ions matching the expected mass of Kdo<sub>2</sub>-L-IIA in different protonation states and with one or two associated sodiums are indicated. Fragments were analyzed in the negative-ion mode.



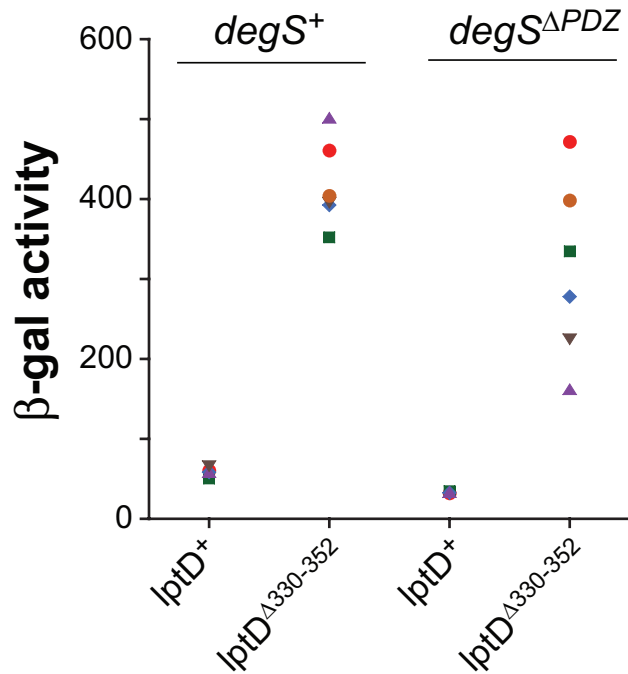
**Supplemental Figure S5:** Competitive inhibition mechanism of L-IIA.

As expected for a competitive-inhibition mechanism, the graph on the left shows that increasing concentrations of the L-IIA fragment decreased the apparent affinity of RseB for fluorescent RseA<sup>P</sup>. Data were fit to a hyperbolic equation, resulting in apparent binding constants ( $K_{app}$ ) of ~160  $\mu$ M (no L-IIA), ~410  $\mu$ M (70  $\mu$ M L-IIA), ~1 mM (105  $\mu$ M L-IIA), and ~ 5.6 mM (140  $\mu$ M L-IIA). The graph on the right is a double-reciprocal plot of the data shown in the graph on the left. Data are plotted as mean  $\pm$  SD ( $N=3$ ).



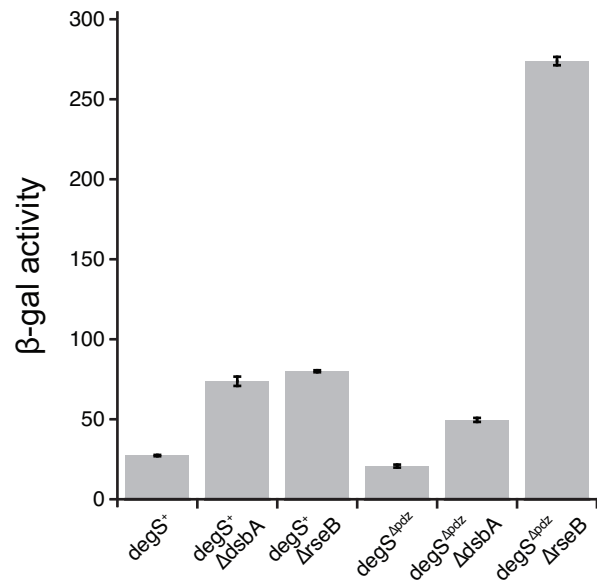
**Supplemental Figure S6:** Gel filtration of RseB with L-IIA fragments.

**(A)** Gel-filtration chromatography of RseB alone (blue), L-IIA alone (green), or a mixture of RseB and L-IIA (red) on a Superose 6 column (10 x 300 mm, 24 mL) equilibrated with 25 mM KPi [8.3], 10 % glycerol. Fractions (~1.5 mL) were collected for each experiment as indicated. The diamonds mark the elution positions of native molecular weight standards (Bio-Rad 151-1901) of 670 kDa (bovine thyroglobulin), 158 kDa (bovine  $\gamma$ -globulin), 44 kDa (chicken ovalbumin), 17 kDa (equine myoglobin), and 1.35 kDa (vitamin B<sub>12</sub>). **(B)** SDS-PAGE (12% bis-tris/acrylamide) and silver staining of fractions from the experiments in panel A. Prior to loading, fractions were adjusted to 0.5 % SDS, boiled for 45 s, and maintained at 50° C to prevent precipitation of potassium- SDS salts. L-IIA alone eluted near the fully retained salt volume (fractions 10-13), but when mixed with RseB, co-eluted at a volume expected for RseB tetramers (fractions 6- 8). In the RseB plus L-IIA experiment, the presence of L-IIA in fraction 9 suggests that some L-IIA initially bound to RseB dissociated during the time required for chromatography.



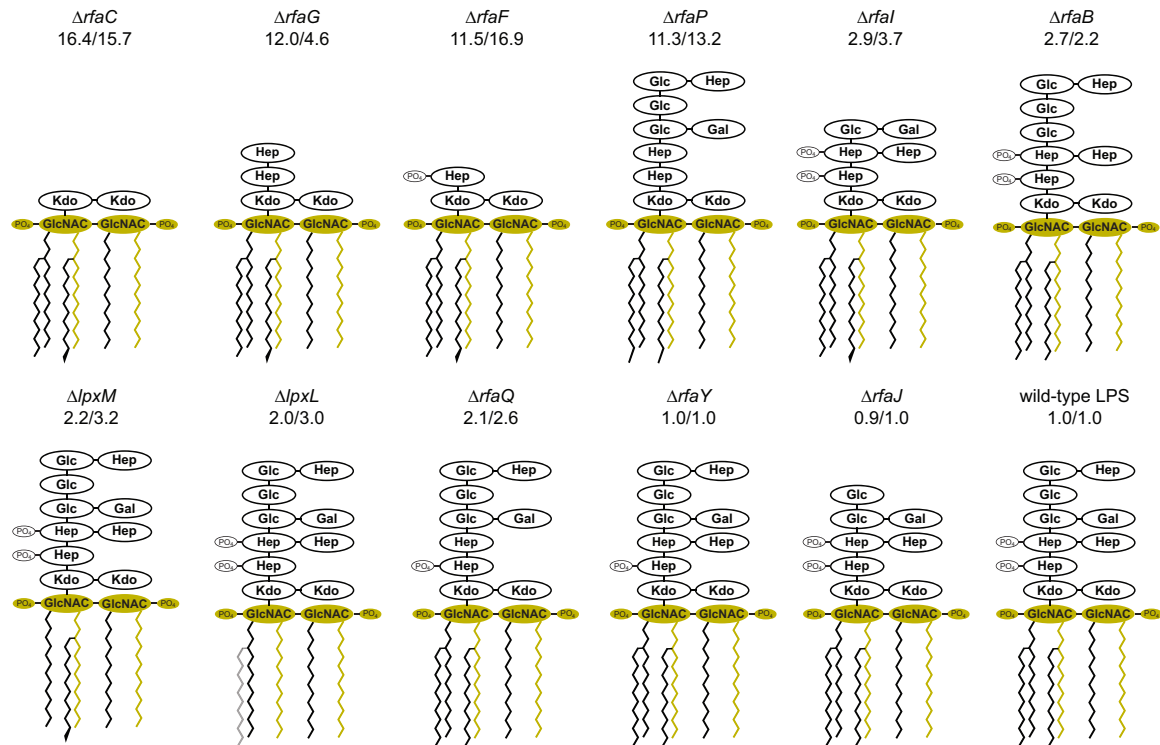
**Supplemental Figure S7:** Individual replicates from Figure 4A.

This figure shows values of the individual replicates from which the average values plotted in Fig. 4A were calculated. The higher variance in strains containing the *lptD*<sup>Δ330-352</sup> allele appears to be caused by suppressor mutations in some isolates that grew faster and had lower activity.



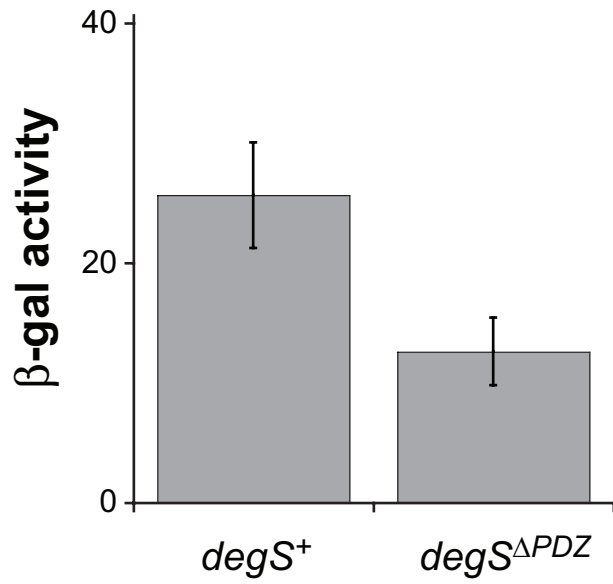
**Supplemental Figure S8:** Δ*dsbA* increases σ<sup>E</sup> activity.

Δ*dsbA*, which reduces the amount of properly disulfide-bonded LptD, increased σ<sup>E</sup> activity in *degS*<sup>+</sup> and in *degS*<sup>ΔPDZ</sup> backgrounds, as measured by expression of the *rpoHP3*-LacZ reporter. For comparison, values are also shown for Δ*rseB* in the *degS*<sup>+</sup> and in *degS*<sup>ΔPDZ</sup> strains. Data are plotted as mean ± SEM (*N* ≥ 2).



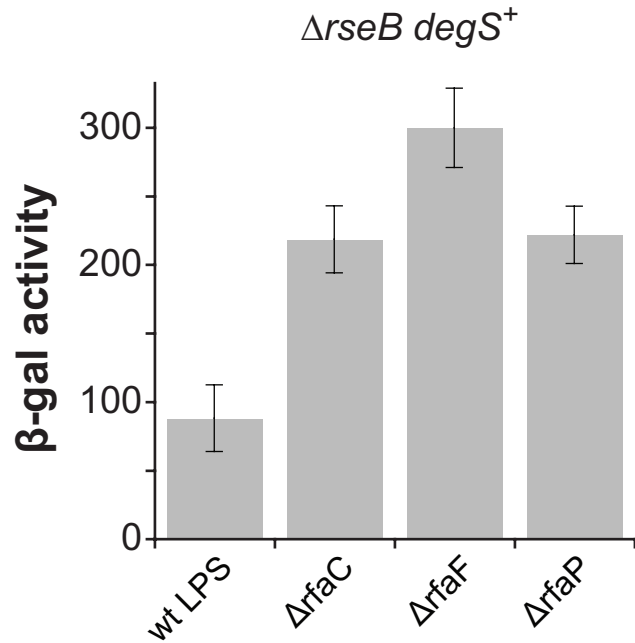
**Supplemental Figure S9:** Structures of mutant LPS species.

Structures of the major LPS species produced by the wild-type and mutant strains assayed for ESR activation in Fig. 4. The numbers listed below each LPS biosynthesis mutation represent the degree of stimulation of the ESR in  $degS^+/degS^{\Delta PDZ}$  strains, respectively. For LPS synthesized by the *lpxL* strain, the acyl chain colored gray is absent in many molecules (48,49). The structural elements colored gold are sufficient for RseB binding.



**Supplemental Figure S10:**  $\sigma^E$  activity in  $DegS^{WT}$  vs  $DegS^{\Delta PDZ}$ .

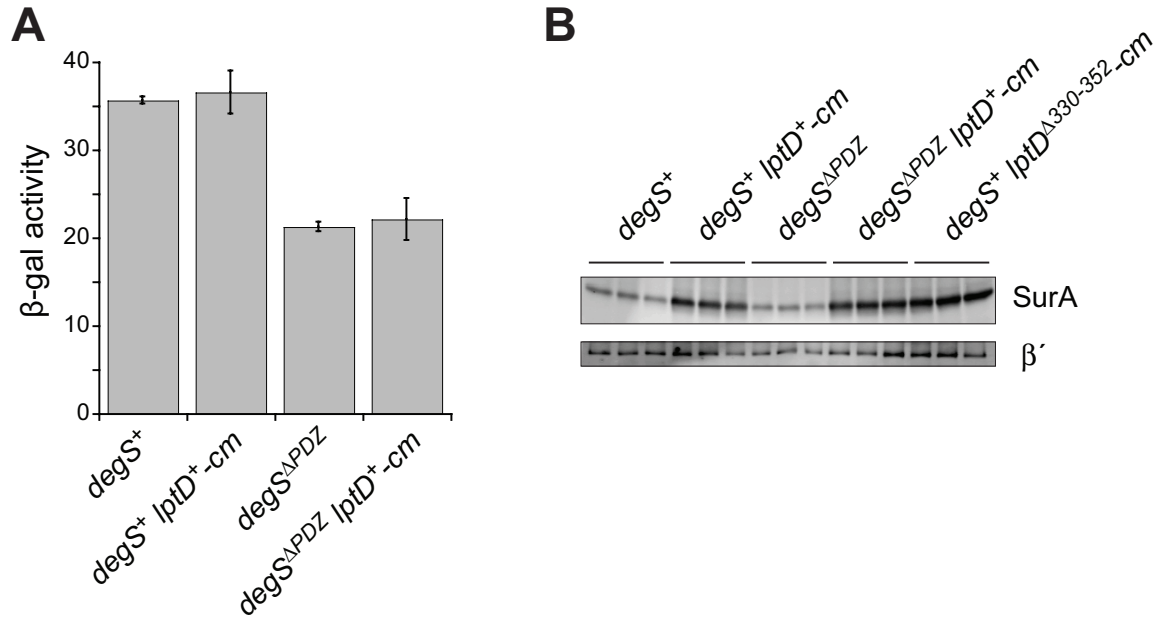
$\sigma^E$  activity from the *rpoHP3-LacZ* reporter was approximately twice as high in a  $degS^+$  strain compared an otherwise isogenic  $degS^{\Delta PDZ}$  strain. Data are plotted as mean  $\pm$  SD ( $N = 16$ ).



**Supplemental Figure S11:** LPS mutants may also generate an OMP signal.

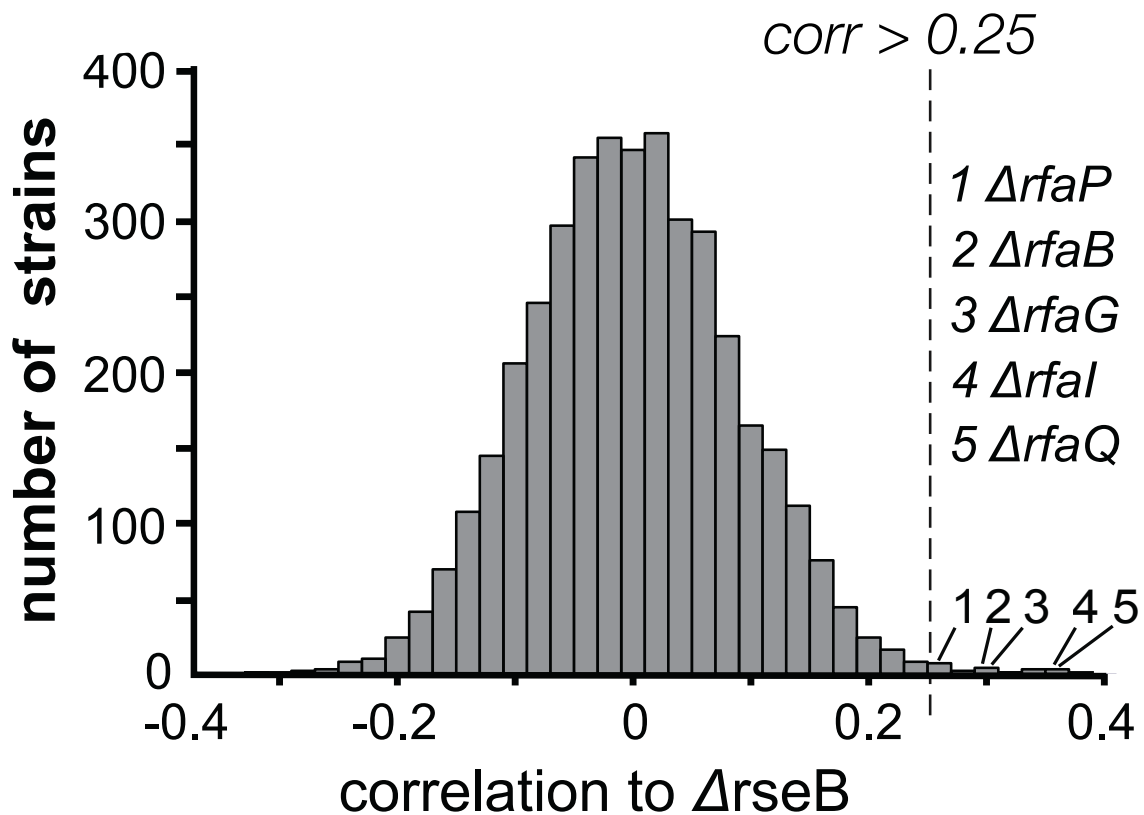
In the *ΔrseB degS<sup>+</sup>* genetic background,  $\sigma^E$  activity was substantially higher in strains producing *rfaC*, *rfaF*, or *rfaP* LPS than producing wild-type LPS. These results support a model in which these LPS biosynthesis mutants also generate an OMP-related signal that activates DegS cleavage of RseA. Data are plotted as mean  $\pm$  1 SEM ( $N \geq 2$ ).



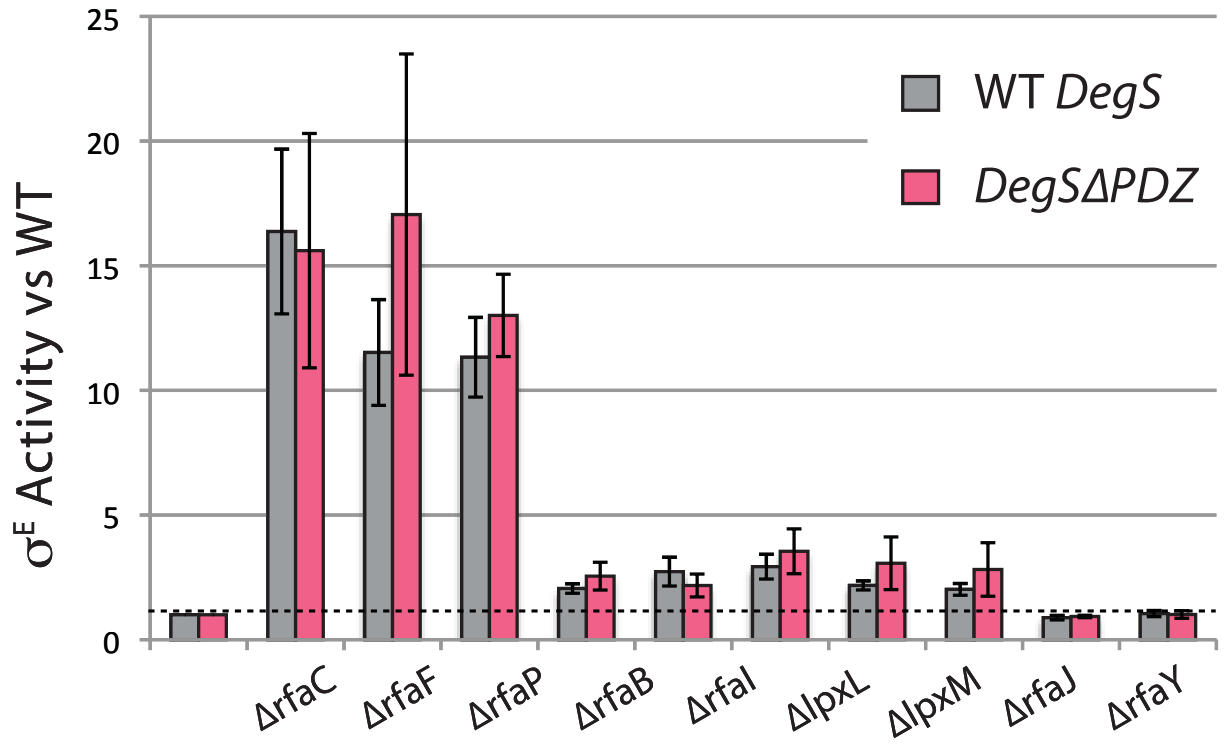


**Supplemental Figure S12:** Effects of the chloramphenicol marker between *lptD* and *surA* on  $\sigma^E$  activity and SurA expression.

(A)  $\sigma^E$  activity from the *rpoHP3*-LacZ reporter in *degS*<sup>+</sup> and *degS* <sup>$\Delta$ PDZ</sup> was not affected by the chloramphenicol marker. (B) SurA levels were increased by the chloramphenicol marker. Western blots of SurA protein levels, with  $\beta'$  as a loading control, for three independent isolates of each strain. SurA levels were increased ~3-fold in the presence of the chloramphenicol marker, and were not affected by the *lptD* <sup>$\Delta$ 330-352</sup> mutation. SurA is a chaperone for LptD, and increased SurA expression should not be detrimental for LptD assembly.



**Supplemental Figure S13:** Histogram of the correlation of the chemical signature of all deletions with  $\Delta rseB$ . Gene deletions in LPS biosynthesis have a similar chemical sensitivity profile as  $\Delta rseB$  in the chemical genomics dataset. 5/9 non-essential genes in LPS core sugar biosynthesis are represented among the to 20 most correlated genes,  $p = 2.8 \times 10^{-10}$ . These gene deletions all truncate the LPS core. *This figure was not included in the Science ms.*



**Supplemental Figure S14:** Mutations in LPS core sugar biosynthesis induce  $\sigma^E$  to similar extents in *DegS*<sup>WT</sup> and in *DegS* <sup>$\Delta$ PDZ</sup> cells.

*This comparison figure was not included in the Science ms.*

**Supplemental Table S1:** Strains used in this study.

| Strain   | Genotype  | Source                         |
|----------|---|--------------------------------|
| MKV12    | W3110 <i>lpxP</i> ::kan   | C. Raetz                       |
| MKV13    | W3110 <i>lpxL</i> ::Tn10, <i>lpxP</i> ::kan   | C. Raetz                       |
| MKV14    | W3110 <i>lpxM</i> ::Ωcam, <i>lpxP</i> ::kan   | C. Raetz                       |
| MKV15b   | W3110 <i>lpxL</i> ::Tn10, <i>lpxM</i> ::Ωcam, <i>lpxP</i> ::kan, uncharacterized suppressor     | C. Raetz; D. Six               |
| D31m4    | <i>proA23, lac-28, tsx-81, trp-30, his-51, rpsL174</i> (strR), <i>rfa-229, rfa-230, ampCp-1</i> | Yale Coli Genetic Stock Center |
| NR698    | MC4100 <i>lptD</i> <sup>Δ330-352</sup> ( <i>imp4213</i> )                                       | T. Silhavy                     |
| NR1216   | MC4100 <i>dsbA</i> ::kan  | D. Kahne                       |
| CAG45114 | MG1655 Δ <i>lacX74</i> ΦI[ <i>rpoHP3-LacZ</i> ]   | ref. 11                        |
| CAG64130 | CAG45114 <i>degS</i> <sup>ΔPDZ</sup> ( <i>degS</i> (Δ757-1065)::kan)                            | <i>This work</i>               |
| CAG64132 | CAG64130 <i>degS</i> <sup>ΔPDZ</sup> ( <i>degS</i> (Δ757-1065)::FRT)                            | <i>This work</i>               |
| CAG64257 | CAG45114 <i>dsbA</i> ::kan  | <i>This work</i>               |
| CAG64258 | CAG64132 <i>dsbA</i> ::kan  | <i>This work</i>               |
| CAG64274 | CAG45114 <i>lptD</i> <sup>Δ330-352</sup> ( <i>lptD4213</i> ::cm)                                | <i>This work</i>               |
| CAG64275 | CAG64294 <i>degS</i> <sup>ΔPDZ</sup> ( <i>degS</i> (Δ757-1065)::kan)                            | <i>This work</i>               |
| CAG64294 | CAG45114 <i>lptD</i> ::cm   | <i>This work</i>               |
| CAG64295 | CAG64130 <i>lptD</i> ::cm   | <i>This work</i>               |
| CAG64801 | CAG45114 <i>lpxL</i> ::kan  | <i>This work</i>               |
| CAG64802 | CAG45114 <i>lpxM</i> ::kan  | <i>This work</i>               |
| CAG64803 | CAG45114 <i>rfaY</i> ::kan  | <i>This work</i>               |
| CAG64804 | CAG45114 <i>rfaQ</i> ::kan  | <i>This work</i>               |
| CAG64830 | CAG45114 <i>rfaF</i> ::kan  | <i>This work</i>               |
| CAG64832 | CAG45114 <i>rfaB</i> ::kan  | <i>This work</i>               |
| CAG64856 | CAG45114 <i>rfaJ</i> ::kan  | <i>This work</i>               |

|          |   |                  |
|----------|---|------------------|
| CAG64858 | CAG45114 <i>rfaG</i> ::kan                            | <i>This work</i> |
| CAG64860 | CAG45114 <i>rfaP</i> ::kan                            | <i>This work</i> |
| CAG64876 | CAG45114 <i>rfaC</i> ::kan                            | <i>This work</i> |
| CAG64878 | CAG45114 <i>rfaI</i> ::kan                            | <i>This work</i> |
| CAG64838 | CAG64132 <i>lpxL</i> ::kan                            | <i>This work</i> |
| CAG64840 | CAG64132 <i>lpxM</i> ::kan                            | <i>This work</i> |
| CAG64842 | CAG64132 <i>rfaQ</i> ::kan                            | <i>This work</i> |
| CAG64844 | CAG64132 <i>rfaY</i> ::kan                            | <i>This work</i> |
| CAG64850 | CAG64132 <i>rfaF</i> ::kan                            | <i>This work</i> |
| CAG64852 | CAG64132 <i>rfaB</i> ::kan                            | <i>This work</i> |
| CAG64866 | CAG64132 <i>rfaJ</i> ::kan                            | <i>This work</i> |
| CAG64868 | CAG64132 <i>rfaG</i> ::kan                            | <i>This work</i> |
| CAG64870 | CAG64132 <i>rfaP</i> ::kan                            | <i>This work</i> |
| CAG64880 | CAG64132 <i>rfaC</i> ::kan                            | <i>This work</i> |
| CAG64882 | CAG64132 <i>rfaI</i> ::kan                            | <i>This work</i> |
| CAG64133 | <i>degS</i> <sup>ΔPDZ</sup> Δ <i>rseB nadB</i> ::Tn10 | <i>This work</i> |
| CAG64881 | CAG64133 <i>rfaC</i> ::kan                            | <i>This work</i> |
| CAG64871 | CAG64133 <i>rfaP</i> ::kan                            | <i>This work</i> |
| CAG64851 | CAG64133 <i>rfaF</i> ::kan                            | <i>This work</i> |
| CAG53505 | CAG45114 Δ <i>rseB nadB</i> ::Tn10                    | <i>This work</i> |
| CAG64831 | CAG53505 <i>rfaF</i> ::kan                            | <i>This work</i> |
| CAG64861 | CAG53505 <i>rfaP</i> ::kan                            | <i>This work</i> |
| CAG64877 | CAG53505 <i>rfaC</i> ::kan                            | <i>This work</i> |

## Supplemental References (27-32)

27. Z. Zhou, S. Lin, R. J. Cotter, C. R. Raetz, Lipid A modifications characteristic of *Salmonella typhimurium* are induced by  $\text{NH}_4\text{VO}_3$  in *Escherichia coli* K12. Detection of 4-amino-4- deoxy-L-arabinose, phosphoethanolamine and palmitate. *J. Biol. Chem.* 274, 18503 (1999). doi:10.1074/jbc.274.26.18503 Medline
28. P. Zhou, E. Altman, M. B. Perry, J. Li, Study of matrix additives for sensitive analysis of lipid A by matrix-assisted laser desorption ionization mass spectrometry. *Appl. Environ. Microbiol.* 76, 3437 (2010). doi:10.1128/AEM.03082-09 Medline
29. E. C. Yi, M. Hackett, Rapid isolation method for lipopolysaccharide and lipid A from gram-negative bacteria. *Analyst* 125, 651 (2000). doi:10.1039/b000368i Medline
30. K. A. Datsenko, B. L. Wanner, One-step inactivation of chromosomal genes in *Escherichia coli* K-12 using PCR products. *Proc. Natl. Acad. Sci. U.S.A.* 97, 6640 (2000). doi:10.1073/pnas.120163297 Medline
31. T. Baba, *et al.*, Construction of *Escherichia coli* K-12 in-frame, single-gene knockout mutants: The Keio collection. *Mol. Syst. Biol.* 2, 2006.0008 (2006).
32. M. K. Vorachek-Warren, S. Ramirez, R. J. Cotter, C. R. Raetz, A triple mutant of *Escherichia coli* lacking secondary acyl chains on lipid A. *J. Biol. Chem.* 277, 14194 (2002). doi:10.1074/jbc.M200409200 Medline

## Chapter 3

MicL, a new  $\sigma^E$ -dependent sRNA, combats envelope stress by repressing synthesis of Lpp, the major outer membrane lipoprotein

**Contributing Authors:** Taylor B. Updegrave, Emily B. Gogol, Svetlana A. Shabalina, Carol A. Gross, and Gisela Storz

*Citation:* Guo, M.S.<sup>†</sup>, Updegrave, T.B.<sup>†</sup>, et al. MicL, a new  $\sigma^E$ -dependent sRNA, combats envelope stress by repressing synthesis of Lpp, the major outer membrane lipoprotein. *Genes & Development* (2014) vol. 28 (14) pp. 1620-34.

<sup>†</sup>These authors contributed equally to this work.

## Preface:

As discussed in the Introduction, the  $\sigma^E$  regulon consists of ~100 genes, which regulate the transport and OM assembly of the OMPs and LPS, and two sRNAs, MicA and RybB that decrease OMP synthesis (Rhodius et al., 2006; Gogol et al., 2011). These sRNAs act in concert with the RNA chaperone, Hfq to target OMP mRNAs for destruction (Vogel and Luisi, 2011).

Importantly, the OM contains a third major component, the OM lipoproteins, which actually represent the majority of proteins transported to the OM. The major lipoprotein is Lpp, which is the most abundant protein in the cell, and serves to structurally link the OM to the peptidoglycan (Braun and Rehn, 1969; Inouye et al., 1972). Previous work has suggested that  $\sigma^E$  may play a role in regulating Lpp, as increased  $\sigma^E$  activity decreases *lpp* mRNA level in an Hfq-dependent fashion (Rhodius et al., 2006; Guisbert et al., 2007). As this effect does not require either of the known  $\sigma^E$ -dependent sRNAs, this suggests that there may be additional  $\sigma^E$ -dependent sRNAs to regulate *lpp* in the cell.

This chapter of my thesis describes the discovery of a third  $\sigma^E$ -dependent sRNA, MicL, which specifically targets *lpp* mRNA. This project was initiated by a previous graduate student in the Gross lab, Emily Gogol, who performed the initial microarrays that discovered a putative  $\sigma^E$ -dependent sRNA (Reg26, later renamed MicL) within the coding region of *cutC*. Emily also performed the microarrays that first showed downregulation of *lpp* by MicL.

Subsequently, I collaborated with Taylor Updegrave in the Gisela Storz lab (NIH) to describe the role of MicL in the cell. Taylor performed all the experiments demonstrating that MicL has the hallmarks of an Hfq-dependent sRNA and demonstrated that MicL is responsible for all known phenotypes of its host gene, *cutC*. Svetlana Shabalina, a staff scientist at NIH, performed sequence analysis to demonstrate conservation of MicL. I performed the mRNA-sequencing and ribosome-profiling and analyzed the data to describe the targets of MicL. I also designed the experiments to test the mechanism of action of MicL and performed the



experiments to demonstrate the role of MicL in the  $\sigma^E$  regulon and the physiology of the cell.

Taylor, Gigi, Carol and I wrote the manuscript, which was published in *Genes & Development* (2014) vol. 28 (14) pp. 1620-34, with Taylor and I as co-first authors, with my name appearing first.

## Abstract

In enteric bacteria, the transcription factor  $\sigma^E$  maintains membrane homeostasis by inducing synthesis of proteins involved in membrane repair and two small, regulatory RNAs (sRNAs) that downregulate synthesis of abundant membrane porins. Here, we describe the discovery of a third  $\sigma^E$ -dependent sRNA, MicL, transcribed from a promoter located within the coding sequence of the *cutC* gene. MicL is synthesized as a 308 nt primary transcript that is processed to an 80 nt form. Both forms possess features typical of Hfq-binding sRNAs, but surprisingly target only a single mRNA, which encodes the outer membrane lipoprotein Lpp, the most abundant protein of the cell. We show that the copper sensitivity phenotype previously ascribed to inactivation of the *cutC* gene is actually derived from the loss of MicL and elevated Lpp levels. This observation raises the possibility that other phenotypes currently attributed to protein defects are due to deficiencies in unappreciated regulatory RNAs. We also report that  $\sigma^E$  activity is sensitive to Lpp abundance and that MicL and Lpp comprise a new  $\sigma^E$  regulatory loop that opposes membrane stress. Together MicA, RybB and MicL allow  $\sigma^E$  to repress the synthesis of all abundant outer membrane proteins in response to stress.

## Introduction

The outer membrane (OM) of gram-negative bacteria is its first line of defense against the environment as it is a barrier against antibiotics and other stresses (reviewed in (Nikaido, 2003)). The OM is a complex environment consisting of outer-leaflet lipopolysaccharide (LPS), inner-leaflet phospholipids, and proteins such as OM porins (OMPs) and lipoproteins (reviewed in (Narita and Tokuda, 2010; Ricci and Silhavy, 2012; Silhavy et al., 2010; Zhang et al., 2013)). The major *E. coli* lipoprotein, Lpp, resides in the OM and is the most abundant protein in the cell (~1 million copies), comprising 2% of its dry weight (Li et al., 2014; Narita and Tokuda, 2010). Approximately a third of the Lpp pool is conjugated to the peptidoglycan layer, serving as a structural element that connects the OM to the peptidoglycan (Braun and Rehn, 1969; Inouye et al., 1972) while the remainder exists, at least in part, as a surface-exposed form that can be recognized by anti-microbial peptides (Chang et al., 2012; Cowles et al., 2011). Since cells synthesize a new OM each cell cycle, OM components are synthesized and transported at a tremendous rate. Indeed, at 37°C more than 5% of all active ribosomes are devoted to Lpp translation (Li et al., 2014). Therefore, balancing the massive flux of membrane components with sufficient transport and assembly factors is vital for OM homeostasis.

In *Escherichia coli* and related  $\gamma$ -proteobacteria, OM homeostasis is monitored by the essential transcription factor  $\sigma^E$ , which responds to perturbations to OMP and LPS folding (Barchinger and Ades, 2013; Lima et al., 2013; Walsh et al., 2003; Zhang et al., 2013).  $\sigma^E$  activity is regulated by the degradation rate of its negative regulator RseA, which holds  $\sigma^E$  inactive in the inner membrane. RseA cleavage is initiated by DegS in response to unfolded OMP stress, but a second regulator, RseB, binds to RseA and protects it from cleavage by DegS (Chaba et al., 2011; Walsh et al., 2003). Off-pathway LPS can bind to RseB and relieve its inhibition of DegS (Lima et al., 2013). Once RseA is cleaved, it undergoes proteolytic degradation and releases  $\sigma^E$  (Chaba et al., 2007). As  $\sigma^E$  activation is thus dependent on two

signals, only concomitant OMP and LPS dysfunction will lead to maximal induction of  $\sigma^E$  (Lima et al., 2013).

Activation of  $\sigma^E$  induces expression of ~100 genes, including all of the machinery required for the transport and assembly of LPS and OMPs into the OM (Braun and Silhavy, 2002; Rhodius et al., 2006; Skovierova et al., 2006; Wu et al., 2005). As the synthesis rate of new OM components is so high, increasing production of chaperones and transport factors may not be sufficient to rapidly restore folding during stress conditions. To combat this problem,  $\sigma^E$  additionally induces expression of two small regulatory RNAs (sRNAs), MicA and RybB, which act to inhibit synthesis of all major OMPs (Johansen et al., 2006; Papenfort et al., 2010; Papenfort et al., 2006; Rasmussen et al., 2005; Thompson et al., 2007; Udekwu et al., 2005; Udekwu and Wagner, 2007).

sRNAs are integral to a myriad of bacterial stress responses, usually interacting with their *trans*-encoded target mRNAs via base pairing to change message stability or translation (reviewed in (Richards and Vanderpool, 2011; Storz et al., 2011)). In enteric bacteria, these base pairing sRNAs are usually associated with the RNA chaperone Hfq, which binds to and protects sRNAs from nuclease degradation, and facilitates the intermolecular contacts between sRNAs and target mRNAs (reviewed in (Vogel and Luisi, 2011)). Only limited base pairing is required for productive interaction. This inherent degeneracy in targeting sequences allows sRNAs to have multiple targets, and conversely, for specific mRNAs to have multiple sRNA regulators.

The  $\sigma^E$ -dependent sRNAs MicA and RybB bind to Hfq and together target 31 messages for degradation, including mRNAs encoding the major porins as well as proteins in metabolism, ribosomal biogenesis, a toxin anti-toxin system, and the transcriptional factor PhoP (Coornaert et al., 2010; Gogol et al., 2011). The promoters of MicA and RybB are the second and third strongest in the  $\sigma^E$  regulon, weaker only than the  $\sigma^E$  promoter itself (Mutalik et al., 2009). These sRNAs have strong protective effects on membrane homeostasis, as they can rescue cell death

resulting from the membrane blebbing and lysis associated with loss of  $\sigma^E$  activity (Gogol et al., 2011; Hayden and Ades, 2008), presumably by downregulating *omp* mRNA and rebalancing the membrane (Gogol et al., 2011; Papenfort et al., 2010).

Here we report the discovery and characterization of a third  $\sigma^E$ -dependent sRNA and show this sRNA is dedicated to the regulation of Lpp. We name this sRNA MicL for mRNA-interfering complementary RNA regulator of Lpp, following the nomenclature of (Mizuno et al., 1984). MicL is transcribed from a strong  $\sigma^E$ -dependent promoter within the *cutC* coding sequence and subsequently processed into a smaller transcript (MicL-S). It is responsible for all phenotypes previously associated with loss of *cutC*. We discuss how our finding that MicL/Lpp constitute a novel regulatory loop modulating  $\sigma^E$  activity expands our view of the cellular mechanism for maintaining OM homeostasis, as well as the implications of sRNAs evolving from the 3' end of transcripts.

## Results

### *MicL is a third $\sigma^E$ regulated sRNA*

To identify novel  $\sigma^E$ -dependent sRNAs in *E. coli*, we used a tiled microarray to examine whole genome expression after ectopic  $\sigma^E$  overexpression. Along with the previously identified  $\sigma^E$ -dependent sRNAs, MicA and RybB, we observed two overlapping transcripts that were strongly upregulated in a  $\sigma^E$ -dependent manner within the 3' end of *cutC* and the intergenic region between *cutC* and *torY* (Fig. 1A). These transcripts are likely the same as RyeF, a putative sRNA previously identified in the *cutC/torY* intergenic region of *E. coli* and *Salmonella* (Chao et al., 2012; Zhang et al., 2003a). We did not observe a  $\sigma^E$ -dependent transcript upstream of *cutC*, suggesting that *cutC* itself is not  $\sigma^E$ -dependent (data not shown). Additionally, we did not observe the previously postulated  $\sigma^E$  regulation of CyaR (Johansen et al., 2008), suggesting that this sRNA is unlikely to be directly regulated by  $\sigma^E$  (data not shown).

Northern analysis of total RNA isolated from cells with and without ectopic expression of  $\sigma^E$  validated the presence of two  $\sigma^E$ -dependent transcripts, a ~300 nt transcript denoted MicL, and an ~80 nt transcript denoted MicL-S, which were detected with a probe to the 3' end of *cutC* (Fig. 1B). Both MicL and MicL-S are induced during transition to stationary phase, a time when  $\sigma^E$  activity increases dramatically (Ades et al., 1999; Costanzo and Ades, 2006). The two bands showed maximal expression during late stationary phase in defined rich media (around ~15 h, Fig. 1C) and in LB (data not shown), consistent with  $\sigma^E$  induction.

Primer extension and total mRNA sequencing analysis revealed that the 308 nt MicL transcript begins within *cutC* (226 nt before *cutC* stop codon) and ends at the *cutC* intrinsic terminator, significantly upstream of the start of *torY* (data not shown and Supplemental Fig. S1A-B). The 80 nt MicL-S begins with the last base of the *cutC* stop codon and ends at the *cutC* terminator. Thus both forms of MicL contain the full *cutC* 3'UTR.

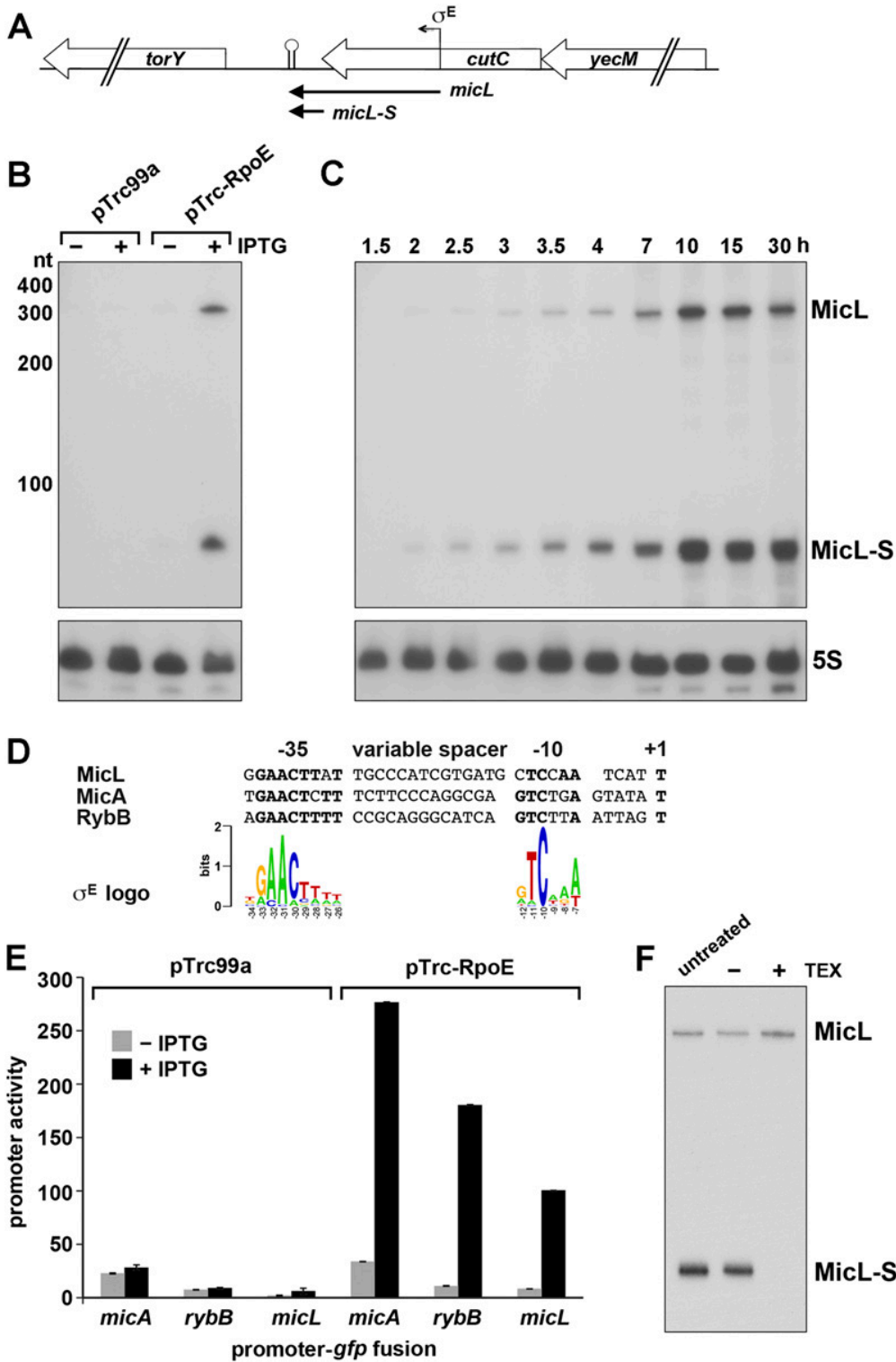


**Figure 1.** MicL expression is regulated by  $\sigma^E$ .

(A) Schematic of genomic context of MicL, its processed transcript MicL-S, and *cutC* (See Supplemental Fig. S1B).

(B) MicL levels increase following  $\sigma^E$  overexpression. Cells harboring either vector or a  $\sigma^E$  expression plasmid

growing exponentially in EZ Rich Defined Media were induced with 1 mM IPTG for 1 h. RNA was extracted and probed for the 3' end of MicL and 5S RNA. **(C)** MicL levels increase in stationary phase. Total RNA was extracted at the indicated times during growth in EZ Rich Defined Media and probed for MicL and 5S RNA. **(D)** The *micL* promoter is similar to a logo for  $\sigma^E$  promoter sequences (Rhodius et al., 2012). **(E)**  $P_{micL}$  is  $\sigma^E$ -dependent. Cells carrying either the vector control or the pTrc-RpoE plasmid, expressing GFP from the indicated minimal promoters (-60 to +20 relative to transcription start site) and growing exponentially in LB were induced with 1mM IPTG, and GFP fluorescence monitored. Promoter activity is measured by normalizing GFP fluorescence by OD (see Materials and Methods). **(F)** MicL-S is a processed transcript. RNA isolated following induction of MicL for 3 h from an IPTG-inducible promoter was: left untreated, incubated in buffer, or incubated in buffer with 5' monophosphate-dependent terminator exonuclease (TEX). MicL-S levels were subsequently probed.



We identified a putative  $\sigma^E$  promoter upstream of the start of MicL ( $P_{micL}$ ) (Fig. 1D) (Rhodius et al., 2006) but not in front of MicL-S. Strong conservation of this sequence within the *cutC* coding sequence is observed in *Shigella*, *Salmonella*, *Citrobacter*, *Klebsiella*, *Cronobacter* and *Enterobacter* species but not in more distantly-related enteric bacteria (Supplemental Fig. S2A-D). A fusion of the minimal putative  $P_{micL}$  promoter (-65 to +20) to GFP is induced by ectopic  $\sigma^E$  overexpression, and is only slightly weaker than the strong  $\sigma^E$ -dependent *micA* and *rybB* promoters in the same vector background (Fig. 1E). Together, these data show that MicL is a third  $\sigma^E$ -dependent sRNA in *E. coli* and likely in related enteric bacteria.

#### *MicL-S is processed from MicL*

MicL-S may be processed from MicL, as we did not observe a promoter for MicL-S. We tested this by treating total RNA with 5' monophosphate-dependent terminator exonuclease (TEX), which degrades processed transcripts, but spares primary transcripts as they have 5' triphosphates. Following TEX treatment, MicL-S is degraded but the MicL level is virtually unchanged (Fig. 1F), suggesting that MicL-S is generated by ribonucleolytic cleavage of MicL. We examined MicL levels after 15 min of MicL induction from  $P_{LacO-1}$  and subsequent IPTG washout (Supplemental Fig. S3A). The observations that MicL-S is detected only after induction of MicL and that MicL and MicL-S disappear with similar kinetics, support the idea that MicL-S is derived from MicL. Importantly, MicL-S expressed independently from the  $P_{LacO-1}$  promoter has the same half-life as MicL-S cleaved from MicL (Supplemental Fig. S3B), demonstrating that cleavage does not impact MicL-S stability.

We next investigated the mechanism of MicL processing. Although the MicL cleavage site is within the *cutC* TGA stop codon, this sequence is not a cleavage signal, as a TGA to GGA mutation did not alter processing (Supplemental Fig. S3C). RNase E is the primary RNase in *E. coli* and mediates processing of other sRNAs (Massé et al., 2003), but production of MicL-S was not abolished in a *rne-3071* mutant (Supplemental Fig. S3D) or in strains lacking various

other RNases (Opdyke et al., 2011), including RNase III (*rnc*), RNase G (*rng*), RNase BN (*elaC*), five toxin endonucleases (Supplemental Fig. S3E), and the broadly conserved YbeY RNase (data not shown). Either uncharacterized ribonucleases mediate MicL processing or other combinations of RNases perform this function.

### *Lpp* is the sole target of MicL

Transcripts from the 3'UTR of *cutC* (RyeF) co-immunoprecipitate with Hfq in *E. coli* and *Salmonella* (Chao et al., 2012; Zhang et al., 2003a). We validated this observation for both MicL and MicL-S, which co-immunoprecipitate with Hfq at ratios consistent with their levels, suggesting that both forms bind Hfq with similar affinity (Fig. 2A). In addition, both MicL transcripts are virtually undetectable in strains lacking Hfq (*hfq-1*), indicating that their stabilities are Hfq-dependent (Fig. 2A).

Hfq-binding sRNAs in *E. coli* have all been found to regulate target mRNAs via limited base pairing, enabling them to regulate expression of multiple targets. With this expectation, we searched for targets of MicL. However, analysis of mRNA-sequencing (mRNA-seq) data taken before and after expression of MicL for 4, 10 and 20 min identified only a single MicL target, *lpp* (Fig. 2B; Supplemental Fig. S4A; Supplemental Table S1). The levels of *lpp* mRNA were reduced starting 4 min after induction and were down regulated by 20-fold after 20 min (Supplemental Fig. S4C). The OM lipoprotein Lpp, the most abundant protein in the cell, is a key component of the membrane.  $\sigma^E$  was previously reported to repress *lpp* via an unknown mechanism that required Hfq (Guisbert et al., 2007; Rhodius et al., 2006). Stunningly, even after the 20-fold reduction in *lpp* mRNA due to MicL overexpression, *lpp* is still the 12<sup>th</sup> most abundant mRNA in the cell (Supplemental Table S1).

We examined the possibility that other MicL targets might be regulated solely at the level of translation by sequencing ribosome-protected mRNA fragments (ribosome profiling) (Ingolia et al., 2009) after ectopic expression of MicL at the same time points used above for mRNA-seq

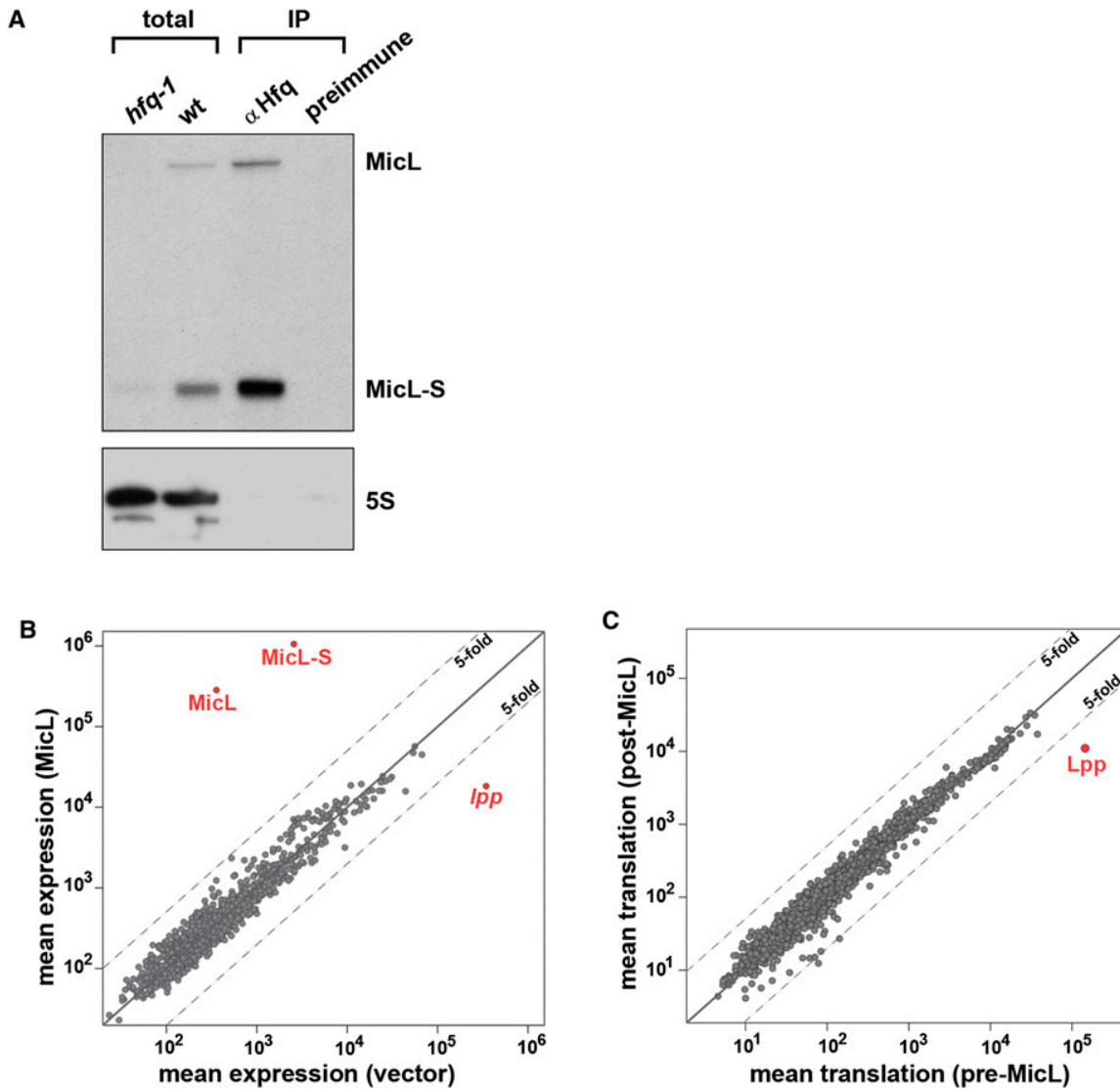


**Figure 2.** *lpp* is the sole target of MicL.

**(A)** MicL interacts with Hfq. Extracts were prepared from wild-type cells after 16 h growth in LB medium and subject to immunoprecipitation with  $\alpha$ -Hfq or preimmune serum. MicL was probed in the immunoprecipitated samples (0.5  $\mu$ g RNA loaded) as well as on total RNA isolated from wild-type and the isogenic *hfq-1* mutant cells (5  $\mu$ g RNA loaded).

**(B)** MicL expression reduces *lpp* mRNA levels ~20-fold. mRNA-seq was performed in exponential phase after 20 min of MicL induction from pBR'-MicL at 30°C in EZ Rich Defined Media and compared to a similarly-treated vector control strain. Expression level in reads per kilobase per million (RPKM).

**(C)** MicL expression reduces translation on *lpp* mRNA ~10-fold. Ribosome profiling was performed in exponential phase after 20 min of MicL induction from pBR'-MicL at 30°C in EZ Rich Defined Media and compared to profiles taken before MicL induction. Relative translation in RPKM. Other genes (*fepA*, *fiu*) close to the 5-fold cutoff are repressed by growth (Supplemental Fig. S4F).

(Fig. 2C and Supplemental Table S2). Similar to what we observed for the steady state mRNA levels, expression of MicL decreased translation of *lpp* ~10-fold after 20 min induction of MicL. For all other transcripts, translation was not significantly altered by MicL overexpression (Supplemental Fig. S4E, F). *lpp* is the most well-translated mRNA in the cell, and remains the 30<sup>th</sup> most well-translated mRNA after MicL expression (Supplemental Table S2). Together, these experiments strongly suggest that *lpp* is the sole MicL target under the conditions tested.

#### *MicL repression of Lpp mimics lpp deletion phenotypes*

Strains lacking *Lpp* were reported to be sensitive to membrane perturbants such as dibucaine, deoxycholate, sodium dodecyl sulfate (SDS) and ethylenediaminetetraacetic acid (EDTA) (Hirota et al., 1977; Nichols et al., 2011; Suzuki et al., 1978). Using the reported concentrations for these chemicals, we found that dibucaine yielded the strongest distinction between wild-type and  $\Delta lpp$  strains, with the latter having small, translucent colonies in the presence of dibucaine. (Fig. 3A). Cells harboring MicL or MicL-S appeared mildly translucent on dibucaine in the absence of inducer, and become markedly translucent after addition of inducer (compare Fig. 3A with Supplemental Fig. S5).  $\Delta lpp$  cells additionally display a small (~10-fold) decrease in viability, but this was not observed for wild-type cells overexpressing either MicL or MicL-S, possibly because such cells still retain some *Lpp*. Overexpression of MicL or MicL-S in a  $\Delta lpp$  background did not further sensitize cells to dibucaine (Fig. 3A), supporting the conclusion that the dibucaine sensitivity associated with MicL overexpression is due to decreased *lpp* levels.

#### *Endogenous levels of MicL are sufficient to repress lpp*

To determine whether MicL expressed from its native locus had the capacity to repress *lpp*, we assayed *lpp* mRNA levels upon  $\sigma^E$  overexpression. Indeed, elevated  $\sigma^E$  led to reduced *lpp* mRNA in wild-type cells but not in a strain lacking MicL ( $\Delta cutC$ ; Fig. 3B). We also tested

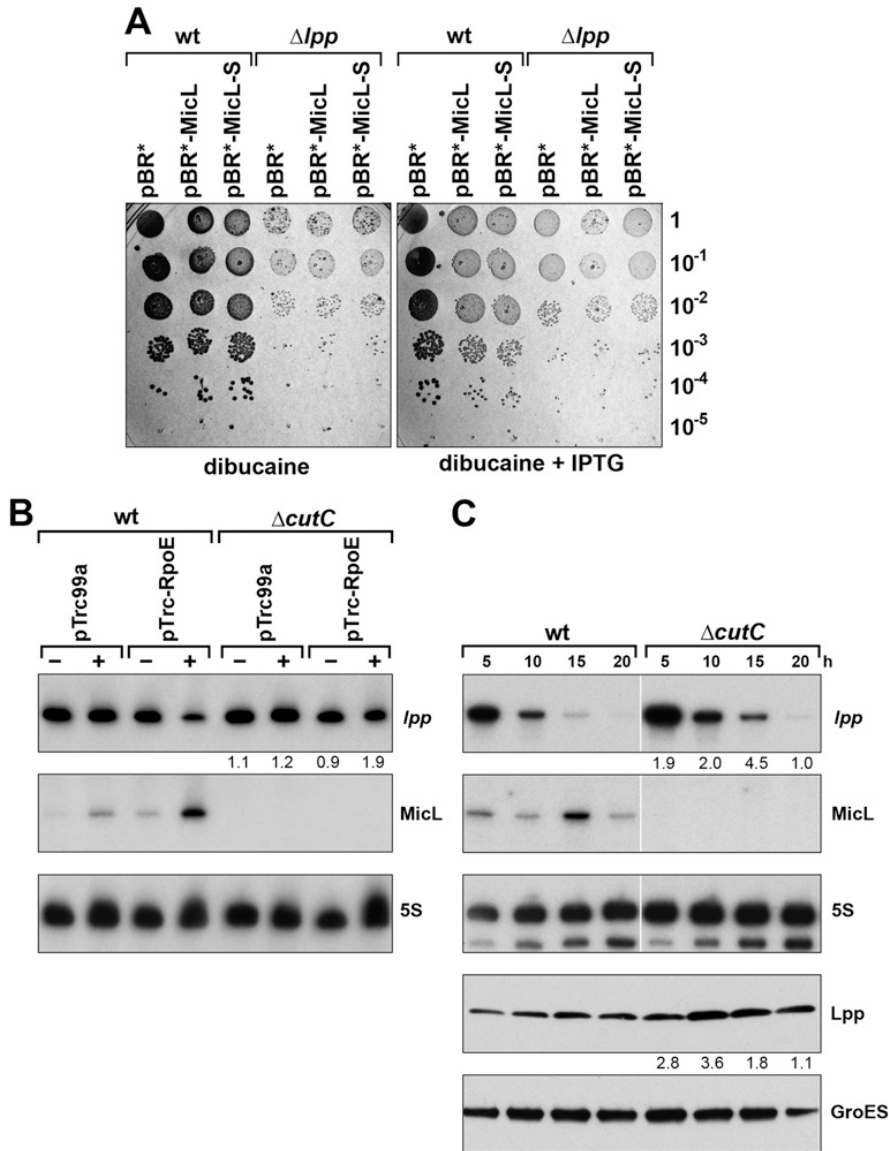


**Figure 3.** MicL repression of *lpp* is physiologically important.

**(A)** Expression of MicL phenocopies the dibucaine sensitivity of  $\Delta lpp$ . Wild-type or  $\Delta lpp$  cells carrying pBR\*-MicL, pBR\*-MicL-S, or empty vector were spotted at the indicated dilutions on LB plates containing 1.4 mM dibucaine with or without 1 mM IPTG. **(B)** MicL represses *lpp* RNA levels following  $\sigma^E$  overexpression. Wild-type and a  $\Delta cutC$  strain with either control vector or pRpoE growing exponentially in LB (OD<sub>600</sub> ~0.1) were induced with 1 mM IPTG for 2 h. Total RNA was isolated and probed for *lpp*, MicL and 5S RNA. **(C)** *lpp* mRNA and Lpp protein levels in wild-type and  $\Delta cutC$  mutant backgrounds. At the indicated times, total RNA was extracted from wild-type and the  $\Delta cutC$  mutant strain grown in LB. Total RNA was probed to examine *lpp*, MicL and 5S RNA levels, and Lpp and GroEL protein levels were examined by immunoblotting protein samples taken at the same time points. For **(B)** and **(C)**, the intensity of the *lpp* RNA or protein band for each strain was quantified using ImageJ software, and the ratios between the corresponding samples for the  $\Delta cutC$  mutant and wild type strains are given.

whether *lpp* mRNA was down regulated in stationary phase when MicL levels are highest (Fig. 1C). As can be seen in Fig. 3C, in stationary phase (10 or 15 h of growth), *lpp* transcript levels are less abundant in wild-type cells than in cells lacking MicL. We also observe higher accumulation of Lpp protein in the  $\Delta cutC$  strain compared to the wild-type strain. The Lpp protein level does not mirror changes in *lpp* mRNA, as the protein is stable and therefore accumulates in stationary phase because proteins are no longer diluted by cell division. Interestingly, even in the  $\Delta cutC$  strain we see a sharp decrease in *lpp* mRNA levels during stationary phase, suggesting the existence of additional regulators of *lpp* expression, and highlighting the importance of reducing Lpp levels in stationary phase (Fig. 3C).

#### *MicL-S base pairs directly with lpp mRNA*

To test for direct base pairing between MicL and *lpp*, we generated a translational fusion by integrating the *lpp* 5'UTR (containing sequences from the transcription start site through 102 nt of the *lpp* coding sequence) in frame to the 7<sup>th</sup> codon of *lacZ* gene, all downstream of the heterologous P<sub>BAD</sub> promoter in the chromosome of PM1205 (Mandin and Gottesman, 2009). The  $\beta$ -galactosidase activity of this reporter strain was reduced >2-fold by ectopic overexpression of both MicL and MicL-S, but not by overexpression of MicA or RybB (Fig. 4A). As both forms of MicL downregulate *lpp*, the region required for regulation must be within MicL-S. To further define the regulatory region, we tested whether 5' truncations of MicL-S retained the ability to regulate the *lpp-lacZ* translational reporter. A MicL-S variant lacking the first 12 nt (MicL-S $\Delta$ 1) fully repressed the fusion while a MicL-S variant lacking the first 45 nt (MicL-S $\Delta$ 2) did not, placing the sequence required for regulation between nt +13-44 of MicL-S (Supplemental Fig. S6). We similarly defined the MicL responsive region of *lpp*, finding that a truncation retaining the first 33 nt of the *lpp* coding sequence is repressed by MicL-S (*lpp* $\Delta$ 2), but a truncation that retains only the first 6 nt of the coding sequence is not (*lpp* $\Delta$ 3), suggesting

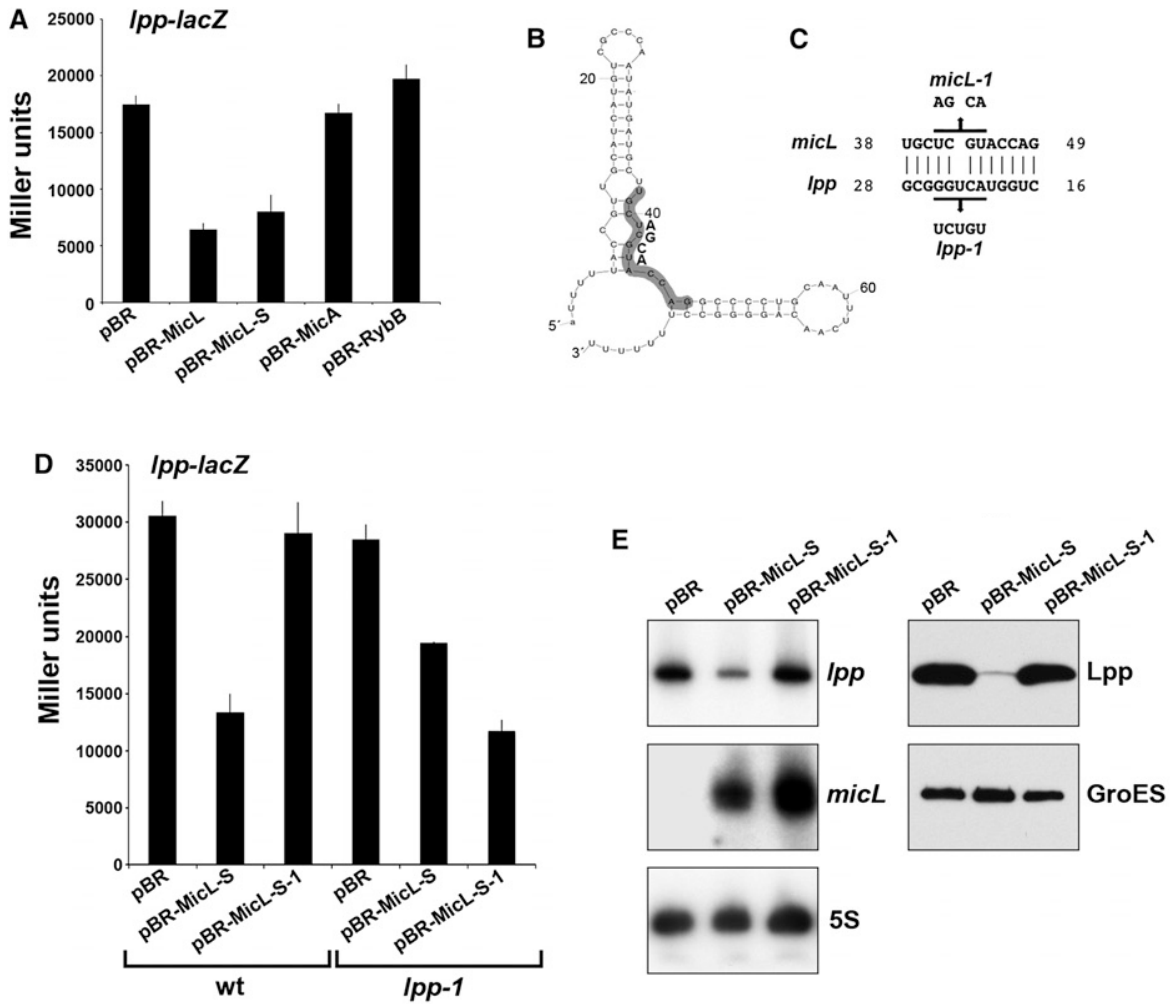


**Figure 4.** MicL base pairs with *lpp*.

**(A)** MicL and MicL-S, but not MicA and RybB, repress an *lpp-lacZ* translational fusion.  $\beta$ -galactosidase activity of the *lpp-lacZ* fusion preceded by a  $P_{BAD}$  promoter was assayed in strains with control vector, pBR-MicL, pBR-MicL-S, pBR-MicA and pBR-RybB plasmids after 3 h induction with 0.2% arabinose (for fusion) and 1 mM IPTG (for sRNA) (final  $OD_{600} \sim 1.0$ ) in LB. Average values and standard deviations from four independent experiments are shown. **(B)** Predicted structure of MicL-S. Nucleotides predicted to base pair with *lpp* are shaded. **(C)** Predicted MicL and *lpp* base pairing with mutations designed to disrupt interaction. **(D)** Effect of disruption and restoration of base pairing on MicL repression of *lpp-lacZ*. Plasmids carrying wild-type MicL-S or the MicL-S-1 derivative were transformed into strains containing *lpp-lacZ* or *lpp-1-lacZ*, which carries compensatory mutations to restore base pairing with MicL-S-1.  $\beta$ -galactosidase activity was assayed as in **(A)**. **(E)** MicL-S but not MicL-S-1 lowers *lpp* RNA and Lpp protein levels. The *lpp-lacZ* fusion strain was transformed with pBR-MicL-S or pBR-MicL-S-1 and induced as in **(A)**. Samples were collected after 3 h and levels of *lpp*, the MicL-S and 5S RNA or the Lpp and GroEL proteins were probed.

that a portion of the sequence targeted by MicL lies between +6-33 nt of the *lpp* coding sequence (+43-70 nt from the start of the of *lpp* mRNA, Supplemental Fig. S6).

Computational analysis of these regions using ThermoComposition software (Matveeva et al., 2007) also suggested possible base pairing between +19-49 of MicL-S (Fig. 4B) and +16-46 of the *lpp* coding sequence. Indeed, MicL-S-1, harboring a 4 nt mutation in the predicted pairing region of MicL-S (Fig. 4C, altered nt +41-44) was unable to repress *lpp-lacZ* reporter (Fig. 4D), but a compensatory mutation in *lpp* (*lpp-lacZ-1*, altered nt +21-25 of the coding sequence) restored repression to levels comparable to wild-type regulation (Fig. 4D). We verified that MicL-S and MicL-S-1 accumulate to similar levels, and while MicL-S noticeably reduced *lpp* mRNA and Lpp protein levels, MicL-S-1 does not (Fig. 4E). Thus, MicL-S is an sRNA that directly base pairs with and represses *lpp*.

Stable duplex predictions between *cutC* and *lpp* in various bacteria revealed that the extensive region of base pairing, and particularly a stable core (seed) interaction between +38-49 of MicL-S and +16-28 of the *lpp* coding sequence, is conserved only in a select group of enteric bacteria, consistent with a recent evolution of the MicL RNA (Supplemental Figs. S1A-D and S7). Interestingly, while *Salmonella enterica* contains two *lpp* genes (LppA and LppB), the long stretch of MicL complementarity is only detected for one of the two *lpp* genes (LppA) found in this organism.

#### *MicL represses lpp by inhibiting translation*

Most sRNAs inhibit translation by sterically occluding the Shine-Dalgarno sequence or the start codon, preventing ribosomes from accessing target mRNA (reviewed in (Desnoyers et al., 2013)). As the core of MicL base pairing with *lpp* is downstream of the translation start site (+16-28 nt of the *lpp* coding sequence, Fig. 5A), at the edge of the region where sRNA binding is known to interfere with translation initiation (Bouvier et al., 2008), it is unclear whether MicL represses translation or affects mRNA stability independently of translation. To examine this, we



tested whether MicL-S overexpression reduces the mRNA levels of *lpp* derivatives harboring early stop mutants (stop codon at start and 2<sup>nd</sup> and 4<sup>th</sup> codons, Fig. 5A). While the *lpp* stop mutant at the start codon cannot be translated, translation should initiate for the other two derivatives. Although the absolute levels of *lpp* mRNA are altered, we no longer observe a significant decrease in *lpp* mRNA levels following MicL-S overexpression in any of these strains (Fig. 5B). This suggests that the primary effect of MicL is to inhibit translation of *lpp* rather than to mediate *lpp* mRNA degradation, and that increased degradation is a consequence of the fact that untranslated mRNAs are not protected from ribonucleolytic cleavage (Nilsson et al., 1984).

Consistent with the idea that *lpp* mRNA is rapidly degraded in the absence of active translation, we observed that expression of MicL did not significantly decrease the translation efficiency (ribosomes per unit mRNA) of *lpp* (Fig. 5C). This suggests that every *lpp* mRNA is being translated by the same number of ribosomes regardless of the level of MicL. Thus *lpp* mRNA is either undergoing active translation or is rapidly cleared when MicL binding blocks translation.

#### *Phenotypes ascribed to $\Delta cutC$ are due to eliminating MicL repression of *lpp**

The *cutC* gene was reported to be involved in copper homeostasis because missense mutations in *cutC* alone and in combination with mutations in *nlpE* lead to copper sensitivity (Gupta et al., 1995). Interestingly, the *cutC* mutations leading to copper sensitivity are clustered around the P<sub>micL</sub> promoter: one lies between the P<sub>micL</sub> -10 and -35 motifs (nt change G197A, amino acid change R66H) and the other is located at -67 from the P<sub>micL</sub> start (nt change A146G, amino acid change K49R), raising the possibility that the copper phenotype of *cutC* could be due to misregulation of MicL. We tested this possibility by determining the copper phenotype of two constructs: a 5' deletion of *cutC* that maintains MicL but deletes the first 104 codons of *cutC* (*cutC* $\Delta$ 5'), and a MicL promoter mutant (point mutations in P<sub>micL</sub> -10 and -35 motifs) that conserves CutC protein sequence (P<sub>micL</sub> mutant). Northern analysis confirmed that MicL and

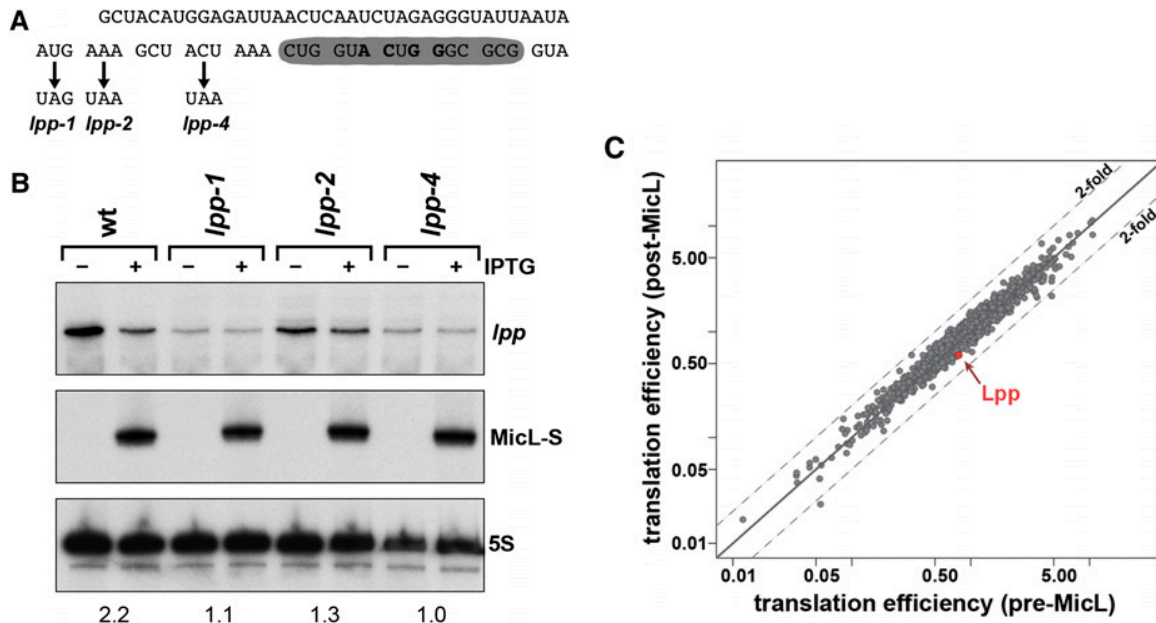


**Figure 5.** MicL repression of *lpp* is dependent on translation.

**(A)** Diagrammatic representation of the derivatives carrying early stop codon mutations: *lpp-1*, ATG to TAG at first codon; *lpp-2*, AAA to TAA at second codon; and *lpp-4*, ACT to TAA at fourth codon. **(B)** The pBR\*-MicL-S plasmid was transformed into wild-type and *lpp* translation-defective cells, MicL-S was induced with 1 mM IPTG in LB for 3 h, and RNA was extracted (final OD<sub>600</sub> ~1.0) and probed for *lpp*, MicL-S and 5S RNA. The intensity of the *lpp* band from each strain was quantified using ImageJ software, and the fold changes listed below are calculated for the corresponding samples with and without IPTG. Immunoblot analysis for Lpp confirmed that translation was eliminated in the stop codon mutants (data not shown). **(C)** Translation efficiency of Lpp is unchanged after MicL expression. Translation efficiency per gene after 20 min of MicL induction is plotted versus translation efficiency before MicL induction. Translation efficiency is calculated as the # of ribosome footprints per gene/mRNA reads per gene from the ribosome profiling and mRNA-seq data.

MicL-S expression was nearly abolished by  $P_{micL}$  mutation (Supplemental Fig. S8B), and western analysis confirmed that CutC is not synthesized in the  $cutC\Delta 5'$  mutant (Supplemental Fig. S1C). The MicL levels were moderately reduced in  $cutC\Delta 5'$  cells, possibly due to effects on  $P_{micL}$  (Supplemental Fig. S8B). However, only the  $P_{micL}$  mutant has a copper sensitivity phenotype that closely matches that of  $\Delta cutC$  (Fig. 6A; Supplemental Fig. S9). Furthermore, ectopic expression of either MicL or MicL-S dramatically increased the viability of  $\Delta cutC$  on copper (Fig. 6B) without affecting growth (Supplemental Fig. S8D). MicL overexpression also enhanced copper resistance in wild-type cells (Fig. 6B).

As *lpp* is the sole target of MicL, we tested whether reduced synthesis of Lpp underlies copper resistance. Indeed, a  $\Delta lpp$  strain was slightly more resistant to copper than wild type cells (Fig. 6A and Supplemental Fig. S9), and overexpression of MicL and MicL-S did not increase the copper resistance of  $\Delta lpp$  mutants (Fig. 6B). Together, these data suggest that high levels of Lpp result in copper sensitivity, and that MicL confers copper resistance by reducing Lpp levels.

#### $\sigma^E$ , MicL, and Lpp form a protective regulatory loop

The essential transcription factor  $\sigma^E$  regulates the folding and levels of abundant membrane proteins such as OM porins (OMPs). In a previously described regulatory loop (Gogol et al., 2011; Papenfort et al., 2010),  $\sigma^E$  is activated by unfolded OMPs, and in turn induces expression of the MicA and RybB sRNAs, which oppose stress by downregulating OMP mRNAs. MicL and Lpp may constitute another  $\sigma^E$ -dependent regulatory loop that opposes stresses associated with Lpp accumulation. We tested whether the MicL, Lpp, and  $\sigma^E$  relationship was similar to that established for RybB and MicA, OMPs, and  $\sigma^E$ . Indeed,  $\sigma^E$  activity responds to Lpp levels. Although Lpp is already the most abundant protein in the cell, mild overexpression of Lpp (~2-fold) leads to activation of the  $\sigma^E$  response and high

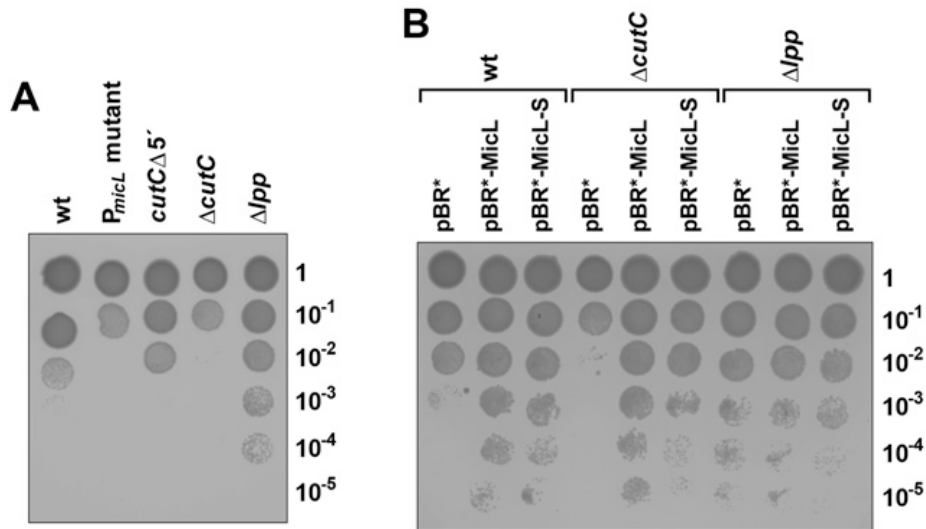


**Figure 6.** Copper sensitivity of  $\Delta cutC$  is due to loss of MicL.

**(A)** Sensitivity of wild-type strains and variants with *P<sub>micL</sub>* mutant (-10C-T/-35A-G), *cutC*Δ5' (which preserves MicL),  $\Delta cutC$  and  $\Delta lpp$  to 4 mM Cu(II)Cl<sub>2</sub>. 3  $\mu$ L of each strain in exponential phase were spotted on LB supplemented with 4 mM Cu(II)Cl<sub>2</sub> at the indicated dilutions (Gupta et al., 1995; Tetaz and Luke, 1983). **(B)** Sensitivity of wild-type cells,  $\Delta cutC$ , and  $\Delta lpp$  transformed with pBR\* control vector, pBR\*-MicL-S and pBR\*-MicL to 4 mM Cu(II)Cl<sub>2</sub> using conditions in **(A)** with the exception that the media was additionally supplemented with kan. Some differences in sensitivity between **(A)** and **(B)** may be due to a synthetic effect between copper and the kan used for plasmid selection in **(B)**.

overexpression (~3-fold) leads to significant  $\sigma^E$  activity and growth arrest (Fig. 7A and Supplemental Fig. S10A).

Others have found that  $\sigma^E$  activity is inhibited in cells that have lost *lpp* (Mecenas et al., 1993). Similarly, we observe that reducing Lpp levels 10-fold by MicL overexpression leads to a reduction in  $\sigma^E$  activity (Fig. 7B and Supplemental S10B). In addition, northern analysis showed that cells lacking MicL ( $\Delta cutC$  strain) have ~1.5-fold higher RybB levels in stationary phase (Supplemental Fig. S10C), consistent with higher  $\sigma^E$  activity.

Finally, and most importantly, overexpression of MicL is able to rescue the growth defect associated with depletion of  $\sigma^E$  activity (Fig. 7C, Supplemental Fig. S10D) (De Las Peñas et al., 1997; Hayden and Ades, 2008) as was observed for MicA and RybB overexpression (Gogol et al., 2011; Papenfort et al., 2010). The ~50- to 100-fold decrease in viability caused by overexpressing the  $\sigma^E$  negative regulators RseA and RseB is rescued comparably by co-expressing either MicL or MicA (Fig. 7C, Supplemental Fig. S10D). We conclude that MicL and Lpp represent an additional protective sRNA loop with similar OM-protective function as the other  $\sigma^E$ -dependent sRNAs.

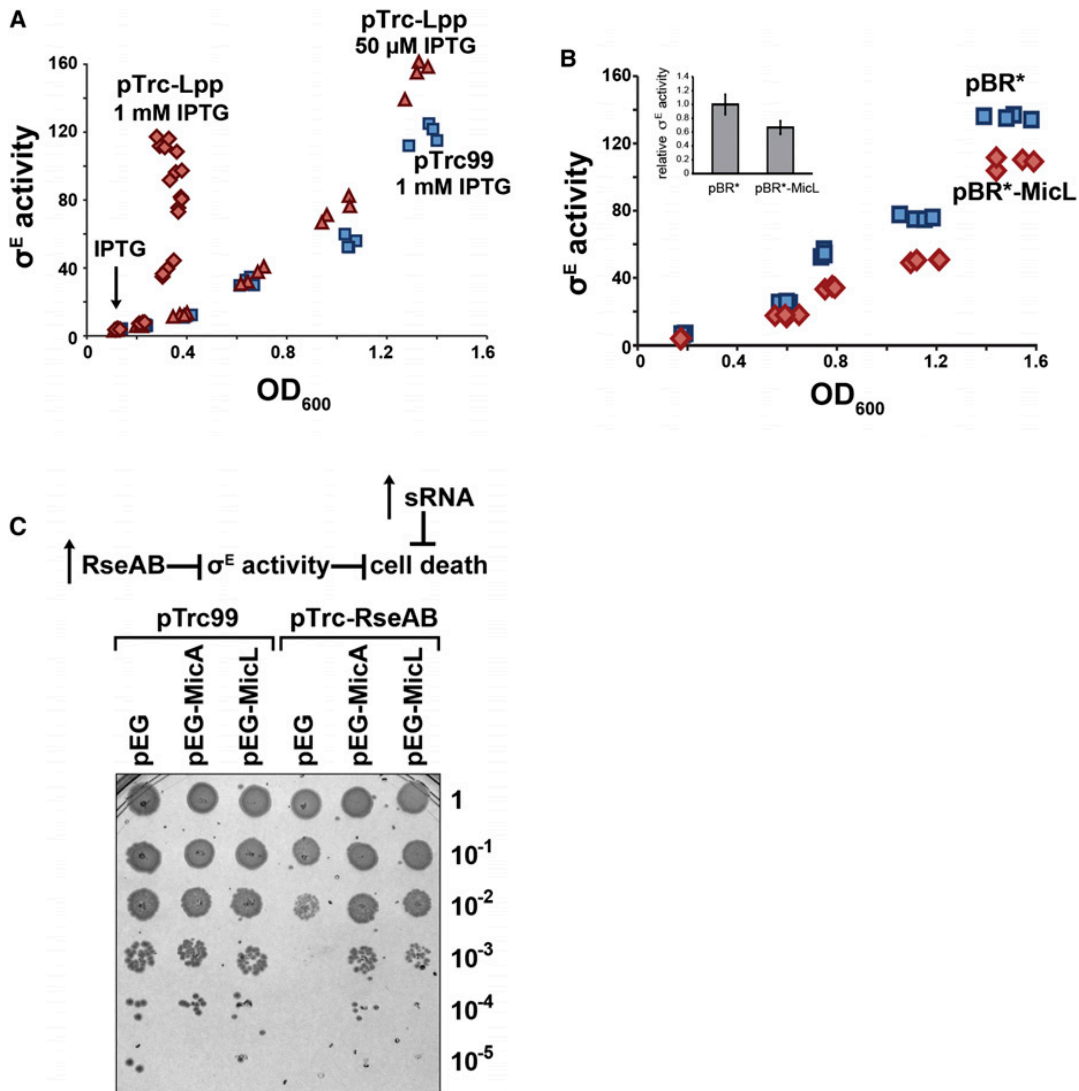


**Figure 7.** MicL and Lpp are part of an envelope-protective regulatory loop.

**(A)** Overexpression of Lpp increases  $\sigma^E$  activity. Cells with either control vector or pTrc-Lpp were induced with either 50  $\mu$ M or 1 mM IPTG (at time indicated).  $\sigma^E$  activity was measured from a  $\sigma^E$ -dependent *rpoHp3-lacZ* reporter. The  $\sigma^E$  activity for the vector control strain treated with 50  $\mu$ M or 1 mM IPTG was similar at all points (data not shown).

**(B)** Overexpression of MicL lowers  $\sigma^E$  activity. Cells with empty vector or pBR\*-MicL were induced with 1 mM IPTG when overnight cultures were diluted to OD<sub>600</sub> ~0.01.  $\sigma^E$  activity was measured as in (A). Notably, MicL overexpression lowers Lpp protein levels to a similar extent as observed in ribosome profiling (~10-fold, compare Fig. 2C and Supplemental Fig. S10B). Inset provides the average and standard deviation for increased  $\sigma^E$  activity for all pBR\* and pBR\*-MicL points, normalized to pBR\* at each timepoint.

**(C)** Shutoff of  $\sigma^E$  activity leads to cell death and can be rescued by concomitant expression of MicA or MicL from derivatives of the pEG plasmid.  $\sigma^E$  activity is shut off by overexpressing the  $\sigma^E$  negative regulators RseA/B from pTrc-RseAB. Aliquots (2  $\mu$ L) of cells growing exponentially in LB with the amp and cm were plated at the indicated dilutions on LB plates  $\pm$  1 mM IPTG, which induces both RseA/B and the sRNA (MicL or MicA).

## Discussion

Lpp is the most abundant protein in the cell and is of central importance in OM homeostasis. It is both embedded in the OM and covalently linked to the peptidoglycan layer, forming an important linkage that connects the OM to the rest of the cell. In this work we have established that MicL, a  $\sigma^E$ -dependent sRNA, specifically targets *lpp* mRNA, preventing its translation. We show that *lpp* is the sole MicL target under conditions we tested. This stands in contrast to most sRNAs, which act via limited base pairing to regulate multiple targets. Additionally, MicL is transcribed from within the coding region of the gene *cutC*, and we show that it is responsible for all known phenotypes of *cutC*. Our results put  $\sigma^E$  at the center of an sRNA and protein network that monitors lipoprotein biogenesis and regulates the majority of proteins destined for the membrane.

### *MicL is a dedicated regulator of Lpp*

Lpp exists in approximately 1 million copies per cell (~2% of dry cell weight) (Li et al., 2014; Narita and Tokuda, 2010) and comprises ~10% of all cellular mRNA and ~8% of all translation events in our conditions. Loss of Lpp leads to a weakened and less tethered OM, causing increased vesiculation, leakage of periplasmic contents, and sensitivity to a variety of compounds (Hirota et al., 1977; Suzuki et al., 1978). Inappropriate up regulation of Lpp likewise is deleterious: defects in Lpp transport or mis-localization of Lpp to the inner membrane leads to cell death (Yakushi et al., 1997). Thus, the levels of this protein must be maintained in a narrow range for optimum growth.

Two unique features of the Lpp lifecycle make post-transcriptional regulation by MicL attractive. First, the cell cannot respond to defects in Lpp transport by upregulating lipoprotein chaperones and transport machines, as these factors utilize some of the same transport machines as Lpp (Narita and Tokuda, 2010). Second, transcriptional repression will not rapidly

lower Lpp flux, since *lpp* mRNA is unusually stable ( $T_{1/2} \sim 10$  minutes *in vivo*) (Ingle and Kushner, 1996; Nilsson et al., 1984). MicL repression of Lpp translation elegantly solves both problems: blocking ribosome initiation on *lpp* decreases Lpp translation and accelerates degradation of *lpp* mRNA to under 4 min based on analysis of our mRNA sequencing data. Increased degradation is likely the result of both increased access to RNases resulting from decreased translation and of recruitment of RNase E through its association with Hfq. MicL-mediated regulation has a further advantage because sRNAs continually inhibit their targets. This is likely to generate less variance in mRNA expression than inhibition of transcription (Levine et al., 2007), which can generate bursts in mRNA synthesis when repressors transiently dissociate from DNA (reviewed in (Eldar and Elowitz, 2010)).

It is notable that MicL has only a single mRNA target. This stands in contrast to all other Hfq-binding sRNA regulators characterized thus far. Lpp might necessitate an sRNA dedicated to controlling the rate of its synthesis, due to its enormous abundance. Since *lpp* is in such high excess over other mRNAs, a second target may be difficult to regulate as competition for base pairing with MicL could prevent the downregulation of the less well-expressed transcript (Levine et al., 2007) such that the secondary mRNA targets would not be regulated until most of the *lpp* mRNA is degraded.

#### *$\sigma^E$ -regulated sRNAs repress protein synthesis of all of the most abundant OM proteins*

Our results place  $\sigma^E$  at the center of an elaborate regulatory system that monitors and responds to defects in all aspects of the OM biogenesis (Fig. 8).  $\sigma^E$  senses OM status through the degradation rate of its negative regulator, RseA, which is mediated by DegS and RseB. DegS and RseB respond respectively to mis-accumulation of OMPs and LPS. Upon stress,  $\sigma^E$  upregulates proteins facilitating OMP and LPS assembly and transport. In addition,  $\sigma^E$  upregulates the MicA and RybB sRNAs to downregulate OMP synthesis, and, as we have shown here, MicL to downregulate Lpp synthesis. The MicA and RybB sRNAs are part of a



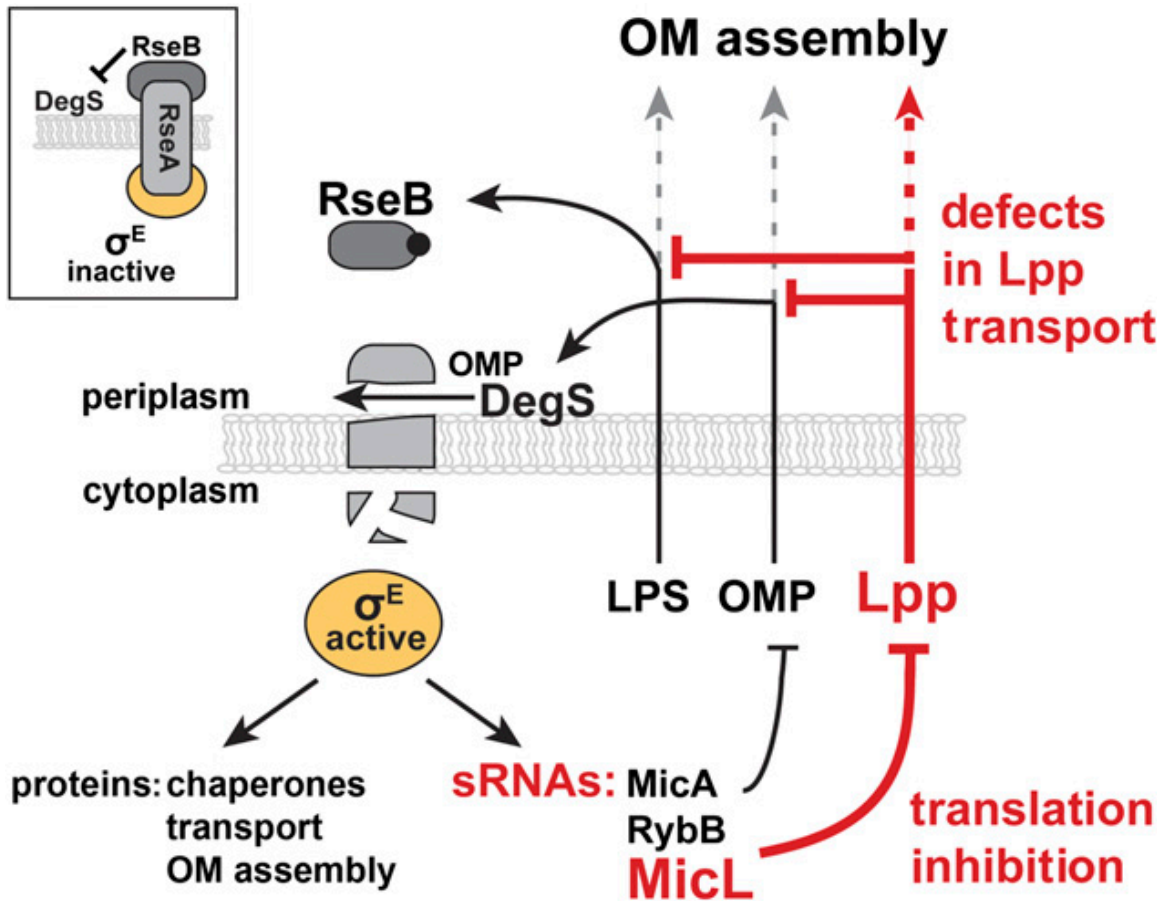


**Figure 8.** Model of the envelope protective  $\sigma^E$ -MicL-Lpp loop.

$\sigma^E$  transcribes genes encoding proteins that relieve folding stress and sRNAs that inhibit new synthesis of the abundant proteins of the OM (OMPs, Lpp). (inset)  $\sigma^E$  is held inactive by RseA in the inner membrane. RseB binds to RseA and prevents DegS from cleaving RseA. (main) Defects in lipoprotein transport inhibit proper OM assembly of both LPS and OMPs, which then bind to RseB and DegS, respectively, inducing RseA cleavage and  $\sigma^E$  activation. In response,  $\sigma^E$  activates the sRNA MicL to specifically downregulate synthesis of Lpp, the major lipoprotein.

regulatory loop that opposes stresses associated with OMP folding and assembly. Our data for MicL/Lpp indicate that they constitute a second  $\sigma^E$ -dependent protective regulatory loop to oppose stresses associated with Lpp folding. We suggest that  $\sigma^E$  senses Lpp status as an indirect consequence of monitoring OMP and LPS assembly. The essential lipoprotein components of the OM assembly machines of OMPs (BamD) and LPS (LptE) (reviewed in (Silhavy et al., 2010)) are in direct competition with Lpp as all lipoproteins are chaperoned by the LolA /LolB system. Thus, transient overexpression of Lpp will decrease OM insertion of the BamD/LptE lipoproteins and assembly of their respective machines. This will disrupt LPS and OMP insertion into the membrane, triggering the concomitant accumulation of both LPS and OMPs and  $\sigma^E$  activation.

Together, MicL, MicA, and RybB regulate not only the majority of protein flux targeted to the OM (>85% of the translation of OM proteins), but also a large fraction of total cell protein (~12% of all translation events) (Supplemental Table S3). As production of OM proteins consumes a large fraction of the cellular resources (~14% of all transcription and translation is devoted to OM proteins, Supplemental Table S3),  $\sigma^E$  is the regulator of a large section of cellular physiology. Given the central role of these sRNAs in controlling flux of membrane proteins, it is not surprising that their overexpression relieves cell death resulting from insufficient  $\sigma^E$ . Although physiological levels of these sRNAs do not fully eliminate Lpp or OMP synthesis, they cause a modest decrease in translation, which nonetheless may have a large effect due to the abundance of these proteins. Even a two-fold change in the availability of *lpp* mRNA would affect 4% of all translation events and alter the composition the membrane.

During transition to stationary phase, nutrient limitation severely curtails cell growth, requiring a significantly reduced rate of membranes synthesis. Indeed, we observe a dramatic decrease in the levels of the *lpp* and *omp* mRNAs during this condition. The necessity of downregulating new synthesis of Lpp and OMPs may explain why there is a dramatic rise in  $\sigma^E$  activity and the levels of MicL, RybB, and MicA during this transition. As both *lpp* and *omp*

mRNAs are exceptionally long-lived and well-translated, upregulating these sRNAs simultaneously inhibits new synthesis of these proteins and allows RNases to degrade the mRNAs, thereby facilitating adaptation to stationary phase.

#### *Copper sensitivity is related to lipoprotein biogenesis*

We found that cells lacking MicL misregulate Lpp and are sensitive to copper stress. Interestingly, defects in other aspects of lipoprotein homeostasis also lead to increased copper sensitivity. Two additional *cut* genes, the OM lipoprotein *nlpE* (*cutF*) and apolipoprotein N-acyltransferase *Int* (*cutE*) (Gupta et al., 1993), are involved in lipoprotein homeostasis. Int is an essential protein that catalyzes lipid attachment to lipoproteins such as Lpp and is the last step in lipoprotein maturation (Narita and Tokuda, 2010). Importantly,  $\Delta$ *lpp* complements the copper sensitivity of partially defective *Int* alleles (Gupta et al., 1993) as well as  $\Delta$ *nlpE* and  $\Delta$ *nlpE*  $\Delta$ *cutC* (data not shown), suggesting that these copper sensitivity phenotypes reflect Lpp misregulation arising from altered Lpp insertion into the OM or an altered OM environment. Thus, monitoring and controlling Lpp biogenesis is a key component of resistance to copper.

The *cutC* gene received its name because mutations in the coding sequence conferred sensitivity to copper. Since our investigations establish that this phenotype instead derives from misregulation of MicL, and consequent alteration of Lpp biogenesis, the function of CutC should be re-examined. However, it is intriguing that CutC, and the YecM protein encoded in the same operon, have been hypothesized to be metal binding proteins (Gupta et al., 1995; Zhang et al., 2003b). While there is no direct evidence for copper association with bacterial CutC, the conserved human variant of CutC has been shown to bind Cu(I) (Li et al., 2010). Are the functions of CutC and MicL related, and are there advantages of hosting MicL within *cutC*? Since MicL-S can be processed from the *cutC* mRNA (Supplemental Fig. S3F), MicL levels could be tied to *cutC* levels, allowing MicL to be made during exponential phase when  $\sigma^E$  activity is low.

*Identification of increasing numbers of 3'UTR-embedded sRNAs warrants reconsideration of phenotypes attributed to proteins*

It is becoming appreciated that sRNAs are not only encoded as independent transcripts in intergenic regions, but also originate from within coding regions. sRNAs can be generated by the processing of a larger transcript, as in the case of s-SodF in *Streptomyces coelicolor* (Kim et al., 2014), or transcribed as a primary transcript like MicL (described here) and DapZ in *S. enterica* (Chao et al., 2012). Intriguingly, many of the other candidate 3'UTR-embedded sRNAs identified in *S. enterica* (Chao et al., 2012) can be observed in our dataset. The fact that the majority of these sRNA transcripts are associated with Hfq strongly implies that they are functional (Chao et al., 2012).

Most sRNA discovery efforts have focused on unique transcripts in intergenic regions, but re-directed searches to identify further coding-region embedded sRNAs are likely to be worthwhile. With the need for bacteria to rapidly generate novel regulators to fine-tune gene expression, 3'UTRs are an ideal region of the genome to evolve novel trans-encoded sRNA regulators. Since Hfq-binding sRNAs appear to require strong transcription terminators, co-opting existing terminators abrogates the need to evolve this structure de novo. Additionally, the untranslated regions of genes are the perfect platform for natural selection to search for beneficial mutations in manner that is less likely to be deleterious. Thus, 3'UTRs may be a reservoir for evolution and may diversify faster than other parts of the genome.

The question of evolution is also interesting to consider in the case of MicL.  $\sigma^E$  and its negative regulators are broadly conserved among the  $\gamma$ -proteobacteria, and the existing data suggest that the pathways activating  $\sigma^E$  are broadly conserved as well. For example, in *Pseudomonas aeruginosa*, homologs of the  $\sigma^E$  regulators respond to the same OMP peptide sequences and LPS stimuli as in the *E. coli* system (Cezairliyan and Sauer, 2009; Lima et al., 2013). Our phylogenetic analysis suggests that MicL, like MicA and RybB, is limited to only a subgroup of  $\gamma$ -proteobacteria (Johansen et al., 2006; Papenfort et al., 2006), but sRNAs whose

expression is  $\sigma^E$ -dependent have been reported for other bacteria in this phylum (Park et al., 2014). Some of these  $\sigma^E$ -dependent sRNAs may fulfill a role similar to *E. coli* MicA, RybB and MicL. Alternatively, MicL, MicA, and RybB could have evolved in response to a particular lifestyle of enteric bacteria. Since the major factors of the OM (OMPs, LPS, Lpp) are recognized by the host immune system (reviewed in (Galdiero et al., 2012)), regulating their levels with sRNAs could be an adaptation to evade detection.

Our study of MicL indicates that investigations of sRNA function continue to provide fundamental insights into bacterial cell physiology. We suggest that additional sRNAs important to cellular physiology are masked in protein-coding regions, and that existing phenotypes associated with protein products may be misattributed and instead arise from misregulation of sRNAs.

## Materials and methods

### *Strains and plasmids*

The bacterial strains and plasmids used in the study are listed in Supplemental Tables S4 and S5, respectively. Gene knockouts or mutants were constructed in strains NM500 or NM400 using  $\lambda$  Red-mediated recombination with DNA fragments generated by PCR using oligonucleotides listed in Supplemental Table S6 (Court et al., 2003; Datsenko and Wanner, 2000; Yu et al., 2000). The mutations linked to markers flanked by FRT sites were moved into new backgrounds by P1 transduction, and where indicated, antibiotic resistance markers were removed using plasmid pCP20 (Cherepanov and Wackernagel, 1995). For the *lpp-lacZ* translational fusions (and mutant derivatives), the entire 5'UTR, beginning with the major *lpp* transcription start at position 1755407 to the indicated position in the coding sequence, was fused to the coding sequence of *lacZ* behind a  $P_{tac}$  promoter (Mandin and Gottesman, 2009). A second *lpp* promoter is annotated in EcoCyc at position 1755320, but only a very weak signal is detected in our deep sequencing analysis (Thomason et al., 2014). In all cases, point mutations were introduced in the fragments used for recombination using overlapping PCR as described previously (Ho et al., 1989).

For plasmid construction, the desired gene fragments were generated by PCR amplification using MG1655 genomic DNA as a template, and after digestion with restriction enzymes, were cloned into the corresponding sites of the indicated vectors. pBR\* is a derivative of the pBR322-derived pBRplac vector (Guillier and Gottesman, 2006) (here denoted pBR) in which the ampicillin (amp) cassette was replaced by the kanamycin (kan) cassette. pBR contains both the amp and the kan cassette. We found transforming with pBR\*-MicL to be more efficient than transforming with pBR-MicL, possibly due to effects of kan versus amp. All cloning was performed using *E. coli* TOP10 cells (Invitrogen), and all mutations and plasmid inserts were confirmed by sequencing.

### *Growth conditions*

Unless indicated otherwise, strains were grown aerobically at 37°C in either LB (10 g tryptone, 5 g yeast extract, 10 g NaCl per liter) or EZ Rich Defined Media (MOPS, Teknova). Copper sensitivity assay was monitored on LB plates supplemented with 4 mM Cu(II)Cl<sub>2</sub> (Sigma; diluted from 1 M stock solution) which were incubated overnight at 30°C (Gupta et al., 1995; Tetaz and Luke, 1983). Where indicated, IPTG was added at a final concentration of 1 mM or as noted and antibiotics and chemicals were added when appropriate at the following concentrations: 100 µg ml<sup>-1</sup> amp, 30 µg ml<sup>-1</sup> kan, 12.5 µg ml<sup>-1</sup> tetracycline (tet), 25 µg ml<sup>-1</sup> chloramphenicol (cat) or 1.4 mM dibucaine.

### *Tiling array analysis*

Cultures of *E. coli* carrying the  $\sigma^E$  overexpression plasmid (pRpoE) were grown to OD<sub>600</sub> ~0.3 at 30°C in LB and pre-induction (0 min) and post-induction (20 min) samples were harvested. After RNA extraction with hot phenol chloroform as described (Massé et al., 2003), each sample was hybridized to a custom Affymetrix *E. coli* tiling array, and an antibody specific for RNA-DNA complexes detected 'ON' tiles as described (Hu et al., 2006). The tiling array tools provided by Affymetrix, Tiling Analysis Software (TAS) and the Integrated Genome Browser (IGB), were used to analyze the data set.

### *Deep sequencing and analysis*

mRNA sequencing and ribosome profiling were performed as previously described, with a few modifications (Ingolia et al., 2009; Li et al., 2012). Briefly, cells were grown in MOPS to OD ~0.3 and induced with 1 mM IPTG, at indicated times 200 mL of cells were harvested. Two replicates were performed for all MicL experiments, with high levels of correlation between experiments. For RNA-seq, the cell pellet was phenol extracted, and ribosomal RNA was removed with the MICROBExpress kit (Life Technologies). tRNAs were not removed to recover

the small RNAs of the cell. For ribosome profiling, ribosome protected fragments were generated as previously described, yielding 25-40 nt footprints (Ingolia et al., 2009; Oh et al., 2011). rRNA was removed, samples were converted to a sequencing library (Ingolia et al., 2009; Li et al., 2012), and sequencing was performed on an Illumina HiSeq2000, and aligned to NC\_000913.fna (MG1655) allowing for 1 mismatch.

Analysis was restricted to genes with more than 128 total counts, a cutoff determined empirically to prevent false-positives (Ingolia et al., 2009). Mean mRNA density and ribosome density was calculated excluding the 5' and 3'UTR and is corrected for total number of reads and the length of each gene and reported in reads per kilobase per million (RPKM) (Ingolia et al., 2009). Translation efficiency (TE) is calculated on a gene-by-gene basis, where TE is the ratio of ribosome footprints to mRNA fragments for that gene (mean translation / mean expression) (Ingolia et al., 2009). To calculate each the fraction of total mRNA and translation each protein represents, the total number of reads per coding region is divided by the total number of reads across all coding regions.

### *Northern analysis*

For Northern analysis, total RNA was extracted by hot acid phenol as described previously (Massé et al., 2003) with minor modifications. Briefly, cells in 1.5 mL of culture (the equivalent of ~3 OD<sub>600</sub>) were collected, resuspended in 650 µL of Buffer A (0.5% SDS, 20 mM NaOAc, and 10 mM EDTA) and immediately added to 750 µL hot acid phenol chloroform (pH 4.5, Ambion). The mixture was vortexed vigorously and incubated for 10 min at 65°C. The sample was then centrifuged 10 min at 30,000 X rpm and the upper aqueous phase was subjected to another round of hot acid phenol chloroform treatment. The aqueous phase from the second acid phenol extraction was added to a Phase Lock Gel Heavy 2.0 ml tube (5Prime) containing 1 mL of phenol chloroform (pH 8, Invitrogen) and mixed and spun 10 min at 30,000X rpm at 4°C. The supernatant was combined with 1 ml of 100% ethanol containing 1 µL of 20



mg/ml glycogen and precipitated at -80°C. The RNA was collected by centrifugation for 30 min at 30,000 X rpm at 4°C, washed twice with 1 mL of 70% ethanol, air dried, and resuspended in nuclease free dH<sub>2</sub>O. Total RNA concentration was determined based on OD<sub>260</sub>.

Northern blots were performed as previously described (Thomason et al., 2012) with minor modifications. Briefly, 10 µg of total RNA was separated on an 8% polyacrylamide-7 M urea gel (USB Corporation) in 1 X TBE and transferred to Zeta-Prove membrane (Bio-Rad) overnight at 20 V in 0.5 X TBE. Oligonucleotides were end-labeled with  $\gamma$ -<sup>32</sup>P-ATP by T4 polynucleotide kinase (New England Biolabs). Membranes were hybridized overnight at 45°C in UltraHyb (Ambion) hybridization buffer. Following hybridization, membranes were washed once with 2X SSC + 0.1% SDS followed by a 10 min incubation at 45°C with 2X SSC + 0.1% SDS. Membranes were subsequently washed 5X with 0.2X SSC + 0.1% SDS, allowed to air dry for 5 min, and exposed to KODAK Biomax X-ray film at -80°C.

#### *Hfq co-immunoprecipitation*

Hfq co-immunoprecipitation was carried out as described (Zhang et al., 2003a). Briefly, cells in 15 ml of wild-type or  $\Delta hfq-1::cm$  cultures grown to late stationary phase (~14 h) were pelleted, resuspended in 400 µL of lysis buffer (20 mM Tris-HCl/pH 8.0, 150 mM KCl, 1 mM MgCl<sub>2</sub>, and 1 mM DTT, 0.2 U RNaseOUT (Ambion)), and lysed by vortexing with glass beads (~0.6 g) for 10 min. To immunoprecipitate Hfq, 200 µL of cell lysate was combined with 24 mg of Protein A Sepharose CL-4B beads (Amersham Biosciences) complexed with 20 µL of  $\alpha$ -Hfq serum and with 200 µL of Net2 Buffer (50 mM Tris-HCl/pH 7.4, 150 mM NaCl, and 0.05% Triton X-100), and 1 µL RNaseOUT. The mixture was incubated at 4°C for 2 h with rotation then washed 5X with 1.5 ml Net2 Buffer. Following the washes, the beads were combined with 400 µL of Net2 Buffer, 50 µL of 3 M NaOAc, 5 µL of 10% SDS, and 600 µL of phenol:chloroform:isoamyl Alcohol (Ambion) and RNA was ethanol precipitated. Total RNA was isolated by Trizol (Invitrogen) extraction followed by chloroform extraction and ethanol

precipitation. Total (5 µg) or co-immunoprecipitated RNA (0.5 µg) were then subject to Northern analysis as described above.

#### *Immunoblot analysis*

Western blot analysis was performed as described previously with minor changes (Beisel and Storz, 2011; Thomason et al., 2012). Samples were separated on a pre-casted 5–20% Tris-Glycine (BioRad) or 16% Tris-Tricine (Invitrogen) and transferred to a nitrocellulose membrane (Invitrogen). Membranes were blocked in 5% milk. To detect Lpp, the blocked membranes were probed with a 1:100,000 dilution of  $\alpha$ -Lpp antibody (kindly provided by the laboratory of T. Silhavy) followed by incubation with a 1:20,000 dilution of HRP-goat-anti-rabbit IgG (Abcam) or with a 1:10,000 dilution of IRDye800-goat-anti-rabbit IgG (Licor). To detect GroEL, the membranes were incubated with a 1:20,000 dilution  $\alpha$ -GroEL mouse monoclonal (Abcam) followed by incubation with 1:40,000 dilution of HRP-goat-anti-mouse IgG (Abcam). For both Lpp and GroEL, the membranes were developed using SuperSignal<sup>®</sup> West Pico Chemiluminescent Substrate (Thermo Scientific) and exposed to KODAK Blue-XB film. To detect RpoA, the membranes were incubated with a 1:1000 dilution of  $\alpha$ -RpoA mouse monoclonal antibody (Neoclone), followed by incubation with 1:10,000 IRDye680-goat-anti-mouse IgG (Licor). Fluorescent antibodies were visualized on an Odyssey imager (Licor).

#### *$\beta$ -galactosidase assays*

$\beta$ -galactosidase assays were performed as described previously (Beisel et al., 2012) with some minor modifications. Briefly, four separate colonies were grown overnight in LB with appropriate antibiotics, diluted 1:200 to OD<sub>600</sub> ~0.03 in the same media supplemented with 1 mM IPTG and 0.02% L-arabinose, and grown to final OD<sub>600</sub> = ~1 at 37°C. 5 µL of cells were lysed in Z buffer (700 µL) with 15 µL of 0.1% SDS and 30 µL of chloroform. The OD<sub>600</sub> and A<sub>420</sub>

of the cultures were measured using an Ultrospec 3080 UV/Vis spectrophotometer (Pharmacia Biotech).

For  $\sigma^E$  activity assays,  $\beta$ -galactosidase activity was measured from an *rpoHp3-LacZ* reporter as described previously (Ades et al., 1999; Costanzo and Ades, 2006). Briefly, cells were grown to  $OD_{600} \sim 0.1$  in LB at 30°C. Four samples were taken at different times, and the  $\beta$ -galactosidase activities of these samples are plotted against their  $OD_{600}$ . The slope of this plot represents  $\sigma^E$  activity. Four independent experiments were performed for each strain. For Fig. 7B, a mean and standard deviation of pMicL to pBR\* was calculated at each timepoint, and aggregated across all timepoints.

#### *Promoter activity assays*

The MicL promoter-GFP fusion were constructed as described previously (Mutalik et al., 2009), placing the  $P_{micL}$  -65 to +5 in front of GFP. Other promoter-GFP fusions are from (Mutalik et al., 2009). GFP fluorescence was measured using a Varioskan (Thermo) as was previously described (Mutalik et al., 2009). Briefly, promoter strength is a function of the fluorescence and the cell density. GFP fluorescence was measured at 4 ODs after  $\sigma^E$  induction, and the fluorescence is plotted versus OD. The slope of the linear portion of this plot is reported as the promoter activity of the specific promoter-GFP fusion in that reporter strain.

#### **Acknowledgments**

We thank A. Zhang for assistance with the tiling array analysis, S. Gottesman for plasmids and strains, T. Silhavy for sharing Lpp antiserum and G.-W. Li and D. Burkhardt for helpful discussions. Work in the Gross laboratory was supported by GM036278 and work in the Storz laboratory was supported by the Intramural Research Program of the Eunice Kennedy Shriver National Institute of Child Health and Human Development.

## References

- Ades, S.E., Connolly, L.E., Alba, B.M., and Gross, C.A. (1999). The *Escherichia coli*  $\sigma^E$ -dependent extracytoplasmic stress response is controlled by the regulated proteolysis of an anti- $\sigma$  factor. *Genes Dev* 13, 2449-2461.
- Barchinger, S.E., and Ades, S.E. (2013). Regulated proteolysis: control of the *Escherichia coli*  $\sigma^E$ -dependent cell envelope stress response. *Subcell Biochem* 66, 129-160.
- Beisel, C.L., and Storz, G. (2011). The base-pairing RNA spot 42 participates in a multioutput feedforward loop to help enact catabolite repression in *Escherichia coli*. *Mol Cell* 41, 286-297.
- Beisel, C.L., Updegrove, T.B., Janson, B.J., and Storz, G. (2012). Multiple factors dictate target selection by Hfq-binding small RNAs. *EMBO J* 31, 1961-1974.
- Bouvier, M., Sharma, C.M., Mika, F., Nierhaus, K.H., and Vogel, J. (2008). Small RNA binding to 5' mRNA coding region inhibits translational initiation. *Mol Cell* 32, 827-837.
- Braun, M., and Silhavy, T.J. (2002). Imp/OstA is required for cell envelope biogenesis in *Escherichia coli*. *Mol Microbiol* 45, 1289-1302.
- Braun, V., and Rehn, K. (1969). Chemical characterization, spatial distribution and function of a lipoprotein (murein-lipoprotein) of the *E. coli* cell wall. The specific effect of trypsin on the membrane structure. *Eur J Biochem* 10, 426-438.
- Cezairliyan, B.O., and Sauer, R.T. (2009). Control of *Pseudomonas aeruginosa* AlgW protease cleavage of MucA by peptide signals and MucB. *Mol Microbiol* 72, 368-379.
- Chaba, R., Alba, B.M., Guo, M.S., Sohn, J., Ahuja, N., Sauer, R.T., and Gross, C.A. (2011). Signal integration by DegS and RseB governs the  $\sigma^E$ -mediated envelope stress response in *Escherichia coli*. *Proc Natl Acad Sci USA* 108, 106-111.

- Chaba, R., Grigorova, I.L., Flynn, J.M., Baker, T.A., and Gross, C.A. (2007). Design principles of the proteolytic cascade governing the  $\sigma^E$ -mediated envelope stress response in *Escherichia coli*: keys to graded, buffered, and rapid signal transduction. *Genes Dev* 21, 124-136.
- Chang, T.W., Lin, Y.M., Wang, C.F., and Liao, Y.D. (2012). Outer membrane lipoprotein Lpp is Gram-negative bacterial cell surface receptor for cationic antimicrobial peptides. *J Biol Chem* 287, 418-428.
- Chao, Y., Papenfort, K., Reinhardt, R., Sharma, C.M., and Vogel, J. (2012). An atlas of Hfq-bound transcripts reveals 3' UTRs as a genomic reservoir of regulatory small RNAs. *EMBO J* 31, 4005-4019.
- Cherepanov, P.P., and Wackernagel, W. (1995). Gene disruption in *Escherichia coli*: TcR and KmR cassettes with the option of Flp-catalyzed excision of the antibiotic-resistance determinant. *Gene* 158, 9-14.
- Coornaert, A., Lu, A., Mandin, P., Springer, M., Gottesman, S., and Guillier, M. (2010). MicA sRNA links the PhoP regulon to cell envelope stress. *Mol Microbiol* 76, 467-479.
- Costanzo, A., and Ades, S.E. (2006). Growth phase-dependent regulation of the extracytoplasmic stress factor,  $\sigma^E$ , by guanosine 3',5'-bispyrophosphate (ppGpp). *J Bacteriol* 188, 4627-4634.
- Court, D.L., Swaminathan, S., Yu, D., Wilson, H., Baker, T., Bubunenko, M., Sawitzke, J., and Sharan, S.K. (2003). Mini-lambda: a tractable system for chromosome and BAC engineering. *Gene* 315, 63-69.
- Cowles, C.E., Li, Y., Semmelhack, M.F., Cristea, I.M., and Silhavy, T.J. (2011). The free and bound forms of Lpp occupy distinct subcellular locations in *Escherichia coli*. *Mol Microbiol* 79, 1168-1181.
- Datsenko, K.A., and Wanner, B.L. (2000). One-step inactivation of chromosomal genes in *Escherichia coli* K-12 using PCR products. *Proc Natl Acad Sci USA* 97, 6640-6645.

- De Las Peñas, A., Connolly, L.E., and Gross, C.A. (1997).  $\sigma^E$  is an essential sigma factor in *Escherichia coli*. *J Bacteriol* **179**, 6862-6864.
- Desnoyers, G., Bouchard, M.P., and Massé, E. (2013). New insights into small RNA-dependent translational regulation in prokaryotes. *Trends Genet* **29**, 92-98.
- Eldar, A., and Elowitz, M.B. (2010). Functional roles for noise in genetic circuits. *Nature* **467**, 167-173.
- Galdiero, S., Falanga, A., Cantisani, M., Tarallo, R., Della Pepa, M.E., D'Oriano, V., and Galdiero, M. (2012). Microbe-host interactions: structure and role of Gram-negative bacterial porins. *Curr Protein Pept Sci* **13**, 843-854.
- Gogol, E.B., Rhodius, V.A., Papenfort, K., Vogel, J., and Gross, C.A. (2011). Small RNAs endow a transcriptional activator with essential repressor functions for single-tier control of a global stress regulon. *Proc Natl Acad Sci USA* **108**, 12875-12880.
- Guillier, M., and Gottesman, S. (2006). Remodelling of the *Escherichia coli* outer membrane by two small regulatory RNAs. *Mol Microbiol* **59**, 231-237.
- Guisbert, E., Rhodius, V.A., Ahuja, N., Witkin, E., and Gross, C.A. (2007). Hfq modulates the  $\sigma^E$ -mediated envelope stress response and the  $\sigma^{32}$ -mediated cytoplasmic stress response in *Escherichia coli*. *J Bacteriol* **189**, 1963-1973.
- Gupta, S.D., Gan, K., Schmid, M.B., and Wu, H.C. (1993). Characterization of a temperature-sensitive mutant of *Salmonella typhimurium* defective in apolipoprotein N-acyltransferase. *J Biol Chem* **268**, 16551-16556.
- Gupta, S.D., Lee, B.T., Camakaris, J., and Wu, H.C. (1995). Identification of *cutC* and *cutF* (*nlpE*) genes involved in copper tolerance in *Escherichia coli*. *J Bacteriol* **177**, 4207-4215.
- Hayden, J.D., and Ades, S.E. (2008). The extracytoplasmic stress factor,  $\sigma^E$ , is required to maintain cell envelope integrity in *Escherichia coli*. *PLoS ONE* **3**, e1573.

- Hirota, Y., Suzuki, H., Nishimura, Y., and Yasuda, S. (1977). On the process of cellular division in *Escherichia coli*: a mutant of *E. coli* lacking a murein-lipoprotein. *Proc Natl Acad Sci USA* 74, 1417-1420.
- Ho, S.N., Hunt, H.D., Horton, R.M., Pullen, J.K., and Pease, L.R. (1989). Site-directed mutagenesis by overlap extension using the polymerase chain reaction. *Gene* 77, 51-59.
- Hu, Z., Zhang, A., Storz, G., Gottesman, S., and Leppla, S.H. (2006). An antibody-based microarray assay for small RNA detection. *Nucleic Acids Res* 34, e52.
- Ingle, C.A., and Kushner, S.R. (1996). Development of an in vitro mRNA decay system for *Escherichia coli*: poly(A) polymerase I is necessary to trigger degradation. *Proc Natl Acad Sci USA* 93, 12926-12931.
- Ingolia, N.T., Ghaemmaghami, S., Newman, J.R.S., and Weissman, J.S. (2009). Genome-wide analysis in vivo of translation with nucleotide resolution using ribosome profiling. *Science* 324, 218-223.
- Inouye, M., Shaw, J., and Shen, C. (1972). The assembly of a structural lipoprotein in the envelope of *Escherichia coli*. *J Biol Chem* 247, 8154-8159.
- Johansen, J., Eriksen, M., Kallipolitis, B., and Valentin-Hansen, P. (2008). Down-regulation of outer membrane proteins by noncoding RNAs: unraveling the cAMP-CRP- and  $\sigma^E$ -dependent CyaR-*ompX* regulatory case. *J Mol Biol* 383, 1-9.
- Johansen, J., Rasmussen, A.A., Overgaard, M., and Valentin-Hansen, P. (2006). Conserved small non-coding RNAs that belong to the  $\sigma^E$  regulon: role in down-regulation of outer membrane proteins. *J Mol Biol* 364, 1-8.
- Kim, H.M., Shin, J.H., Cho, Y.B., and Roe, J.H. (2014). Inverse regulation of Fe- and Ni-containing SOD genes by a Fur family regulator Nur through small RNA processed from 3'UTR of the *sodF* mRNA. *Nucleic Acids Res* 42, 2003-2014.
- Levine, E., Zhang, Z., Kuhlman, T., and Hwa, T. (2007). Quantitative characteristics of gene regulation by small RNA. *PLoS Biol* 5, e229.

- Li, G.-W., Burkhardt, D.H., Gross, C.A., and Weissman, J.S. (2014). Quantifying absolute protein synthesis rates reveals principles underlying allocation of cellular resources. *Cell* 157, 624-635.
- Li, G.-W., Oh, E., and Weissman, J.S. (2012). The anti-Shine-Dalgarno sequence drives translational pausing and codon choice in bacteria. *Nature* 484, 538-541.
- Li, Y., Du, J., Zhang, P., and Ding, J. (2010). Crystal structure of human copper homeostasis protein CutC reveals a potential copper-binding site. *J Struct Biol* 169, 399-405.
- Lima, S., Guo, M.S., Chaba, R., Gross, C.A., and Sauer, R.T. (2013). Dual molecular signals mediate the bacterial response to outer-membrane stress. *Science* 340, 837-841.
- Mandin, P., and Gottesman, S. (2009). A genetic approach for finding small RNAs regulators of genes of interest identifies RybC as regulating the DpiA/DpiB two-component system. *Mol Microbiol* 72, 551-565.
- Massé, E., Escorcia, F.E., and Gottesman, S. (2003). Coupled degradation of a small regulatory RNA and its mRNA targets in *Escherichia coli*. *Genes Dev* 17, 2374-2383.
- Matveeva, O., Nechipurenko, Y., Rossi, L., Moore, B., Saetrom, P., Ogurtsov, A.Y., Atkins, J.F., and Shabalina, S.A. (2007). Comparison of approaches for rational siRNA design leading to a new efficient and transparent method. *Nucleic Acids Res* 35, e63.
- Mecenas, J., Rouviere, P.E., Erickson, J.W., Donohue, T.J., and Gross, C.A. (1993). The activity of  $\sigma^E$ , an *Escherichia coli* heat-inducible  $\sigma$ -factor, is modulated by expression of outer membrane proteins. *Genes Dev* 7, 2618-2628.
- Mizuno, T., Chou, M.Y., and Inouye, M. (1984). A unique mechanism regulating gene expression: translational inhibition by a complementary RNA transcript (micRNA). *Proc Natl Acad Sci USA* 81, 1966-1970.
- Mutalik, V.K., Nonaka, G., Ades, S.E., Rhodius, V.A., and Gross, C.A. (2009). Promoter strength properties of the complete sigma E regulon of *Escherichia coli* and *Salmonella enterica*. *J Bacteriol* 191, 7279-7287.



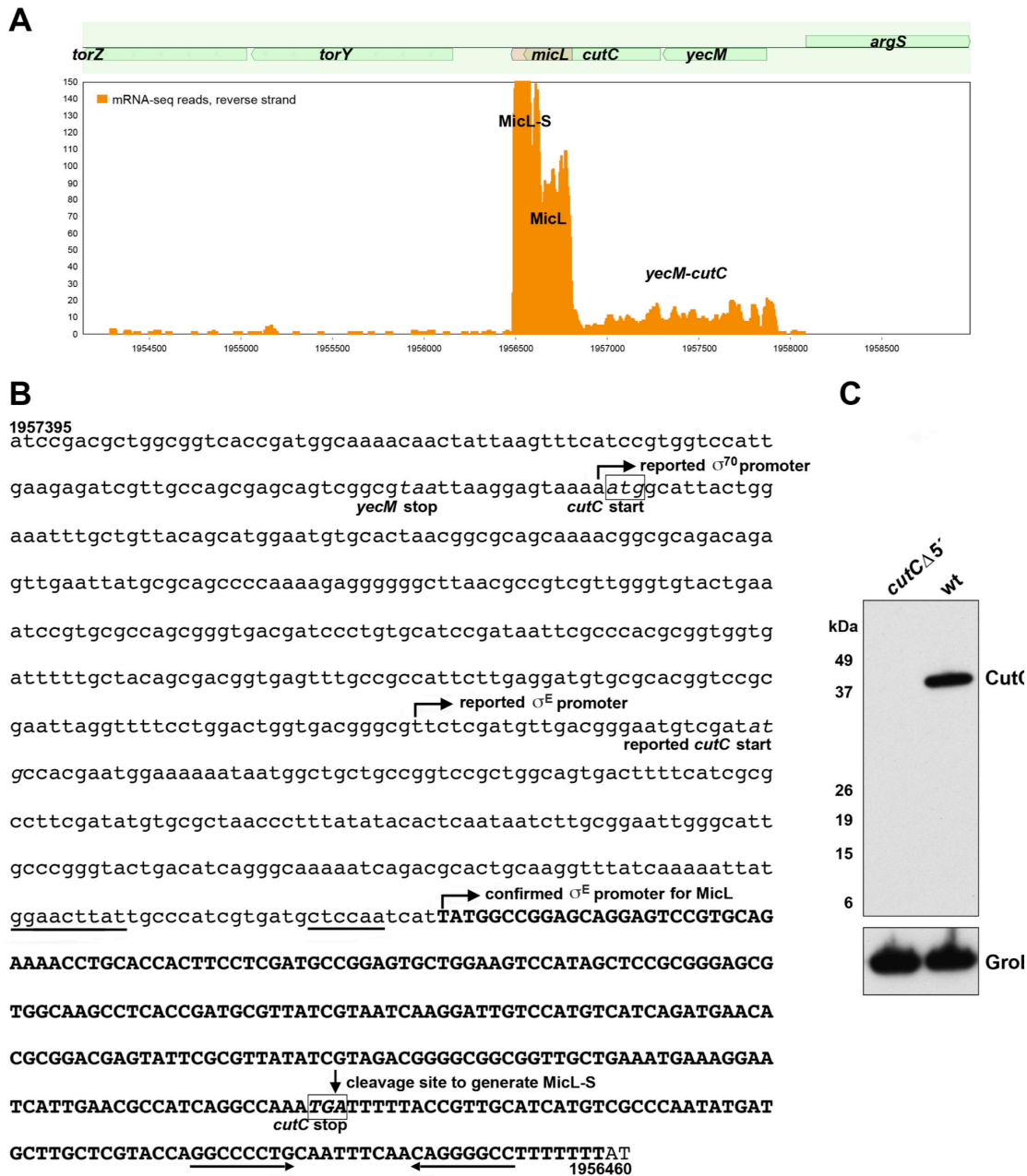
- Narita, S., and Tokuda, H. (2010). Biogenesis and membrane targeting of lipoproteins. In EcoSal Plus 2010.
- Nichols, R.J., Sen, S., Choo, Y.J., Beltrao, P., Zietek, M., Chaba, R., Lee, S., Kazmierczak, K.M., Lee, K.J., Wong, A., *et al.* (2011). Phenotypic landscape of a bacterial cell. *Cell* 144, 143-156.
- Nikaido, H. (2003). Molecular basis of bacterial outer membrane permeability revisited. *Microbiol Mol Biol Rev* 67, 593-656.
- Nilsson, G., Belasco, J.G., Cohen, S.N., and von Gabain, A. (1984). Growth-rate dependent regulation of mRNA stability in *Escherichia coli*. *Nature* 312, 75-77.
- Oh, E., Becker, A.H., Sandikci, A., Huber, D., Chaba, R., Gloge, F., Nichols, R.J., Typas, A., Gross, C.A., Kramer, G., *et al.* (2011). Selective ribosome profiling reveals the cotranslational chaperone action of trigger factor in vivo. *Cell* 147, 1295-1308.
- Opdyke, J.A., Fozo, E.M., Hemm, M.R., and Storz, G. (2011). RNase III participates in GadY-dependent cleavage of the *gadX-gadW* mRNA. *J Mol Biol* 406, 29-43.
- Papenfort, K., Bouvier, M., Mika, F., Sharma, C.M., and Vogel, J. (2010). Evidence for an autonomous 5' target recognition domain in an Hfq-associated small RNA. *Proc Natl Acad Sci USA* 107, 20435-20440.
- Papenfort, K., Pfeiffer, V., Mika, F., Lucchini, S., Hinton, J.C., and Vogel, J. (2006).  $\sigma^E$ -dependent small RNAs of *Salmonella* respond to membrane stress by accelerating global omp mRNA decay. *Mol Microbiol* 62, 1674-1688.
- Park, S.H., Bao, Z., Butcher, B.G., D'Amico, K., Xu, Y., Stodghill, P., Schneider, D.J., Cartinhour, S., and Filiatrault, M.J. (2014). Analysis of the small RNA *spf* in the plant pathogen *Pseudomonas syringae* pv. *tomato* strain DC3000. *Microbiology* 160, 941-953.
- Rasmussen, A.A., Eriksen, M., Gilany, K., Udesen, C., Franch, T., Petersen, C., and Valentin-Hansen, P. (2005). Regulation of *ompA* mRNA stability: the role of a small regulatory RNA in growth phase-dependent control. *Mol Microbiol* 58, 1421-1429.

- Rhodium, V.A., Mutalik, V.K., and Gross, C.A. (2012). Predicting the strength of UP-elements and full-length *E. coli*  $\sigma^E$  promoters. *Nucleic Acids Res* 40, 2907-2924.
- Rhodium, V.A., Suh, W.C., Nonaka, G., West, J., and Gross, C.A. (2006). Conserved and variable functions of the  $\sigma^E$  stress response in related genomes. *PLoS Biol* 4, e2.
- Ricci, D.P., and Silhavy, T.J. (2012). The Bam machine: a molecular cooper. *Biochim Biophys Acta* 1818, 1067-1084.
- Richards, G.R., and Vanderpool, C.K. (2011). Molecular call and response: the physiology of bacterial small RNAs. *Biochim Biophys Acta* 1809, 525-531.
- Silhavy, T.J., Kahne, D., and Walker, S. (2010). The bacterial cell envelope. *Cold Spring Harb Perspect Biol* 2, a000414.
- Skovierova, H., Rowley, G., Rezuchova, B., Homerova, D., Lewis, C., Roberts, M., and Kormanec, J. (2006). Identification of the  $\sigma^E$  regulon of *Salmonella enterica* serovar Typhimurium. *Microbiology* 152, 1347-1359.
- Storz, G., Vogel, J., and Wassarman, K.M. (2011). Regulation by small RNAs in bacteria: expanding frontiers. *Mol Cell* 43, 880-891.
- Suzuki, H., Nishimura, Y., Yasuda, S., Nishimura, A., Yamada, M., and Hirota, Y. (1978). Murein-lipoprotein of *Escherichia coli*: a protein involved in the stabilization of bacterial cell envelope. *Mol Gen Genet* 167, 1-9.
- Tetaz, T.J., and Luke, R.K. (1983). Plasmid-controlled resistance to copper in *Escherichia coli*. *J Bacteriol* 154, 1263-1268.
- Thomason, M.K., Bischler, T., Eisenbart, S.K., Förstner, K.U., Zhang, A., Herbig, A., Nieselt, K., Sharma, C.M., and Storz, G. (2014). Global transcriptional start site mapping using dRNA-seq reveals novel antisense RNAs in *Escherichia coli*. Submitted.
- Thomason, M.K., Fontaine, F., De Lay, N., and Storz, G. (2012). A small RNA that regulates motility and biofilm formation in response to changes in nutrient availability in *Escherichia coli*. *Mol Microbiol* 84, 17-35.

- Thompson, K.M., Rhodius, V.A., and Gottesman, S. (2007).  $\sigma^E$  regulates and is regulated by a small RNA in *Escherichia coli*. *J Bacteriol* *189*, 4243-4256.
- Udekwi, K.I., Darfeuille, F., Vogel, J., Reimegård, J., Holmqvist, E., and Wagner, E.G.H. (2005). Hfq-dependent regulation of OmpA synthesis is mediated by an antisense RNA. *Genes Dev* *19*, 2355-2366.
- Udekwi, K.I., and Wagner, E.G.H. (2007). Sigma E controls biogenesis of the antisense RNA MicA. *Nucleic Acids Res* *35*, 1279-1288.
- Vogel, J., and Luisi, B.F. (2011). Hfq and its constellation of RNA. *Nat Rev Microbiol* *9*, 578-589.
- Walsh, N.P., Alba, B.M., Bose, B., Gross, C.A., and Sauer, R.T. (2003). OMP peptide signals initiate the envelope-stress response by activating DegS protease via relief of inhibition mediated by its PDZ domain. *Cell* *113*, 61-71.
- Wu, T., Malinverni, J., Ruiz, N., Kim, S., Silhavy, T.J., and Kahne, D. (2005). Identification of a multicomponent complex required for outer membrane biogenesis in *Escherichia coli*. *Cell* *121*, 235-245.
- Yakushi, T., Tajima, T., Matsuyama, S., and Tokuda, H. (1997). Lethality of the covalent linkage between mislocalized major outer membrane lipoprotein and the peptidoglycan of *Escherichia coli*. *J Bacteriol* *179*, 2857-2862.
- Yu, D., Ellis, H.M., Lee, E.C., Jenkins, N.A., Copeland, N.G., and Court, D.L. (2000). An efficient recombination system for chromosome engineering in *Escherichia coli*. *Proc Natl Acad Sci USA* *97*, 5978-5983.
- Zhang, A., Wassarman, K.M., Rosenow, C., Tjaden, B.C., Storz, G., and Gottesman, S. (2003a). Global analysis of small RNA and mRNA targets of Hfq. *Mol Microbiol* *50*, 1111-1124.
- Zhang, G., Meredith, T.C., and Kahne, D. (2013). On the essentiality of lipopolysaccharide to Gram-negative bacteria. *Curr Opin Microbiol* *16*, 779-785.

Zhang, R.G., Duke, N., Laskowski, R., Evdokimova, E., Skarina, T., Edwards, A., Joachimiak, A., and Savchenko, A. (2003b). Conserved protein YecM from *Escherichia coli* shows structural homology to metal-binding isomerases and oxygenases. *Proteins* 51, 311-314.

## Supplemental Figures



### Supplemental Figure S1. Re-annotation of *cutC* region.

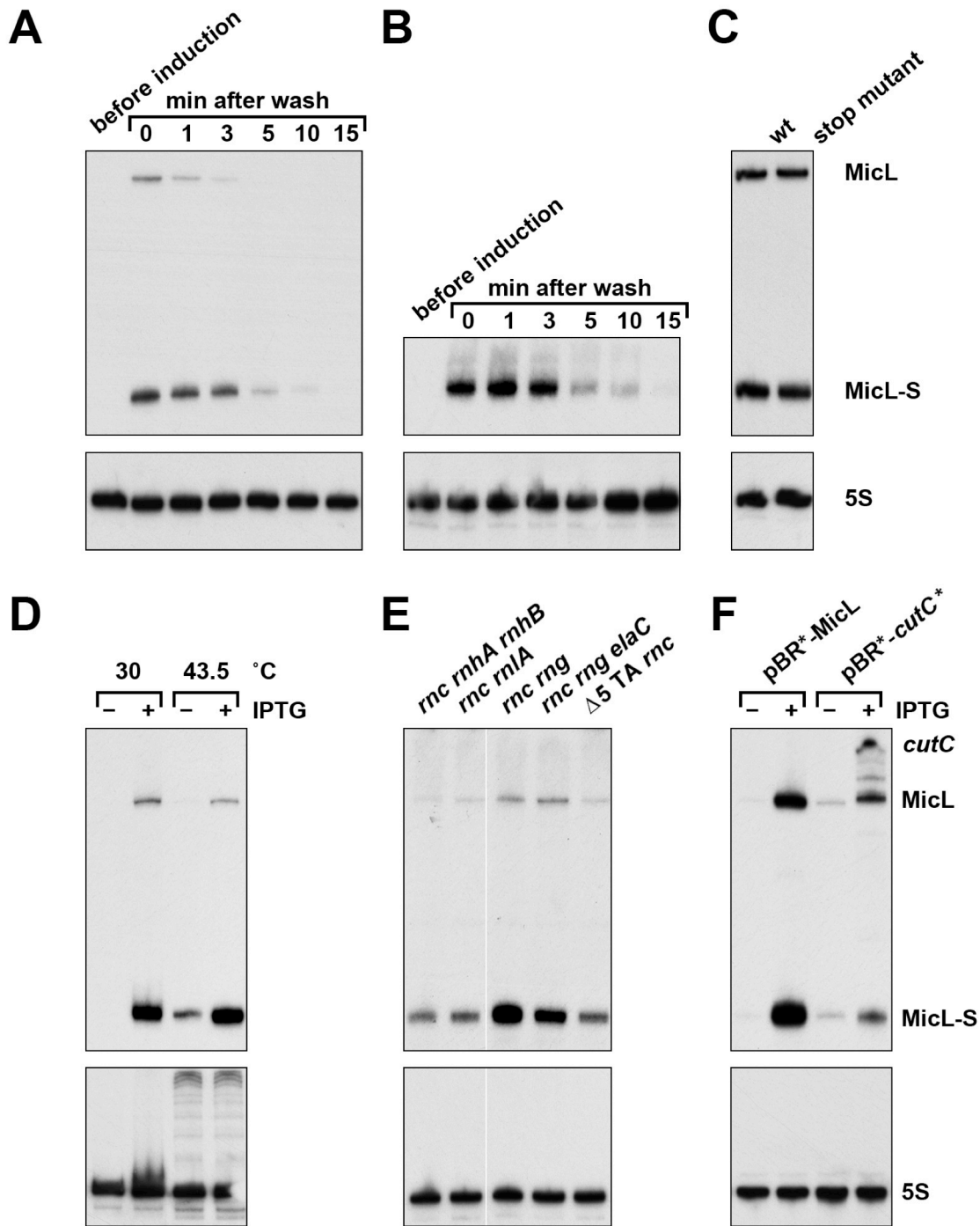
(A) Transcription of the *yecM-cutC* region as observed in mRNA-seq. *cutC* appears to be co-transcribed with *yecM* in all conditions tested. (B) Sequence of *micL-cutC* genomic region. MicL (chromosome positions 1956771 to 1956462) and MicL-S (chromosome positions 1956544 to 1956462) terminate within the poly(T) stretch of the rho-independent terminator of *cutC* (stem indicated by arrows). The predicted -10 and -35  $\sigma^E$  promoter elements of *micL* are

underlined and the site of cleavage to generate MicL-S is indicated by the vertical arrow. A previous study reported a  $\sigma^E$ -dependent promoter for *cutC* at position 1957010 (Dartigalongue et al., 2001). We find no evidence for this site in our tiling array, deep sequencing and Northern data upon  $\sigma^E$  overexpression. Our data sets also do not support a reported  $\sigma^{70}$ -dependent promoter at position 1957291 (Huerta and Collado- Vides, 2003). While it is possible that there is transcription from these reported promoters under conditions not tested in this study, we suggest that *cutC* is in an operon with the upstream *yecM* gene. We also note that based on phylogenetic conservation and ribosome profiling data, the *cutC* coding sequence initiates at the AUG at position 1957290 (indicated by box) instead of the AUG at position 1956984 annotated in the EcoCyc database (<http://ecocyc.org/>). The close proximity to *yecM* suggests that these two genes are likely transcribed together. **(C)** Detection of CutC-SPA. A SPA tag fused in frame to the 3' end of the *cutC* gene prior to the stop codon was integrated into the wild type strain CAG1684 and isogenic mutant *cutC* $\Delta$ 5'. Both strains were grown to OD<sub>600</sub> ~1.0 in LB media and 1 mL of cells harvested. SPA-tagged CutC was detected as in Materials and Methods with the exception that the membrane was incubated with 1:1,000 dilution HRP-mouse-anti-FLAG (Sigma) prior to developing the membrane. The predicted sizes of CutC initiated from the first start codon and the SPA tag are 26.76 kDa and 10 kDa, respectively, consistent with the ~37 kDa band seen in lane 2. Lack of signal in lane 1 shows no CutC-SPA is produced in the *cutC* $\Delta$ 5' strain (see Fig. 6A). Note that the published annotation of the *cutC* start codon at position 1956984 in EcoCyc would yield a protein of molecular weight 15.87 kDa (25.87 kDa tagged with SPA), which is not observed.



the same region. **(C)** Multiple alignment of the *micL* promoter regions from several species showing ambiguous similarity in the same region. For **(A)**, **(B)** and **(C)**, positions of 100% sequence conservation are marked by stars. The positions of the -35 and -10 regions are shown in bold. The consensus sequence of a  $\sigma^E$ -dependent promoter (Rhodius et al., 2006), with the invariable C residue in the -10 box underlined, is shown for comparison above the alignments. An AT-rich element is present upstream of the -35 box. Abbreviations of species and accession numbers of aligned sequences: *EsCo* - *Escherichia coli* NC\_000913; *ShSo* – *Shigella sonnei* NC\_007384; *ShBo* – *Shigella boydii* NC\_007613; *CiKo* – *Citrobacter koseri* NC\_009792; *SaEn* - *Salmonella enterica* NC\_003197; *KIPn* – *Klebsiella pneumoniae* NC\_011283; *EnCl* – *Enterobacter cloacae* NC\_016514; *CrTu* – *Cronobacter turicensis* NC\_013282; *PaVa* – *Pantoea vagans* NC\_014562; *ErAm* – *Erwinia amylovora* NC\_013961; *ErTa* – *Erwinia tasmaniensis* NC\_010694; *DiDa* – *Dickeya dadantii* NC\_014500; *SoGl* – *Sodalis glossinidius* NC\_007712; *RaSp* – *Rahnella sp* NC\_015061; *PeAt* – *Pectobacterium atrosepticum* NC\_004547; *SeSp* – *Serratia sp* NC\_017573; *EdTa* – *Edwardsiella tarda* NC\_013508; *YePs* – *Yersinia pseudotuberculosis* NC\_006155; *PrMi* – *Proteus mirabilis* NC\_010554; *XeNe* – *Xenorhabdus nematophila* NC\_014228; *PhAs* – *Photorhabdus asymbiotica* NC\_012962; *PrSt* – *Providencia stuartii* NC\_017731. **(D)** Maximum-likelihood tree of *cutC* genes/*micL* promoter regions based on the multiple alignment of sequences present in *Enterobacteria* and *Vibrio*. For individual sequences, the species name and the genome identification numbers are indicated; triangle denote multiple, collapsed *Vibrio* sp. sequences. Presence of two other  $\sigma^E$ -dependent sRNAs, MicA and RybB, in the individual genomes is indicated in red and green, respectively. It should be noted that sequences with ambiguous hits to MicA and RybB are present in the genomes for which no sRNA is listed.

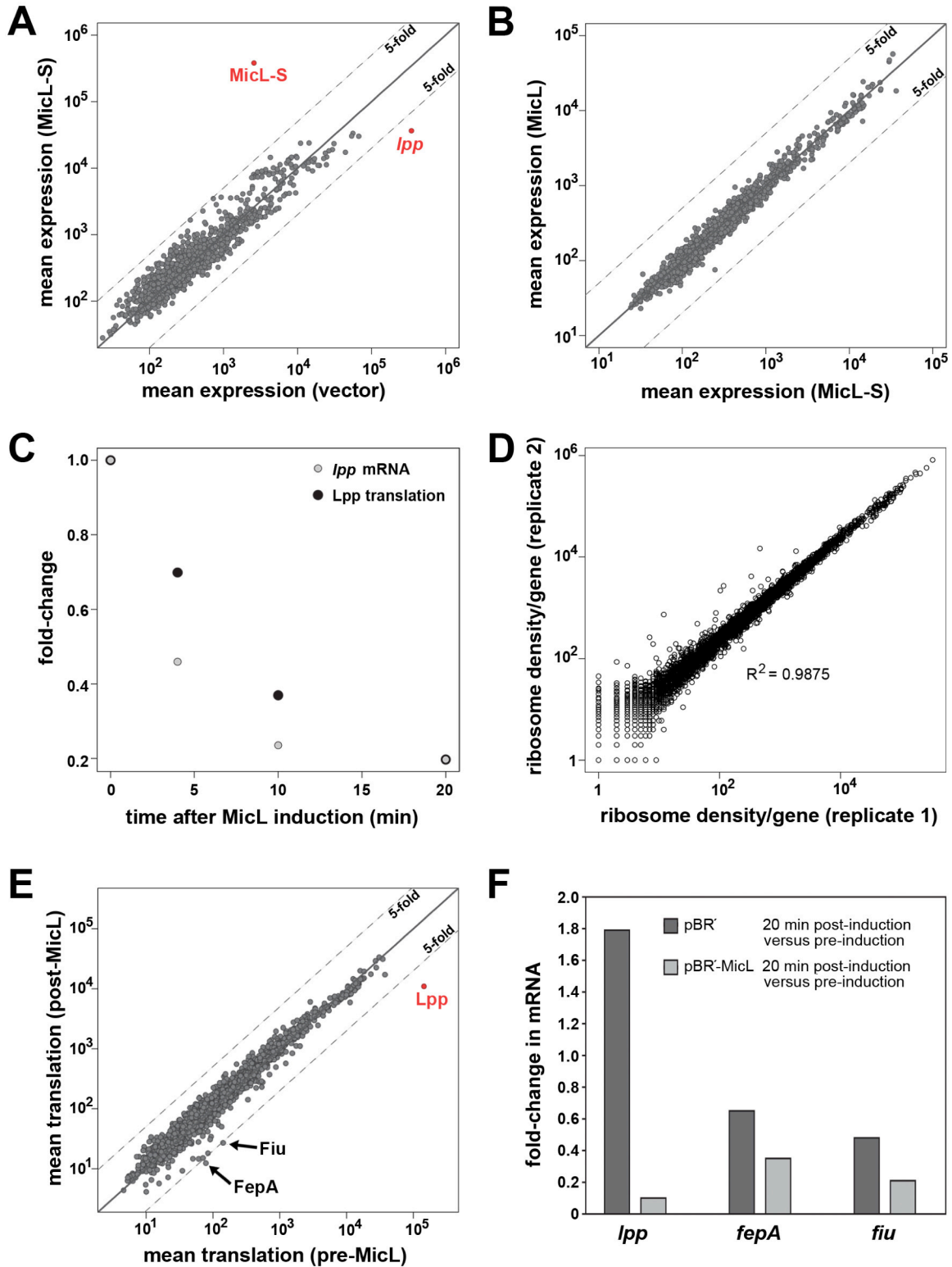




**Supplemental Figure S3.** Processing of MicL-S.

(A) Stability of MicL and MicL-S. Strain CAG64307 HK::lacIq  $\Delta cutC$  carrying pBR<sup>+</sup>-MicL was grown to OD<sub>600</sub> ~0.4 and MicL expression was induced with 100  $\mu$ M IPTG for 15 min. Samples were collected at the indicated time periods after washing out the inducer. (B) Stability of MicL-S only. Samples of CAG64307 HK::lacIq  $\Delta cutC$  carrying pBR<sup>+</sup>-MicL-S were obtained as above. (C) Levels of MicL and MicL-S expressed from a *cutC* stop codon mutant. Strain

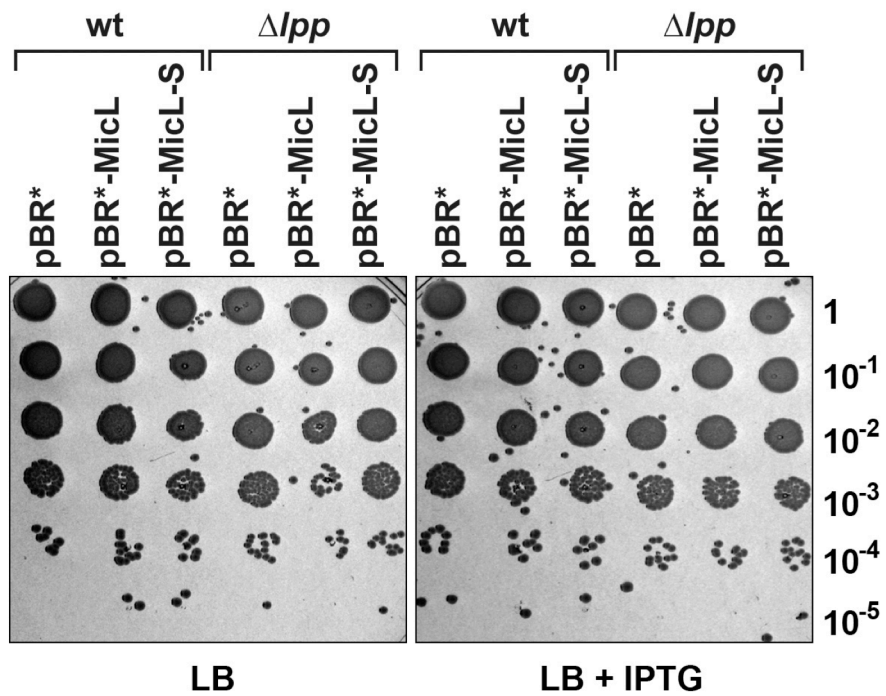
CAG1684  $\Delta cutC$  was transformed with pBR\*-MicL or pBR\*-MicL<sub>UGA to GGA</sub> mutant and grown in LB media with kanamycin to final OD<sub>600</sub> ~1.0. **(D)** MicL levels in *rne-3071*  $\Delta mg$  mutant. Strains CAG64307  $\Delta mg$  and the isogenic mutant carrying the temperature sensitive *rne-3071* allele were transformed with pBR\* and pBR\*-MicL and grown at 30°C to an OD<sub>600</sub> ~0.4 in LB with kanamycin. Cultures were split and incubated at either 30°C or 43.5°C. After 25 min, either water or 1 mM IPTG was added and cells were allowed to continue to grow an additional 45 min (final OD<sub>600</sub> ~0.8). **(E)** MicL levels in RNase mutant strains. Total RNA was isolated from *rnc::Tn10 rnhA::cat rnhB::kan* (GSO675), *rnc::cat rnlA::kan* (GSO420), *rnc mg* (GSO419), *rnc mg elaC* (GSO429) and *rnc 5* toxin (GSO676) mutant strains after 16 h growth in LB media. **(F)** MicL and MicL-S derived from *cutC*. A PCR fragment of the entire *cutC* gene (from the RBS to 3'UTR) containing the same point mutation as the P<sub>micL</sub>-mutant (See Supplemental Fig. S8) was cloned into pBR\* (pBR\*-*cutC*\*) and transformed, along with plasmid pBR\*-MicL, into the CAG64307  $\Delta cutC$  strain. Both strains were grown in LB with kanamycin to OD<sub>600</sub> ~0.1. Cultures were split and either water or 1 mM IPTG was added. Cultures were harvested at OD<sub>600</sub> ~1.0. For all samples in **(A-F)**, total RNA isolated was separated on a denaturing gel and subjected to Northern analysis using probes specific for the MicL 3' end and the 5S RNA. Note that higher molecular weight bands in the pBR\*-*cutC*\* + IPTG sample represents processed fragments with 5' OH groups as they are susceptible, along with MicL-S, to TEX treatment (data not shown).



**Supplemental Figure S4.** *lpp* is the sole target of MicL and MicL-S.

(A) mRNA-seq following 20 min of MicL-S overexpression from pBR'-MicL-S versus similarly treated vector control using identical conditions as described in Fig. 3A. (B) High correlation between samples after MicL or MicL-S

induction. We observe no major changes in mRNA levels after 20 min of MicL or MicL-S overexpression. **(C)** Change in Lpp in mRNA-seq (gray) and ribosome profiling (black) after MicL overexpression. **(D)** High correlation between two replicate ribosome profiling experiments (pre-induction). **(E)** Two other genes (*fepA*, *fiu*) are slightly repressed when comparing ribosome profiles pre and 20 min post MicL induction. **(F)** Comparison of mRNA-seq levels for *lpp*, *fepA* and *fiu*, showing that *fepA* and *fiu* mRNAs are repressed by growth both in the presence and absence of MicL overexpression. Fold-change in mRNA level of *lpp*, *fepA*, and *fiu* at 20 min post induction versus pre-induction in pBR vector control cells (dark gray) and in MicL expressing cells (light gray). While *lpp* is not repressed in the vector control strain, *fepA* and *fiu* mRNA levels significantly decrease during the 20 min induction period, possibly reflecting iron depletion in the medium during growth.

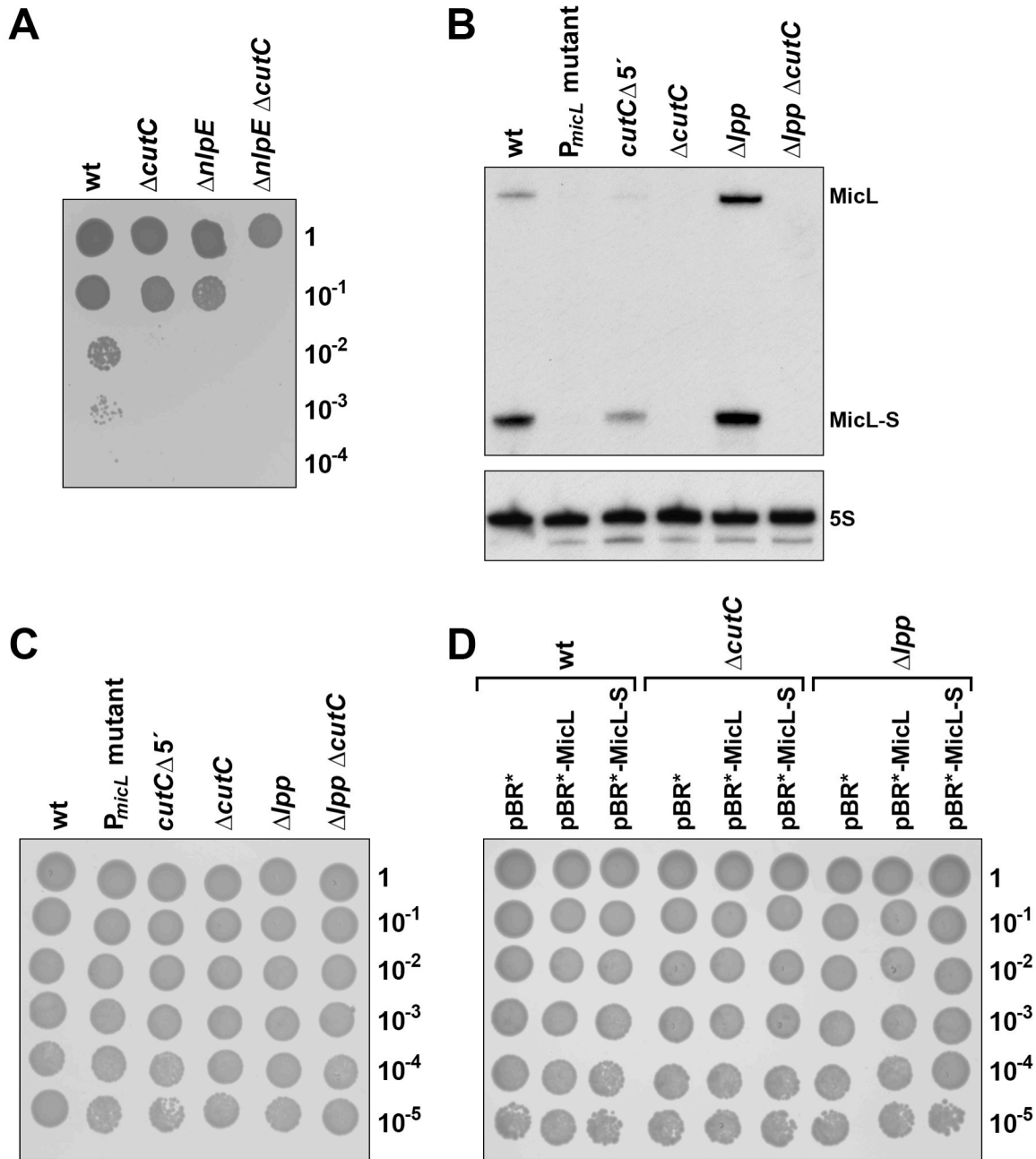


**Supplemental Figure S5.** MicL repression of Lpp induces sensitivity to dibucaine. LB and LB + IPTG control plates for Fig. 3A.



|                               |    |    |                                  |        |             |
|-------------------------------|----|----|----------------------------------|--------|-------------|
| <i>Escherichia coli</i>       | 19 | 49 | UGucGCCCAauAUgAUgcuUGCUC-GUACCAG | -25.40 | MicL        |
|                               |    |    |                                  |        |             |
|                               | 46 | 16 | AUcuUGGGUccUAaUGgc-GCGGGuCAUGGUC |        | <i>lpp</i>  |
| <i>Shigella sonnei</i>        | 19 | 49 | UGucGCCCAauAUgAUgcuUGCUC-GUACCAG | -25.40 | MicL        |
|                               |    |    |                                  |        |             |
|                               | 46 | 16 | AUcuUGGGUccUAaUGgc-GCGGGuCAUGGUC |        | <i>lpp</i>  |
| <i>Shigella boydii</i>        | 19 | 49 | UGucGCCCAauAUgAUgcuUGCUC-GUACCAG | -25.40 | MicL        |
|                               |    |    |                                  |        |             |
|                               | 46 | 16 | AUcuUGGGUccUAaUGgc-GCGGGuCAUGGUC |        | <i>lpp</i>  |
| <i>Citrobacter koseri</i>     | 19 | 49 | UGucGCCCAauAUgAUgcuUGCUC-GUACCAG | -25.40 | MicL        |
|                               |    |    |                                  |        |             |
|                               | 46 | 16 | AUcuUGGGUccUAaUGgc-GCGGGuCAUGGUC |        | <i>lpp</i>  |
| <i>Salmonella enterica</i>    | 19 | 49 | UGucGCCCAauAUgAUgcuUGCUC-GUACCAG | -25.40 | MicL        |
|                               |    |    |                                  |        |             |
|                               | 46 | 16 | AUcuUGGGUccUAaUGgc-GCGGGuCAUGGUC |        | <i>lppA</i> |
| <i>Salmonella enterica</i>    | 19 | 49 | UGucGCCCAauAUgA-UGCUGcUcGuAcCAG  | -16.10 | MicL        |
|                               |    |    |                                  |        |             |
|                               | 49 | 19 | ACcuUGGGUcuUGaUgACGuG-GAuUcUaGUC |        | <i>lppB</i> |
| <i>Klebsiella pneumoniae</i>  | 19 | 49 | UGucGCCCAauAUgAUgauUGCCC-GUACCAG | -28.40 | MicL        |
|                               |    |    |                                  |        |             |
|                               | 46 | 16 | AUcuUGGGUccUAaUGgc-GCGGGuCAUGGUC |        | <i>lpp</i>  |
| <i>Enterobacter cloacae</i>   | 19 | 49 | UGucGCCCAauAUgAUgcuUGCUC-GUACCAG | -23.40 | MicL        |
|                               |    |    |                                  |        |             |
|                               | 46 | 16 | AUcuUGGGUccUAaUGgc-GCGGGuCAUGGUC |        | <i>lpp</i>  |
| <i>Cronobacter turicensis</i> | 19 | 49 | UGucGCCCAauAUgAUgcuUGCUC-GUACCAG | -25.40 | MicL        |
|                               |    |    |                                  |        |             |
|                               | 46 | 16 | AUcuUGGGUccUAaUGgc-GCGGGuCAUGGUC |        | <i>lpp</i>  |

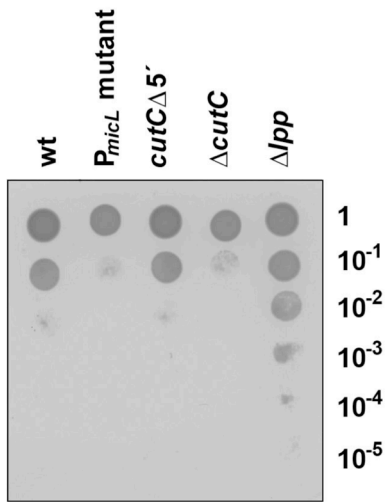
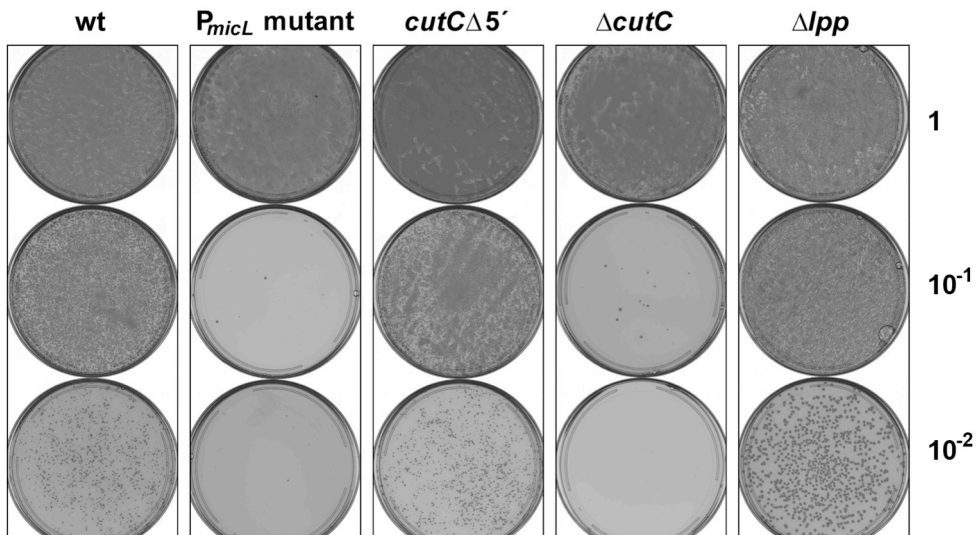
**Supplemental Figure S7.** Prediction of potential MicL sRNA targets in *lpp* mRNAs from several enterobacteria. The ThermoComposition software (Matveeva et al., 2007) was used to predict optimal targets for MicL sRNAs in *lpp* mRNAs from different enterobacteria. The tool allows calculations of duplex stabilities ( $\Delta G$  kcal/mol) for potential targets and searches for optimal interactions between two RNA molecules by using the nearest neighbor model and the same thermodynamic parameters as the Afold and Mfold programs (Mathews et al., 2007; Ogurtsov et al., 2006). Complete *lpp* mRNAs and MicL-S sequences were used for the analysis. Predicted core (seed) regions of complementary interactions are shown in red.



**Supplemental Figure S8.** MicL repression of *lpp* confers copper resistance.

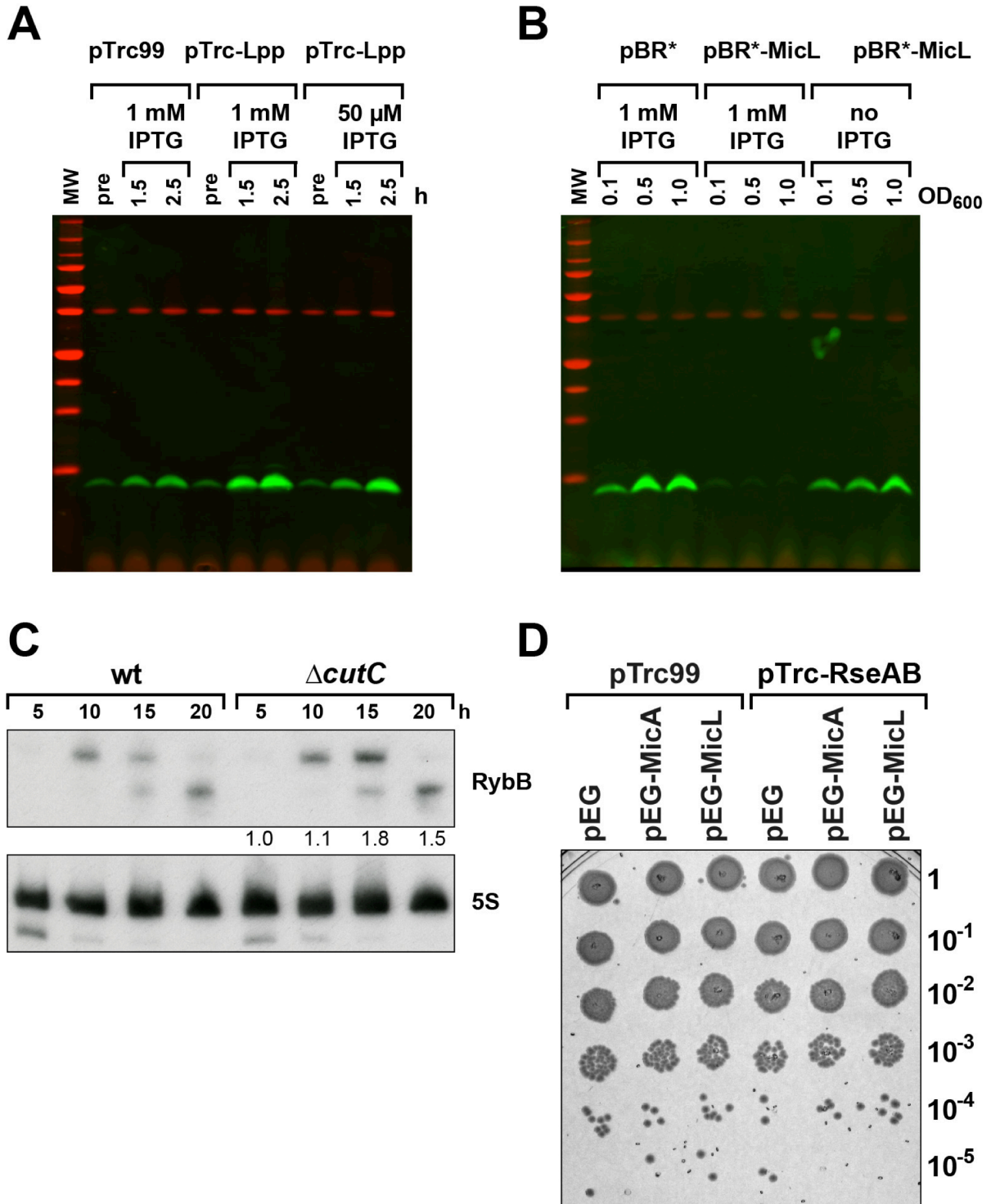
**(A)** Plate assay showing sensitivity of the CAG1684 wild-type and isogenic mutant strains  $\Delta cutC$ ,  $\Delta nlpE$  and  $\Delta cutC \Delta nlpE$  to 4 mM Cu(II)Cl<sub>2</sub> using conditions in Fig. 6A. **(B)** Northern blot assay of MicL and MicL-S RNA levels in the *cutC* chromosomal mutant backgrounds used in Fig. 6A. Total RNA isolated from the wild-type CAG1684 strain along with the isogenic mutant strains P<sub>micL</sub> mutant, *cutC*Δ5',  $\Delta cutC$ ,  $\Delta lpp$  and  $\Delta cutC \Delta lpp$  grown for 10 h at 37 °C was subjected to Northern analysis with probe specific for the MicL 3' end and the 5S RNA. **(C)** LB control plate for Fig. 6A. **(D)** LB with kanamycin control plate for Fig. 6B.



**A****B**

**Supplemental Figure S9.** MicL is responsible for *cutC* copper sensitivity phenotype.

**(A)** Plate assay showing sensitivity of the CAG1684 wild-type and isogenic mutant strains P<sub>micL</sub> mutant, *cutC*Δ5', Δ*cutC* and Δ*lpp* carried out exactly as in Fig 6A. **(B)** Aliquots (80 μl) of each culture in **(A)** were spread onto 4mM copper supplemented LB plates and grown for 48 hrs at 30°C.

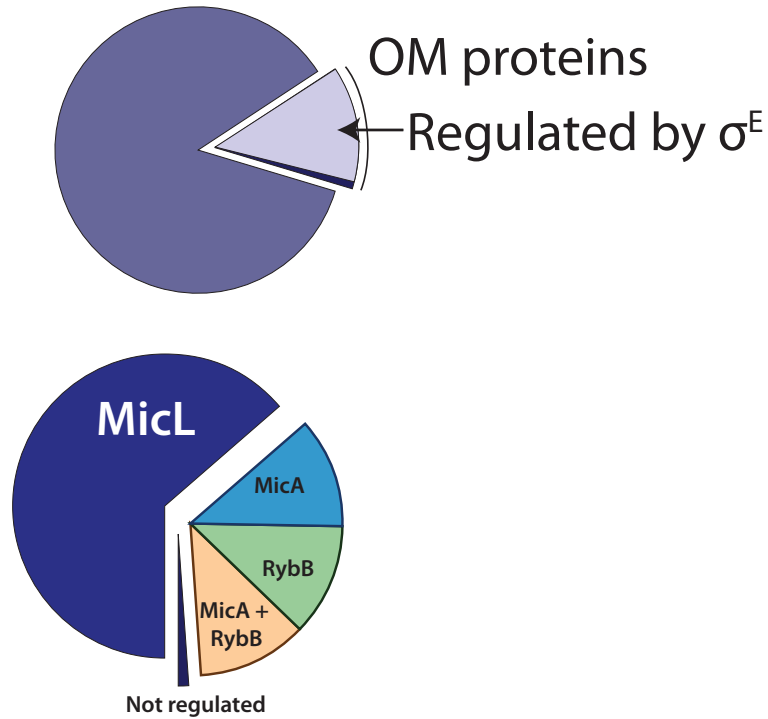


**Supplemental Figure S10.** MicL and Lpp are part of an envelope-protective regulatory loop.

(A) Western blot of Lpp (green) and RpoA (red) after Lpp overexpression as in Fig. 7A. Samples were normalized by OD<sub>600</sub>. Strains with pTrc99 and pTrc-Lpp were grown to OD<sub>600</sub> ~0.1, samples were taken and IPTG was added to the

remaining cultures as indicated. Two additional samples were taken 1.5 and 2.5 h post-induction. pTrc99 + 1 mM IPTG was sampled at  $OD_{600} \sim 0.1, 0.5, \text{ and } 1.0$ ; pTrc-Lpp + 1 mM IPTG was sampled at  $OD_{600} \sim 0.1, 0.3, \text{ and } 0.3$  (because cultures cease to grow); pTrc-Lpp + 50  $\mu\text{M}$  IPTG was sampled at  $OD_{600} \sim 0.1, 0.5, \text{ and } 1.0$ . At 1.5 h, the pTrc-Lpp + 1 mM IPTG cultures are ceasing growth. Lpp quantification per lane: 1.0, 1.9, 2.4, 1.1, 4.2, 6.0, 1.2, 2.3, 4.4. **(B)** Western blot of Lpp and RpoA after MicL overexpression as in Fig. 7B. Samples were normalized by  $OD_{600}$ . Strains with pBR\* and pBR\*-MicL were diluted into either LB or LB + 1 mM IPTG, and samples were collected at  $OD_{600} \sim 0.1, 0.5, \text{ and } 1.0$ . Lpp quantification per lane: 1.0, 2.6, 2.7, 0.1, 0.1, 0.1, 1.0, 1.3, 2.0. For both **(A)** and **(B)**, quantification was performed with ImageJ software, and normalized against RpoA levels. **(C)** RybB RNA levels in wild type and  $\Delta\text{cutC}$  mutant cells. RybB is known to be processed in late stationary phase (Vogel et al., 2003) as we observe. Total RNA samples analyzed in Fig. 3D were probed for RybB and 5S RNA. The intensity of the RybB RNA band for each strain was quantified using ImageJ software, and the ratios between the corresponding samples for the  $\Delta\text{cutC}$  mutant and wild type strains are given. The same differences were observed for total RNA isolated from independent samples grown for 22 h. **(D)** LB control plates for Fig. 7C.

## Total Translation



**Supplemental Figure S11.**  $\sigma^E$  regulates the majority of OM proteins through its sRNAs.

A graphic representation taken from values generated in Supplemental Table S3. **(Top)**  $\sigma^E$  regulates the majority of translation events of the OM through its sRNAs. Dark slice: ~13% of all translation events are of OM proteins. Light slice:  $\sigma^E$  regulates >90% of all translation events destined for the OM. **(Bottom)** MicL regulates the majority of OM protein flux. MicL regulates ~60% of all OM translation, with MicA, RybB, and those regulated jointly by MicA and RybB comprising 11% of translation. Only ~1% of OM translation events are not regulated.

**Supplemental Table S1.** All mRNA sequencing data. mRNA sequencing data for empty vector, MicL-S, and MicL before (0) and 4, 10, and 20 min after induction by IPTG. Mean expression of each gene is normalized by total number of reads and reported.

**Supplemental Table S2.** All ribosome profiling data. Ribosome profiling of MicL before (0) and 4, 10 and 20 min after induction by IPTG. Two experiments were performed, and reported separately. Experiment 1 shows before (0) and 10 and 20 min after MicL induction, experiment 2 shows before (0) and 4 min after MicL induction. Mean translation of each gene is normalized by total number of reads and reported.

**Supplemental Table S6:** Oligonucleotides used for this study.

These tables are not reproduced here, but can be found at <http://genesdev.cshlp.org/content/28/14/1620/suppl/DC1>.

**Supplemental Table S3.** Outer membrane and MicA, RybB, and MicL regulated proteins as a fraction of total.

**(A)** Outer membrane proteins as a fraction of total transcription and translation. OM proteins were those annotated in (Riley et al., 2006) and are reported as a percent of total.

| GeneNames | mRNA Pre-MicL | mRAN 20 min Post-MicL | Rib fp Pre-MicL | Rib fp 20min Post-MicL |
|-----------|---------------|-----------------------|-----------------|------------------------|
| lpp       | 9.77          | 1.05                  | 7.98            | 0.67                   |
| ompF      | 1.47          | 1.45                  | 1.05            | 1.24                   |
| ompX      | 0.67          | 0.80                  | 0.91            | 1.26                   |
| ompC      | 0.40          | 0.41                  | 0.38            | 0.48                   |
| ompA      | 0.39          | 0.42                  | 1.48            | 1.77                   |
| ecnB      | 0.21          | 0.43                  | 0.19            | 0.44                   |
| pal       | 0.19          | 0.27                  | 0.35            | 0.43                   |
| slyB      | 0.12          | 0.12                  | 0.09            | 0.12                   |
| nlpI      | 0.12          | 0.12                  | <.01            | <.01                   |
| ompT      | 0.09          | 0.07                  | 0.10            | 0.07                   |
| spr       | 0.08          | 0.11                  | 0.04            | 0.05                   |
| nlpD      | 0.08          | 0.10                  | <.01            | 0.01                   |
| bamD      | 0.07          | 0.08                  | 0.05            | 0.06                   |
| bamC      | 0.06          | 0.08                  | 0.02            | 0.03                   |
| mltD      | 0.06          | 0.05                  | <.01            | <.01                   |
| yjeI      | 0.05          | 0.09                  | 0.06            | 0.11                   |
| osmE      | 0.05          | 0.08                  | 0.04            | 0.05                   |
| borD      | 0.05          | 0.03                  | 0.04            | 0.03                   |
| vacJ      | 0.04          | 0.04                  | 0.02            | 0.02                   |
| smpA      | 0.03          | 0.04                  | 0.05            | 0.06                   |
| bamA      | 0.03          | 0.04                  | 0.03            | 0.04                   |
| yedD      | 0.03          | 0.03                  | 0.03            | 0.03                   |
| bamB      | 0.02          | 0.03                  | 0.02            | 0.03                   |
| ygdR      | 0.02          | 0.04                  | 0.02            | 0.03                   |
| yjaH      | 0.02          | 0.03                  | <.01            | <.01                   |
| ecnA      | 0.02          | 0.02                  | <.01            | <.01                   |
| mipA      | 0.02          | 0.02                  | 0.06            | 0.07                   |
| yeaY      | 0.02          | 0.01                  | <.01            | <.01                   |
| mltA      | 0.01          | 0.01                  | <.01            | <.01                   |
| nlpC      | 0.01          | 0.02                  | <.01            | <.01                   |
| tolC      | 0.01          | 0.02                  | 0.04            | 0.05                   |
| ycfL      | 0.01          | 0.02                  | <.01            | <.01                   |
| ydbJ      | 0.01          | 0.02                  | 0.02            | 0.02                   |
| ybaY      | 0.01          | 0.02                  | 0.02            | 0.04                   |
| yidQ      | 0.01          | 0.02                  | <.01            | <.01                   |
| fimD      | <.01          | <.01                  | <.01            | <.01                   |
| imp       | <.01          | 0.01                  | 0.02            | 0.02                   |
| yraP      | <.01          | 0.01                  | 0.01            | 0.01                   |
| tsx       | <.01          | 0.01                  | 0.04            | 0.05                   |
| fhuA      | <.01          | <.01                  | <.01            | <.01                   |
| yfeY      | <.01          | 0.01                  | <.01            | <.01                   |
| yggG      | <.01          | 0.01                  | <.01            | <.01                   |
| ybhC      | <.01          | <.01                  | 0.01            | 0.01                   |

|      |      |      |      |      |
|------|------|------|------|------|
| pIdA | <.01 | <.01 | <.01 | <.01 |
| rlpA | <.01 | <.01 | <.01 | 0.01 |
| amiD | <.01 | <.01 | <.01 | <.01 |
| ydcL | <.01 | <.01 | <.01 | 0.01 |
| ygdI | <.01 | <.01 | <.01 | 0.01 |
| panE | <.01 | <.01 | <.01 | <.01 |
| ycfM | <.01 | 0.01 | 0.01 | 0.02 |
| yfaZ | <.01 | <.01 | <.01 | <.01 |
| btuB | <.01 | <.01 | 0.01 | 0.01 |
| slp  | <.01 | <.01 | <.01 | <.01 |
| emtA | <.01 | 0.01 | 0.01 | 0.01 |
| fadL | <.01 | <.01 | 0.02 | 0.02 |
| nmpC | <.01 | <.01 | 0.01 | 0.01 |
| ytfM | <.01 | <.01 | <.01 | <.01 |
| hslJ | <.01 | <.01 | <.01 | <.01 |
| yajG | <.01 | <.01 | 0.04 | 0.05 |
| cirA | <.01 | <.01 | <.01 | <.01 |
| yfhG | <.01 | <.01 | <.01 | <.01 |
| ynbE | <.01 | <.01 | <.01 | <.01 |
| yaiW | <.01 | <.01 | <.01 | <.01 |
| yoaF | <.01 | <.01 | <.01 | <.01 |
| nlpE | <.01 | <.01 | <.01 | <.01 |
| yceB | <.01 | <.01 | <.01 | <.01 |
| lolB | <.01 | <.01 | 0.02 | 0.02 |
| yiaD | <.01 | <.01 | <.01 | <.01 |
| ygeR | <.01 | <.01 | <.01 | <.01 |
| mltC | <.01 | <.01 | <.01 | <.01 |
| yidX | <.01 | <.01 | <.01 | <.01 |
| ybfN | <.01 | <.01 | <.01 | <.01 |
| ybbC | <.01 | <.01 | <.01 | <.01 |
| nmpC | <.01 | <.01 | <.01 | <.01 |
| fiu  | <.01 | <.01 | <.01 | <.01 |
| csgG | <.01 | <.01 | <.01 | <.01 |
| yncD | <.01 | <.01 | <.01 | <.01 |
| osmB | <.01 | <.01 | <.01 | <.01 |
| yjfO | <.01 | <.01 | <.01 | <.01 |
| yhfL | <.01 | <.01 | <.01 | <.01 |
| fepA | <.01 | <.01 | <.01 | <.01 |
| fliL | <.01 | <.01 | <.01 | <.01 |
| yajI | <.01 | <.01 | <.01 | <.01 |
| yddW | <.01 | <.01 | <.01 | <.01 |
| rcsF | <.01 | <.01 | 0.01 | 0.02 |
| ydhA | <.01 | <.01 | <.01 | <.01 |
| yegR | <.01 | <.01 | <.01 | <.01 |
| yaeF | <.01 | <.01 | <.01 | <.01 |
| mltB | <.01 | <.01 | <.01 | <.01 |
| yaiT | <.01 | <.01 | <.01 | <.01 |
| yoeA | <.01 | <.01 | <.01 | <.01 |
| ysaB | <.01 | <.01 | <.01 | <.01 |

|      |      |      |      |      |
|------|------|------|------|------|
| ycgH | <.01 | <.01 | <.01 | <.01 |
| pagP | <.01 | <.01 | <.01 | <.01 |
| yaiT | <.01 | <.01 | <.01 | <.01 |
| yhcD | <.01 | <.01 | <.01 | <.01 |
| viaT | <.01 | <.01 | <.01 | <.01 |
| phoE | <.01 | <.01 | <.01 | <.01 |
| ompN | <.01 | <.01 | <.01 | <.01 |
| bcsZ | <.01 | <.01 | <.01 | <.01 |
| ybjP | <.01 | <.01 | <.01 | 0.02 |
| fhuE | <.01 | <.01 | <.01 | <.01 |
| fecA | <.01 | <.01 | <.01 | <.01 |
| flgH | <.01 | <.01 | <.01 | <.01 |
| nfrA | <.01 | <.01 | <.01 | <.01 |
| pgaA | <.01 | <.01 | <.01 | <.01 |
| ypjA | <.01 | <.01 | <.01 | <.01 |
| ydeK | <.01 | <.01 | <.01 | <.01 |
| srlD | <.01 | <.01 | <.01 | <.01 |
| ompW | <.01 | <.01 | <.01 | <.01 |
| ybfP | <.01 | <.01 | <.01 | <.01 |
| blc  | <.01 | <.01 | <.01 | 0.01 |
| rzoD | <.01 | <.01 | <.01 | <.01 |
| ybeT | <.01 | <.01 | <.01 | <.01 |
| gfcE | <.01 | <.01 | <.01 | <.01 |
| yafT | <.01 | <.01 | <.01 | <.01 |
| gfcB | <.01 | <.01 | <.01 | <.01 |
| yhdV | <.01 | <.01 | <.01 | <.01 |
| pgaB | <.01 | <.01 | <.01 | <.01 |
| yraJ | <.01 | <.01 | <.01 | <.01 |
| yfiB | <.01 | <.01 | <.01 | <.01 |
| mdtP | <.01 | <.01 | <.01 | <.01 |
| ycaL | <.01 | <.01 | <.01 | <.01 |
| yfeN | <.01 | <.01 | <.01 | <.01 |
| yqhH | <.01 | <.01 | <.01 | <.01 |
| yfgH | <.01 | <.01 | <.01 | <.01 |
| flu  | <.01 | <.01 | <.01 | <.01 |
| nrfG | <.01 | <.01 | <.01 | <.01 |
| yoeA | <.01 | <.01 | <.01 | <.01 |
| uidC | <.01 | <.01 | <.01 | <.01 |
| yjbF | <.01 | <.01 | <.01 | <.01 |
| yecR | <.01 | <.01 | <.01 | <.01 |
| ycbS | <.01 | <.01 | <.01 | <.01 |
| lamB | <.01 | <.01 | <.01 | <.01 |
| ybfM | <.01 | <.01 | <.01 | <.01 |
| yehB | <.01 | <.01 | <.01 | <.01 |
| yqiH | <.01 | <.01 | <.01 | <.01 |
| yqiG | <.01 | <.01 | <.01 | <.01 |
| yghG | <.01 | <.01 | <.01 | <.01 |
| cusC | <.01 | <.01 | <.01 | <.01 |
| sfmD | <.01 | <.01 | <.01 | <.01 |



|       |       |      |       |      |
|-------|-------|------|-------|------|
| bglH  | <.01  | <.01 | <.01  | <.01 |
| ycjN  | <.01  | <.01 | <.01  | <.01 |
| htrE  | <.01  | <.01 | <.01  | <.01 |
| ompL  | <.01  | <.01 | <.01  | <.01 |
| ompG  | <.01  | <.01 | <.01  | <.01 |
| wza   | <.01  | <.01 | <.01  | <.01 |
| ybgQ  | <.01  | <.01 | <.01  | <.01 |
| rzoR  | <.01  | <.01 | <.01  | <.01 |
| ypdI  | <.01  | <.01 | <.01  | <.01 |
| yfiL  | <.01  | <.01 | <.01  | <.01 |
| yqiG  | <.01  | <.01 | <.01  | <.01 |
| Total | 14.27 | 6.25 | 13.30 | 7.54 |

**Supplemental Table S3.** Outer membrane and MicA, RybB, and MicL regulated proteins as a fraction of total.

**(B)** Outer membrane proteins regulated by MicA, RybB, or MicL as a fraction of total transcription and translation.

| GeneNames | mRNA Pre-MicL | mRAN 20 min<br>Post-MicL | Rib fp Pre-MicL | Rib fp 20min<br>Post-MicL | sRNA Regulator |
|-----------|---------------|--------------------------|-----------------|---------------------------|----------------|
| lpp       | 9.77          | 1.05                     | 7.98            | 0.67                      | MicL           |
| ompF      | 1.47          | 1.45                     | 1.05            | 1.24                      | RybB           |
| ompX      | 0.67          | 0.80                     | 0.91            | 1.26                      | MicA           |
| ompC      | 0.40          | 0.41                     | 0.38            | 0.48                      | RybB           |
| ompA      | 0.39          | 0.42                     | 1.48            | 1.77                      | RybB, MicA     |
| ecnB      | 0.21          | 0.43                     | 0.19            | 0.44                      | MicA           |
| pal       | 0.19          | 0.27                     | 0.35            | 0.43                      | MicA           |
| tsx       | <.01          | 0.01                     | 0.04            | 0.05                      | RybB, MicA     |
| fadL      | <.01          | <.01                     | 0.02            | 0.02                      | RybB           |
| fiu       | <.01          | <.01                     | <.01            | <.01                      | RybB           |
| ompW      | <.01          | <.01                     | <.01            | <.01                      | RybB, MicA     |
| lamB      | <.01          | <.01                     | <.01            | <.01                      | RybB, MicA     |
| sum       | 13.10         | 4.84                     | 12.41           | 6.37                      |                |

**Supplemental Table S4:** Strains used in this study.

| Name    | TU Name  | Relevant genotype   | Source                     |
|---------|--|---|----------------------------|
| Top10   | Top10  | F- <i>mcrA</i> $\Delta$ ( <i>mrr</i> - <i>hsdRMS</i> - <i>mcrBC</i> ) $\phi$ 80 <i>lacZ</i> $\Delta$ M15 $\Delta$ <i>lacX74</i> <i>nupG</i> <i>recA1</i> <i>araD139</i> $\Delta$ ( <i>ara</i> - <i>leu</i> )7697 <i>galE15</i> <i>galK16</i> <i>rpsL</i> (Str <sup>R</sup> ) <i>endA1</i> $\lambda$ | lab stock                  |
| PM1205  | PM1205   | MG1655 <i>mal::lacI<sup>q</sup></i> , <i>DaraBAD</i> <i>araC<sup>+</sup></i> , <i>lacI<sup>l</sup>::P<sub>BAD</sub>-cat-sacB-lacZ</i> , <i>mini</i> $\lambda$ <i>tet<sup>R</sup></i>  | Mandin and Gottesman, 2009 |
| GSO677  | <i>lppS-lacZ</i>   | PM1205 $\Delta$ <i>cat-sacB::lpp1755407-1755547-lacZ</i>  | this study                 |
| GSO678  | <i>lpp-lacZ</i> trunc 1  | PM1205 $\Delta$ <i>cat-sacB::lpp1755407-1755511-lacZ</i>  | this study                 |
| GSO679  | <i>lpp-lacZ</i> trunc 2  | PM1205 $\Delta$ <i>cat-sacB::lpp1755407-1755478-lacZ</i>  | this study                 |
| GSO680  | <i>lpp-lacZ</i> trunc 3  | PM1205 $\Delta$ <i>cat-sacB::lpp1755407-1755451-lacZ</i>  | this study                 |
| GSO681  | <i>lppS</i> -HPI <i>mutI</i> comp- <i>lacZ</i> -1                          | PM1205 $\Delta$ <i>cat-sacB::lpp1755407-1755547-lacZ</i> mutation ACTGG to TGTCT  | this study                 |
| EM1279  | EM1279   | EM10552 <i>zce-726::Tn102</i>   | Massé et al., 2008         |
| EM1277  | EM1277   | EM1055 <i>rne-3071 zce-726::Tn102</i>   | Massé et al., 2008         |
| NM400   | NM400  | MG1655 <i>mini-<math>\lambda</math>-cm</i>  | N. Majdalani               |
| GSO682  | NM400 $\Delta$ <i>cutC::kan</i>  | NM400 $\Delta$ <i>cutC::kan</i>   | this study                 |
| GSO683  | NM400 $\Delta$ <i>lpp::kan</i>   | NM400 $\Delta$ <i>lpp::kan</i>  | this study                 |
| NM500   | NM500  | MG1655 <i>mini-<math>\lambda</math>-tet</i>   | N. Majdalani               |
| GSO684  | NM500 $\Delta$ <i>nlpE::cm</i>   | NM500 $\Delta$ <i>nlpE::cm</i>  | this study                 |
| GSO685  | NM500 $\Delta$ <i>cutC5'::cm</i>   | NM500 $\Delta$ <i>cutC5'::cm</i>  | this study                 |
| GSO688  | NM500 <i>PmicL</i> mutant:: <i>kan</i>                                     | NM500 <i>PmicL</i> mutant:: <i>kan</i>  | this study                 |
| CAG1684 | CAG1684  | MG1655 $\Delta$ <i>lacX74</i>   | lab stock                  |
| GSO688  | CAG1684 $\Delta$ <i>cutC::kan</i>  | MG1655 $\Delta$ <i>lacX74</i> $\Delta$ <i>cutC::kan</i>   | this study                 |
| GSO690  | CAG1684 $\Delta$ <i>cutC</i>   | MG1655 $\Delta$ <i>lacX74</i> $\Delta$ <i>cutC</i>  | this study                 |
| GSO691  | CAG1684 $\Delta$ <i>nlpE::cm</i>   | MG1655 $\Delta$ <i>lacX74</i> $\Delta$ <i>nlpE::cm</i>  | this study                 |
| GSO692  | CAG1684 $\Delta$ <i>cutC</i> $\Delta$ <i>nlpE::cm</i>                      | MG1655 $\Delta$ <i>lacX74</i> $\Delta$ <i>cutC</i> $\Delta$ <i>nlpE::cm</i>   | this study                 |
| GSO693  | CAG1684 $\Delta$ <i>lpp::kan</i>   | MG1655 $\Delta$ <i>lacX74</i> $\Delta$ <i>lpp::kan</i>  | this study                 |
| GSO694  | CAG1684 $\Delta$ <i>lpp</i> $\Delta$ <i>cutC::kan</i>                      | MG1655 $\Delta$ <i>lacX74</i> $\Delta$ <i>lpp</i> $\Delta$ <i>cutC::kan</i>   | this study                 |
| GSO695  | CAG1684 $\Delta$ <i>lpp</i> $\Delta$ <i>cutC</i>                           | MG1655 $\Delta$ <i>lacX74</i> $\Delta$ <i>lpp</i> $\Delta$ <i>cutC</i>  | this study                 |
| GSO696  | CAG1684 $\Delta$ <i>lpp</i> $\Delta$ <i>nlpE::cm</i>                       | MG1655 $\Delta$ <i>lacX74</i> $\Delta$ <i>lpp</i> $\Delta$ <i>nlpE::cm</i>  | this study                 |
| GSO697  | CAG1684 $\Delta$ <i>lpp</i> $\Delta$ <i>nlpE</i>                           | MG1655 $\Delta$ <i>lacX74</i> $\Delta$ <i>lpp</i> $\Delta$ <i>nlpE</i>  | this study                 |
| GSO698  | CAG1684 $\Delta$ <i>lpp</i> $\Delta$ <i>nlpE</i> $\Delta$ <i>cutC::kan</i> | MG1655 $\Delta$ <i>lacX74</i> $\Delta$ <i>lpp</i> $\Delta$ <i>nlpE</i> $\Delta$ <i>cutC::kan</i>  | this study                 |
| GSO699  | CAG1684 $\Delta$ <i>lpp</i> $\Delta$ <i>nlpE</i> $\Delta$ <i>cutC</i>      | MG1655 $\Delta$ <i>lacX74</i> $\Delta$ <i>lpp</i> $\Delta$ <i>nlpE</i> $\Delta$ <i>cutC</i>   | this study                 |
| GSO700  | CAG1684 $\Delta$ <i>cutC5'::cm</i>   | MG1655 $\Delta$ <i>lacX74</i> $\Delta$ <i>cutC5'::cm</i>  | this study                 |
| GSO701  | CAG1684 $\Delta$ <i>cutC5'</i>   | MG1655 $\Delta$ <i>lacX74</i> $\Delta$ <i>cutC5'</i>  | this study                 |
| GSO702  | CAG1684 <i>PmicL</i> mut:: <i>kan</i>                                      | MG1655 $\Delta$ <i>lacX74</i> <i>PmicL</i> mut:: <i>kan</i>   | this study                 |
| GSO703  | CAG1684 <i>PmicL</i> mut   | MG1655 $\Delta$ <i>lacX74</i> <i>PmicL</i> mut  | this study                 |
| GSO704  | CAG1684 <i>cutC</i> -SPA   | MG1655 $\Delta$ <i>lacX74</i> <i>cutC</i> -SPA  | this study                 |

|          |   |  |                      |
|----------|---|--|----------------------|
| GSO705   | CAG1684 $\Delta$ cutC5'-SPA                                 | MG1655 $\Delta$ lacX74 $\Delta$ cutC5'-SPA   | this study           |
| GSO706   | CAG1684 $\Delta$ hfq1-cm (P1 from AZ270)                    | MG1655 $\Delta$ lacX74 $\Delta$ hfq1-cm  | this study           |
| GSO707   | CAG1684 $\Delta$ rnc-cm (P1 from AZ275)                     | MG1655 $\Delta$ lacX74 $\Delta$ rnc-cm   | this study           |
| CAG64307 | CAG64307  | MG1655 $\Delta$ lacX74 HK::lacIq   | lab stock            |
| GSO708   | CAG64307 $\Delta$ cutC::kan                                 | MG1655 $\Delta$ lacX74 HK::lacIq $\Delta$ cutC::kan  | this study           |
| GSO709   | CAG64307 $\Delta$ cutC                                      | MG1655 $\Delta$ lacX74 HK::lacIq $\Delta$ cutC   | this study           |
| GSO710   | CAG64307 lpp-Stop1-cm                                       | MG1655 $\Delta$ lacX74 HK::lacIq lpp-Stop1-cm  | this study           |
| GSO711   | CAG64307 lpp-Stop2-cm                                       | MG1655 $\Delta$ lacX74 HK::lacIq lpp-Stop2-cm  | this study           |
| GSO712   | CAG64307 lpp-Stop4-cm                                       | MG1655 $\Delta$ lacX74 HK::lacIq lpp-Stop4-cm  | this study           |
| GSO713   | CAG64307 lpp-cm   | MG1655 $\Delta$ lacX74 HK::lacIq lpp-cm  | this study           |
| GSO675   | JO145   | MG1655 $\Delta$ lacZ $\Delta$ gadXY::Plac-lacZgadX $\Delta$ rnc::Tn10 $\Delta$ rnhA::cm $\Delta$ rnhB::kan | Opdyke et al., 2011  |
| GSO420   | JO146   | MG1655 $\Delta$ lacZ $\Delta$ gadXY::Plac-lacZgadX $\Delta$ rnc::cm $\Delta$ rnlA::kan                     | Opdyke et al., 2011  |
| GSO676   | JO147   | MG1655 $\Delta$ lacZ $\Delta$ gadXY::Plac-lacZgadX $\Delta$ 5 TA $\Delta$ rng::cm                          | Opdyke et al., 2011  |
| GSO419   | GSO419  | MG1655 $\Delta$ lacZ $\Delta$ gadXY::Plac-lacZgadX $\Delta$ rnc::cat $\Delta$ rng::kan                     | Opdyke et al., 2011  |
| GSO429   | GSO429  | MG1655 $\Delta$ lacZ $\Delta$ gadXY::Plac-lacZgadX $\Delta$ elaC $\Delta$ rnc::cat $\Delta$ rng::kan       | Opdyke et al., 2011  |
| CAG55860 | CAG64114 pTrc99a pUA-E60-MicA                               | MG1655 $\Delta$ lacX74 rpoHp3-lacZ pTrc99a pUA-E60-MicA  | Mutalik et al., 2009 |
| CAG55851 | CAG64114 pTrc99a pUA-E51-RybB                               | MG1655 $\Delta$ lacX74 rpoHp3-lacZ pTrc99a pUA-E51-RybB  | Mutalik et al., 2009 |
| GSO714   | CAG64114 pTrc99a pUA-E-MicL                                 | MG1655 $\Delta$ lacX74 rpoHp3-lacZ pTrc99a pUA-E-MicL  | this study           |
| CAG55760 | CAG64114 pRpoE pUA-E60-MicA                                 | MG1655 $\Delta$ lacX74 rpoHp3-lacZ pRpoE pUA-E60-MicA  | Mutalik et al., 2009 |
| CAG55751 | CAG64114 pRpoE pUA-E51-RybB                                 | MG1655 $\Delta$ lacX74 rpoHp3-lacZ pRpoE pUA-E51-RybB  | Mutalik et al., 2009 |
| GSO715   | CAG64114 pRpoE pUA-E-MicL                                   | MG1655 $\Delta$ lacX74 rpoHp3-lacZ pRpoE pUA-E-MicL  | this study           |
| CAG64334 | CAG45114 pTrc99a pEG  | MG1655 $\Delta$ lacX74 rpoHp3-lacZ pTrc99a pEG   | Gogol et al., 2011   |
| CAG64335 | CAG45114 pTrc99a pEG-MicA                                   | MG1655 $\Delta$ lacX74 rpoHp3-lacZ pTrc99a pEG-MicA  | Gogol et al., 2011   |
| GSO716   | CAG45114 pTrc99a pEG-MicL                                   | MG1655 $\Delta$ lacX74 rpoHp3-lacZ pTrc99a pEG-MicL  | this study           |
| CAG64337 | CAG45114 pRseAB pEG   | MG1655 $\Delta$ lacX74 rpoHp3-lacZ pRseAB pEG  | Gogol et al., 2011   |
| CAG64338 | CAG45114 pRseAB pEG-MicA                                    | MG1655 $\Delta$ lacX74 rpoHp3-lacZ pRseAB pEG-MicA   | Gogol et al., 2011   |
| GSO717   | CAG45114 pRseAB pEG-MicL                                    | MG1655 $\Delta$ lacX74 rpoHp3-lacZ pRseAB pEG-MicL   | this study           |
| GSO720   | CAG64307 $\Delta$ cutC $\Delta$ rng::kan                    | MG1655 $\Delta$ lacX74 HK::lacIq $\Delta$ cutC $\Delta$ rng::kan   | this study           |
| GSO721   | CAG64307 $\Delta$ cutC $\Delta$ rng                         | MG1655 $\Delta$ lacX74 HK::lacIq $\Delta$ cutC $\Delta$ rng  | this study           |
| GSO722   | CAG64307 $\Delta$ cutC $\Delta$ rng rne-3071 zce-726::Tn102 | MG1655 $\Delta$ lacX74 HK::lacIq $\Delta$ cutC $\Delta$ rng rne-3071 zce-726::Tn102                        | this study           |
| GSO723   | MC4100 $\Delta$ ybeY  | MC4100 $\Delta$ ybeY   | Jacob et al., 2013   |

**Supplemental Table S4: Plasmids used in this study.**

| Name                | TU Name                       | Brief discription  | Source  |
|---------------------|-------------------------------|--|---|
| pBR                 | pBRplac                       | p15A ori, Amp, contains pLacO-1 promoter   | lab stock; Thomason et. al., 2012                           |
| pBR-MicL-S          | pBRplac-Reg26-80              | micL-S (80nt) cloned into pBRplac at the HindIII/AatII site  | this study  |
| pBR-MicL-S-1mut     | pBRplac-Reg26-80 HPImutII     | Generated TCGT to AGCA mutation into pBR-MicL-S  | this study  |
| pBR-MicL-S Δ1-12    | pBRplac-Reg26-80 Δ1-12        | Deleted <i>micL</i> -S nucleotides 1-12 of pBR-MicL-S  | this study  |
| pBR-MicL-S Δ1-45    | pBRplac-Reg26-80 Δ1-45        | Deleted <i>micL</i> -S nucleotieds 1-45 of pBR-MicL-S  | this study  |
| pBR-MicL            | pBRplac-Reg26-FL              | micL (308 nt) cloned into pBRplac at the HindIII/AatII site  | this study  |
| pBR-MicA            | pBRplac-MicA                  | MicA cloned into pBRplac at the HindIII/EcoRI site   | kindly provided by S. Gottesman, De Lay and Gottesman, 2012 |
| pBR-RybB            | pBRplac-RybB                  | RybB cloned into pBRplac at the HindIII/EcoRI site   | kindly provided by S. Gottesman, De Lay and Gottesman, 2012 |
| pBR'                | pMSG13                        | p15A ori, Amp, Kan, contains pLacO-1 promoter, derived from pBRplac vector   | this study  |
| pBR'-MicL-S         | pMSG13-Reg26-80               | micL-S (80nt) cloned into pBR' at the HindIII/AatII site   | this study  |
| pBR'-MicL           | pMSG13-Reg26-FL               | micL (308nt) cloned into pBR' at the HindIII/AatII site  | this study  |
| pBR*                | pMSG14                        | p15A ori, Kan, contains pLacO-1 promoter; derived from pBR' vector   | this study  |
| pBR*-MicL-S         | pMSG14-Reg26-80               | micL-S (80nt) cloned into pMSG14 at the HindIII/AatII site   | this study  |
| pBR*-MicL           | pMSG14-Reg26-FL               | micL (308nt) cloned into pMSG14 at the HindIII/AatII site  | this study  |
| pBR*-MicL-TGAmut    | pMSG14-Reg26LTGAmut           | micL (308 nt) with cutC stop codon mutation (TGA to GGA) cloned into pMSG14 at the HindIII/AatII site  | this study  |
| pBR*- <i>cutC</i> * | pMSG14-cutC MicL promoter mut | cutC (from ribosome binding site through transcription terminator) with MicL -10/-35 promoter mutation cloned into pMSG14 at the HindIII/AatII site. | this study  |
| pTrc99a             | pTrc99a                       | pBR322 ori, Amp, contains pTrc promoter  | lab stock; Rhodius et al., 2006                             |
| pRpoE (pLC245)      | pRpoE (pLC245)                | rpoE coloned into pTrc99a  | lab stock; Rhodius et al., 2006                             |
| pKD3                | pKD3                          | Used as template plasmid for PCR amplification of cat cassette with FRT flanking sequence  | lab stock; Datsenko & Wanner, 2000                          |
| pKD4                | pKD4                          | Used as template plasmid for PCR amplification of kan cassette without FRT flanking sequence for pMSG13  | lab stock; Datsenko & Wanner, 2000                          |
| pKD13               | pKD13                         | Used as template plasmid for PCR amplification of kan cassette with FRT flanking sequence  | lab stock; Datsenko & Wanner, 2000                          |
| pCP20               | pCP20                         | Used for removing atibiotic resistance gene with flanking FRT sequence   | lab stock; Cherepanov & Wackernagel, 1996                   |
| pLpp                | pLpp                          | Lpp cloned into pTrc99a using EcoRI/XbaI   | this study  |
| pRseAB (pLC253)     | pRseAB (pLC253)               | RseAB cloned into pTrc99a  | lab stock; De Las Penas et al., 1997                        |
| pEG                 | pEG                           | p15A ori, Cm, modified pBAD with modified Trc promoter   | lab stock; Gogol et al., 2011                               |
| pEG-MicA            | pEG-MicA                      | p15A ori, Cm, modified pBAD with MicA under a modified Trc promoter  | lab stock; Gogol et al., 2011                               |
| pEG-MicL            | pEG-MicL                      | <i>micL</i> cloned into pEG using PstI/HindIII, under a modified Trc promoter  | this study  |
| pUA-E-MicA          | pUA-E60-MicA                  | pSC101 ori, Kan, contains MicA promoter (-65 to +5) GFP fusion   | lab stock; Mutalik et al., 2009                             |
| pUA-E-RybB          | pUA-E51-RybB                  | pSC101 ori, Kan, contains RybB promoter (-65 to +5) GFP fusion   | lab stock; Mutalik et al., 2009                             |
| pUA-E-MicL          | pUA-E-MicL                    | pSC101 ori, Kan, contains MicL promoter (-65 to +5) GFP fusion, cloned using XhoI/BamHI  | this study  |

## Conclusions

In this thesis, I have described several important discoveries elucidating how Gram-negative bacteria assemble their envelope. For *E. coli* and related Gram-negative bacteria, the  $\sigma^E$  pathway is a comprehensive envelope-monitoring system that is able to integrate multiple signals of OM dysfunction and regulate multiple folding pathways to effectively repair this dysfunction. I have shown that  $\sigma^E$  not only monitors unfolded OMPs, but also monitors misfolding of LPS through its negative regulator RseB (Chapter 1 and Chapter 2). Additionally, I have shown that while the protein-encoding members of  $\sigma^E$  regulon are specialized for OMP and LPS transport and repair, a third  $\sigma^E$ -dependent sRNA is responsible for regulating lipoprotein transport by modulating the flux of the most abundant protein in the cell, Lpp (Chapter 3). By monitoring and modulating all major components of the OM, this allows  $\sigma^E$  to control a major portion of protein synthesis and effectively assemble the OM.

However, many questions remain. How does  $\sigma^E$  sense lipoprotein status, and is Lpp a direct inducer of  $\sigma^E$ ? How do other bacteria, e.g.,  $\alpha$ -proteobacteria, which do not have  $\sigma^E$ , regulate their outer membranes? While  $\sigma^E$  is essential in *E. coli*,  $\sigma^E$  may not be essential in other, related organisms. How do these organisms deal with OM stress, and are there compensatory pathways that regulate OM assembly? Why is  $\sigma^E$  essential in *E. coli*? OM assembly is likely highly coordinated with cell-division, thus, is  $\sigma^E$  regulated by cell-cycle? These questions, and others have yet to be investigated.

## Appendix 1

Suppressors of the lethality due to  $\sigma^E$  activity depletion

**Contributing Authors:** Sarah E. Ades, Carol A. Gross

## Introduction

$\sigma^E$  is an essential gene in *E. coli*, but the reason for its essentiality is unknown [1]. Depletion of  $\sigma^E$  activity by overexpression of the  $\sigma^E$  negative regulators RseA and RseB leads to membrane defects and eventual cell lysis [2]. Intriguingly, this loss of viability can be rescued by concomitant overexpression of the proteins YhbW, PtsN or the  $\sigma^E$ -dependent sRNAs MicA, RybB, and as was shown in Chapter 3, MicL [2-4]. YhbW, a conserved bacterial protein, is highly conserved in enterobacteriaceae and encodes a predicted flavin-using monooxygenase [5]. PtsN is thought to be a component in the PTS phosphorelay system and may regulate the transcription of many genes through altering  $\sigma$  competition [5,6]. It is not understood how YhbW or PtsN might act to rescue this lethality, but several hypotheses have been put forward [2].

In contrast, the fact that the  $\sigma^E$ -dependent sRNAs can rescue this lethality suggests an attractive model for the cellular defects that occur when  $\sigma^E$  activity is decreased. As  $\sigma^E$  transcribes the essential machines that transport and assemble LPS and OMPs into the membrane [7], perhaps when  $\sigma^E$  activity is decreased there are insufficient levels of these assembly factors, thus weakening the membrane. The sRNAs can rescue this lethality by decreasing new synthesis of the abundant proteins of the OM, thus rebalancing the protein folding load with the level of assembly factors.

To test this model, I verified that overexpression of MicA/RybB/MicL could rescue lethality when  $\sigma^E$  activity is depleted, and I tested whether deletions in the abundant proteins of the OM ( $\Delta ompA$ ,  $\Delta ompC$ , and  $\Delta lpp$ ) could also rescue this defect. I additionally tested whether the presence of additional stressors (42°C, EDTA, SDS, and NaCl) could reveal differences between the rescue phenotypes of the different strains. Indeed, loss of these abundant proteins rescues the lethality, with the strongest rescue in  $\Delta ompA$  cells, which are almost fully suppressed under all the conditions tested.



## Results

### *Rescue of $\sigma^E$ activity depletion by MicA/RybB under stress conditions*

I verified that overexpression of MicA and RybB indeed rescued the lethality due to expression of the  $\sigma^E$  anti- $\sigma_S$ , RseA and RseB (at 30°C). I further tested this at 37°C, 42°C, and in media containing either 0.1 mM EDTA, or 300 mM NaCl, or 1.0% SDS (Figure 1). Importantly, I observed that even under basal expression of RseAB (no inducer), RseAB hosting cells were significantly sick at 42°C, but not at lower temperatures. However, I found that the sickness and rescue phenotype was highly variable in my hands, and after a significant amount of troubleshooting, I realized that this was due to the way the MicA/RybB overexpression and control plasmids were constructed. I describe the reconstruction of these plasmids in the following section, but the phenotype of MicA/RybB under these stress conditions needs to be revisited.

### *Reconstruction of MicA/RybB overexpression plasmids*

These plasmids were supposed to be constructed using a pSC101 origin harboring a  $\text{Cm}^R$  marker (in pXG10) so that they would be compatible with the pRseAB plasmid ( $\text{Amp}^R$  and pBR origin) [3]. However, I realized that while the control plasmid was pXG10, the pMicA/pRybB plasmids actually had a pBR origin (backbone pBAD24) with a  $\text{Cm}^R$  marker and a section from pXG10 (Figure 2). Since both the pMicA/pRybB plasmids and pRseAB had the same origins, competition from these origins could be the reason why these sRNAs can rescue the RseAB overexpression phenotype.

To circumvent this issue, I constructed a new series of plasmids (pEG aka pMSG15) that were  $\text{Cm}^R$  with a p15A origin and the same fragment from pXG10 (using pBAD33 as a backbone; Figure 3). I inserted a BbsI restriction site (type II enzyme) immediately after the promoter +1 to allow for cloning in of future sRNAs without linker. In this reconstructed plasmid

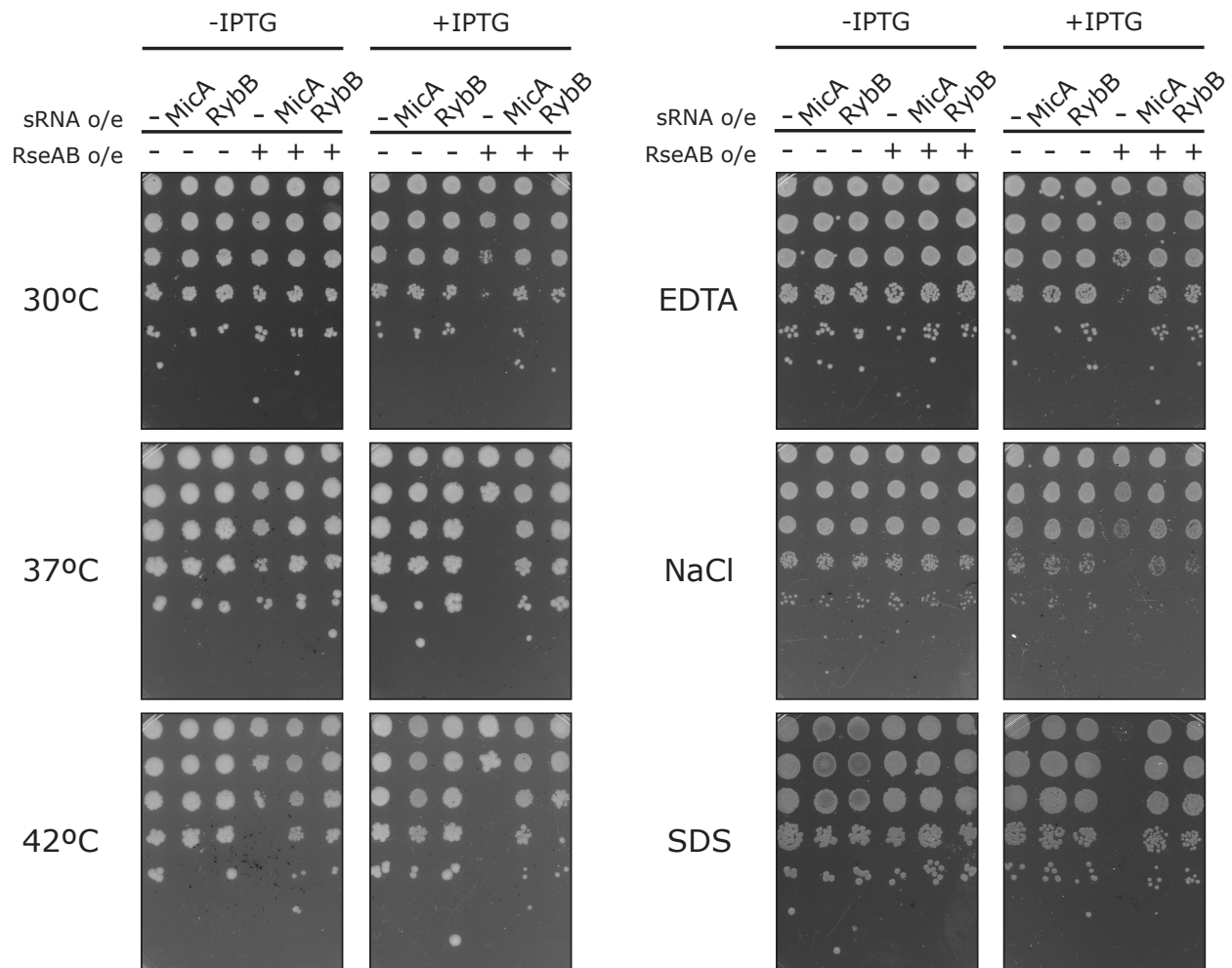


**Figure 1.** Rescue of lethality from loss of  $\sigma^E$  activity by sRNA under various stress conditions.

When  $\sigma^E$  activity is repressed by the overexpression of its negative regulators (RseA and RseB), viability decreases. Under heat stress, overexpression of MicA but not RybB rescues cells with low  $\sigma^E$  activity from death. In other stresses, overexpression of either sRNA rescues this phenotype. Strains containing IPTG-inducible RseAB (pRseAB) and/or IPTG-inducible sRNA (pMicA or pRybB) were grown in LB to OD600 0.1 without inducer, serially 10-fold diluted, and plated on LB±IPTG with various treatments/additives. (A) 30°C; (B) 37°C; (C) 42°C; (D) 0.1mM EDTA; (E) 300mM NaCl; (F) 1.0% SDS. Strains: no o/e, MicA o/e, RybB o/e, RseAB o/e, RseAB MicA o/e, RseAB RybB o/e. At least three independent platings were conducted for each condition, with one representative experiment shown.

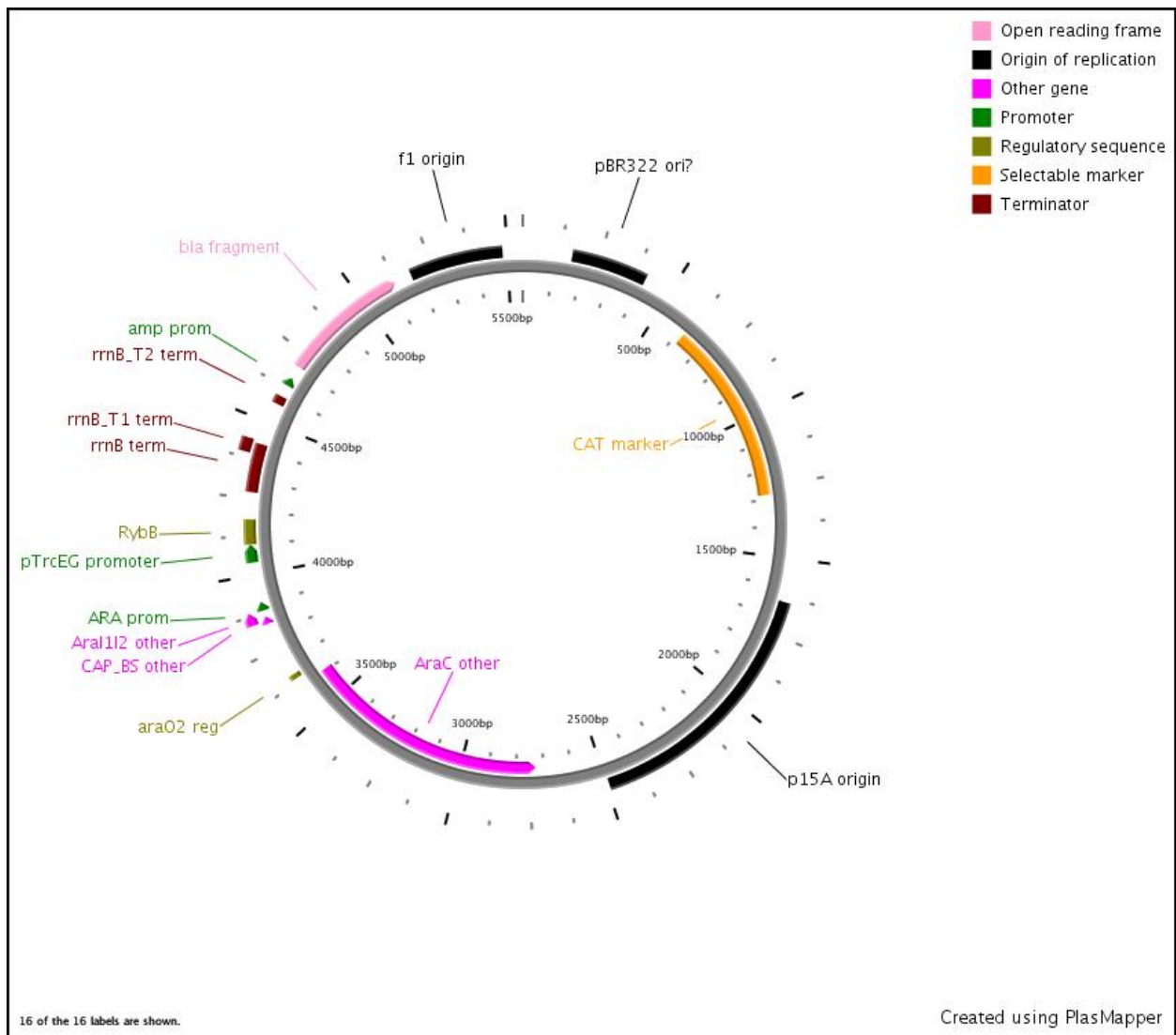


**Figure 2.** Plasmid map for pXG10-RybB.

Plasmid map was generated by fully sequencing pXG-RybB, and constructing a new vector map from the sequencing results. Similar results were obtained by doing the same with pXG-MicA, which was identical other than the sRNA sequence.

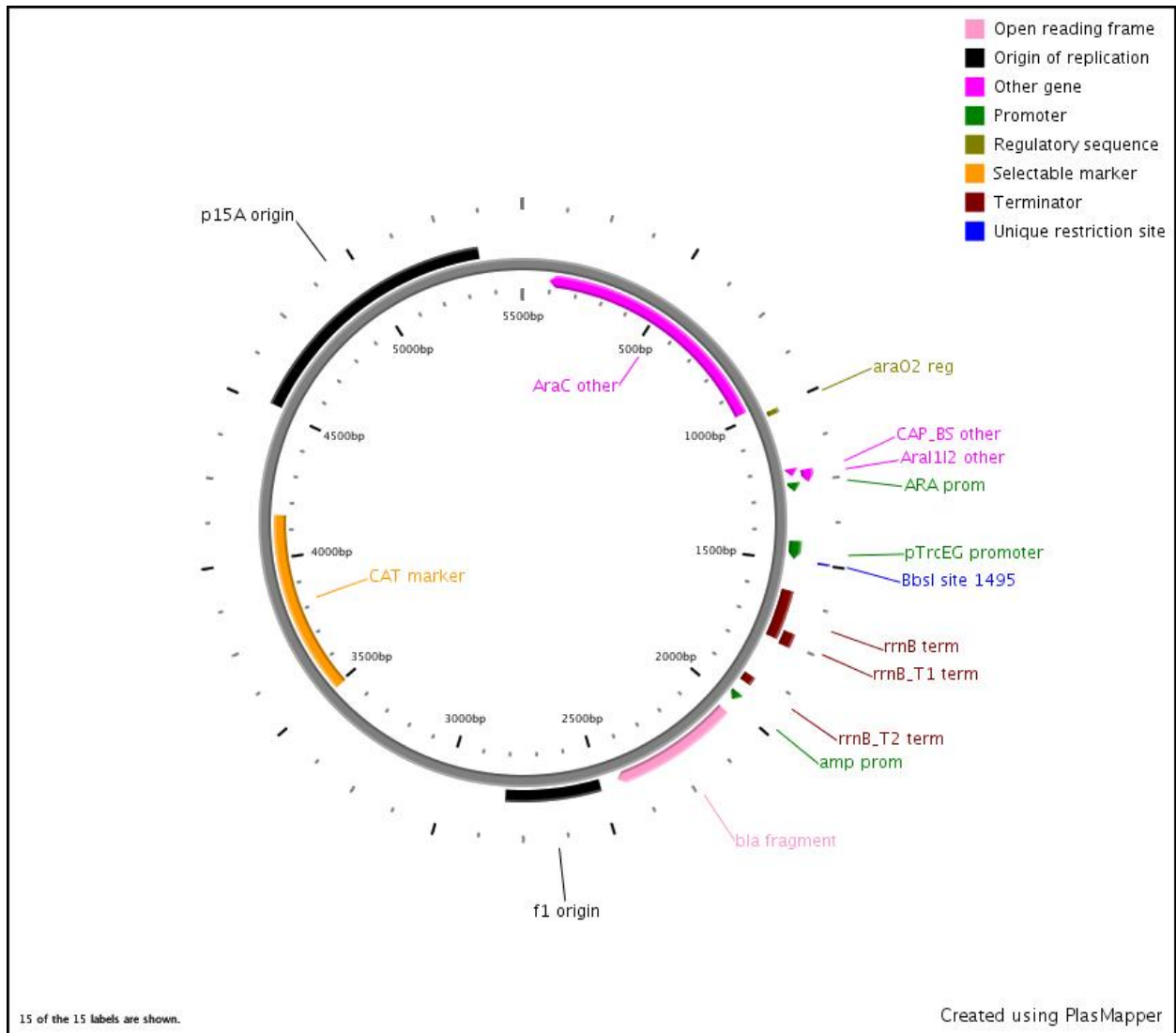


**Figure 3.** New plasmid (pMSG15) for sRNA cloning.

This is the reconstructed pXG10-sRNA plasmid. *MicA/RybB* were cloned in with *BbsI/HindIII* from pXG10. *BbsI* is a type II restriction enzyme, so sRNAs can be cloned in without linker.

background, I verified that indeed, overexpression of MicA/RybB can rescue the lethality due to depletion of  $\sigma^E$  activity (Figure 3, Chapter 3, Figure 7C). This is also the background where I performed the experiments in Chapter 3 to show that overexpression of MicL can rescue depletion of  $\sigma^E$  activity [4].

Importantly, I also tested whether expression of MicA or RybB from a different, more controlled promoter (pMSG11: p15A, Kan<sup>R</sup>, PLacO-1, LacIq) could also rescue this lethality. Interestingly, MicA and RybB expressed from the pMSG11 plasmid was unable to rescue the lethality of RseAB overexpression (data not shown). This may be due to the fact that the promoter in pXG/pEG is a modified Trc promoter (from pTrc99), and it is much leakier than the PLacO-1 promoter. Additionally, the Trc promoter is downstream from the natural pBAD promoter. Together, this suggests that a high basal level of sRNA may be required in addition to the overexpression of sRNA to fully rescue the cells when  $\sigma^E$  activity is depleted. This hypothesis has not been tested.

#### *Deletion of abundant OM proteins rescues $\sigma^E$ activity depletion*

$\Delta ompC$  or  $\Delta ompA$  cells were able to rescue the lethality when RseAB were overexpressed, with  $\Delta ompA$  cells showing full rescue and  $\Delta ompC$  cells showing partial rescue (Figure 4). Stress conditions (42°C or with EDTA, SDS, NaCl) exacerbated this difference, with  $\Delta ompA$  cells showing nearly full rescue on NaCl but  $\Delta ompC$  cells being nearly dead (Figure 4). In comparison, both  $\sigma^E$ -dependent sRNAs showed full rescue (Figure 3).

$\Delta lpp$  cells were also able to partially rescue this lethality, albeit with at most a 10-fold increase in viability (Figure 5). This is in contrast to the fact that overexpression of MicL shows nearly complete rescue [4]. This might be due to the fact that Lpp is an integral structural protein of the OM, so that partial loss of Lpp rebalances folding but complete loss of Lpp may negatively perturb the membrane in RseAB overexpressing cells.

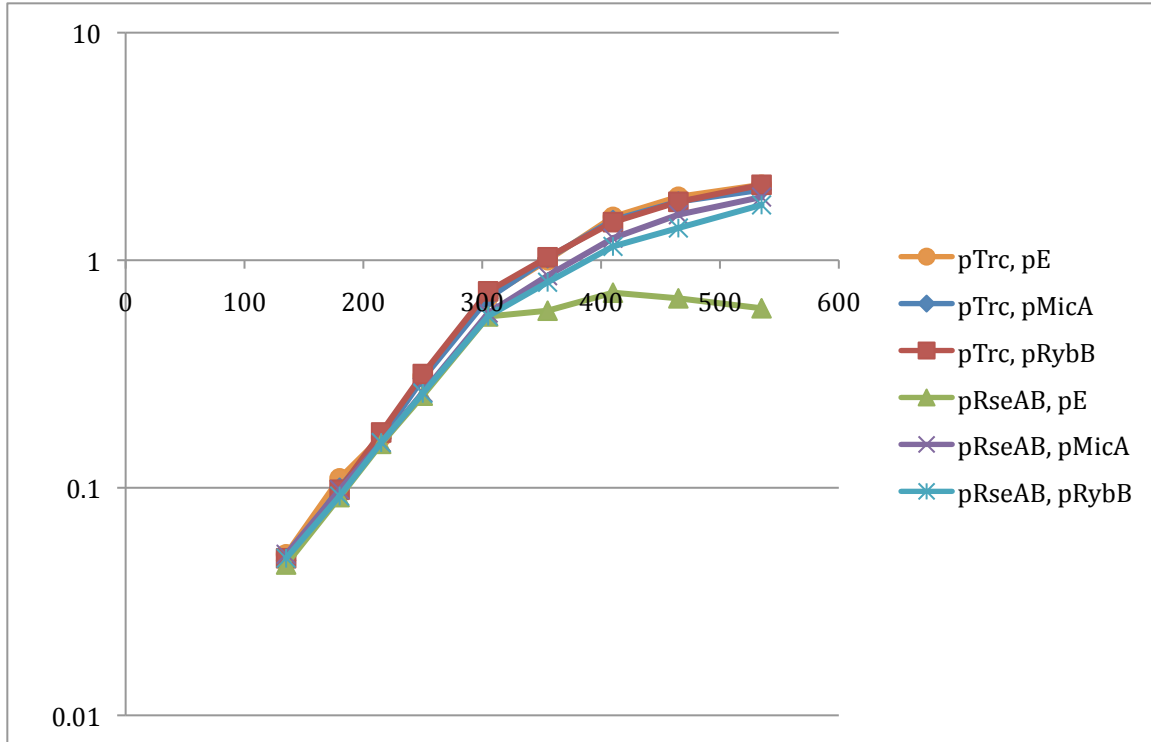


**Figure 3.** Overexpression of new sRNA plasmids rescues growth defect of pRseAB overexpression. IPTG is added at OD 0.1 which induces both expression of sRNA and expression of RseAB. pTrc, vector control for pRseAB. pE, vector control for pMicA/RybB. See also, Chapter 3, Figure 7C.

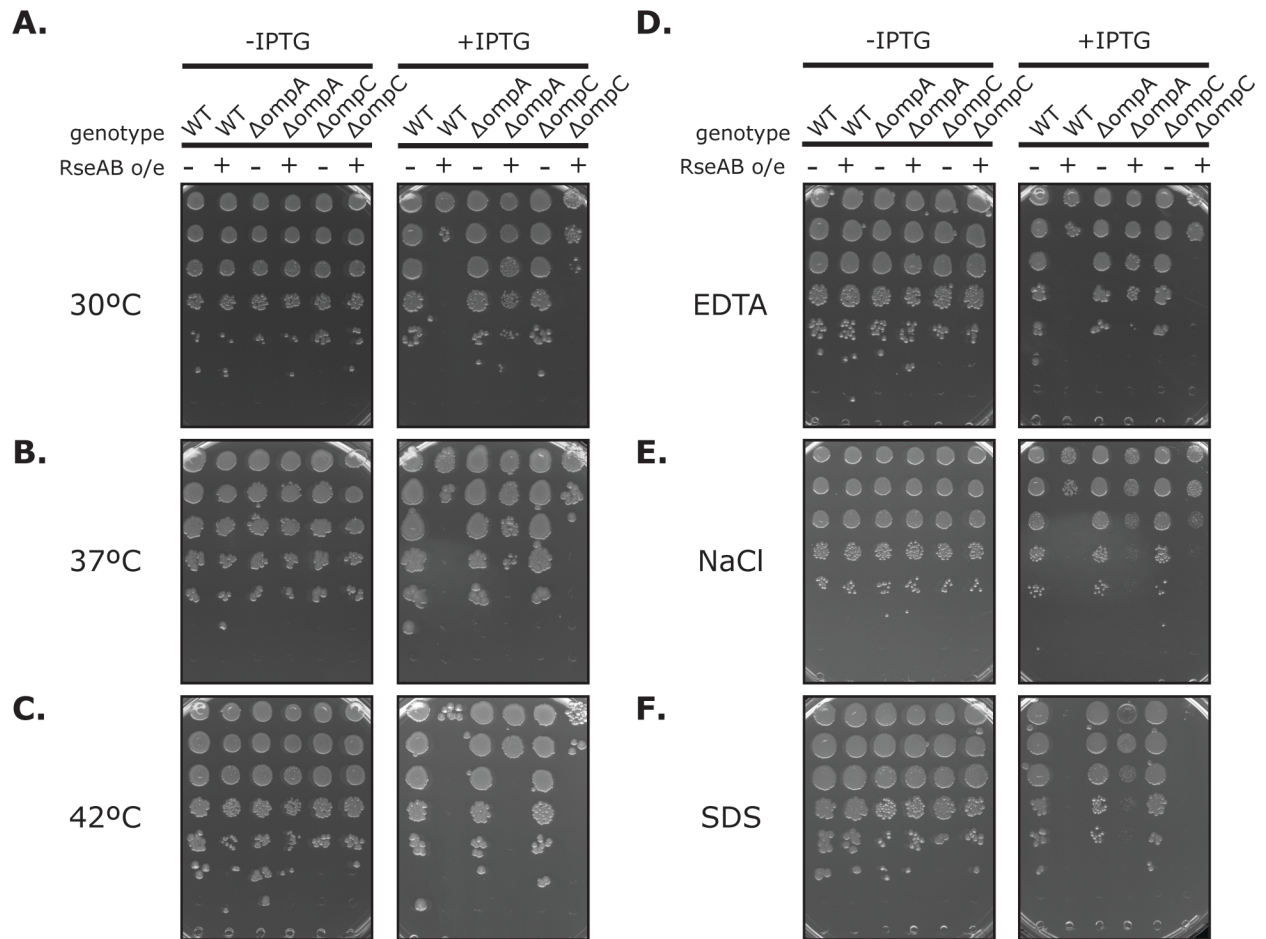
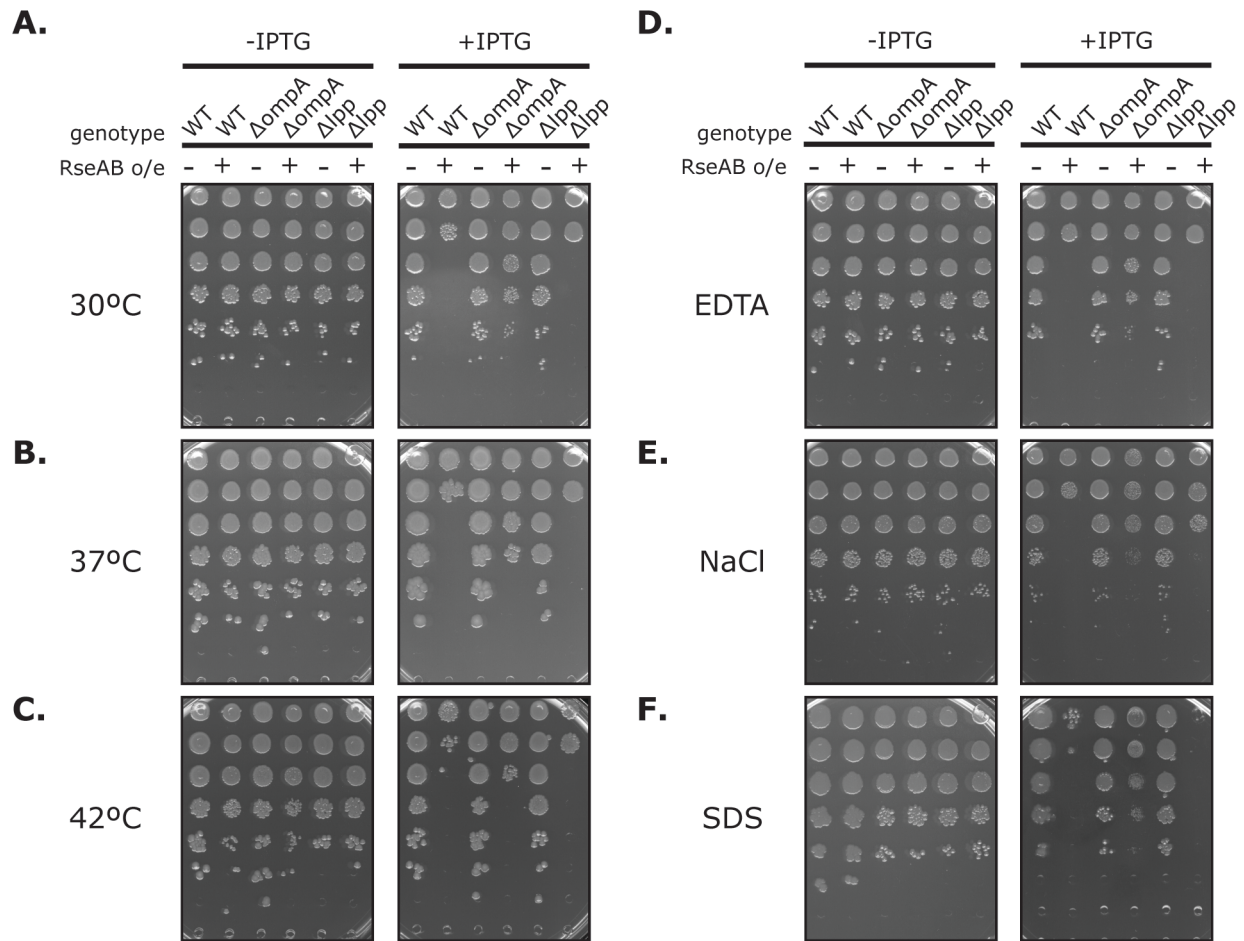


**Figure 4.** Deletion of major OM porins rescues viability when RseA and RseB are overexpressed. Strains containing IPTG-inducible RseAB (pRseAB) or its vector control (pTrc99) in WT,  $\Delta ompA$ , and  $\Delta ompC$  backgrounds were grown in LB to OD600 0.1 without inducer, serially 10-fold diluted, and plated on LB $\pm$ IPTG in various conditions/stresses. **(A)** 30°C; **(B)** 37°C; **(C)** 42°C; **(D)** 0.1mM EDTA; **(E)** 300mM NaCl; **(F)** 1.0% SDS. Strains: WT pTrc99, WT pRseAB,  $\Delta ompA$  pTrc99,  $\Delta ompA$  pRseAB,  $\Delta ompC$  pTrc99,  $\Delta ompC$  pRseAB. At least three independent platings were conducted for each condition, with one representative experiment shown.





## Discussion/Future Directions

These experiments are consistent with a model where cells that have reduced  $\sigma^E$  activity must reduce the flux of proteins to the membrane to survive. Since OMPs and Lpp are assembled into the OM in separate pathways (OMPs by the BAM complex, Lpp by the Lol system) why do they have the same rescue phenotype in  $\sigma^E$  activity depleted cells? In fact, both of these proteins are transported across the IM via the Sec pathway. This suggests that decreasing  $\sigma^E$  activity causes a defect in transport through Sec, thus preventing proper translocation of proteins into the periplasm/IM, leading to lysis. This model makes an important prediction: decreasing  $\sigma^E$  activity causes OMPs/Lpp to build up in the IM and overexpressing sRNA decreases these proteins in the IM, allowing the essential proteins of the OM to be translocated across and assembled. This can be tested by separating the OM/IM and interrogating the levels of OMPs/Lpp under these conditions. Given this model, it is interesting to speculate if defects in OM assembly “back up” into the IM, and prevent proper translocation of these proteins. As OMPs are thought to diffuse freely across the periplasm once across the IM, an interesting possibility could be that there is a “bridge” for OMPs and for Lpp that is analogous to the Lpt bridge that transports LPS [8].

Additionally, it is interesting to consider how could the overexpression suppressors PtsN and YhbW (and the deletion suppressor, YdcQ) alter OMP transport or translocation by Sec. Do these suppressors alter OMP/Lpp level or sRNA expression? Can they alter translocation through the IM? An additional idea could be that there are essential proteins that are not efficiently transported by Sec when OMP/Lpp levels are too high, and that the function of these other suppressors may be to support translocation of these other essential factors.

## Methods

### *Strain construction*

MG1655 (CAG45114) was used as the wild-type strain.  $\Delta ompA$ ,  $\Delta ompC$ , and  $\Delta lpp$  were obtained from the KEIO collection, and transduced into CAG45114.

### *Growth conditions*

Strains were grown aerobically at 30°C unless specified in LB (10 g tryptone, 5 g yeast extract, 10 g NaCl per liter). Where indicated, IPTG was added at a final concentration of 1 mM and antibiotics and chemicals were added when appropriate.

### *Pinning experiments*

Overnight cultures were diluted at 1:100 and grown at 30°C for 1:15 hr, and then serially diluted as specified. Either a 48-well frogger or 2.5  $\mu$ L of each dilution was spotted onto a LB plate with the appropriate additives. Spotted plates were allowed to dry, and were grown overnight at the appropriate temperature.

## References

1. De Las Peñas et al. SigmaE is an essential sigma factor in *Escherichia coli*. *J Bact* (1997) vol. 179 (21) pp. 6862-4.
2. Hayden, J.D., and Ades, S.E. (2008). The extracytoplasmic stress factor,  $\sigma^E$ , is required to maintain cell envelope integrity in *Escherichia coli*. *PLoS ONE* 3, e1573.
3. Gogol et al. Small RNAs endow a transcriptional activator with essential repressor functions for single-tier control of a global stress regulon. *Proc Natl Acad Sci USA* (2011) vol. 108 (31) pp. 12875-80.
4. Guo et al. MicL, a new  $\sigma^E$ -dependent sRNA, combats envelope stress by repressing synthesis of Lpp, the major outer membrane lipoprotein. *Genes Dev* (2014) vol. 28 (14) pp. 1620-34.
5. Keseler et al. EcoCyc: fusing model organism databases with systems biology. *Nuc Acids Res* (2013) vol. 41 pp. D605-12.
6. Lee et al. Potassium mediates *Escherichia coli* enzyme IIA(Ntr) -dependent regulation of sigma factor selectivity. *Mol Micro* (2010) vol. 78 (6) pp. 1468-83.
7. Rhodius et al. Conserved and variable functions of the sigmaE stress response in related genomes. *Plos Biol* (2006) vol. 4 (1) pp. e2.
8. Ruiz et al. Transport of lipopolysaccharide across the cell envelope: the long road of discovery. *Nat Rev Micro* (2009) vol. 7 (9) pp. 677-83.

## Appendix 2

### MicL overexpression alters global sRNA regulation

*Raw data published in:* Guo, M.S.<sup>†</sup>, Updegrave, T.B.<sup>†</sup>, et al. MicL, a new  $\sigma^E$ -dependent sRNA, combats envelope stress by repressing synthesis of Lpp, the major outer membrane lipoprotein. *Genes & Development* (2014) vol. 28 (14) pp. 1620-34.

## Introduction

The majority of known bacterial sRNAs are stabilized by the RNA chaperone Hfq, which facilitates the sRNA-target interaction [1,2]. It has recently been appreciated that Hfq might be limiting within the cell, and thus sRNAs are in active competition for Hfq [3]. The Gottesman Lab have investigated *in vivo* the effect of overexpression of several sRNAs on the mRNA levels and Hfq association of a small subset of other sRNAs [3]. These experiments suggested that different sRNAs might largely compete with only a subset of the Hfq-binding sRNAs [3]. While this could be a simple matter of binding affinity to Hfq, it has been suggested that sRNAs that have even highly variable structures have similar affinity for Hfq [4]. An alternative explanation arises from the fact that sRNAs can interact with one of a number of regions on Hfq (proximal, distal, rim helices), thus sRNAs may mostly be competitive with others that bind in similar regions on Hfq [2, 5]. The only thing that is clear is that the rules and physiological implications of Hfq competition have yet to be fully understood.

As I described in Chapter 3, I examined a time course of gene expression profiles using mRNA-seq after MicL overexpression and compared these profiles to those from a similarly treated vector control [6]. This dataset provides an excellent platform to investigate the question of Hfq competition, as all previous investigations have only examined the competitiveness of a small subset of cellular sRNAs. Additionally, this is the first investigation of a  $\sigma^E$ -dependent sRNA. By re-analyzing this dataset, I hope to answer the question of how does MicL compete for Hfq?

## Results

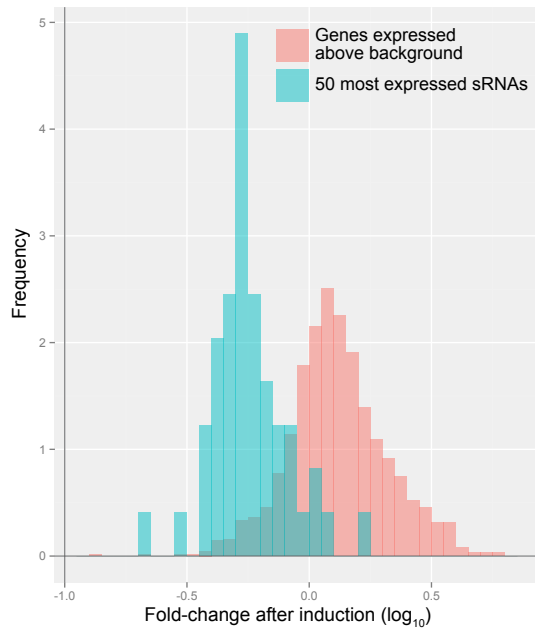
### *MicL overexpression reduces mRNA levels of global sRNAs*

As described in Chapter 3, I induced MicL-S with 1 mM IPTG for 20 min and then performed mRNA-seq. At this time, MicL-S is induced  $> 10^5$ -fold vs the vector control (Supplemental Figure 1). Strikingly, MicL-S overexpression leads to a small, but significant change in global sRNA level ( $p = 2 \times 10^{-16}$ , student's two-tailed t-test; Figure 1A). The top 5 most affected sRNAs were repressed approximately 2-fold, which is a similar fold-change as was observed in previous sRNA competition experiments (Figure 1B) [3]. Interestingly, the sRNAs who were most sensitive to MicL levels were not the most sensitive sRNAs from [3], again highlighting the fact that sRNA competition is most pronounced among specific subgroups of sRNAs.

### *MicL overexpression does not alter Hfq mRNA levels or translation*

While MicL overexpression alters the RNA levels of sRNAs, it was not known if this would affect Hfq levels in any way. I observed that after MicL overexpression, there was no change in either the level of Hfq mRNA or in the amount of translation on Hfq (Figure 2), suggesting that there is no feedback to upregulate Hfq transcription/translation when sRNAs compete.

A)



B)

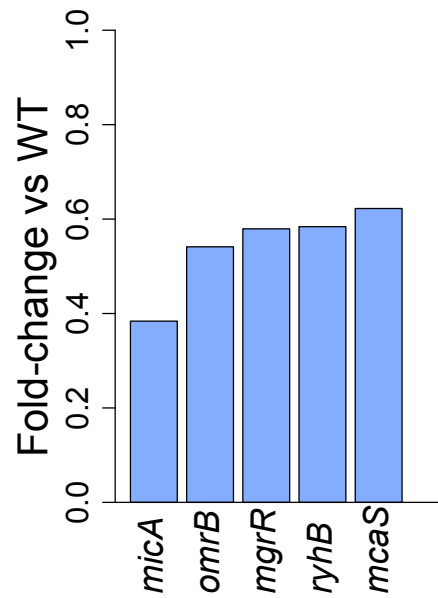


**Figure 1.** Global change in sRNA levels after 20 mins of MicL-S overexpression.

**(A)** The mRNA levels of the 50 most expressed sRNAs (cyan) are significantly decreased compared to bulk mRNA (salmon,  $p = 2 \times 10^{-16}$ ). Fold-change is normalized to vector control after 20 mins induction. **(B)** Change in sRNA levels (for 5 most repressed sRNAs) after 20 mins of MicL-S induction, normalized to vector control. Similar results are obtained with MicL overexpression.

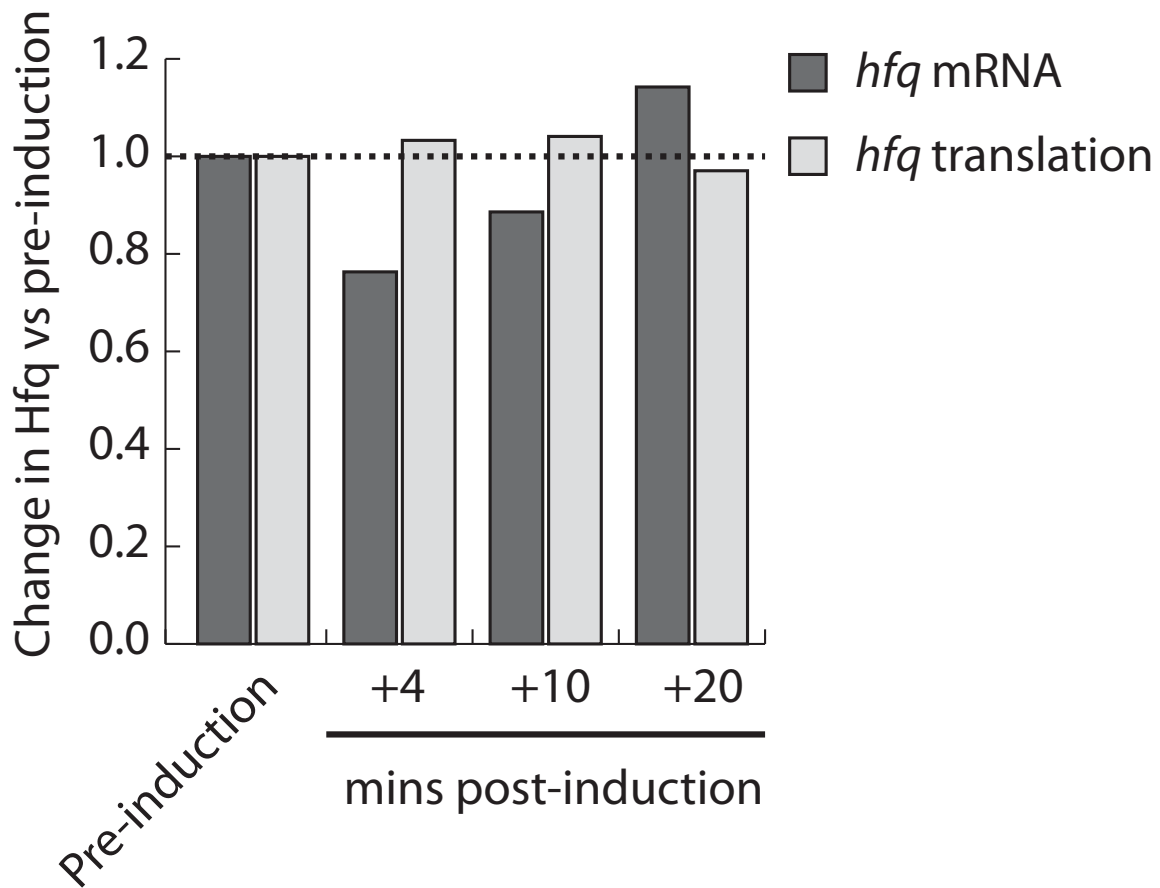


**Figure 2.** Effect of MicL-S overexpression on *hfq*.

*hfq* mRNA and translation at each timepoint was normalized to a pre-induced sample. **(Dark bars)** Effect of MicL-S overexpression on *hfq* mRNA levels. **(Light bars)** Effect MicL-S overexpression on relative translation of *hfq*. Similar results are obtained after MicL overexpression.



## Discussion

As expected, MicL overexpression affected the level of other sRNAs that are stabilized by Hfq. Interestingly, the suite of sRNAs that are most affected by MicL overexpression are not the same as those that were most sensitive to perturbation of OxyS or other sRNAs tested in [3]. When OxyS was overexpressed, CyaR, DsrA, ArcZ, and ChiX were strongly inhibited, but of these, only CyaR was strongly inhibited when MicL was overexpressed (top 10). Interestingly, both MicA and RybB levels were significantly inhibited when MicL was overexpressed (3-fold for MicA, 2-fold for RybB). An interesting hypothesis might be that MicL, MicA, and RybB may have evolved to compete for the same binding region on Hfq. Since these sRNAs are likely highly induced by  $\sigma^E$  activation, competition for the same face of Hfq might ensure that high expression of these sRNAs would still permits other sRNAs to interact efficiently with Hfq.

As Hfq transcription and translation are not affected by changes in sRNA level, future experiments with sRNAs must be carefully interpreted, as any subtle phenotypes could easily be due to global sRNA misregulation.

## References

1. Waters and Storz. Regulatory RNAs in bacteria. *Cell* (2009) vol. 136 (4) pp. 615-28.
2. De Lay et al. Bacterial small RNA-based negative regulation: Hfq and its accomplices. *J Biol Chem* (2013) vol. 288 (12) pp. 7996-8003.
3. Moon and Gottesman. Competition among Hfq-binding small RNAs in Escherichia coli. *Mol Micro* (2011) vol. 82 (6) pp. 1545-62.
4. Olejniczak. Despite similar binding to the Hfq protein regulatory RNAs widely differ in their competition performance. *Biochemistry* (2011) vol. 50 (21) pp. 4427-40.
5. Zhang et al. Mutations in Interaction Surfaces Differentially Impact E. coli Hfq Association with Small RNAs and Their mRNA Targets. *J Mol Biol* (2013) vol. 425 (19) pp. 3678-97.
6. Guo et al. MicL, a new  $\sigma$ E-dependent sRNA, combats envelope stress by repressing synthesis of Lpp, the major outer membrane lipoprotein. *Genes Dev* (2014) vol. 28 (14) pp. 1620-34.

## **Appendix 3**

### Comparison of sequencing approaches to identify TSS

**Contributing Authors:** Irene Ong, Sean Dorlan, Robert Landick

## Introduction

Few methods exist for identifying transcriptional start sites (TSS). One method is to use terminator exonuclease (TEX), an enzyme that specifically degrades away 5' monophosphate ends, to distinguish between bona fide TSS, have 5' triphosphates and other processed mRNA species, which have 5' monophosphates [1]. Conversion of TEX treated total mRNA into a sequencing library (TSS-seq) and subsequently mapping the start of all reads leads to a genome-wide prediction of TSS [1]. There are several caveats with this technology, as TEX has some ability to degrade 5' triphosphates and often leaves degradation products, which can make it difficult to distinguish genuine 5' ends. Comparison with an untreated library, and careful analysis is required to differentiate between the bona fide TSS and background noise generated by treatment.

In contrast, identifying TSS using mRNA-seq poses a slightly different challenge. Many mRNA-seq protocols discard the information of the 5' or 3' ends of the nascent mRNA. Importantly, mRNA-seq protocols developed for ribosome profiling from protocols for microRNA sequencing avoids biases that would distort the distribution of the RNA species [2, 3]. This protocol relies on a 3' linker ligation, followed by circularization of the ssDNA, preserving the precise 5' ends and adding minimal distortion to the 3' end [2, 3].

I analysed several mRNA-seq datasets generated from these protocols, and I realized that the 5' and 3' ends of these mRNA-seq reads were sometimes highly enriched at annotated promoter and terminator sequences. As I was collaborating with Irene Ong, Sean Dorlan, and Robert Landick at the UW-Madison Bioenergy Institute, I had access to their TSS-seq dataset (unpublished), which was gathered in a very different condition. I wanted to know how accurate mRNA-seq could be at predicting TSS, and I thought that I could use this TSS-seq dataset to find out. The results that follow detail several of my observations comparing mRNA-seq to TSS-seq.

## Results

### *Promoters in mRNA-seq and TSS-seq are highly correlated*

While the TSS-seq and mRNA-seq datasets were gathered in a vastly different conditions (mRNA-seq in MOPS glucose complete, and TSS-seq in a corn hydrolysate media), many promoters are still likely to be in common between the two datasets. I was able to find many positions where putative TSS-seq peaks correspond with putative 5' ends in the mRNA-seq (example in Figure 1). I subsequently made a list of positions where high TSS-seq peaks were correlated (within 1 nucleotide) of an mRNA-seq 5' peak (Table 1). This finding was very similar to the finding of Schrader et al, who also observed that mRNA-seq 5' peaks in *Caulobacter* were highly correlated with a 5' RACE dataset (5' RACE data not published) [4].

### *Algorithm for discovery of 5' ends of mRNA using mRNA-seq*

As putative 5' ends of mRNAs are easily identified in RNA-seq and are highly correlated with TSS, it would be a major advantage to develop methods to predict transcript boundaries from just mRNA-seq data. This has several advantages – 1) as it only relies on one technique, this method would be cheaper and more rapid than those that require additional (TSS-seq, ribosome profiling) datasets; 2) mRNA-seq also provides information of relative transcription levels and is helpful in predicting ORFs; 3) mRNA-seq will also provide information regarding the ends of transcripts, and may allow prediction of sRNAs.

I developed a simple algorithm based on the algorithm of [5]. Briefly, 100 nucleotides of mRNA sequence (using mRNA-seq data that has been mapped to every position) is correlated against a vector of 100 zeros followed by 100 ones ( $[0_{100}, 1_{100}]$ ). Regions with correlation  $\geq 0.86$  are then examined for a local 5' maxima in mRNA-seq (using mRNA-seq 5' mapping). These 5' maxima report many true transcriptional units and are very close to genuine TSS (assessed by comparison to TSS-seq data). This rough algorithm finds 83 5' ends in the first 300,000 nt of the

genome (~2500 events total per genome). However, this algorithm generates many false positives (due to fluctuations in the mRNA-seq density, which is captured by the window size).

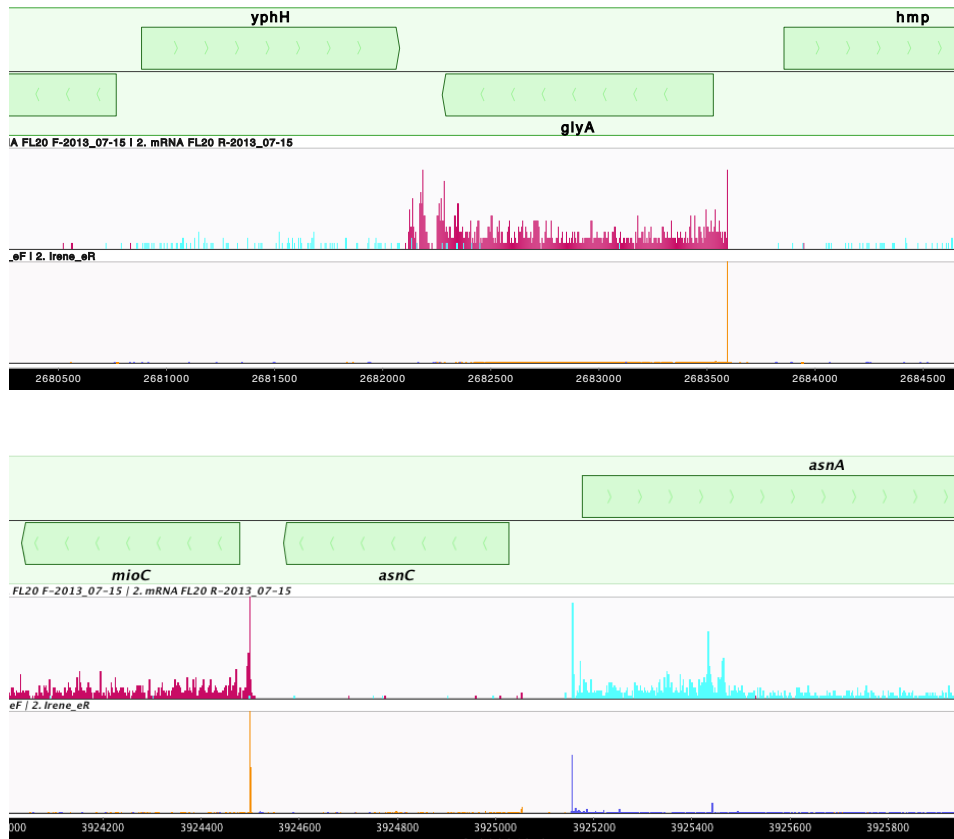


**Figure 1.** Examples comparing promoters in mRNA-seq with TSS-seq.

From top: gene orientation, mRNA-seq, TSS-seq. Cyan/Blue – forward strand; Red/Orange – reverse strand.

*glyA*: Ecocyc mapped start of transcription 2683596; mRNA/TSS-seq 2683593.

*mioC*: Ecocyc mapped start of transcription 3924498; mRNA/TSS-seq 3924499.

*asnA*: Ecocyc mapped start of transcription 3925152; mRNA/TSS-seq 3925155.

Notice high correlation of peaks between mRNA-seq and TSS-seq and mapped promoters.

**Table 1:** Sites in TSS-seq that correspond with peaks in mRNA-seq

| TSS_site | Strand |         |   |
|----------|--------|---------|---|
|          |        | 3171142 | + |
| 148      | +      | 3208669 | + |
| 12048    | +      | 3208671 | + |
| 89589    | +      | 3208738 | + |
| 107668   | +      | 3208740 | + |
| 141360   | +      | 3236395 | + |
| 194784   | +      | 3352533 | + |
| 257810   | +      | 3378148 | + |
| 443882   | +      | 3403267 | + |
| 458037   | +      | 3436023 | + |
| 458039   | +      | 3483975 | + |
| 496357   | +      | 3607940 | + |
| 742021   | +      | 3607942 | + |
| 773934   | +      | 3635635 | + |
| 779734   | +      | 3646085 | + |
| 816137   | +      | 3646316 | + |
| 849436   | +      | 3662887 | + |
| 931551   | +      | 3882140 | + |
| 938587   | +      | 3882265 | + |
| 960941   | +      | 3925155 | + |
| 982246   | +      | 3946073 | + |
| 1145872  | +      | 3963673 | + |
| 1150799  | +      | 3963675 | + |
| 1298694  | +      | 3984454 | + |
| 1306787  | +      | 4047922 | + |
| 1620611  | +      | 4049059 | + |
| 1625515  | +      | 4049061 | + |
| 1735712  | +      | 4098782 | + |
| 1739225  | +      | 4116450 | + |
| 1755407  | +      | 4130573 | + |
| 1860641  | +      | 4130575 | + |
| 1891360  | +      | 4173696 | + |
| 1899959  | +      | 4176377 | + |
| 1921089  | +      | 4198199 | + |
| 2051590  | +      | 4213427 | + |
| 2151335  | +      | 4255110 | + |
| 2267832  | +      | 4328343 | + |
| 2518942  | +      | 4368639 | + |
| 2518944  | +      | 4370786 | + |
| 2555334  | +      | 4374822 | + |
| 2555336  | +      | 4390335 | + |
| 2598459  | +      | 4397421 | + |
| 2751577  | +      | 4397824 | + |
| 2753615  | +      | 4494428 | + |
| 2945404  | +      | 4494430 | + |
| 3053781  | +      | 4526044 | + |
| 3053996  | +      |         |   |



| TSS_site | Strand |         |   |
|----------|--------|---------|---|
|          |        | 2689362 | - |
| 4633376  | -      | 2642401 | - |
| 4604457  | -      | 2597806 | - |
| 4447709  | -      | 2529302 | - |
| 4231560  | -      | 2468687 | - |
| 4117379  | -      | 2468685 | - |
| 4051800  | -      | 2278566 | - |
| 3958003  | -      | 2192222 | - |
| 3957864  | -      | 2096355 | - |
| 3957862  | -      | 1990207 | - |
| 3924499  | -      | 1914191 | - |
| 3865541  | -      | 1914189 | - |
| 3851215  | -      | 1820307 | - |
| 3810019  | -      | 1800757 | - |
| 3723377  | -      | 1800755 | - |
| 3717120  | -      | 1785185 | - |
| 3628952  | -      | 1762793 | - |
| 3599025  | -      | 1715311 | - |
| 3517403  | -      | 1676038 | - |
| 3475488  | -      | 1675998 | - |
| 3464769  | -      | 1669157 | - |
| 3451463  | -      | 1396683 | - |
| 3451461  | -      | 1386868 | - |
| 3451459  | -      | 1292180 | - |
| 3430625  | -      | 1120243 | - |
| 3309808  | -      | 1049924 | - |
| 3309806  | -      | 1049922 | - |
| 3268615  | -      | 1019409 | - |
| 3193262  | -      | 925702  | - |
| 3192887  | -      | 788233  | - |
| 3182740  | -      | 786893  | - |
| 3084431  | -      | 786852  | - |
| 3070879  | -      | 696389  | - |
| 3067893  | -      | 696053  | - |
| 3056478  | -      | 607015  | - |
| 3039121  | -      | 584889  | - |
| 2967027  | -      | 584887  | - |
| 2922546  | -      | 214197  | - |
| 2866139  | -      | 185978  | - |
| 2866137  | -      | 185976  | - |
| 2820112  | -      | 179181  | - |
| 2748769  | -      | 142703  | - |
| 2744276  | -      | 83735   | - |
| 2732315  | -      | 75608   | - |

## References

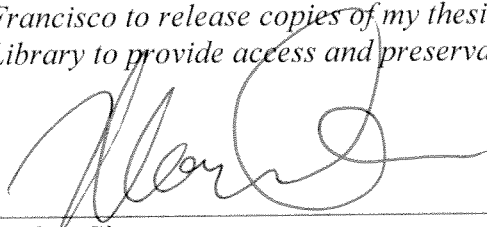
1. Sharma et al. The primary transcriptome of the major human pathogen *Helicobacter pylori*. *Nature* (2010) vol. 464 (7286) pp. 250-5.
2. Ingolia et al. Genome-wide analysis in vivo of translation with nucleotide resolution using ribosome profiling. *Science* (2009) vol. 324 (5924) pp. 218-23.
3. Lamm et al. Multimodal RNA-seq using single-strand, double-strand, and CircLigase-based capture yields a refined and extended description of the *C. elegans* transcriptome. *Genome Res* (2011) vol. 21 (2) pp. 265-75.
4. Schrader et al. The Coding and Noncoding Architecture of the *Caulobacter crescentus* Genome. *PLoS Genet* (2014) vol. 10 (7) pp. e1004463.
5. Güell et al. Transcriptome complexity in a genome-reduced bacterium. *Science* (2009) vol. 326 (5957) pp. 1268-71.

**Publishing Agreement**

*It is the policy of the University to encourage the distribution of all theses, dissertations, and manuscripts. Copies of all UCSF theses, dissertations, and manuscripts will be routed to the library via the Graduate Division. The library will make all theses, dissertations, and manuscripts accessible to the public and will preserve these to the best of their abilities, in perpetuity.*

***Please sign the following statement:***

*I hereby grant permission to the Graduate Division of the University of California, San Francisco to release copies of my thesis, dissertation, or manuscript to the Campus Library to provide access and preservation, in whole or in part, in perpetuity.*



\_\_\_\_\_  
Author Signature

9/16/14  
\_\_\_\_\_  
Date